DOCTORAL THESIS

Multiuser Non Coherent Massive MIMO Schemes based on DPSK for Future Communication Systems

Author: *VÍCTOR MONZÓN BAEZA*

Supervised by: *ANA GARCÍA ARMADA*

A doctoral thesis submitted in partial fulfilment
of the requirements for the award of Doctor of Philosophy at

Multimedia and Communication PHD Program

University Carlos III of Madrid
Department Signal Theory and Communications

Leganes, May 2019

Tesis Doctoral: Multiuser Non Coherent Massive MIMO Schemes based on DPSK for Future Communication Systems

Autor: Víctor Monzón Baeza

Directora: Dra. Ana García Armada

El tribunal nombrado para juzgar la tesis doctoral arriba citada, compuesto por los doctores

Presidente: Ana Isabel Pérez Neira

Vocal: M. Carmen Aguayo Torres

Secretario: Máximo Morales Céspedes

acuerda otorgarle la calificacin de **SOBRESALIENTE CUM LAUDE**

Leganés, a 30 de Mayo 2019

This thesis is dedicated to:
my mother and brother,
To my father's memory

El logro de un objetivo debe ser el punto de partida de otro.

Alexander Graham Bell

Dadme un punto de apoyo y moveré al mundo.

Arquímedes

Nada tiene tanto poder para ampliar la mente
como la capacidad de investigar de forma
sistemática y real todo lo que es
susceptible de observación en la vida.

Marco Aurelio

La única forma de tener un gran trabajo,
es amando lo que haces.

Steve Jobs

It is an old maxim of mine that when you have
excluded the impossible, whatever remains,
however improbable, must be the truth

Arthur Conan Doyle

Cualquier tecnologa lo suficientemente
avanzada es totalmente indistinguible de la magia

Arthur C. Clarke

Abstract

The explosive usage of rich multimedia content in wireless devices has overloaded the communication networks. Moreover, the fifth generation (5G) of wireless communications involves new requirements in the radio access network (RAN) which require higher network capacities and new capabilities such as ultra-reliable and low-latency communication (URLLC), vehicular communications or augmented reality. All this has encouraged a remarkable spectrum crisis in the RF bands. A need for searching alternative techniques with more spectral efficiency to accommodate the needs of future emerging wireless communications is emerging. In this context, massive MIMO (m-MIMO) systems have been proposed as a promising solution for providing a substantial increase in the network capacity, becoming one of the key enabling technologies for 5G and beyond. m-MIMO provides high spectral- and energy-efficiency thanks to the deployment of a large number of antennas at the BS. However, we have to take into account that the current communication technologies are based on coherent transmission techniques so far, which require the transmission of a huge amount of signaling. This drawback is escalating with the excessive available number of antennas in m-MIMO. Therefore, the differential encoding and non coherent (NC) detection are an alternative solution to circumvent the drawbacks of m-MIMO in coherent systems. This Ph.D. Thesis is focused on signal processing techniques for NC detection in conjunction with m-MIMO, proposing new constellation designs and NC detection algorithms, where the information is transmitted in the signal differential phase.

First, we design new constellation schemes for an uplink multiuser NC m-MIMO system in Rayleigh fading channels. These designs allow us to separate the users' signals at the receiver thanks to a one-to-one correspondence between the constellation for each user and the received joint constellation. Two approaches are considered in terms of BER: each user achieves a different performance and, on the other hand, the same performance is provided for all users. We analyze the number of antennas needed for those designs and compare to the required number by other designs in the literature. It is shown that our designs based on DPSK require a lower number of antennas than that required by their counterpart schemes based on energy. In addition, we compare the performance to their coherent counterpart systems, resulting NC-m-MIMO based on DPSK capable of outperforming the coherent systems with the suitable designs.

Second, in order to reduce the number of antennas required for a target performance we propose a multi-user bit interleaved coded modulation - iterative decoding (BICM-ID)

scheme as channel coding for a NC-m-MIMO system based on DPSK. We propose a novel NC approach for calculating EXIT curves based on the number of antennas. Then using the EXIT chart we find the best channel coding scheme for our NC-m-MIMO proposal. We show that the number of users served by the BS can be increased with a 70% reduction in the number of antennas with respect to the case without channel coding. In particular, we show that with 100 antennas for error protection equal design for all users and a coding rate of 1/2 we achieve the minimum probability of error.

Third, we consider that current scenarios such as backhaul wireless systems, rural or suburban environments, and even new device-to-device (D2D) communications or the communications in higher frequencies (millimeter and the emerging ones in terahertz frequencies) can have a predominant line-of-sight (LOS) component, modeled by Rician fading. For all these new possible scenarios in 5G, we analyze the behavior of the NC m-MIMO systems when we have a Rician fading. We present a new constellation design to overcome the problem of the LOS channel component, as well as an associated detection algorithm to separate each user in reception taking into account the characterization of the constellation. In addition, for contemplating a more realistic scenario, we propose grouping users which experience a Rayleigh fading with those with Rician fading, analyzing the SINR and the performance of such combination in a multi-user NC m-MIMO system based on M-DPSK. The adequate user grouping allows unifying the constellation for both groups of users and the detection algorithm, reducing the complexity of the receiver. Also, the number of users that may be multiplexed may be further increased thanks to the improved performance.

In the fourth part of this Thesis, we analyse the performance of multi-user NC m-MIMO based on DPSK in real environments and practical channels defined for the current standards such as LTE, the future technologies such as 5G and even for communications in the terahertz band. For this purpose, we use a metric to model the time-varying characteristics of the practical channels. We employ again the EXIT charts tool for analyzing and designing iteratively decoded systems. This analysis allows us to obtain an estimate of the degradation of the system's performance imposed by realistic channels. Hence, we show that our proposed system is robust to temporal variations, thus it is more recommendable the employment of NC-m-MIMO-DPSK in the future communication standards such as 5G. In order to reduce the number of hardware resources required in terms of RF chains, facilitating its implementation in a real system, we propose incorporating differential spatial modulation (DSM). We present and analyze a novel multiuser scheme for NC-m-MIMO combined with DSM with which we can see that the number of antennas is not affected by the incorporation of DSM, even we have an improvement on the performance with respect to the coherent case.

Finally, we study the viability of multiplexing users by constellation schemes against classical multiplexing techniques such as time division multiple access (TDMA). In order to fully characterize the system performance we analyze the block error rate (BLER) and the throughput of a NC-m-MIMO system. The results show a significant advantage regarding the number of antennas for multiplexing in the constellation against TDMA. However, in some cases, the demodulation of multiple users in constellation could require an excessively large number of antennas compared to TDMA. Therefore, it is necessary to properly manage the tradeoff between throughout and the number of antennas, to reach an optimal operational point, as shown in this Thesis.

Resumen

El inmenso uso de contenido multimedia en los dispositivos inalámbricos ha sobrecargado las redes de comunicaciones. Además, la quinta generación (5G) de sistemas de comunicaciones demanda nuevos requisitos para la red de acceso radio, la cual requiere ofrecer capacidades de red mayores y nuevas funcionalidades como comunicaciones ultra fiables y con muy poca letancia (URLLC), comunicaciones vehiculares o aplicaciones como la realidad aumentada. Todo esto ha propiciado una crisis notable en el espectro electromagnético, lo que ha llevado a una necesidad por buscar técnicas alternativas con más eficiencia espectral para acomodar todos los requisitos de las tecnologías de comunicaciones emergentes y futuras. En este contexto, los sistemas multi antena masivos, conocidos como *massive MIMO, m-MIMO*, han sido propuestos como una solución prometedora que proporciona un incremento substancial de la capacidad de red, convirtiéndose en una de las tecnologías claves para el 5G. Los sistemas m-MIMO elevan enormemente el número de antenas en la estación base, lo que les permite ofrecer alta eficiencia espectral y energética. No obstante, tenemos que tener en cuenta que las actuales tecnologías de comunicaciones emplean técnicas coherentes, las cuales requieren de información del estado del canal y por ello la transmisión de una enorme cantidad de información de señalización. Este inconveniente se ve agravado en el caso del m-MIMO debido al enorme número de antennas. Por ello, la codificación diferencial y la detección no coherente (NC) son una solución alternativa para solventar el problema de m-MIMO en los sistemas coherentes. Esta Tesis se centra en las técnicas de procesado de señal para detección NC junto con m-MIMO, proponiendo nuevos esquemas de constelación y algoritmos de detección NC, donde la información sea transmitida en la diferencia de fase de la señal.

Primero, diseñamos nuevas constelaciones para un sistema multi usuario NC en m-MIMO en enlace ascendente (*uplink*) en canales con desvanecimiento tipo Rayleigh. Estos diseños nos permiten separar las señales de los usuarios en el receptor gracias a la correspondencia unívoca entre la constelación de cada usuario individual y la constelación conjunta recibida en la estación base. Hemos considerado dos enfoques para el diseño en términos de probabilidad de error: cada usuario consigue un rendimiento distinto, mientras que por otro lado, todos los usuarios son capaces de recibir las mismas prestaciones de probabilidad de error. Analizamos el número de antenas necesario para estos diseños y comparamos con el número requerido por otros diseños propuestos en la literatura. Nuestro diseño basado en DPSK requiere un número menor de antenas comparado con los sistemas basados en detección de energía. También comparamos con su homólogo coher-

ente, resultando que NC-m-MIMO basado en DPSK es capaz de superar a los sistemas coherentes con los diseños adecuados.

En segundo lugar, para reducir el número de antenas requerido para un rendimiento dado, proponemos incluir un esquema de codificación de canal. Hemos optado por un esquema de modulación codificado por bit entrelazado y decodificación iterativa (BICM-ID). Hemos empleado la herramienta EXIT chart para el diseño de la codificación de canal, proponiendo un nuevo enfoque para calcular las curvas EXIT de forma NC y basadas en el número de antennas. Los resultados muestran que el número de usuarios servidos por la estación base puede ser incrementado reduciendo un 70% el número de antenas con respecto al caso sin codificación de canal. En particular, para un array de 100 antenas y un diseño que ofrezca iguales prestaciones a todos los usuarios, con un código de tasa 1/2, podemos conseguir la mínima probabilidad de error.

En tercer lugar, consideramos escenarios donde el canal tenga una componente predominante de visión directa (LOS) con la estación base modelada mediante un desvanecimiento tipo Rician. Por ejemplo, sistemas inalámbricos de backhaul, entornos rurales o sub urbanos, comunicaciones entre dispositivos (D2D), también cuando nos movemos hacia frecuencias superiores como son en la banda de milimétricas o más recientemente, la banda de terahercios para buscar mayores anchos de banda. Todos estos escenarios están contemplados en el futuro 5G. Los diseños presentados para canales Rayleigh ya no son válidos debido a la componente LOS del canal, por ello presentamos un nuevo diseño de constelación que resuelve el problema de la componente LOS, así como una guía para diseñar nuevas constelaciones. También proponemos un algoritmo asociado al diseño de la constelación para poder separar a los usuarios en recepción. Además, para contemplar un escenario más realista donde podamos encontrar tanto desvanecimiento Rayleigh como Rice, proponemos agrupar usuarios de ambos grupos, analizando su rendimiento y relación señal a interferencia en la combinación. El adecuado agrupamiento permite unificar el diseño de la constelación para ambos desvanecimientos y por tanto reducir la complejidad en el receptor. También, el número de usuarios multiplicados en la constelación podría ser incrementado, gracias a la mejora en el rendimiento.

El cuarto módulo de esta tesis es dedicado a analizar el rendimiento de los diseños propuestos en presencia de canales reales, donde disponemos de variabilidad temporal y en frecuencia. Proponemos usar una métrica que modela las características de la variabilidad temporal y, usando de nuevo la herramienta EXIT, analizamos los sistemas decodificados iterativamente considerando ahora los parámetros prácticos del canal. Este análisis nos permite obtener una estimación de la degradación que sufre el rendimiento del sistema impuesto por canales reales. Los resultados muestran que los sistemas NC-m-MIMO basados en DPSK son muy robustos a la variabilidad temporal por lo que son recomendables para los nuevos escenarios propuestos por el 5G, donde el canal cambia rápidamente.

Otra consideración para introducir los sistemas NC con m-MIMO es la problemática de necesitar muchas cadenas de radio frecuencia que llevarían a tamaños de dispositivos enormes. Para reducir este número se propone la modulación espacial. En esta Tesis, estudiamos su uso con los sistemas NC, proponiendo una solución de modulación espacial diferencial para esquemas con multiples usuarios combinado con NC-m-MIMO.

Finalmente, estudiamos la viabilidad de multiplexar usuarios en la constelación frente a usar técnicas clásicas de multiplexación como TDMA. Para caracterizar completamente el rendimiento del sistema, analizamos la tasa de error de bloque (BLER) y el *throughput* de un sistema NC-m-MIMO. Los resultados muestran una ventaja significativa en cuanto al número de antenas para multiplexar usuarios en la constelación frente al requerido por TDMA. No obstante, en algunos casos, la demodulación de múltiples usuarios en la constelación podría requerir un número de antennas excesivamente grande comparado con la multiplexación en el tiempo. Por ello, es necesario gestionar adecuadamente un balance entre el *throughput* y el número de antenas para alcanzar un punto operacional óptimo, como se muestra en esta Tesis.

Acknowledgements

Una vez más agradecer a mis padres, y en especial a mi madre, todo el trabajo y esfuerzo que han realizado durante estos años para que yo pueda llegar hasta aquí. El duro y a veces amargo camino que comenzaron ellos y que con mucha valentía y fuerza ha continuado mi madre hasta permitirme lograr cualquier reto que me he planteado. Con estas palabras darle mil gracias por su apoyo incondicional y compresión en los momentos difíciles. Agradecerle el ánimo y la fuerza que tanto he necesitado en esta larga y dura etapa, sin los cuales seguramente esto hubiese sido mucho más duro. Mi agradecimiento a mi hermano, Alejandro, por su apoyo y esos consejos valiosos que se reflejan en esta Tesis. Su perseverancia en las recaídas para continuar hasta el final.

Además del pilar fundamental de mi padres y mi hermano, tengo que agradecer a otras personas que han estado ahí apoyándome. Gracias a Carmen Rodal que no solo confió en mi durante mis años de instituto como profesora, sino que hasta el día de hoy me ha dado consejos hasta alcanzar esta Tesis, al igual que Antonio Vilchez. Gracias a Rafael Arellano por sus ánimos durante estos años. Por supuesto, no me olvido también de vuestros ánimos Nuria Montero y Elena Huerta, esos viajes inmemorables a los ensayos, en los momentos de bloqueo que me liberaban la mente y que sin duda han aportado a este trabajo. Igualmente, me gustará agradecer a Pilar y Esther Castellanos por hacerme el trabajo más llevadero en el día a día.

Agradecer a mi tutora Ana García Armada la oportunidad de realizar esta Tesis, su dedicación y trabajo para alcanzar el éxito de la misma.

I would like to thank all people that I had the pleasure of meeting during the time I spent in Southampton. I would specially like to thank Professor Lajos Hanzo for his invaluable comments and suggestions, also Mohammed and Wenbo.

A todos ellos, **GRACIAS**

CONTENIDOS PUBLICADOS Y PRESENTADOS

At the time of writing this Thesis had been published in the following papers, which will be related to the content of this Thesis in the introduction:

Book Chapter

1. **V. M. Baeza** and A. G. Armada "Non-Coherent Massive MIMO" in Book "Radio Technologies for 5G". Wiley, 2019.

Journal Papers

1. **V. M. Baeza and A. G. Armada**, "Non-Coherent Massive SIMO System based on M-DPSK for Rician Channels", IEEE Transactions on Vehicular Technology, January 2019, pp. 849-853.

2. **V. M. Baeza, A. G. Armada, W. Zhang, M. El-Hajjar and L. Hanzo**, "A Noncoherent Multiuser Large-Scale SIMO System Relying on M-Ary DPSK and BICM-ID", IEEE Transactions on Vehicular Technology, Feb 2018, pp. 2450-2454.

Conference Papers

1. **V. M. Baeza and A. G. Armada**, "User Grouping for Non-Coherent DPSK Massive SIMO with Heterogeneous Propagation Conditions" to be published on 2019 20th IEEE International Workshop on signal processing advances in wireless communications, Cannes, Jul. 2019.

2. **V. M. Baeza and A. G. Armada**, "Performance and Complexity Tradeoffs of Several Constellations for Non Coherent Massive MIMO" The 22nd International Symposium on Wireless Personal Multimedia Communications (WPMC)

3. **V. M. Baeza and A. G. Armada**, "Analysis of the Performance of a Non-Coherent Large Scale SIMO System Based on M-DPSK Under Rician Fading', European Signal Processing Conference (EUSIPCO), Kos, Greece, Sep 2017, pp. 732-736.

4. **V. M. Baeza, A. G. Armada, M. El-Hajjar and L. Hanzo**, "Performance of a non-coherent massive SIMO M-DPSK System", Proceedings of IEEE Vehicular Technology Conference (VTC) Fall, Toronto, Canada, September 2017, pp. 3031-3035.

OTROS MÉRITOS DE INVESTIGACIÓN

1. **V. M. Baeza**, M. Sánchez-Fernández, A. G. Armada and A. Royo "Testbed for a LiFi system integrated in streetlights" 2015 European Conference on Networks and Communications (EuCNC), Paris, 2015, pp. 517-521.

2. **V. M. Baeza**, M. J. Fernández-Getino and A. G. Armada "Análisis de sistemas de comunicación por luz visible (VLC) basados en FBMC/OQAM para 5G" 2015 Simposium Nacional de la Unión Internacional de Radio (URSI 2015).

3. **V. M. Baeza**, J.J. García Fernández and A. G. Armada "Bitloaded Modified Enhanced Subcarrier Index Modulation OFDM for Visible Light Communications" 2nd International Conference on Wireless Communication Systems and Networks (MIC-Wireless 2015)

4. Finalist at the II Edition 3 Minutes Thesis Talk Contest.

5. Local Chairman in 2nd International Conference on Wireless Communication Systems and Networks, Barcelona Spain 2015.

6. Technical Committee Member of GC-Technology Valencia, Spain 2020

Contents

Chapter 1

Introduction

1.1 Non Coherent techniques for communication systems

Wireless and cellular technologies are based on coherent transmission techniques so far, from the first generation 1G till the fourth one, 4G [1–5]. These coherent communication systems require the transmission of a huge amount of signaling or reference information, also known as *pilot signals*, to estimate the communication channel in the demodulation procedure. Another disadvantage of the coherent communications is the detection of the information when the channel changes rapidly such as in fast-fading scenarios. Moreover, multiple antennas are incorporated in the 4G systems in both handsets and base station (BS), known as multiple-input multiple output (MIMO) systems. For the future wireless technologies such as the fifth generation, 5G and beyond, the number of antennas is expected to continue rising towards higher numbers at the BS, so-called massive MIMO (m-MIMO) systems, even far beyond those used in the current operational standards such as Long Term Evolution (LTE) [5]. In these systems, the estimation of the channel state information (CSI) is worsened since a large number of channels have to be estimated. The CSI may be obtained using the pilot signals mentioned, transmitted from each user to the BS, assuming reciprocity in the radio link when employing time division duplex (TDD). Due to the fact that the pilot signals used in the adjacent cells are not completely orthogonal, the performance of the m-MIMO systems is degraded by the widely-recognized pilot contamination [6]. In addition, it is frequently assumed that the transmitter and/or receiver have knowledge of the exact channel impairments. However, this is an impractical assumption as well as obtaining the channel information is undesirable, particularly for m-MIMO.

The differential encoding (DE) and non coherent (NC) detection are an alternative solution to circumvent the two drawbacks of m-MIMO: the difficulty in estimating large amounts of CSI and the pilot contamination. The non coherent communications carry out the data detection without any knowledge of the channel information at the receiver side. However, the receiver may possess statistical information of the channel; *e.g.*, statistical descriptors of random variables such as mean, variance and autocorrelation. These techniques require of a detailed transmitted signals scheme, which can allow approaching the channel capacity of the coherent system at high signal to noise ratios (SNR). In a NC transmission, a reference symbol is transmitted, which is normally set to unity, and subsequent symbols are a differentially encoded version of the symbol in the previous time instant.

Instead of encoding information into absolute phases, the information is now encoded using phase differences between successive signal transmission. The receiver compares the phase during each symbol interval with the phase used during the previous symbol interval. However, these demodulators produce slightly more demodulation errors causing a known loss of 3 dB in their performance with respect to the coherent counterpart system.

The design dilemma between coherent and NC communication has intrigued the community for decades [7]. NC detection has indeed compelling benefits in terms of dispensing with power-thirsty channel estimation, as also argued in [8, 9]. The emphasis in this thesis will be the NC detection on m-MIMO systems. Indeed, we will demonstrate that NC systems are potentially capable of outperforming their coherent counterparts with the suitable designs.

1.2 New technologies for Radio Access

New scenarios emerging with 5G technology involve new requirements for the wireless communications systems [10–13]. Primarily, an increased usage of mobile multimedia services (*e.g.* video streaming applications) has conducted an exponential increase in wireless traffic demand and volume. 5G spreads the usage of the communications to include human-to-machine and machine-to-machine communications. Therefore, the new technologies for radio access networks (RAN) will have to satisfy the high variety of different new services and new context for the communication systems. Moreover, the new RAN must provide more flexibility, scalability and higher data rates. Some of the radio access technologies addressing the aforementioned issues, emerging as candidates for 5G are described below.

Massive MIMO:

It is the essential and promising technology as candidate in contributing to the new

RAN in 5G [14–19]. It has already been anticipated in the previous section that m-MIMO technology is defined as a system which utilizes a large number of antennas at least at one side of a wireless communications link, conventionally equipped at the BS side. In radar systems, large antennas arrays have been considered since years ago [20, 21], however, for mobile communications systems are being taken into account recently. T. Marzietta pioneered on m-MIMO in [22]. In this work showed that assuming the dimensions of a MIMO system grow large then the results of Random Matrix Theory (RMT) makes linear processing simpler which approaches optimal performance. More precisely, even with simple maximum-ratio combining (MRC) in the uplink, the effects of uncorrelated noise, the intra cell interference and fast fading tend to disappear as the number of antennas at BS grows large.

The main advantages of m-MIMO are summarized in [23] as:

- High spectral efficiency.
- High energy efficiency.
- Simple signal processing.

New waveforms:

For new RAN new waveforms are proposed [24] as evolution of the classical multi-carrier Orthogonal Frequency Division Multiplexing (OFDM) waveform by a filtering component. This provides good spectral containment properties of the transmit signals which can lead minimum interference between sub bands and, therefore facilitate the transmission of independent and uncoordinated different services. All of this enables a flexible air interface for future communications systems.

Two candidates are under research: Filter-Bank Multi-Carrier (FBMC) [25] and Universal Filtered Multi-Carrier (UFMC) [26]. FBMC offers more degrees of freedom in the design than UFMC due to individual filtering of the single subcarriers. On the other hand, UFMC maintains the conventional OFDM structure being sub bands constituted by a minimum number of filtered subcarriers.

Non-orthogonal multiple access:

To the new waveforms for future communications system is added the novel non-orthogonal schemes for efficient multiple access [27, 28] which allow for overloading the spectrum by multiplexing users typically in the power and the code domain. The candidate schemes are *e.g.* Non-Orthogonal Multipole Access (NOMA) which uses the power domain to multiplex users; both Interleave Division Multiple Access (IDMA) and Sparse Code Multiple Access (SCMA) which use the code domain. These schemes applied to m-MIMO can further reduce the signaling overhead.

Spatial Modulation (SM):

This is a newly and promising modulation scheme for MIMO communications [29,30], especially for m-MIMO. A key drawback of m-MIMO in the practical realization is the need to have a lot of radio frequency (RF) chains as it increases the complexity of the system. SM scheme can alleviate this disadvantage by the usage of fewer transmit RF chains than number of transmit antennas without compromising on the spectral efficiency. This reduces the RF hardware complexity, cost and size in m-MIMO systems [31]. SM uses multiple antennas in the transmitter, but only a single RF chain. The novelty of this modulation scheme is that it conveys information in the indices of the chosen antennas for data transmission, apart from the information conveyed through classical modulation schemes like phase shift keying (PSK) or quadrature amplitude modulation (QAM). In order to detect spatial modulation signals, low complexity detection algorithm can be used. In the literature, space shift keying (SSK) is referred as a special case of SM, where only the information of the transmitting antennas is conveyed. On the other hand, generalized spatial modulation (GSM) is the generalized version of SM [32].

Vehicle to Anything (V2X) communication:

This type of RAN technologies are being considered as solutions tailored for use cases of 5G. The safety-critical nature of V2X communications requires the ultra-reliable links. In this regard, channel estimation or channel prediction in V2X environments is significant, hence the non coherent detection may be of the greatest importance to avoid any errors made in the estimation of the channel [33]. Another advantage deriving from non coherent techniques is low delay in the communications which can provide high data rates for the new services envisaged for 5G. In order to achieve the safety requirement, the device-to-device (D2D) links are the most attractive [34].

Visible Light Communications (VLC) or Light Fidelity (LiFi):

The looming electromagnetic spectrum crisis -due to the fact of the explosive growth in the increasing user data demand- has encouraged the emergence of new wireless technologies. Currently, 16,000 million devices in the world and with an expected increase of 23% for the year 2021. The wide use of these devices is promoted by the emerging multimedia applications such as augmented and virtual reality or video streaming services. These technologies require very high bandwidth and data rate which are clogging the RF band. On the other hand, even with advances in wireless technology, there are locations such as hospitals, aircrafts or industry where the RF signals interfere with the electronic devices, which cause serious health and security problems. The data rate is still not large enough even through m-MIMO to meet the demand of unforeseen applications. To circumvent all these impediments, Visible Light Communications (VLC) [35] or its commercial version, the Light Fidelity (LiFi) promising technology [36] is emerging as one of the best technol-

ogy of the Era to support the growth of the demand for higher transmission speeds as well as ensuring RF interference-free environments, offering a 10,000 times larger bandwidth.

Massive machine-type communication:

In the machine-to-machine (M2M) communications [37] is typical transmitting small data packets in order not to saturate the channel. In this regard, the pilot signals for CSI and channel estimation introduce a high signaling overhead. Again, the non coherent techniques help to avoid this issue through savings in CSI.

Millimeter waves:

The lack of spectrum has caused to continually seek new frequency bands to accommodate the desire by higher data rates for the communication services. The millimeter wave (mmWaves) spectrum can offer from 10 up to 100 more bandwidth than is available for conventional and current systems such as Wireless Fidelity (WiFi), 4G or older cellular systems. Currently, the mmWaves spectrum is used by military, radar and as backhaul, applications where the non coherent techniques already are in usage. The large amount of spectrum available offers new opportunity for future wireless communications [38] and hence for the non coherent detection schemes. In addition, the short carrier wavelength allows incorporating antenna arrays an easier way in the handsets facilitating the deployment of m-MIMO.

1.3 Overview of Massive MIMO Systems

The large number of antennas at the BS or terminals, called m-MIMO, has been gradually explained in this introduction as a novel technique to increase the capacity and performance of the communication systems. Hence, it is a primary part for 5G. Thus, it is time to review the key aspects of this technology.

M-MIMO renders the benefits of the conventional MIMO to a much larger scale. Specifically, this technology can offer higher power efficiency, higher throughput and communication reliability than current standard with a low-complexity linear processing. In order to carry out this processing, m-MIMO exploits the concept of *favorable propagation* (FP) as argued in [39] and [40]. This property involves that the channel responses h defined between J users and the BS are mutually orthogonal to each other as the number of antennas R increases without limit, backed by the law of Large Numbers [41] and expressed as

$$h_j^H h_k = \begin{cases} \|h_j\|^2 \neq 0, & k = j = 1, \cdots, J \\ \frac{h_j^H h_k}{R} \to 0, & R \to \infty;\ j, k = j = 1, \cdots, J \text{ and } j \neq k \end{cases} \tag{1.1}$$

The capacity of a m-MIMO system is defined as

$$C = \log_2 |\mathbf{I}_J + P\mathbf{H}^H\mathbf{H}| \tag{1.2}$$

where P is the average transmit power and $\mathbf{H}$ is the channel matrix. When FP conditions in (1.1) are achieved, (1.2) is converted as $R \to \infty$ in

$$C \approx \sum_{j=1}^{J} \log_2(1 + P\,\|h_j\|^2), \tag{1.3}$$

which entails a gain with respect to R which is translated in:

- A reduction of transmitted power denoting an increased energy-efficiency, the exploitation of extra degrees of freedom provided by the excess of service antennas, reducing internal power consumption. We can reduce the transmitted power of each user proportionally to $1/R$ if the BS has perfect channel state information (CSI), and proportionally to $1/\sqrt{R}$ if CSI is estimated from uplink pilots.
- The inter-user interference vanishes as R grows. Extra antennas help by focusing energy into ever smaller regions of space to bring huge improvements in throughput and radiated energy contributing to improving the spectral- and energy-efficiency.
- Linear processing becomes optimal when R is close to infinite value. For m-MIMO conventional linear detectors maximum-ratio combining (MRC), zero-forcing (ZF), and minimum mean-squared error (MMSE) are considered. MRC has the advantage that it can be implemented in a distributed manner, i.e., each antenna performs multiplication of the received signals with the conjugate of the channel, without sending the entire baseband signal to the BS for processing. ZF is typically used to suppress the Interference between terminals. Moreover, these improvements in performance can be achieved with the aid of a low-complexity linear processing.
- The throughput is optimized offering an increased spectral-efficiency also.

The tradeoff between the energy efficiency measured in bits per joules (b/J) and spectral efficiency as *bits/channel use/terminal* is shown in Figure 1.1 [39]. It is shown that the use of large antenna arrays can improve the spectral and energy efficiency with orders of magnitude compared to a single-antenna system using simple lineal detectors.

In order for the channel estimation to be feasible, m-MIMO systems tend to assume TDD operation, where the pilot sequences are transmitted in the uplink (UL) for estimating the UL channel and then the downlink (DL) channel is assumed to be identical to that of the UL during the Transmit Pre-Coding (TPC) transmission. The issue is the pilot contamination due to the non-orthogonality of the pilot sequences used in neighboring

Figure 1.1 Energy efficiency versus spectral efficiency in m-MIMO from [39].

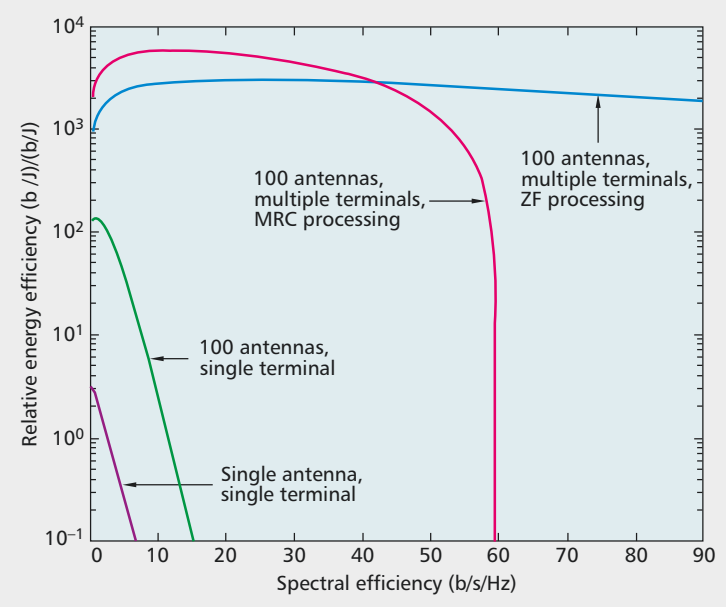

cells seriously compromises the performance of these systems [22]. Even though there is some ongoing research on ameliorating this problem [6], there are still open challenges for further research. Additionally, mitigating the impact of other impairments, such as phase noise [42] is needed.

The capacity increase results from the aggressive spatial multiplexing used in m-MIMO. The fundamental principle that makes the dramatic increase in energy efficiency possible is that, with a large number of antennas, energy can be focused with extreme sharpness into small regions in space. The underlying physics is coherent superposition of wavefronts. By appropriately shaping the signals sent out by the antennas, the base station can make sure that all wavefronts collectively emitted by all antennas add up constructively at the locations of the intended terminals, but destructively (randomly) almost everywhere else.

Other advantages of m-MIMO, due to the law of large numbers, are that noise, fading, and hardware imperfections average out when signals from a large number of antennas are combined in the air. Therefore, there is a reduction of the constraints on accuracy and linearity of each individual amplifier and RF chain. One of the main bottlenecks of m-MIMO due to the large number of antennas is the need to obtain the CSI of numerous channels for coherent detection or for TPC. The number of channel responses each terminal must estimate is also proportional to the number of base station antennas. Hence, the uplink resources needed to inform the base station of the channel responses would be up to 100 times larger than in conventional systems.

Hence, in order to circumvent the drawbacks and exploit the full potential of all these advantages raised with m-MIMO, the non coherent techniques emerge for incorporating in the future communication systems.

1.4 Analysis of the State of Art

The major part of this thesis is devoted to the multiuser non coherent detection for m-MIMO systems using DPSK schemes. Popularly, the basis for a DPSK modulation scheme and non coherent detection may be consulted in Proakis's book [43]. However, for decades before that, many works have contributed to the inclusion of these techniques in the communication systems. Although the lack of hardware and advanced signal processing techniques have delayed their practical application in these systems. In this section we give a detailed review of the existing literature in the field of NC communications, from single user (SU) systems to multiuser, and from single-input single-output (SISO) until modern communication systems which include m-MIMO.

1.4.1 Non Coherent versus Coherent

Communication systems over years have been responding to challenges posed by channel estimation. In view of increasing demand for high date rates, dispensing with CSI using m-MIMO is attracting increasing attention among the research community on wireless communications. Several studies have been devoted to highlight the performance of the non coherent systems against their counterpart coherent schemes [44–50]. In [44] aeronautical systems that adaptively switch between coherent and non-coherent schemes based on high doppler were proposed, demonstrating that the usage of a sphere detector and feedback detection as NC solutions are capable of outperforming their coherent counterparts at high normalized Doppler frequencies, being the reason for NC schemes to be more preferable for aeronautical environments..

In the context of impulse radio ultra-wideband (IR-UWB) communications, [45] compared coherent and non-coherent schemes that exploit the spatial diversity in a distributed manner among the different terminals of a wireless network. From point of view of cooperative network, [46] studied the NC scheme against coherent. In [47, 48] the comparison is based on the complexity of the system, being NC scheme more attractive than the coherent one.

1.4.2 Single and Multi-user Non Coherent SISO

The performance of non coherent (NC) communications has been theoretically studied against their coherent counterpart since the 1960s [51–55]. At the start of the NC detection, the predominant three schemes were on-off-keying (OOK), NC frequency-shift-keying (FSK) and differential phase-shift-keying (DPSK), used exclusively for binary signals. FSK was considered as the representative scheme for NC detection. The technical features for all of them are described in [56] and compared to coherent schemes such as ASK, coherent FSK and PSK according to their complexity, spectral properties, performance and effects provided by delay distortion, fading and interference from point of view of digital radio. In [53,54], FSK schemes were extended to continuous phase FSK (CPFSK), although the constraints of the FSK schemes such as the high bandwidth utilization or the difficulties in establishing a reference carrier in the receiver, converts DPSK scheme in a better candidate for NC detection. Therefore, it was in the 1990s when DPSK schemes took advantage over FSK, as shown in [57, 58]. For these years, [59] presented an evolutioned Viterbi algorithm for differential detection using DPSK. Also, adaptive differential detection was studied for $M-$ary DPSK in [60], extending NC schemes to multilevel signals. Other contributions for multilevel DPSK were [61–65].

The general structure proposed for an optimum NC detector in all these early contributions consists of a matched filter followed by an envelope detector and a comparator as shown in Figure 1.2 (a). There are practical difficulties in implementing optimum detectors for FSK and DPSK, and hence sub-optimum solutions, such as discriminators and phase-locked loops, have usually been adopted [66]. It is possible, however, to adapt the pulse-compression techniques widely used in radar systems to facilitate the implementation of a matched filter in the form of a pulse-compressor matched filter (PCMF) [67] as shown in Figure 1.2 (b). This has led the development of NC detection techniques primarily in radar technology [20,68]. The application of this technology in military communications introduces the direct-sequence spread-spectrum (DSSS) modulation schemes in the NC detection [69, 70].

The envelope detection can easily be achieved with a diode element. In addition, due to the light properties, the NC demodulation has evoked also great interest for optical communications: *e.g.* [71] using DPSK scheme, [72] for OOK scheme and [73] for FSK scheme.

The scenarios for wireless communications have gradually driven towards fast fading environment over years. In this background, NC detection type based on energy have gained importance against envelope detection due to the fact that the envelope detection is difficult to achieve when it changes rapidly.

Figure 1.2 Non Coherent detector based on envelope detection.

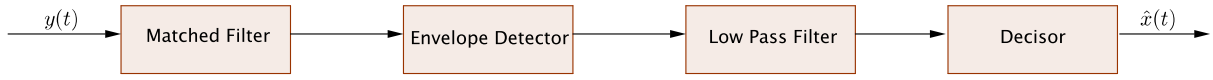

(a) NC Detector with Matched Filter

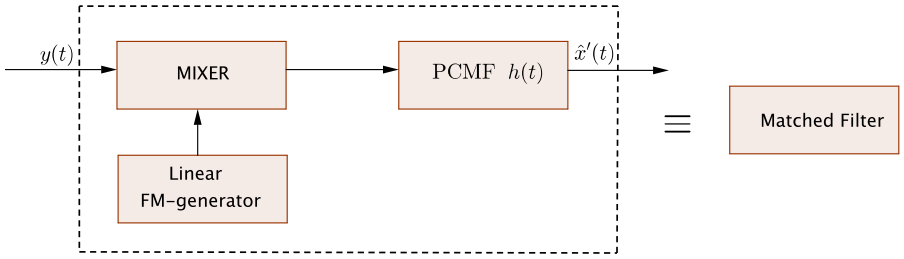

(b) Matched Filter as PCMF

More recently, NC techniques have been enjoying a new boom [74–77]. For energy harvesting communications systems, the need for the CSI which requires extra power consumption in the coherent schemes, is promoting the use of NC techniques as shown in [74, 75]. A novel NC scheme is proposed in [76] based on a combination of DPSK with Quadrature Amplitude Modulation (QAM). This scheme tranmists one or several QAM symbols inserted between two DPSK symbols providing a power gain compared to solely DPSK due to the usage of high SNR, although it leads to additional complexity and costs. In [77] an analysis of the effect of phase-quadrature (I/Q) imbalance on the carrier when we employ NC schemes is shown, more pronounced with the use of mmWaves. All these works can serve as a basis for advances towards the path of NC-m-MIMO.

Despite efforts to improve the performance for single user systems, the communication systems implement multi-user detection (MUD), where the basis is sharing the same physical resource by all users, to increase the spectral efficiency and, thus, the opportunity of higher data rates. The main issue for MUD is the inter-user interference (IUI) which limits the performance of these systems. This is a recurrent problem in any new generation of communication technologies.

MUD for coherent schemes have been widely studied for years and integrated in the current operational standards [78–81]. Meanwhile, for non coherent MUD (NC-MUD) the research dates back to the 2000s, when only single-input single-output (SISO) systems were proposed with non coherent schemes. In those works, the NC-MUD was classified into two groups: the prior non coherent MUD (prior-NC-MUD) and the posterior non coherent MUD (post-NC-MUD). In the first group, the operations related to MUD are carried out before the non coherent processing [82–84], while in the second one the operations for users

detection is carried out after the non coherent processing [85,86]. The performance results of these studies were proposed in the context of the time-hopping/multi-carrier code division multiple access (TH/MC CDMA) systems, then present in the 3G systems and which will be possible to extend to other schemes. In [87], NC receivers for differentially encoded CDMA are proposed with DPSK. As with the single user scheme, the main modulation technique used firstly in NC-MUD was MFSK and the non coherent processing consisting only of the square-law nonlinearity based on envelope signal.

The prior-NC-MUD can achieve the full diversity gain. However, the number of users supportable was in general low. Conversely, the post-NC-MUD was capable of supporting a high number of users by a trade-off with the diversity gain achievable. Both NC-MUDs can retain an optimum bit error rate (BER) performance, but with an extremely high complexity, making them unfeasible for real implementation.

1.4.3 Single and Multi-user Non Coherent MIMO

On a par with NC-MUD for SISO systems, the research on multiuser MIMO (MU-MIMO) technology is carried out. At the end of the year 2000, the Differential Unitary Space-Time Modulation (DUSTM) [88] and subsequently in [89] scheme spearhead the background of non-coherent MIMO systems. This scheme was a higher dimensional extension of the standard DPSK modulation to attain non-coherent communication with MIMO channels. In DUSTM, the channel is used in blocks of R_t transmissions, where R_t is the number of transmitting antennas. The transmitted signals belong to a codebook comprising a predefined set of $R_t \times R_t$ unitary matrices. The main advantage of DUSTM is its efficient decoding, which can be carried out through Multiple-Symbol Differential Detection (MSDD) at the receiver side [90]. In [88] the authors proposed unitary space-time modulation for avoiding the need for CSI estimation at the receiver. This scheme was shown to work well for long coherence time intervals or for high SNR. Here we focus our attention on the energy-efficiency potential of increasing the number of antennas and we will seek solutions that work at low SNRs. Other works with DUSTM can be found in [91, 92].

Other alternatives for non coherent MIMO communication were codebooks of unitary matrices isotropically distributed on the compact Grassmannian manifold [93, 94]. These schemes were designed in particular for block-fading channels. The codebooks exploit the MIMO channels characteristics, considering orthogonal subspaces which distinguish the transmitted symbols at the non coherent receiver. The design of Grassmannian Constellations (GC) was becoming important, although so far from a theoretical point of view [94]. There exist many designs of GC, some of them systematic [95] and others non-systematic [94]. Regarding the decoding of GC, these constellations cannot exploit MSDD due to their non-differential construction. Nevertheless, GC can be non-coherently

decoded using generalized likelihood ratio test (GLRT) receivers. The GC works well for frequency flat MIMO channel and for high SNR. On the contrary, in the DUSTM schemes, GC is specifically designed for single user MIMO system.

1.4.4 Non Coherent Massive MIMO

After years of research on MU-MIMO technology, its new version called *massive MIMO* is being considered as a key technology for 5G and beyond. The above-mentioned issues are emphasized with m-MIMO. Again, the non coherent techniques emerge to circumvent the drawbacks of MIMO, now aggravated by large number of antennas. We propose four groups or categories, as shown in Figure 1.3, in order to classify the designs proposed in the literature for NC-m-MIMO as well as ongoing research. First, one category pertains to the works developed on the basis of the constellation design. The modulation schemes considered for this group are ASK, hexagonal schemes, QAM, Space-time scheme and DPSK. The second category is based on the channel coding scheme used in conjunction with the NC techniques. Notable in this group are GC coding, random coding which goes typically hand in hand with ASK constellation and the last, Bit-Interleaved Coded Modulation (BICM) and iterative decoding (ID), proposed with DPSK, QAM and space-time constellations. However, not all of them for m-MIMO. The third and fourth group are related to the detection procedure, which is divided from the point of view of signal processing or from size of time window used in the differential detection. The signal processing is classified in envelope detector, energy-based detector and phase-based detector. The first one has been inherited from the beginning of NC schemes in SISO system, however it was more used in FSK which is not proposed for m-MIMO. The energy-based detector is the most popular because of its simplicity, but its performance is not so good against differential phase detection. Therefore, in this work we focus on phase-based detector.

In 2013, A. Schenk *et.al* presented the first proposal on non coherent detection for m-MIMO systems [96]. The scheme was based on a Differential Quaternary Phase Shift Keying (DQPSK) system with a particular channel that resembles an Impulse Radio-Ultra Wide Band (IR-UWB) system, where the users can be spatially separated based on their non-overlapping power-space profiles. However this channel model cannot be exploited in general.

The rest of studies on NC-m-MIMO are based on energy detection. The model based on amplitude shift keying (ASK) is the most commonly used so far for the energy-based detection schemes. The main reason behind this is which ASK is a simple scheme regarding complexity in the receiver for m-MIMO, albeit its performance is not so good regarding to the number of antennas compared to its differential phase counterparts, as proposed

Figure 1.3 Classification for analyzing non coherent m-MIMO schemes proposed in the literature.

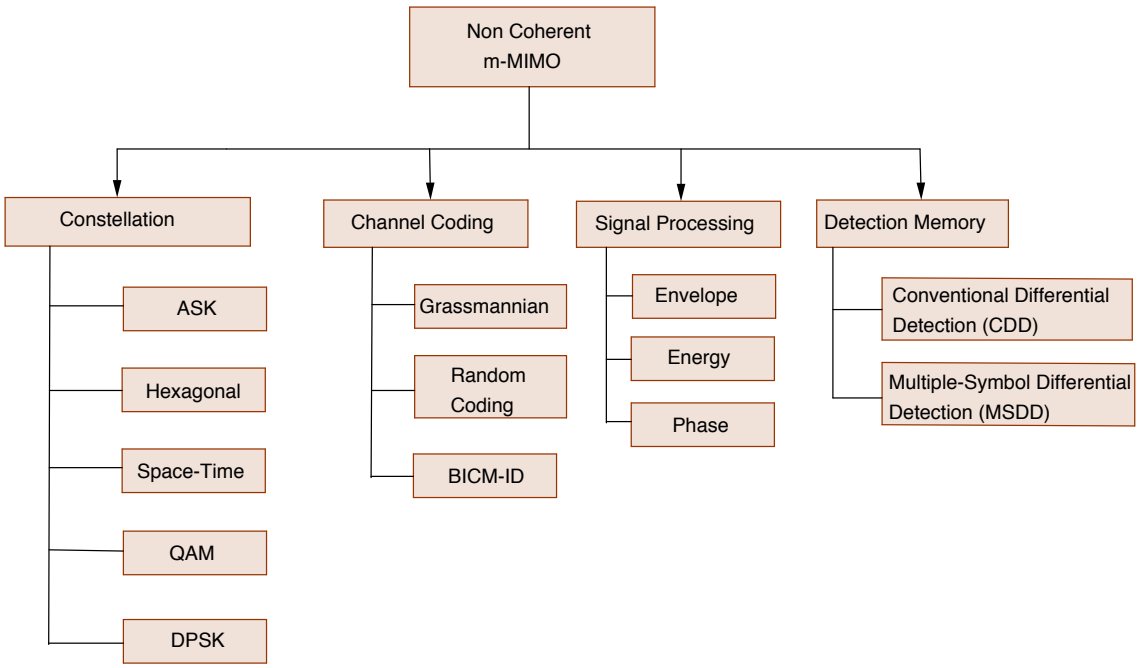

in this Thesis. Although the ASK constellations do not make differential encoding, they do use NC techniques for detection.

A. Goldsmith and her research group have presented several works in this area [97–99]. In [97] was shown that in terms of the scaling law of achievable rates, the performance of the proposed NC system is no different from that achievable under the idealized simplifying assumption of having perfect CSI at the transmitters and the receiver. A comparison between coherent and NC detection for massive single input multiple output (m-SIMO) and single-user systems was presented in [98] which emphasizes that NC schemes can outperform coherent schemes. The constellation designs for energy-based schemes are shown in [99], specifically, based on NC-ASK modulation technique.

On the other hand, in [100] other design which uses the energy of the signal received was shown. Another recent design used for NC SIMO is focused on hexagonal uniquely factorable constellation [101], not developed for m-MIMO though. Thus, the superposition principle used by this is the precursor for the designs in this work, which we scale up for m-MIMO. In [102], a preliminary design is presented for a differential QAM (DQAM) scheme. Both hexagonal and QAM constellations present best performance compared to DPSK schemes, however they are more complex to detect them. In addition, due to the transmission on amplitude too, they have an extra power consumption against DPSK schemes.

Against the energy-based designs, [103] proposes several constellations based on M-ary Differential Phase Shift Keying (MDPSK) that allow us to use differential detection and separate the signals of multiple users merely relying on the knowledge of their received signal powers whilst leveraging the advantages of using an increased number of receive antennas.

However, the greatest disadvantage for all these designs is that they require an excessive number of antennas for a reasonable performance. Therefore, some studies have researched to include channel coding schemes, which drastically improve the system performance, hence reducing the number of antennas required for attaining a given performance. Goldsmith's contributions in [99] has also been extended in [104, 105], for ASK scheme, exploring the impact of random coding for reducing the number of antennas, nevertheless it is still inadequate for practical systems.

Recent works show the utility of GC in BICM systems with Iterative Demodulation and Decoding (IDD) [106] in the future communication systems. However, as abovemention it is not developed for m-MIMO yet.

We have to highlight that these works focused on channels which experience a Rayleigh fading. However, current scenarios such as rural or suburban environments, backhaul wireless systems [107], and even new D2D communications [34] can have a predominant line-of-sight (LOS) component, consequently , they are better modeled by Rician fading [108, 109]. The same happens when using higher frequencies, looking for wider spectrum availability, such as in millimeter frequency bands [38]. In [110], some performance results for a single-user system were shown for Rician channels, but with high number of antennas still. Hence, the NC m-MIMO proposals have to be extended and analyzed for considering them in Rician channels for multiuser systems. Going back to the first group in Figure 1.3, the ASK model in [99] considers Rician fading in its constellation design, which is built again depending on the statistics of the channel. Here, for ASK, the LOS component does not pose issues for NC detection since there is not differential encoding. However, multiuser m-MIMO creates problems for NC detection where we have Rician propagation as was anticipated in [111]. In this work, we propose solutions for this drawback.

From the point of view the detection memory, the fourth group as shown in Figure 1.3, we divide it into those that perform a differential encoding with the previous symbol and those employ a window of N_S symbols, as shown in Figure 1.4. The first one is referred to as conventional differential detection (CDD). The second one performs the detection procedure over multiple symbols (MSDD) by maximum likelihood (ML) for optimum design. By contrast, for sub optimum designs we can use decision-feedback differential detection (DFDD) criteria.

Figure 1.4 Classification for multiple-symbol differential detection.

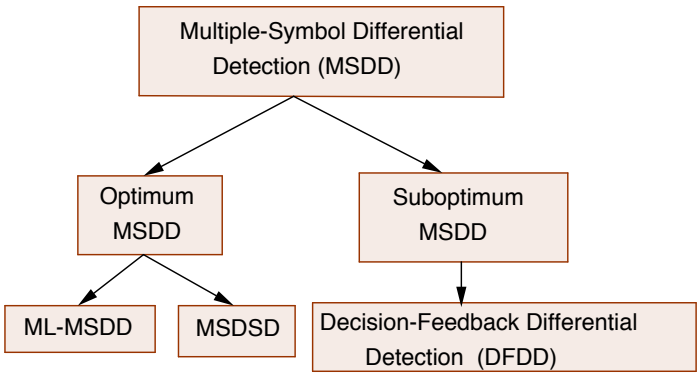

1.4.5 Capacity of Non Coherent Massive MIMO

A benchmark parameter for designing any communication system is the capacity of the system. As mentioned in Section 1.3, with MIMO the higher number of antennas the higher capacity. Hence, since in m-MIMO this number is extremely large we can achieve increasing hugely the capacity.

For the same number of transition and reception antennas, the NC capacity is less than its coherent counterpart. Thus, the NC channel requires a larger bandwidth in order to achieve the same throughput as the coherent channel. However, in the limit of infinite bandwidth, Zheng and Tse [3] show that the capacities per degree of freedom for the coherent and non-coherent MIMO channels are the same.

The capacity of NC MIMO channels for uncorrelated Rayleigh fading was shown in [112] when there is only an average power constraint on the input signal as

$$C_{NC\ MIMO} = \frac{1}{2}\log(\frac{R_r}{2\pi}) + \log(\varepsilon) + \frac{\mathsf{P}}{\varepsilon R_t(1+\frac{\mathsf{P}}{R_t})}, \tag{1.4}$$

where P is the input power, R_t and R_r the number of antennas in the transmitter and receiver, recpectively, and the function ε is

$$\varepsilon = \int_0^\infty \frac{dy}{1+y}\exp\left[-\frac{y}{1+\frac{\mathsf{P}}{R_t}}\right]. \tag{1.5}$$

In addition to the pair (R_t, R_r) and SNR received in each antennas, other works have studied the capacity in terms of coherence length or time (T_c) per degree of freedom [113, 114], proving that the NC channel has a near coherent performance when this is working on the wideband regime, being equivalent to the number of antennas as follows

$$\lim_{SNR\to 0}\frac{C_{coherent}(SNR)}{SNR} = \lim_{SNR\to 0}\frac{C_{NC}(SNR)}{SNR} = R_r, \tag{1.6}$$

then, the capacity can thus be expressed as

$$C(SNR) = R_r SNR + o(SNR)\ nats/channel\ use. \tag{1.7}$$

The term $o(SNR)$ is the sub-lineal term which differences NC capacity from coherent. Also [114] showed that this term is

$$o(SNR) \approx \frac{R_r SNR}{\log(\frac{R_r}{SNR})}. \tag{1.8}$$

A property of the NC capacity is that it tends towards the coherent capacity as the coherence length increases.

For the design based on energy detection, the Goldsmith's studies showed that in terms of the scaling law of achievable symmetric rates for two users, the performance for NC detection is no different from that achievable with perfect CSI at the transmitters and the receiver [97].

However, a general expression for the capacity of the NC-m-MIMO systems has not been proposed yet. Therefore, based on the performance results for NC systems, it offers a great deal of exciting research for NC techniques.

1.5 Motivation, Objectives and Contributions

The explosive usage of rich multimedia content in wireless devices has overloaded the communication networks. As aforementioned, this has resulted in a remarkable spectrum crisis in the overcrowded RF bands. Hence, there is a need for searching alternative techniques with more spectral efficiency to accommodate the needs of emerging wireless communications systems. In this context, m-MIMO systems have been proposed as a promising solution for providing a substantial increase in the attainable network capacity, becoming one of the key enabling technologies for future 5G communication systems and beyond [16–19]. They provide high spectral- and energy-efficiency thanks to the deployment of a large number of antennas at the BS. However, the most research has been focused on designs based on energy detection. These proposals trow high number of antennas and need the knowledge of the channel statistics in the detection procedure, forgetting the existing barriers in the coherent communications. In addition, they are only proposed for single user and Rayleigh channel. Other works such as those proposed in Grassmannian domain are not developed for m-MIMO yet.

Against limitations of the coherent communications for further progress, the initial research of this thesis was focused on modulation designs and signal processing techniques for non coherent massive MIMO systems where the information is transmitted in the signal differential phase, instead of the amplitude like energy-based schemes.

The basis for our NC massive MIMO scheme was proposed at the beginning of the work shown in [103]. From this conference work, which outperformed the benchmarker of the designs based on energy detection, some questions arise such as:

1. *Is there an optimal constellation design?*
2. *How to reduce the number of antennas to a large number but feasible?*
3. *Is this scheme valid for any type of channel fading?*
4. *What is the performance of a NC-m-MIMO-DPSK system in real channels?*
5. *Can a NC-m-MIMO-DPSK system be applied to the new radio access technologies?*
6. *How to increase the number of users?*

The above discussion and all these questions have motivated the work performed in this Ph.D. Thesis whose main goal is marked by designing an attractive, operational and easy-to-adopt solution for multi-users non coherent massive MIMO (MU-NC-m-MIMO) based on DPSK schemes, which comes closest to the performance of the coherent communication systems.

In order to answer the questions posed above the following objectives are raised:

- Design new efficient constellation schemes in multiuser NC-m-MIMO, first for Rayleigh fading channels. Analyze the number of antennas needed for those designs and compare to the required number by other designs in the literature.
- Analyze possible channel coding schemes to reduce the large number of antennas keeping the initial performance for non coherent m-MIMO system and outperforming the energy-based detection schemes.
- Analyze the behavior of the NC-m-MIMO systems when we have a Rician fading for possible emerging scenarios with 5G technology.

The novel contributions of this thesis are as follows:

- Previous contributions in the state of the art are focused on single user systems. Here, we propose multi-user schemes.
- We evaluate different schemes for non coherent massive MIMO based on DPSK. We compare the performance to their coherent counterpart systems and other NC schemes proposed in the literature for Rayleigh fading. The results drawn are published in [115].

- We present a new constellation design to overcome the problem of the LOS channel component in Rician channels, as well as an associated detection algorithm to separate each user in reception taking into account the characterization of the constellation. This research was presented in [116, 117].
- We analyse the performance of multi-user NC m-MIMO based on DPSK in real environments for the current standards such as LTE and the future technologies such as 5G. This analysis was published in [118].
- We study the viability of multiplexing users by constellation schemes against classical multiplexing techniques such as time division multiplexing access (TDMA).

1.6 Organization of this Thesis

After this introduction, the outline of the thesis is presented as follows:

- **Chapter 2** presents a reference system model for Non Coherent Massive MIMO systems based on DPSK schemes as starter. This chapter introduces the system variables to be designed in the next chapters considering different channel fading. The proposed model for Rayleigh channels was presented in [115, 118], and for Rice channels in [116, 117]
- **Chapter 3** presents the proposed constellations for channels with Rayleigh fading. We propose designs based on two approaches. The first one is for unequal performance among users, while the other is relying on obtaining the same performance for all users. In addition, we derivate the total interference power and signal to interference plus noise ratio (SINR) for Rayleigh channels. The proposed schemes are compared to their counterpart in coherent systems. Furthermore, we compare the performance with other constellation designs proposed for m-MIMO in the literature such as ASK, DAPSK or DQAM. The content therein was presented in [115].
- **Chapter 4** presents a powerful channel coding scheme construction based on the principle of bit-interleaved coded modulation and iterative decoding (BICM-ID), which is intrinsically amalgamated with the NC m-MIMO system based on M-ary DPSK. We present a novel analysis using the EXIT chart tool in order to study the effect of the number of antennas on the system performance, demonstrating that the employment of coding considerably reduces the number of receive antennas required. The research comprising this chapter is presented in [115].

- **Chapter 5** analyses the behavior of the NC m-MIMO systems when we have a Rician fading, presenting a new constellation design to overcome the problem of the LOS channel component. Furthermore we develop a decoding algorithm, that taking into account the characteristics of the new constellation and interference, outperforms exiting algorithms for NC detection. In addition, we propose some guidelines to design other constellations for NC massive MIMO systems based on DPSK modulation. The results in this chapter were included in [116, 117].

- **Chapter 6** explores and discusses the practical issues emerged for the NC-m-MIMO systems. On the one hand, it analyses the SINR and the performance in terms of symbol error rate (SER) of DPSK based NC-m-MIMO in heterogeneous propagation conditions. We propose user grouping to effectively combat the effects of the LOS component. We also quantify the advantage of the mixed-propagation in terms of complexity. On the other hand, it extends the analysis of NC-m-MIMO systems to include the impact of time-varying channels on the required number of antennas and maximum achievable rate (MAR). We present a novel metric on the performance which reflects the channel's variability. Furthermore, we illustrate the analysis with the aid of practical channels on LTE, beyond 5G, even for new mmW and THz bands communications. Finally, we study the performance of our proposed system by empirical simulations with OFDM and with emerging techniques such as spatial modulation. The analysis contained in this chapter was published in [118].

- **Chapter 7** analyses the block error rate (BLER) and the throughput to validate the behavior of the proposed multiuser NC-m-MIMO system based on DPSK in a communication network. In addition, we assess the multiplexing of users in constellation against other physical resources such as time, frequency or code.

- **Chapter 8** summarizes the presented work, highlighting the main contributions of this thesis and devises the research lines to be potentially considered as future work.

1.7 Relation with published works

The work developed in this Ph.D. Thesis is relying on, and consequently, partially coincides with the following published contributions:

- **Chapters 3 and 4**:

  V. M. Baeza, A. G. Armada, W. Zhang, M. El-Hajjar and L. Hanzo, "A Noncoherent Multiuser Large-Scale SIMO System Relying on M-Ary DPSK and BICM-ID," in IEEE Transactions on Vehicular Technology, vol. 67, no. 2, pp. 1809-1814, Feb. 2018. doi: 10.1109/TVT.2017.2750114 [115].

V. M. Baeza and A. G. Armada, "Performance and Complexity Tradeoffs of Several Constellations for Non Coherent Massive MIMO" to be published on 2019 IEEE European Conference Networks and Communications, Valencia, Spain, Jun. 2019.

- **Chapters 5**:

  V. Monzon Baeza and A. Garcia-Armada, "Non-Coherent Massive SIMO System based on M-DPSK for Rician Channels," in IEEE Transactions on Vehicular Technology, vol. 1, pp. 1-14, Jan. 2019. doi: 10.1109/TVT.2019.2892390 [117].

  V. M. Baeza and A. G. Armada, "Analysis of the performance of a non-coherent large scale SIMO system based on M-DPSK under Rician fading," 2017 25th European Signal Processing Conference (EUSIPCO), Kos, 2017, pp. 618-622. doi: 10.23919/EUSIPCO.2017.8081281 [116].

- **Chapters 6**:

  V. M. Baeza and A. G. Armada, "User Grouping for Non-Coherent DPSK Massive SIMO with Heterogeneous Propagation Conditions" to be published on 2019 20th IEEE Internatinal Workshop on signal processing advances in wireless communications (SPAWC), Cannes, Jul. 2019.

  V. M. Baeza, A. G. Armada, M. El-Hajjar and L. Hanzo, "Performance of a Non-Coherent Massive SIMO M-DPSK System," 2017 IEEE 86th Vehicular Technology Conference (VTC-Fall), Toronto, 2017, pp. 1-5. doi: 10.1109/VTCFall.2017.8288015 [118].

The thesis is also related to conference publication [103]. We also issued a book chapter as result of the conclusions obtained in this thesis concerning the non coherent massive MIMO techniques:

"Non-Coherent Massive MIMO" in Book "Radio Technologies for 5G". Wiley, 2019. [119]

Chapter 2

System Model for multiuser non coherent m-MIMO based on DPSK

In this chapter we introduce the system model as reference for the rest of the thesis. The different components of this model will be extended and explained in a thorough manner in each chapter, where we show the design in details for each one of them. The model which we use here mainly is based on a system with differential phase modulation and encoding at the transmitter side and non coherent detection in the receiver side. We consider a multi-user massive MIMO uplink scenario, where a single base station (BS) is equipped with R receive antennas (RA) to receive the signals transmitted from J mobile stations (MSs), or users as shown in Figure 2.1.

Figure 2.1 System model for multi-user uplink scenarios in massive MIMO.

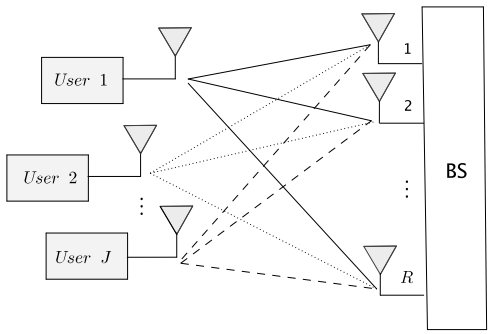

The interest shown in the uplink scenario is due to there being a greater complexity since the users are uncoordinated. This system model could apply to a beyond 5G cellular network where several users are communicating with the BS. It could also represent a wireless backhaul where several BS are transmitting towards a central baseband unit (BBU), or even an evolved WiFi system where several terminals are accessing the access point. In all these scenarios it is likely that the channel follows Rician fading. Therefore, we design and analyse this system and its performance for environments with

Rayleigh fading conditions and then we extend the design to scenarios where there exits Rician fading propagation. In addition, a new possible scenario is forecasted, visible light communications such as LiFi technology where LED transmitters access a receiver with multiple photodetectors.

2.1 Classical DPSK scheme

We start with a brief review of the differential encoding and detection procedure. The coherent systems derive a frequency or phase reference from a carrier synchronization loop, which may introduce a phase ambiguity providing an error detection of the information. As a solution, in a differential phase shift keying (DPSK) scheme the information is encoded using phase differences between successive signal transmission instead of absolute phases. This technique enables the receiver to make reliable data estimations without explicit knowledge of the channel information. As it was explained in the Introduction chapter, this is an advantage for m-MIMO systems..

The differential signaling process begins transmitting a single reference symbol $x[0]$, followed by differential recursive encoding, as is illustrated in Figure 2.2 and expressed as follows

$$x[n] = s[n]x[n-1],\ n > 1, \tag{2.1}$$

where the information sequence $s[n]$ is now carried by phase difference. D represents the delay between the sample in the current and previous time instants. Typically $D = 1$ which is is equivalent to encoding only with the previous symbol.

Figure 2.2 A classical DPSK modulation scheme.

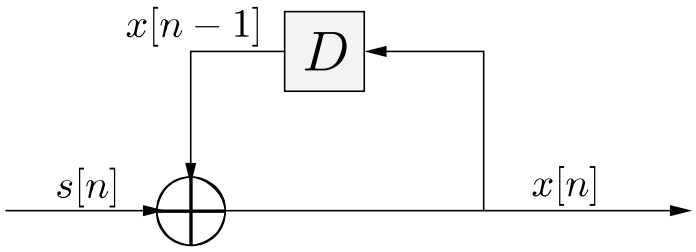

The receiver can effectively recover the symbols $s[n]$ using the received symbols during the n^{th} and $(n-1)^{th}$ time slots, respectively, represented as

$$y[n-1] = h[n-1]x[n-1] + \nu[n-1], \tag{2.2}$$

$$y[n] = h[n]x[n] + \nu[n], \tag{2.3}$$

where ν is the additive white Gaussian noise (AWGN). Assuming a slow-fading channel, meaning $h[n-1] = h[n]$, then by using (2.1) in (2.3), the received symbol is as follows

$$\begin{aligned} y[n] &= h[n-1]x[n-1]s[n] + \nu[n], \\ y[n] &= y[n-1]s[n] + \underbrace{\nu[n] - \nu[n-1]s[n]}_{\nu'}. \end{aligned} \tag{2.4}$$

This way, as (2.4) the differentially encoded data $s[n]$ can be recovered multiplying the received symbol in the time instant n by the conjugated received symbol in $n-1$, this is $y[n]y^*[n-1]$, as shown in Figure 2.3.

Figure 2.3 A classical DPSK demodulation scheme.

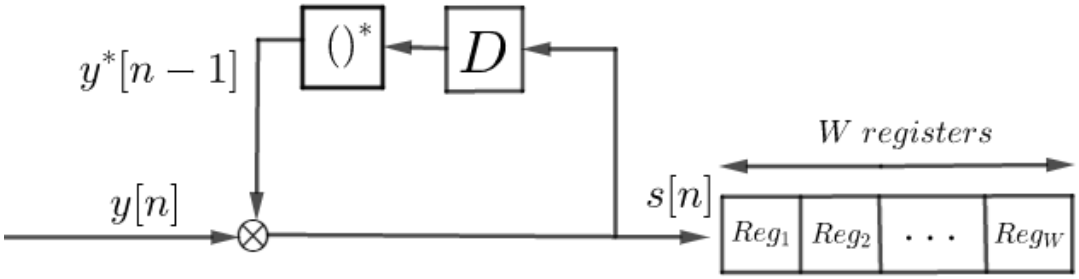

When in the receiver the decision is based on only one symbol we have a conventional differential detection (CDD), while if we wait W symbols to decide, this is referred as multiple symbol differential detection (MSDD). Remember the classification in Figure 1.4 presented in Section 1.3.

Comparing to coherent, here we do not need CSI in the receiver side at the cost of a 3 dB performance loss in comparison with its coherent counterpart provided by the doubled noise (ν') in the decision process (2.4). Secondly, due to the time varying nature of the channel, also DPSK scheme presents other performance limitation, an error floor associated with CDD in fast fading channels. All these issues will be minimized in m-MIMO as we demonstrate throughout this thesis.

2.2 Transmitter

In the transmitter shown in Figure 2.4 we can see the next procedure: an user j transmits a block of bits $\mathbf{b}_j$ which are encoded by a channel encoder based on the principle of bit-interleaved coded modulation (BICM). This module will be expanded in details in Chapter 4. After bit encoding, the bits $\mathbf{b}_j$ are grouped in sets of p bits, $\{b_1^j, b_2^j, ..., b_p^j\}$, in order to be mapped to symbols $s_j[n]$. These symbols are independent of each other, unit

Figure 2.4 Transmitter system model for NC-m-MIMO based on DPSK.

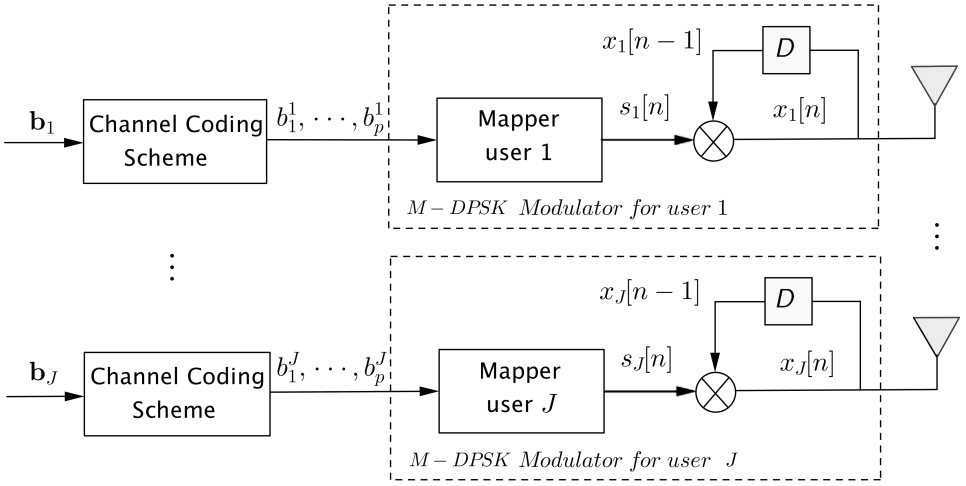

symbols ($|s_{m,j}[n]| = 1$) and belong to an M-ary PSK constellation, $\mathfrak{M}_j = \{s_{m,j},\ m = 0, 1, ...,\ M-1\}$ where M is the order of the constellation defined as $M = 2^p$. We refer to the user constellations as individual constellations since it may in fact be different for each user, as we will demonstrate in the next chapters where it will be designed depending on the channel fading conditions. Considering a Rayleigh fading we design the constellation for NC m-MIMO in Chapter 3, whilst for Rice fading the constellation scheme will be designed in Chapter 5. The mapping scheme is jointly designed with the encoder to optimize the number of antennas needed in our m-MIMO system, this is explained in Chapter 4.

Once the symbols are mapped, each user j transmits a signal $x_j[n]$ at time instant n, which is a differentially encoded version of $s_j[n]$ following the DPSK model presented in Section 2.1 as

$$x_j[n] = s_j[n]x_j[n-1],\ n > 1. \tag{2.5}$$

In order to carry out the non coherent detection in the receiver side, the $x_j[0]$ is a first symbol known at the transmitter and receiver which is taken from the individual user constellation $\mathfrak{M}_j$.

2.3 Channel Model

We present the channel model for two cases. First, the model used in general for analyzing and designing our NC m-MIMO proposals. Second, we will analyze the proposed schemes for practical channels, hence we show the characteristics and parameters imposed by realistic channels.

2.3.1 MIMO channel

The propagation channel is represented by the $(R \times J)$-element channel matrix $\widetilde{\mathbf{H}}$ with the components $h_{r,j}$ modeling the propagation from user j to the r-th antenna of the BS, as is shown in Figure 2.5. The coefficients $h_{r,j} \sim CN(0,1)$ are circularly symmetric complex Gaussian random variables that account for Rayleigh fading with zero mean and variance $\sigma_h^2 = 1$ (Rayleigh case).

Figure 2.5 Channel model for m-MIMO.

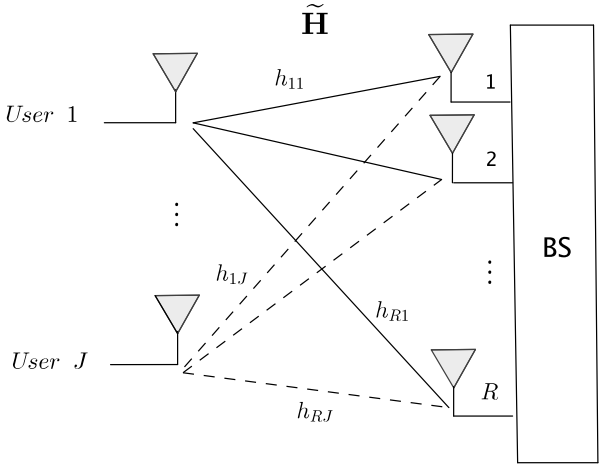

In the case, we extend the system model to support Rician propagation conditions, the channel matrix is modeled as $\widetilde{\mathbf{H}} = \mathbf{H} + \mu$, whose components $\widetilde{h_{rj}}$ represent the propagation from the user j-th to the r-th antenna of the BS. These elements $\widetilde{h}_{rj} = h_{rj} + \mu$, where $h_{rj} \sim CN(0, \sigma_h^2)$. Hence, we have extracted the mean of the channel μ to remark the effect of the LOS channel component in the expressions.

We assume that the statistics of the channel are defined as follows

$$\mu^2 = \frac{K}{K+1} \tag{2.6}$$

and

$$\sigma_h^2 = \frac{1}{K+1}, \tag{2.7}$$

being μ and σ_h^2 the mean and variance respectively, and where K is the Rician factor ($K > 0$), which characterizes the fading model [120]. This factor characterizes a propagation with LOS between the BS and the user. Note that when K=0 we have a Rayleigh channel in which there is no dominant propagation along the LOS and in this case, we can use interchangeably the channel matrix $\widetilde{\mathbf{H}} = \mathbf{H}$. For simplicity of the presentation, we assume that all the channels experience Rician fading with the same K-factor, unless otherwise stated.

Regarding channel coefficients, in order to make possible a non coherent detection, we assume that $h_{rj}[n-1] = h_{rj}[n] = h_{rj}$, with $r = 1, ..., R$ and $j = 1, ..., J$, meaning that the

channel stays time-invariant for two consecutive symbols. In a real scenario there will be a small variation between these two channels, this is just an assumption for the analysis. In Chapter 6 we analyse the effect of this assumption and show that our scheme is very robust to the channel variability that is likely to happen in realistic scenarios.

The effects of large-scale fading are taken into account with an additional power term. Explicitly, the signals of the different users may be received at a different average power, either because they are allowed to use a different transmit power or because their path loss is not compensated by power control. Without loss of generality we will assume that the signal of user one is received with unit power and the others have a relative gain of α_j with respect to user one.

2.3.2 Channel for practical scenarios

A typical fading channel has a time-variant impulse response, characterized by the Doppler shift which characterizes the speed of variation of the channel. The Doppler shift (f_D) is defined in [43] as

$$f_D = f_c \frac{v}{c} \cos\gamma \tag{2.8}$$

where f_c is the carrier frequency which is shifted to f_D when the transmitter is moving with a speed v. c is the light speed and γ is the angle between the direction of propagation of the electromagnetic wave and the direction of the motion. An alternative to measure the channel variability is the coherence time T_c of the channel, which is related in [121] to f_D as

$$T_c = \frac{1}{16\pi f_D}. \tag{2.9}$$

So far, this parameter in (2.9) is which we have considered large enough so that the channel does not vary when making NC detection.

In order to study the behavior of the system in time-varying channels, we normalize the signal's bandwidth (BW) by f_D to define a metric that relates both parameters as follows

$$\beta = \frac{BW}{f_D}. \tag{2.10}$$

The advantage of using this metric is that it allows us to characterize the system independently of the physical system parameters such as the carrier frequency (f_c), bandwidth or Doppler effect. Thus, it is a beneficial metric for designing new systems for practical time-variant wireless channels.

We may interpret β-value as follows: for high values of β the channel experiences low time variability, whilst lower values can be seen as high f_D which lead to low coherence time in (2.9), therefore high time variability. As increasing β, the time variability is negligible, hence we can consider that the channel is time-invariant, so-called here *constant*

channel condition. In this situation, the channel is static in the transmission of a large symbol burst and changes randomly between them. Therefore, another important parameter here is the length of the transmission frame, defined as the number of the symbols transmitted. We must bear in mind the longer the frame is, the higher time variability of the channel is in the signal duration.

In order to simulate the temporal correlation imposed by time variability of the channel in the coefficients h_{rj}, we generate these coefficients following the procedure shown in Figure 2.6. First, we generate complex white Gaussian random variables in the frequency domain for two branches, one for a real part and the other for an imaginary part. Then, low-pass Doppler filters characterized by a bandwidth of f_D and an inverse fast Fourier transform (IFFT) which transforms the signal into the time-domain, are applied. Since the output of the IFFT block must be a real signal, its input must be always conjugate symmetric. Then, we can build a complex channel gain using the first branch as real part and the second one as imaginary part, and adding both. This way, a channel with Rayleigh distributed-magnitude is generated.

Figure 2.6 Schematic for generation channel filter.

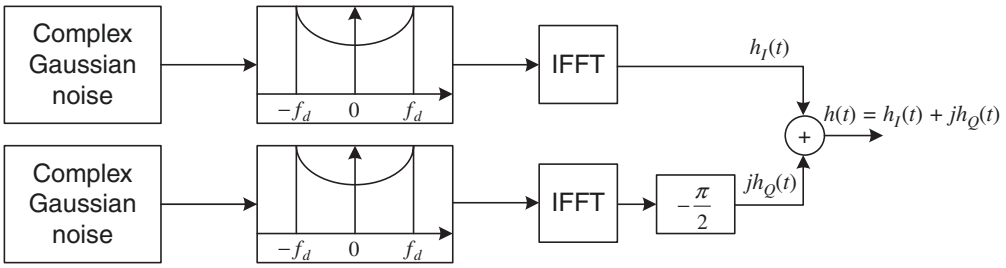

The model illustrated in Figure 2.6 and explained above is known as Clarke-Gans model, which has been designed under the assumption that scattering components around a mobile station are uniformly distributed with an equal power for each component [122]. This model can be applied both for conventional frequencies and also for mmWave or THz frequencies [38].

2.4 Receiver

In this section, we explain the model for the received signal which influences on each module designed of our NC-m-MIMO receiver shown in Figure 2.7. In addition, the joint constellation concept is illustrated in this section since in the next chapters, the individual constellations are designed for different scenarios keeping in mind the joint constellation. The *Joint Demapper* and *Channel Decoding Scheme* blocks will be explained in details in Chapter 4.

Figure 2.7 Receiver system model for a NC-m-MIMO system based on DPSK.

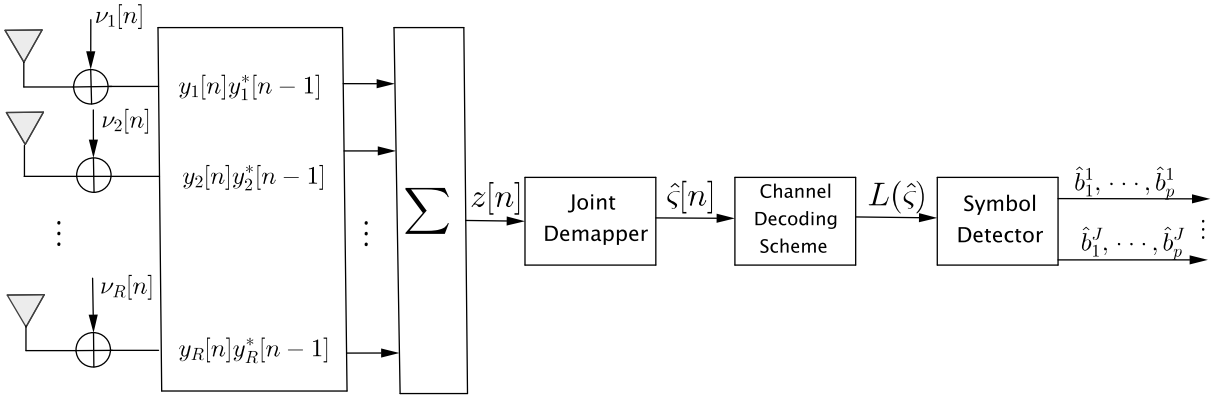

2.4.1 Received signal

In each of the BS antennas at time instant n is received the signal in (2.3) and all the signals from all antennas are grouped in the $(R \times 1)$-element vector $\mathbf{y}[n]$. Then, $\mathbf{y}[n]$ is obtained as follows

$$\mathbf{y} = \widetilde{\mathbf{H}}\boldsymbol{\alpha}\mathbf{x} + \nu, \tag{2.11}$$

where we will remove the time dependency n to facilitate the notation. The AWGN is represented by the $(R \times 1)$-element vector, where the AWGN in the antenna r is $\nu_r[n] \sim CN(0, \sigma^2)$. The diagonal matrix $\boldsymbol{\alpha}$= $diag\{\sqrt{\alpha_j}\}$ contains the power terms associated with the transmission of the different user $j = 1, \cdots, J$, being $\alpha_1 = 1$ and $\alpha_j \geq 1$ for $j \neq 1$.

The power of the signal received at each antenna is

$$E\{||\widetilde{\mathbf{H}}\mathbf{x}||^2\} = \sum_{j=1}^{J} \alpha_j |s_j|^2 (\sigma_h^2 + \mu^2) = \sum_{j=1}^{J} \alpha_j, \tag{2.12}$$

as $|s_j|^2 = 1$ and $(\sigma_h^2 + \mu^2) = 1$. Then we define the reference SNR as

$$\rho = \frac{E\{||\widetilde{\mathbf{H}}x||^2\}}{\sigma^2} = \frac{\sum_{j=1}^{J} \alpha_j}{\sigma^2}. \tag{2.13}$$

When all users are received with the same power, the reference SNR ρ depends on the number of users as

$$\rho = \frac{J}{\sigma^2}. \tag{2.14}$$

In the case we include a channel coding scheme, for the sake of performing a fair comparison of the schemes with different channel coding rate η, we also define the ratio of bit energy to noise spectral density E_b/N_0 as

$$\frac{E_b}{N_0} = \frac{\rho}{\eta} = \left.\frac{\sum_{j=1}^{J} \alpha_j}{\eta\sigma^2}\right|_{\alpha_j=1,\forall j} = \frac{J}{\eta\sigma^2}. \tag{2.15}$$

Most of the proposed designs in this thesis are for the same power lever for all users.

As shown in Figure 2.7, the phase difference is non-coherently detected for two consecutive symbols received at each antenna. The resulting received symbol is the decision variable $z[n]$ defined as follows

$$z[n] = \frac{1}{R}\sum_{r=1}^{R} y_r[n]y_r^*[n-1], \tag{2.16}$$

that contains information and interference gleaned from all antennas and users. This variable will be analyzed for each fading conditions in the next chapters which establish criteria and procedures for the constellation designs.

In general, taking into account $(\sigma_h^2 + \mu^2) = 1$ by channel definition in (2.6), (2.7) and according to the law of Large Numbers [41], we approximate the decision variable $z[n]$ as R goes to infinity as follows

$$z[n] \overset{R\to\infty}{=} \sum_{j=1}^{J} \alpha_j s_j[n] + \ interfering\ terms \tag{2.17}$$

where we define the joint symbol as

$$\varsigma[n] = \sum_{j=1}^{J} \alpha_j s_j[n] \tag{2.18}$$

which shapes the joint constellation in the receiver side. This constellation $\mathcal{M} = \{\varsigma_k, k = 0, ..., \mathfrak{K}\}$ of cardinality $\mathfrak{K} = M^J$ is obtained from adding combinations of the individual constellation points of all $\mathfrak{M}_j$ as

$$\mathcal{M} = \{\alpha_1 s^1_{m^{(1)}} + \alpha_2 s^2_{m^{(2)}} + ... + \alpha_J s^J_{m^{(j)}}, \quad m^{(j)} = 0, 1, ..., M-1\}. \tag{2.19}$$

In Chapter 3 we will show more details on criteria to design the constellations for the Rayleigh fading case, and in Chapter 5 for the case with Rice fading. Then, as R grows bigger, we have that (2.17) can be reformulated as

$$z[n] \overset{R\to\infty}{=} \varsigma[n] + \ interfering\ terms. \tag{2.20}$$

More explicitly, the superimposed transmitted constellation $\mathcal{M}$, obtained from all legitimate combinations of the constellation points of $\mathfrak{M}_j$, should have M^J uniquely distinguishable points. As long as this is accomplished, the individual users' encoded data symbols $s_j[n]$ can be directly obtained from the detected joint symbols $\hat{\varsigma}[n]$ by demapping in the joint constellation.

In the case of a system with channel coding scheme, the detected joint symbols are fed through a decoder to achieve soft information $L(\varsigma)$ due to the iterative decoding process, as we will explain in Chapter 4. Then, from these values we obtain the estimated p bits for user j, $\hat{b_1^j}, \cdots, \hat{b_p^j}$.

2.4.2 Example of joint constellation construction

As an example in order to build the joint constellation from the individual user constellations, we present a system for two users ($J = 2$), where the symbols $s[n]$ transmitted by user 1 belong to the constellation $\mathfrak{M}_1$ which is a classical binary phase shift keying (BPSK), $M = 2$. The second user transmits symbols that belong to $\mathfrak{M}_2$, a different BPSK as follows:

$$\begin{cases} user\ 1 : \mathfrak{M}_1 = \{s_1^1, s_2^1\} \in BPSK_1 \\ user\ 2 : \mathfrak{M}_2 = \{s_1^2, s_2^2\} \in BPSK_2. \end{cases} \tag{2.21}$$

Then, the general joint constellation is the result of combining all user 1's symbols with the user 2 ones as (2.19)

$$\varsigma \in \mathcal{M} = \{s_1^1 + s_1^2; s_1^1 + s_2^2; s_2^1 + s_1^2; s_2^1 + s_2^2\}. \tag{2.22}$$

Considering the BPSK, the values for joint symbol ς are summarized in Table 2.1 for $\alpha_j = 1$. These values are represented in Figure 2.8. The labelling for ς is by concatenation

Table 2.1: Information for composition of the joint constellation for two users transmitting with BPSK..

User 1			**User 2**			**Joint Symbol**		
Binary Mapping	**Symbols**	**Labelling**	**Binary Mapping**	**Symbols**	**Labelling**	**Binary Mapping**	**Symbol**	**Labelling**
0	$s_1^1 = 1$	A	0	$s_1^2 = j$	C	[0 0]	$\varsigma_1 = 1 + j$	AC
0	$s_1^1 = 1$	A	1	$s_2^2 = -j$	D	[0 1]	$\varsigma_2 = 1 - j$	AD
1	$s_2^1 = -1$	B	0	$s_1^2 = j$	C	[1 0]	$\varsigma_3 = -1 + j$	BC
1	$s_2^1 = -1$	B	1	$s_2^2 = -j$	D	[1 1]	$\varsigma_4 = -1 - j$	BD

of individual symbols, as it can be seen in Table 2.1. As we can see in (2.22), we have $M^J = 4$ points which must be uniquely distinguishable to detect each user separately thanks to the one-to-one relationship between (2.21) and (2.22).

Figure 2.8 Example of joint constellation composition for $J = 2$ users transmitting with BPSK.

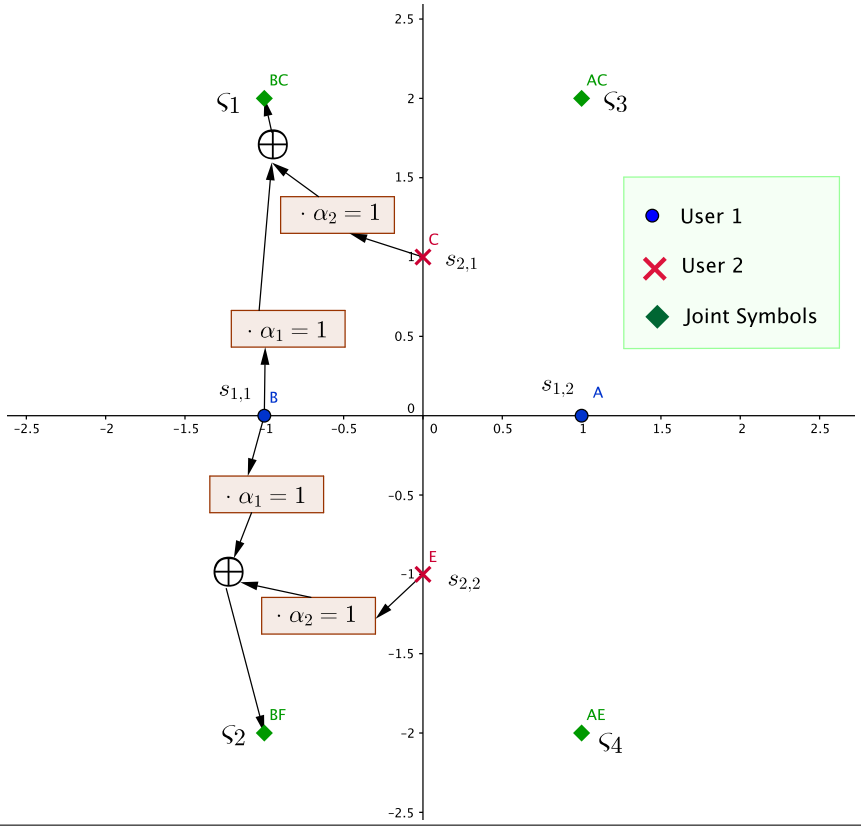

Chapter 3

New Constellation Schemes based on DPSK for Rayleigh Channels

In the previous chapter, we focused on the system model to know how the received signal is able to detect all users from a joint constellation. In order to separate the users' signals at the BS, the constellations $\mathfrak{M}_j$ must be specifically designed so that their symbols can still be uniquely and unambiguously distinguished upon superimposing the transmitted signals from all users, which have formed the joint constellation $\mathcal{M}$.

In this chapter, we propose several constellation designs based on two approaches to separate the users. On the one hand, we design the constellation discerning between schemes with different performance level among users called *unequal error protection* (UEP) scheme and a new design to achieve the same performance for all users, named *Equal Error Protection* (EEP) scheme. On the other hand, we consider different power levels for each user in each design. Moreover, it must be highlighted that in this chapter the encoding scheme is not considered.

This chapter begins by discussing the full developing of the decision variable $z[n]$ defined in the previous chapter for propagation in Rayleigh channels. This analysis is the framework for the design requirements of the constellation which will be all proposed in this chapter are developed for a Rayleigh fading conditions. We continue analyzing the SINR, likewise for Rayleigh channels. Then, we derivate some bounds for the error probability in order to validate the performance of our designs. On this bases, we present seven different constellation designs and we compare them to the previous non coherent proposals in the literature. In addition, we present a comparative study with its coherent counterparts.

3.1 Non coherent design for constellation schemes in channels with Rayleigh fading

We consider the decision variable $z[n]$ defined in (2.16). In this case, we assume a channel matrix $\mathbf{H}$ with Rayleigh fading according to the model explained in Chapter 2. Then, we develop the terms in (2.16) as follows:

$$\begin{aligned} z[n] = & \frac{1}{R}\sum_{j=1}^{J}\sum_{r=1}^{R}|h_{rj}|^2\alpha_j s_j[n] + \frac{1}{R}\sum_{j=1}^{J}\sum_{\substack{k=1\\k\neq j}}^{J}\sum_{r=1}^{R}h_{rj}h_{rk}^*\sqrt{\alpha_j\alpha_k}x_j[n]x_k^*[n-1]+ \\ & + \frac{1}{R}\sum_{r=1}^{R}\nu_r^*[n-1]\sum_{j=1}^{J}h_{rj}\sqrt{\alpha_j}x_j[n] + \frac{1}{R}\sum_{r=1}^{R}\nu_r[n]\sum_{j=1}^{J}h_{rj}^*\sqrt{\alpha_j}x_j^*[n-1] \\ & + \frac{1}{R}\sum_{r=1}^{R}\nu_r^*[n-1]\nu_r[n]. \end{aligned} \tag{3.1}$$

From the Law of Large Numbers we know almost surely that [41]

$$\frac{1}{R}\sum_{i=1}^{R}|h_{ij}|^2 \overset{R\to\infty}{=} 1. \tag{3.2}$$

$$\frac{1}{R}\sum_{r=1}^{R}\sum_{j=1}^{J}\sum_{\substack{k=1\\k\neq j}}^{J}h_{rj}h_{rk}^*\sqrt{\alpha_j\alpha_k}x_j[n]x_k^*[n-1] \overset{R\to\infty}{=} 0, \tag{3.3}$$

$$\frac{1}{R}\sum_{r=1}^{R}\nu_r[n]\sum_{j=1}^{J}h_{rj}^*\sqrt{\alpha_j}x_j^*[n-1] \overset{R\to\infty}{=} 0, \tag{3.4}$$

$$\frac{1}{R}\sum_{r=1}^{R}\nu_r^*[n-1]\nu_r[n] \overset{R\to\infty}{=} 0, \tag{3.5}$$

Then, we remember from (2.18) and (2.20)

$$z[n] \overset{R\to\infty}{=} \varsigma[n] + i[n], \tag{3.6}$$

where $i[n]$ are the noise terms and the interference imposed by all the antennas and users. Then, we can obtain an estimate of $\varsigma[n]$ from $z[n]$ as

$$\hat{\varsigma}[n] = \arg\min\{|\hat{\varsigma}[n] - z[n]|, \hat{\varsigma}[n] \in \mathcal{M}\}. \tag{3.7}$$

Once we have the joint symbol $\hat{\varsigma}$, we can obtain an estimate of $s_j[n]$ for user j as[1]

$$\hat{s_j}[n] = \arg\min\{|\sum_{j=1}^{J} \alpha_j \hat{s_j}[n] - z[n]|, \hat{s_j}[n] \in \mathfrak{M}_j\}. \tag{3.8}$$

3.2 Analysis of Signal to Interference plus Noise Ratio for Rayleigh fading

The Signal to Interference plus Noise Ratio (SINR) is defined as the ratio of the signal power to the power of AWGN noise plus interference created by the detection process. When detecting $\hat{\varsigma}[n]$ from $z[n]$, the interference plus noise arises from the noise terms in (3.6) and from equality in (3.2)-(3.5) not being met due to a finite value of R. Hence the interference plus noise term $i[n]$ is shown in (3.9).

$$i[n] = \varsigma[n] - z[n] = \underbrace{\sum_{j=1}^{J}[\alpha_j s_j[n](1 - \frac{1}{R}\sum_{r=1}^{R}|h_{rj}|^2)] - \frac{1}{R}\sum_{j=1}^{J}\sum_{\substack{k=1 \\ k\neq j}}^{J}\sum_{r=1}^{R} h_{rj}h_{rk}^{*}\sqrt{\alpha_j\alpha_k}x_j[n]x_k^{*}[n-1]}_{i_1[n]}$$
$$\underbrace{-(\frac{1}{R}\sum_{r=1}^{R}\nu_r^{*}[n-1]\sum_{j=1}^{J}h_{rj}\sqrt{\alpha_j}x_j[n] + \frac{1}{R}\sum_{r=1}^{R}\nu_r[n]\sum_{j=1}^{J}h_{rj}^{*}\sqrt{\alpha_j}x_j^{*}[n-1]}_{i_2[n]} \underbrace{+\frac{1}{R}\sum_{r=1}^{R}\nu_r^{*}[n-1]\nu_r[n])}_{i_3[n]} \tag{3.9}$$

where the term $i[n]$ is separated in sub-terms $i_1[n]$, $i_2[n]$ and $i_3[n]$ for the convenience of analysis. The interference power for any terms in (3.9) is defined as $I_x = E\{|i_x[n]|^2\}$, while the total interference power is derivate as follows

$$\mathfrak{I} = \sum_{x=1}^{3} I_x = I_1 + I_2 + I_3. \tag{3.10}$$

In order to obtain $\mathfrak{I}$, first we demonstrate that all interference terms in (3.9) are independent and, thus, can be linearly added in (3.10).

We started to calculate the power for the first term, I_1. Since $E\{x_k^{*}[n-1]x_j[n]\} = 0$

[1] In this chapter we do not use the channel coding scheme.

for $j \neq k$, we have

$$\begin{aligned} I_1 =& E\left\{\left|\sum_{j=1}^{J}\alpha_j s_j[n](1-\frac{1}{R}\sum_{r=1}^{R}|h_{rj}|^2)-\frac{1}{R}\sum_{j\neq k}^{J}\sum_{r=1}^{R}h_{rj}h_{rk}^*\sqrt{\alpha_j\alpha_k}x_j[n]x_k^*[n-1]\right|^2\right\} \\ =& E\left\{\left|\sum_{j=1}^{J}\alpha_j s_j[n](1-\frac{1}{R}\sum_{r=1}^{R}|h_{rj}|^2)\right|^2\right\}+E\left\{\left|\frac{1}{R}\sum_{j\neq k}^{J}\sum_{r=1}^{R}h_{rj}h_{rk}^*\sqrt{\alpha_j\alpha_k}x_j[n]x_k^*[n-1]\right|^2\right\} \end{aligned} \tag{3.11}$$

and because $E\{\sum_{r=1}^{R}|h_{rj}|^2\}=R$ and $E\{(\sum_{r=1}^{R}|h_{rj}|^2)^2=R(R+1)$ for $h_{rj}\sim CN(0,1)$ [41], we have

$$E\left\{\left|\sum_{j=1}^{J}\alpha_j s_j[n](1-\frac{1}{R}\sum_{r=1}^{R}|h_{rj}|^2)\right|^2\right\}=\frac{1}{R}\left(\sum_{j=1}^{J}\alpha_j\right)^2, \tag{3.12}$$

while

$$E\left\{\left|\frac{1}{R}\sum_{j\neq k}^{J}\sum_{r=1}^{R}h_{rj}h_{rk}^*\sqrt{\alpha_j\alpha_k}x_j[n]x_k^*[n-1]\right|^2\right\}=\frac{2}{R^2}E\left\{\sum_{j\neq k}^{J}\sum_{r=1}^{R}|h_{rj}|^2|h_{rk}|^2\alpha_j\alpha_k\right\}=\frac{2}{R}\sum_{j\neq k}^{J}\alpha_j\alpha_k, \tag{3.13}$$

because

$$E\{h_{rj}h_{rk}^*h_{lj}h_{lk}^*\}=\begin{cases}0, r\neq l\\ 1, r=l\end{cases} \tag{3.14}$$

So, finally

$$I_1=\frac{1}{R}\left(\sum_{j=1}^{J}\alpha_j\right)^2. \tag{3.15}$$

For I_2, since $E\{v_r^*[n-1]v_r[n]\}=0$, $v_r[n]\sim CN(0,\sigma^2)$ and $h_{rj}\sim CN(0,1)$, we have

$$\begin{aligned} I_2 &= E\left\{\left|\frac{1}{R}\sum_{r=1}^{R}\nu_r^*[n-1]\sum_{j=1}^{J}h_{rj}\sqrt{\alpha_j}x_j[n]+\frac{1}{R}\sum_{r=1}^{R}\nu_r[n]\sum_{j=1}^{J}h_{rj}^*\sqrt{\alpha_j}x_j^*[n-1]\right|^2\right\} \\ &= \frac{2}{R^2}E\left\{\left|\sum_{r=1}^{R}\nu_r^*[n-1]\sum_{j=1}^{J}h_{rj}\sqrt{\alpha_j}x_j[n]\right|^2\right\} \end{aligned} \tag{3.16}$$

and because $E\{|h_{rj}|^2\}=1$ and $E\{|x_j[n]|^2\}=1$, we have

$$I_2=\frac{2\sigma^2}{R}\sum_{j=1}^{J}\alpha_j. \tag{3.17}$$

For I_3, since $v_r[n-1]\sim CN(0,\sigma^2)$ and $v_r[n]\sim CN(0,\sigma^2)$ are independent each other, we can derivate the third sub-term as follows

$$\begin{aligned} I_3 &= E\left\{\left|\frac{1}{R}\sum_{r=1}^{R}\nu_r^*[n-1]\nu_r[n]\right|^2\right\} \\ &= \frac{1}{R^2}\sum_{r=1}^{R}E|v_r^*[n-1]|^2E|v_r[n]|^2=\frac{1}{R}\sigma^4. \end{aligned} \tag{3.18}$$

Also, we have to demonstrate that the interference plus noise components are independent and uncorrelated. To this end, they have to fulfill

$$\begin{aligned} Cov(i_1, i_2) = E\{i_1[n]i_2[n]\} - E\{i_1[n]E\{i_2[n\} = 0 \\ E\{i_1[n]i_2[n]\} = E\{i_1[n]E\{i_2[n\} \end{aligned} \tag{3.19}$$

$$\begin{aligned} Cov(i_1, i_3) = E\{i_1[n]i_3[n]\} - E\{i_1[n]E\{i_3[n\} = 0 \\ E\{i_1[n]i_3[n]\} = E\{i_1[n]E\{i_3[n\} \end{aligned} \tag{3.20}$$

$$\begin{aligned} Cov(i_2, i_3) = E\{i_2[n]i_3[n]\} - E\{i_2[n]E\{i_3[n\} = 0 \\ E\{i_2[n]i_3[n]\} = E\{i_2[n]E\{i_3[n\} \end{aligned} \tag{3.21}$$

where $Cov(x, y)$ is the covariance between the random variables x and y. We assume that the power for all user is unitary, that means $\alpha_j = 1\ \forall j$, since it does not influence in the expectation.

First, let us obtain the expectation for each term $i_x[n]$ in (3.9).

$$\begin{aligned} E\{i_1[n]\} &= E\{\sum_{j=1}^{J}[s_j[n](1 - \frac{1}{R}\sum_{r=1}^{R}|h_{rj}|^2)] - \frac{1}{R}\sum_{j=1}^{J}\sum_{\substack{k=1 \\ k\neq j}}^{J}\sum_{r=1}^{R} h_{rj}h_{rk}^* x_j[n]x_k^*[n-1]\} \\ &= \sum_{j=1}^{J} E\{s_j[n]\} - \frac{1}{R}E\{\sum_{r=1}^{R}|h_{rj}|^2\} - \frac{1}{R}\sum_{j=1}^{J}\sum_{\substack{k=1 \\ k\neq j}}^{J}\sum_{r=1}^{R} E\{h_{rj}h_{rk}^* x_j[n]x_k^*[n-1]\}, \end{aligned} \tag{3.22}$$

where we assume that all constellation points s_j are independent and based on M-DPSK, then $E\{s_j[n]\} = 1$. In the last line in (3.22) we make use of the fact that the channel h_{rj} and the noise v_r are independent and have zero mean, so (3.22) results to be $E\{i_1[n]\} = 0$.

Similarly, we derive the expectation for the second term as follows

$$\begin{aligned} E\{i_2[n]\} =& E\{-\frac{1}{R}\sum_{r=1}^{R}\nu_r^*[n-1]\sum_{j=1}^{J}h_{rj}x_k[n] - \frac{1}{R}\sum_{r=1}^{R}\nu_r[n]\sum_{j=1}^{J}h_{rj}^* x_j^*[n-1]\} \\ =& -\frac{1}{R}\sum_{r=1}^{R}\sum_{j=1}^{J}E\{\nu_r^*[n-1]h_{rj}x_k[n]\} - \frac{1}{R}\sum_{r=1}^{R}\sum_{j=1}^{J}E\{\nu_r[n]h_{rj}^* x_j^*[n-1]\} \\ =& -\frac{1}{R}\sum_{r=1}^{R}\sum_{j=1}^{J}E\{\nu_r^*[n-1]\}E\{h_{rj}x_k[n]\} - \frac{1}{R}\sum_{r=1}^{R}\sum_{j=1}^{J}E\{\nu_r[n]\}E\{h_{rj}^* x_j^*[n-1]\}, \end{aligned} \tag{3.23}$$

by applying the independence between the channel and the noise, we have

$$E\{i_2[n]\} = -\frac{1}{R}\sum_{r=1}^{R}\sum_{j=1}^{J} E\{\nu_r^*[n-1]\}E\{h_{rj}x_j[n]\} - \frac{1}{R}\sum_{r=1}^{R}\sum_{j=1}^{J} E\{\nu_r[n]\}E\{h_{rj}^*x_j^*[n-1]\}, \tag{3.24}$$

so, following the same reasoning, finally $E\{i_2[n]\} = 0$. For the third term, the expectation is

$$\begin{aligned} E\{i_3[n]\} =& E\{-\frac{1}{R}\sum_{r=1}^{R}\nu_r^*[n-1]\sum_{j=1}^{J}h_{rj}x_j[n] - \frac{1}{R}\sum_{r=1}^{R}\nu_r[n]\sum_{j=1}^{J}h_{rj}^*x_j^*[n-1]\} \\ =& -\frac{1}{R}\sum_{r=1}^{R}\sum_{j=1}^{J} E\{\nu_r^*[n-1]\}E\{h_{rj}x_k[n]\} - \frac{1}{R}\sum_{r=1}^{R}\sum_{j=1}^{J} E\{\nu_r[n]\}E\{h_{rj}^*x_j^*[n-1]\}, \end{aligned} \tag{3.25}$$

that results in $E\{i_3[n]\} = 0$.

Once the expectation is derived, the cross expectations of each of the terms have to fulfill

$$E\{i_1[n]i_2[n]\} = 0 \tag{3.26}$$

$$E\{i_1[n]i_3[n]\} = 0 \tag{3.27}$$

$$E\{i_2[n]i_3[n]\} = 0. \tag{3.28}$$

We obtain the cross expectations as

$$\begin{aligned} E\{i_1[n]i_3[n]\} =& -\frac{1}{R}\sum_{j=1}^{J}\sum_{r=1}^{R} E\{s_j[n]\}E\{\nu_r^*[n-1]\}E\{\nu_r[n]\} \\ &+ \frac{1}{R^2}\sum_{j=1}^{J}\sum_{r=1}^{R}\sum_{r=1}^{R} E\{\nu_r^*[n-1]\}E\{\nu_r[n]\}E\{|h_{rj}|^2 s_j[n]\} \\ &+ \frac{1}{R^2}\sum_{j=1}^{J}\sum_{\substack{k=1\\k\neq j}}^{J}\sum_{r=1}^{R}\sum_{r=1}^{R} E\{h_{rj}^*\}E\{h_{rj}\}E\{x_j^*[n-1]x_k[n]\}E\{\nu_r^*[n-1\}E\{\nu_r[n]\} \end{aligned} \tag{3.29}$$

$$
\begin{aligned}
E\{i_1[n]i_2[n]\} =& E\{-\sum_{j=1}^{J} s_j[n]\frac{1}{R}\sum_{r=1}^{R}\nu_r^*[n-1]\sum_{j=1}^{J}h_{rj}x_j[n] - \sum_{j=1}^{J} s_j[n]\frac{1}{R}\sum_{r=1}^{R}\nu_r[n]\sum_{j=1}^{J}h_{rj}^*x_j^*[n-1] \\
&+ \sum_{j=1}^{J}\frac{1}{R}\sum_{r=1}^{R}|h_{rj}|^2\frac{1}{R}\sum_{r=1}^{R}\nu_r^*[n-1]\sum_{j=1}^{J}h_{rj}x_j[n] \\
&+ \sum_{j=1}^{J}\frac{1}{R}\sum_{r=1}^{R}|h_{rj}|^2\frac{1}{R}\sum_{r=1}^{R}\nu_r[n]\sum_{j=1}^{J}h_{rj}^*x_j^*[n-1] \\
&+ \frac{1}{R}\sum_{j=1}^{J}\sum_{\substack{k=1\\k\neq j}}^{J}\sum_{r=1}^{R}h_{rj}^*h_{rj}x_j^*[n-1]x_k[n]\frac{1}{R}\sum_{r=1}^{R}\nu_r^*[n-1]x_k[n]\sum_{j=1}^{J}h_{rj} \\
&+ \frac{1}{R}\sum_{j=1}^{J}\sum_{\substack{k=1\\k\neq j}}^{J}\sum_{r=1}^{R}h_{rj}^*h_{rj}x_j^*[n-1]x_k[n]\frac{1}{R}\sum_{r=1}^{R}\nu_r[n]\sum_{j=1}^{J}h_{rj}^*x_j^*[n-1]\}
\end{aligned}
\tag{3.30}
$$

$$
\begin{aligned}
E\{i_2[n]i_3[n]\} =& \left(\frac{1}{R}\sum_{r=1}^{R}E\{\nu_r^*[n-1]\}\right)^2\sum_{j=1}^{J}E\{h_{rj}\}E\{x_j[n]\}E\{\nu_r[n]\}+ \\
&+\left(\frac{1}{R}\sum_{r=1}^{R}E\{\nu_r[n]\}\right)^2\sum_{j=1}^{J}E\{\nu_r^*[n-1]\}E\{h_{rj}^*\}E\{x_j^*[n-1]\}
\end{aligned}
\tag{3.31}
$$

Due to the independence between the channel and the noise, the cross terms (3.29), (3.30) and (3.31) are zero, therefore the expressions in (3.26), (3.27) and (3.28) are fulfilled. Hence the interference terms $i_1[n]$, $i_2[n]$ and $i_3[n]$ are independent and uncorrelated, consequently they can be linearly added in (3.10). The outcome of the expectation of the power of the different terms of $i[n]$ can be summarized as follows

$$
I_1 = \frac{1}{R}\left(\sum_{j=1}^{J}\alpha_j\right)^2 \tag{3.32}
$$

$$
I_2 = \frac{2}{R}\sigma^2\sum_{j=1}^{J}\alpha_j \tag{3.33}
$$

$$
I_3 = \frac{1}{R}\sigma^4, \tag{3.34}
$$

resulting the total interference power for $i[n]$ as

$$
\mathfrak{I} = \frac{(\sum_{j=1}^{J}\alpha_j)^2 + 2\sigma^2\sum_{j=1}^{J}\alpha_j + \sigma^4}{R}, \tag{3.35}
$$

that depends on the number of antennas R, the number of users J and the noise variance σ^2. Then the SINR obeys

$$SINR = \frac{E\{|\varsigma|^2\}}{\mathfrak{I}} = \frac{R\sum_{j=1}^{J}\alpha_j^2}{(\sum_{j=1}^{J}\alpha_j)^2 + 2\sigma^2\sum_{j=1}^{J}\alpha_j + \sigma^4}. \tag{3.36}$$

For a high reference SNR, given by ρ in (2.14), only the term I_1 is significant, so that we have a upper bound for the SINR in (3.36)

$$SINR_H = R\frac{\sum_{j=1}^{J}\alpha_j^2}{(\sum_{j=1}^{J}\alpha_j)^2}, \tag{3.37}$$

while for a low SNR, the main dominant term is I_3 so that we find a lower bound for (3.36)

$$SINR_L = \frac{R\sum_{j=1}^{J}\alpha_j^2}{\sigma^4}. \tag{3.38}$$

We can see that upon increasing the R at the BS, the SINR increases proportionately. Hence, the energy-efficiency increases with R, obeying the same scaling law as for coherent systems associated with perfect CSI, as predicted [39].

Table 3.1 summarizes the interference terms, the SINR and its bounds derived in this section for the particular case where the power of each user is $\alpha_j = 1$. This case is considered for the EEP constellation design which we will present in Section 3.5. In this design all users will have the same power profile.

interfering terms, I_x	$I_1 = \frac{1}{R}$	$I_2 = \frac{2J}{R}\sigma^2$	$I_3 = \frac{\sigma^4}{R}$
Total Interference power	$\mathfrak{I} = \frac{J^2+2\sigma^2J+\sigma^4}{R}$	**Total SINR**	$SINR = \frac{RJ}{J^2+2\sigma^2J+\sigma^4}$
Bounds	$SINR_H = \frac{R}{J}$		$SINR_L = \frac{RJ}{\sigma^4}$

Table 3.1: Summary of SINR and interference for $\alpha_j = 1$, EEP design.

In Figure 3.1 the SINR obtained by simulation is compared to that in the theoretical expression (3.36) according to reference SNR (ρ), for $R = 100$ antennas and $J = 2$ users. Two cases are shown. First, the second user has the same power level than the first user, this is mean $\alpha_1 = 1 = \alpha_2$, while in the other case, the second user has $\alpha_2 = 8$. Also the bounds for high and low ρ and, $\alpha_2 = 1$ and $\alpha_2 = 8$ are shown. The value of $\alpha_2 = 8$ is the highest value to appreciate differences in the SINR in terms of α. We can see that the approximation for the bound in Figure 3.1 is valid approximately below $\rho = -10$ dB and above $\rho = 10$ dB. By contrast, between $(-10, 10)$ dB, there is a distinction between the bound for the SINR and the theoretical expression (3.36) which we quantify in Figure 3.2, according to the number of antennas for $\rho = -10$, 10 and 0 dB. This difference is small for R in the limits of the interval, while acquires the largest $R-$value in the middle of the

Figure 3.1 Validation of SINR (3.36) and approximation bounds (3.37)-(3.38). Example for $R = 100$ antennas and J= 2 users.

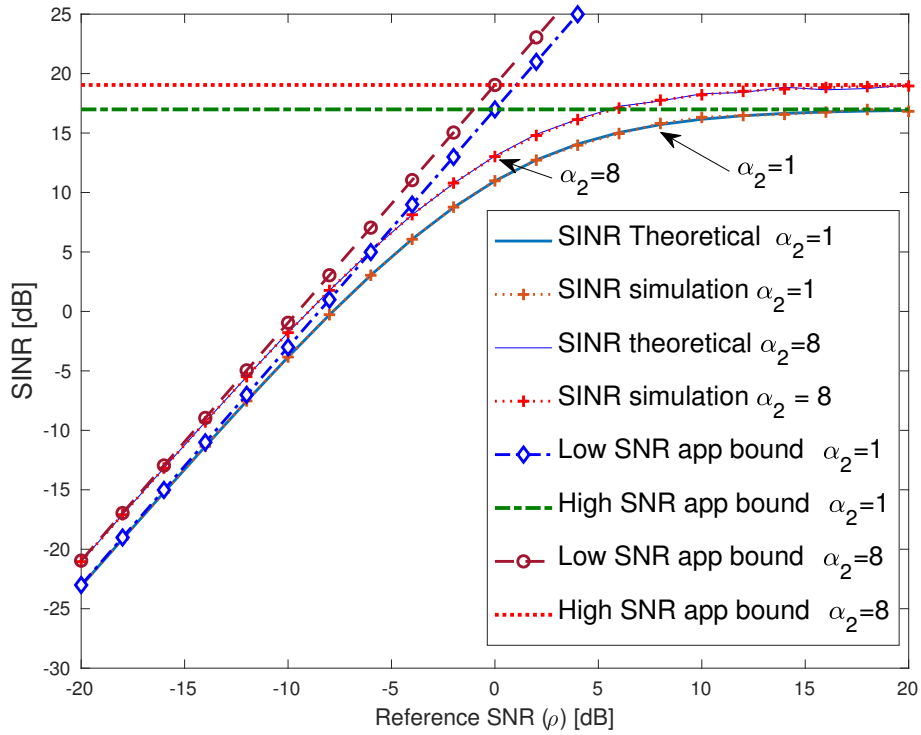

Figure 3.2 Deviations between SINR expression and bounds as the number of antennas R for $\rho = 10$, -10 and 0 dB.

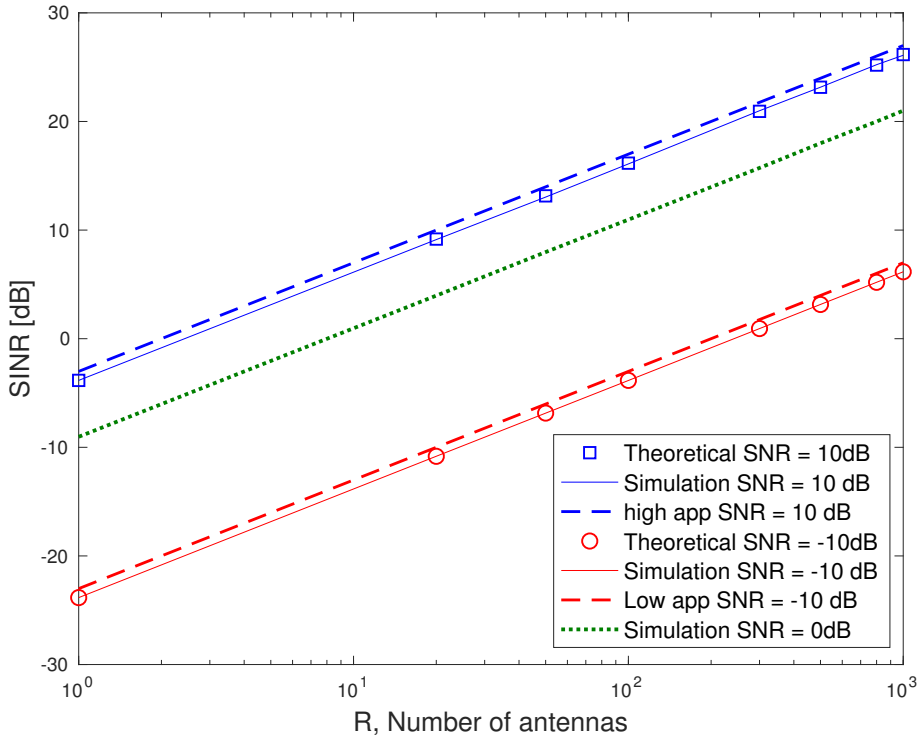

range, this is for $\rho = 0$ dB. By contrast, for $\rho = 15$ and -15 dB, the bounds perfectly match the theoretical expression in (3.36) and the difference in R is zero, as is shown in Figure 3.3.

Figure 3.3 Deviations between SINR expression and bounds as the number of antennas R for $\rho = 15$ dB and -15 dB.

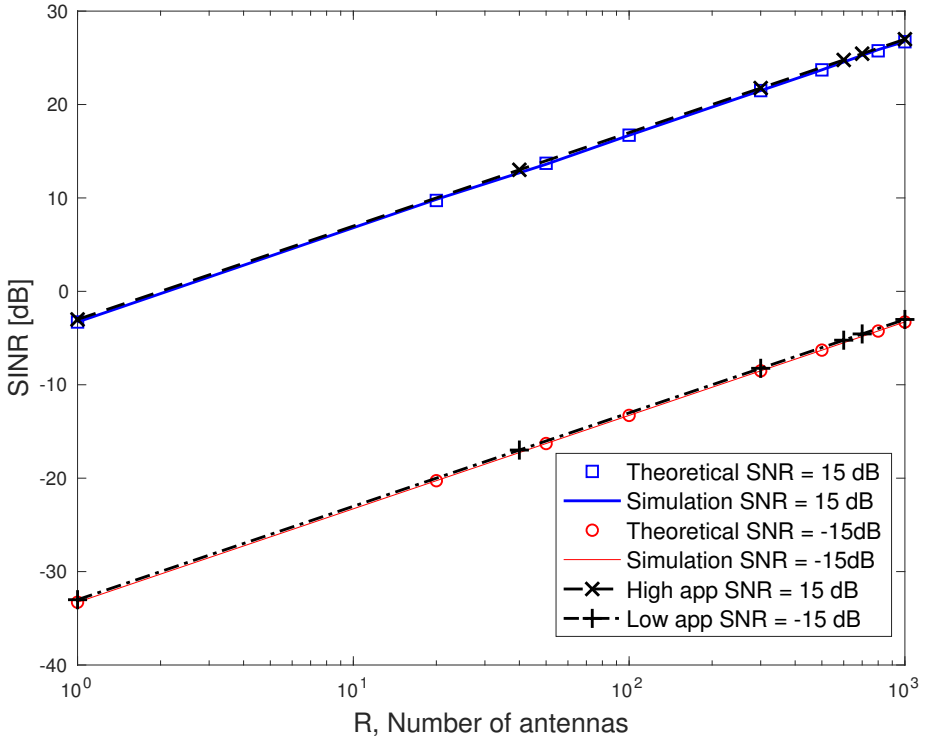

3.3 Bounds for Error Probability

The error probability of the joint symbols $\varsigma[n]$ may be found using the Union Bound and assuming that the interference plus noise $i[n]$ in (3.9) is Gaussian, which is justified by the Central Limit Theorem. Let us first define the pairwise error probability as the probability of detecting symbol m', when symbol m was transmitted, that is, as defined in [43]

$$Pe_{mm'} = Q\left(\sqrt{\frac{d^2_{mm'}}{2\mathfrak{I}}}\right), m, m' \in \{0, 1, ...\mathfrak{K} - 1\}, m' \neq m, \tag{3.39}$$

where the distance between points m and m' of the joint constellation is $d_{mm'} = |\varsigma_m - \varsigma_{m'}|$. Then we can upper-bound the symbol error probability (SEP) P_e as

$$P_e \leq \frac{1}{\mathfrak{K}} \sum_{m=0}^{\mathfrak{K}-1} \sum_{\substack{0 \leq m' \leq \mathfrak{K}-1 \\ m' \neq m}} Q\left(\sqrt{\frac{d^2_{mm'}}{2\mathfrak{I}}}\right). \tag{3.40}$$

The error probability of the joint symbols $\varsigma[n]$ may be found using the Union Bound as was shown in [115]. By considering the minimum distance of the constellation between the symbols ς_m and $\varsigma_{m'}$ as

$$d_{min} = min\{|\varsigma_m - \varsigma_{m'}|, 1 \leq m \leq \mathfrak{K}, 1 \leq m' \leq \mathfrak{K}, m' \neq m\}, \tag{3.41}$$

and being d^m_{min} the minimum distance (MD) of the constellation point m to its nearest neighbor[2], then we can use an approximated bound for SEP [43] as follows

$$Pe \approx \frac{1}{\mathfrak{K}} \sum_{m=0}^{\mathfrak{K}-1} Q\left(\frac{d^m_{min}}{\sqrt{2\mathfrak{I}}}\right). \tag{3.42}$$

Considering the minimum constellation distance d_{min} (3.41), we can further upper-bound the SEP as

$$P_e \leq (\mathfrak{K}-1)\, Q\left(\sqrt{\frac{d^2_{min}}{2\mathfrak{I}}}\right). \tag{3.43}$$

We can also find a lower bound to the SEP using the minimum distance to its nearest neighbor, d^m_{min}, as can be found in [43], being the lower bound for SEP the following

$$Pe \geq \frac{1}{\mathfrak{K}} \sum_{m=0}^{\mathfrak{K}-1} Q\left(\frac{d^m_{min}}{\sqrt{2\mathfrak{I}}}\right). \tag{3.44}$$

For all these bounds, the power of the noise plus interference $\mathfrak{I}$ is defined in (3.35) and with $\alpha_j = 1$ in Table 3.1. Recalling that we have $\mathfrak{I} = \frac{\sum_{j=1}^{K} \alpha_j^2}{SINR}$ (3.36), we can also express (3.43) as

$$Pe \leq (\mathfrak{K}-1)\, Q\left(\sqrt{\frac{d^2_{min}}{2\sum_{j=1}^{J}\alpha_j^2} SINR}\right)\Bigg|_{\alpha=1} = (\mathfrak{K}-1)\, Q\left(\sqrt{\frac{d^2_{min}}{2J} SINR}\right). \tag{3.45}$$

From (3.45) we define the normalized minimum distance (NMD) as follows

$$\overline{d_{min}} = \frac{d_{min}}{\sqrt{\sum_{j=1}^{J}\alpha_j^2}}\Bigg|_{\alpha=1} = \frac{d_{min}}{J}, \tag{3.46}$$

This implies that for a given SINR, the error performance depends on the normalized d_{min} (3.46). We can find the constellation parameters that optimize the error probability by maximizing the normalized d_{min}. As we will demonstrate in the next sections, the EEP designs show a better performance for $\overline{d_{min}}$ than UEP.

The same approximations also apply to the individual SEP of each of the users, provided that the distances between the constellation points that encode the same user's symbol are not evaluated.

[2]For the next sections, for convenience we denote MD d_{min} for each user j as $d_{min,j}$.

Performance bounds are a useful tool to assess the quality of coded systems and to gain insights into the effect of coding parameters on the system performance. We compare the corresponding sections the performance for our designs to these performance bounds.

3.4 Designs for Unequal Error Performance (UEP)

In this section, we present the constellation designs for the approach where each user experiences a different performance, so-called UEP scheme. We apply two design criteria: one based on the fact that the signal of all the users is received with the same or different average power level, this is depending on α_j-value. The other one is based on MD which is obtained in the joint constellation.

3.4.1 UEP design with equal power per user

In this design, all users transmit with unit power without relative power gain with respect to the user 1, $\alpha_j = 1\ \forall j$. The basic constellation scheme belongs to the phase-modulation family PSK. Here, we propose three designs.

- *Constellation A*:

  The purpose for building the constellation A is intercalating the last user between the first two symbols of the previous user along unit circle. Then, the points for the individual constellations $\mathfrak{M}_j^A$, for each user j, are defined as

$$\mathfrak{M}_j^A = \left\{ \frac{2\pi m}{M} \mathsf{L}^{1-j}, m = 0, 1, ..., M-1 \right\}, j = 1, ..., J, \mathsf{L} \geq M, \tag{3.47}$$

  where L is the number of symbols of the user j for $j \neq 1$ which are intercalated. An example for $J = 2$ users and a size of constellation of $M = \mathsf{L} = 4$ symbols per user for (3.47) is shown in Figure 3.4. In this example, the constellation for user 1 ($\mathfrak{M}_1^A$) corresponds to Figure 3.4 (a), the user 2 uses the constellation in Figure 3.4 (b) ($\mathfrak{M}_2^A$), while the resulting joint constellation ($\mathcal{M}^A$) is represented in Figure 3.4 (c), following the superposition principle from individual constellations, as was explained in Section 2.4.2.

  In this design we can see a different individual MD[3] between users, this is $d_{min,1}^A \neq d_{min,2}^A$. This is the reason why each user experiences an unequal performance. Moreover, $d_{min,1}^A$ is different to the MD in the joint constellation, as noted in Figure 3.4.

[3] $d_{min,j}^A$ is the minimum distance in the constellation A for user j.

Figure 3.4 Design A for UEP criterion: (a) User 1 ($\alpha_1 = 1$), (b) user 2 ($\alpha_2 = 1$) and (c) joint constellation.

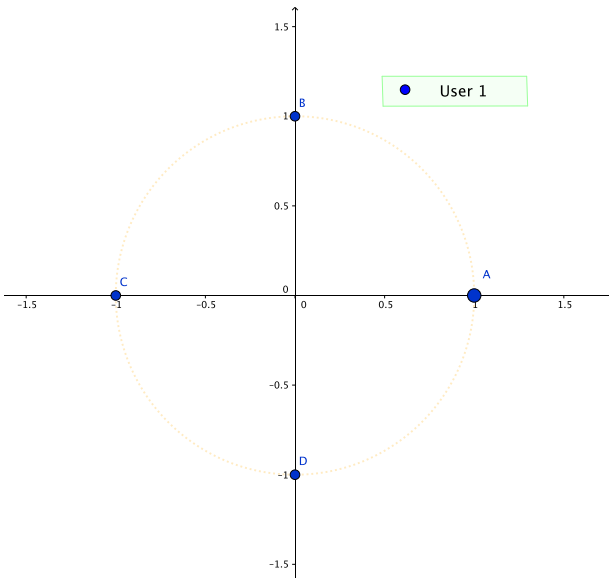

(a) User 1, $\mathfrak{M}_1^A$

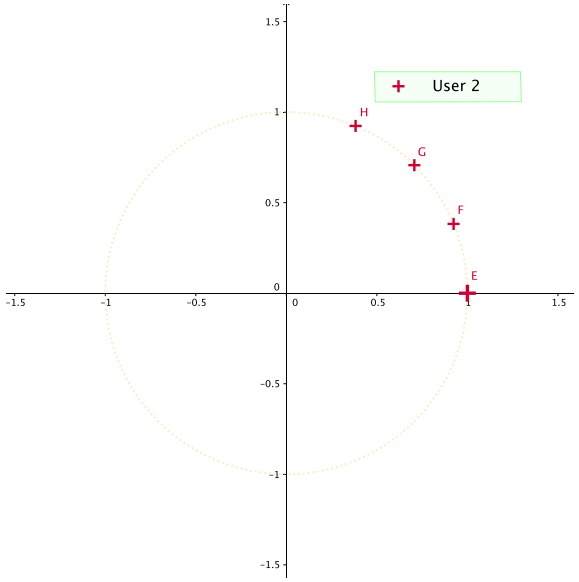

(b) User 2, $\mathfrak{M}_2^A$

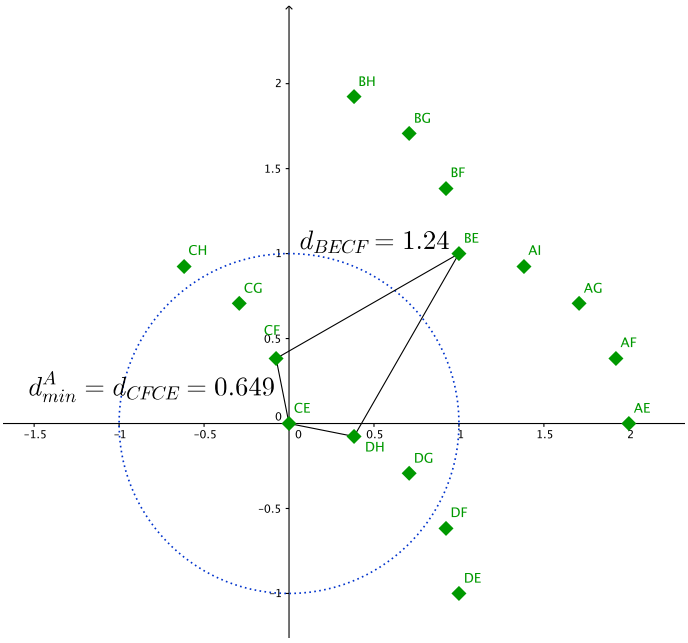

(c) Joint constellation A

For this constellation design with J users, considering $\mathsf{L} = M$ and $\alpha_j = 1$ we can see that the MD imposed by worse user (lower individual MD) is given by

$$d^A_{min} = |1 - e^{\frac{j2\pi}{M^2}}| \approx \sin\left(\frac{2\pi}{M^J}\right) \approx \frac{2\pi}{M^J}, \tag{3.48}$$

while the NMD for constellation A using (3.46) is

$$\overline{d^A_{min}} \approx \frac{2\pi}{M^J\sqrt{J}}. \tag{3.49}$$

The issue for this design is increasing the number of users, since the distance decreases exponentially with J. The more symbols are intercalated, the worse the performance is for the last user (intercalated user).

- *Constellation B*:

  For alleviating the degradation on the performance due to the fact that intercalating all user's symbols between only two symbols belong to other user, we propose other scheme.

  In this case, with the goal of increase the distance for the intercalated user, maintaining the unequal performance and the same power gain α, we intercalate half of the constellation for the last user between the first half of the previous user while the second one is placed in the opposed quadrants. An example for $J = 2$ users and $M = \mathrm{L} = 4$ symbols is shown in Figure 3.5 (a) and (b) for the user 1's and user'2 constellation, respectively. In Figure 3.5 (c) the resulting joint constellation is shown. The points for this scheme are calculated for the user 1 as

$$\mathfrak{M}^B_1 = \left\{\frac{2\pi m}{M},\ \ m = 1, \cdots, M\right\}\ for\ user\ 1, \tag{3.50}$$

while for the remaining users have to be intercalated as

$$\mathfrak{M}^B_j = \left\{\begin{array}{c} \frac{2\pi m}{M}(\mathrm{L}-1)^{1-j},\ \ m = 1, \cdots, \mathrm{L}/2 \\ \pi + \frac{2\pi m}{M}(\mathrm{L}-1)^{1-j},\ \ m = \mathrm{L}/2, \cdots, M \end{array}\right\}\ for\ j > 1. \tag{3.51}$$

Now, the NMD for the constellation B is expressed as

$$\overline{d^B_{min}} \approx \frac{4\pi}{M^J\sqrt{J}} \tag{3.52}$$

which is duplicated with respect to the case A.

Figure 3.5 Design B for UEP criterion: (a) User 1 ($\alpha_1 = 1$), (b) user 2 ($\alpha_2 = 1$) and (c) joint constellation.

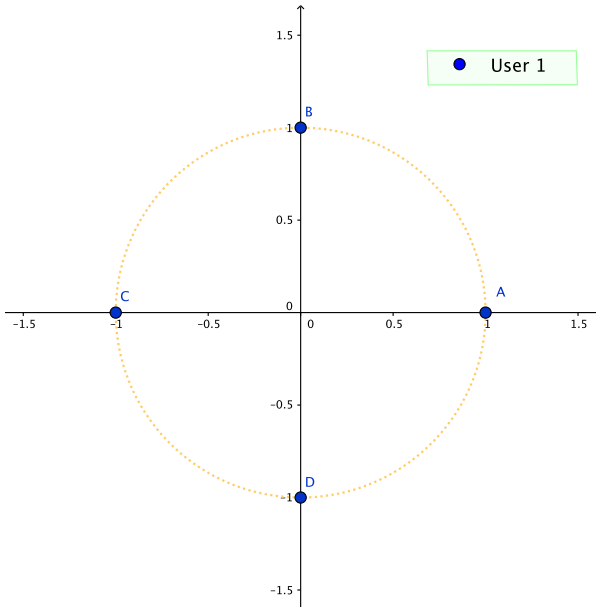

(a) User 1, $\mathfrak{M}_1^B$

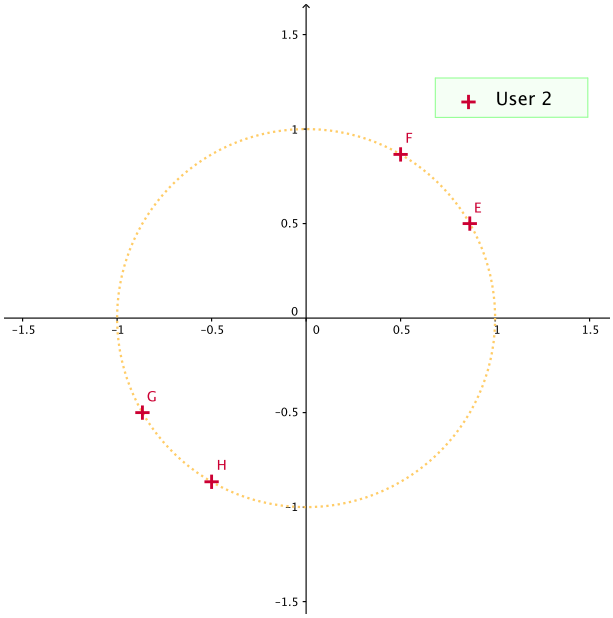

(b) User 2, $\mathfrak{M}_1^B$

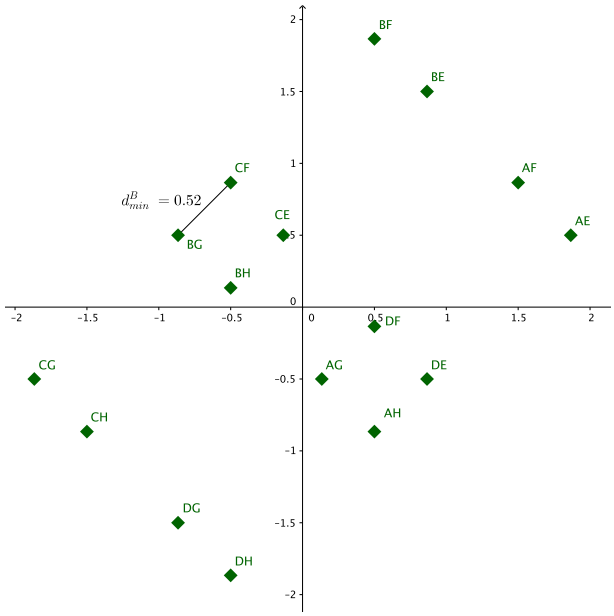

(c) Joint constellation B

- *Constellation C*:

  The third design is build to obtain the same distance for all adjacent symbols in the joint constellation, maintaining the same average power level among users. The MD is referred now between joint symbols which is searched by a comprehensive search as

$$d_{opt}^{C} = \underbrace{arg\ min}_{\forall j,k\ k\neq j} \sqrt{\varsigma - s_j s_k}, \tag{3.53}$$

  being the optimal distance $d = 0.56$. In Figure 3.6 we show the obtained constellations for the case of $J = 2$ users and $M = 4$. In addition, in Figure 3.6 we can see how the second user is intercalated inside user 1. Note that the MD for user 2 is increased which will be reflected in better performance compared to those obtained in constellation A, with the cost of reducing the performance for user 1, but without reaching the user 2 in B. This will be analyzed in detail in the Section 3.4.3 with every design proposed.

Figure 3.6 Design C for UEP criterion: (a) User 1 ($\alpha_1 = 1$), (b) user 2 ($\alpha_2 = 1$) and (c) joint constellation.

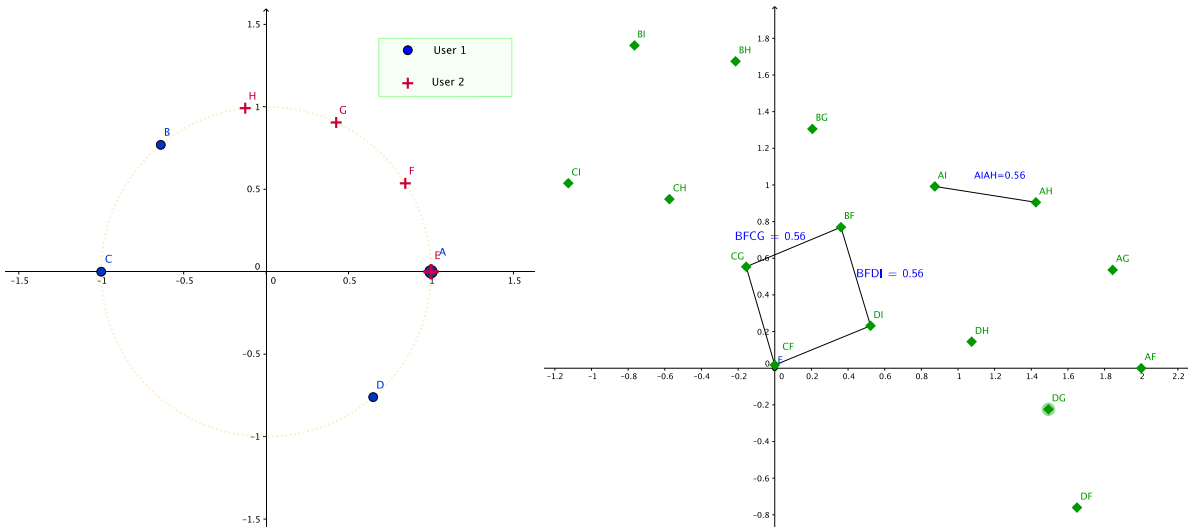

(a) User 1 $\mathfrak{M}_1^C$ and 2 $\mathfrak{M}_2^C$ (b) Joint Constellation C

3.4.2 UEP design with unequal power per user

In this case, all the users transmit symbols of the same standard M-DPSK constellation. Hence, their signals require different powers α_j to be separated in the receiver. The user 1 transmits with unit power ($\alpha_1 = 1$), while the rest of the users transmit with a power gain with respect to the user 1. Other reason why the signals of the different users may be received at a different average power is because their path loss is not compensated by

power control. Here, the unequal power level is the reason for the different performance among users.

As happened for the UEP case with equal power for all users, we use two design criteria: on the one hand, designing the joint constellation with same distance between symbols and, on the other hand, the case where all symbols are in the same distance in the individual constellation.

- *Constellation D*:

  As already mentioned, all users employ the same constellation scheme, hence $\mathfrak{M}^D$ does not depend on the subindex j as the previous designs. The points for the individual constellation are defined as

  $$\mathfrak{M}^D = \left\{ \frac{2\pi m}{M}, m = 0, 1, ..., M-1 \right\}, j = 1, ..., J. \tag{3.54}$$

  In this case, the joint constellation formed by superposition of J-user constellation contains separate replicas of the smaller constellations obtained for $(J-1)$ users, with a separation of at least d_{min}.

  This implies that the NMD decreases as α_j is increased, so that the maximum normalized d_{min} is achieved for $\alpha_j = 2^{j-1}$, which has a value of

  $$\overline{d_{min}^D} = \frac{d_{min}^{(l)}}{\sqrt{\sum_{j=1}^{J} 2^{2(j-1)}}} = \frac{\sqrt{3} d_{min}^{(l)}}{\sqrt{4^J - 1}}, l = 1, 2. \tag{3.55}$$

  From this equation we can observe a less substantial reduction of the maximum $\overline{d_{min}}$, when J is increased for design D. For $M > 4$ the geometry becomes more complicated and the values of α_j that maximize $\overline{d_{min}^D}$ can be found by exhaustive search. However, they do not in general obey $\alpha_j = 2^{j-1}$. For example, for $M = 8$ and $J = 2$ users, the maximum $\overline{d_{min}^D}$ is found to be for $\alpha_2 = 1.765$.

  The MD for this individual users is given by the unit-energy DPSK constellations. For example, considering the size of constellation of $M = 2$, $M = 4$ and $M = 8$, the MD are $d_{min} = 2$, $d_{min} = \sqrt{2}$ and $d_{min} = 2 - \sqrt{2}$, respectively. In the joint constellation, the MD can be preserved, provided that $\alpha_j \geq 2^{j-1}$ for the case $M = 2$ and $M = 4$.

  An example of design D for $J = 2$ users and $M = 4$ is shown in Figure 3.7. Both users employ the same scheme shown in Figure 3.7(a), while the resulting joint constellation is Figure 3.7(b), which shows a $d_{min} = 1.41$ just like the individual constellation. However, a target symbol does not have all its neighbour symbols at the same distance. For example, in Figure 3.7(b) the distance between the symbol DG and BH is 2.

Figure 3.7 Design D for UEP criterion: (a) User 1 ($\alpha_1 = 1$), (b) user 2 ($\alpha_2 = 2$) and (c) joint constellation.

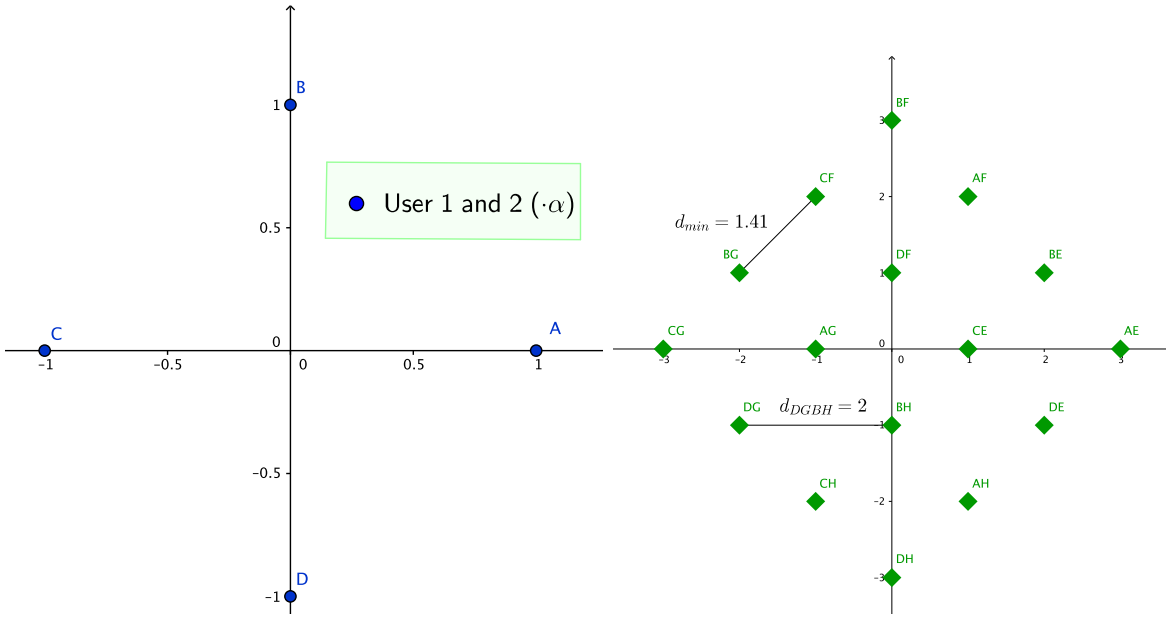

(a) User 1 $\mathfrak{M}_1^D$ and user 2 $\mathfrak{M}_2^D$ (b) Joint constellation D

- *Constellation E*:

  From the design D, now the purpose is obtaining the same distance among all joint symbols. We keep the unequal power between individual user signals. In this case, the design E is created by a rotation of the individual constellations in D. The points for the individual constellations $\mathfrak{M}^E$ are defined as

$$\mathfrak{M}^E = \left\{ \frac{\pi(2m+1)}{M}, m = 0, 1, ..., M-1 \right\}. \tag{3.56}$$

  As with constellation D, $\mathfrak{M}^E$ does not depend on j.

  An example of the users' and joint constellations is shown in Figure 3.8 for $J = 2$ users and $M = 4$ symbols. We can see that the resulting joint constellation in Figure 3.8(b) is equivalent to QAM scheme, where MD is defined as $d_{min} = 2$. However, in our DPSK we do not have to worry by the amplitude detection, merely making MD with the joint symbol and the direct mapping between individual constellation.

Figure 3.8 Design E for UEP criterion: (a) User 1 ($\alpha_1 = 1$), (b) user 2 ($\alpha_2 = 2$) and (c) joint constellation.

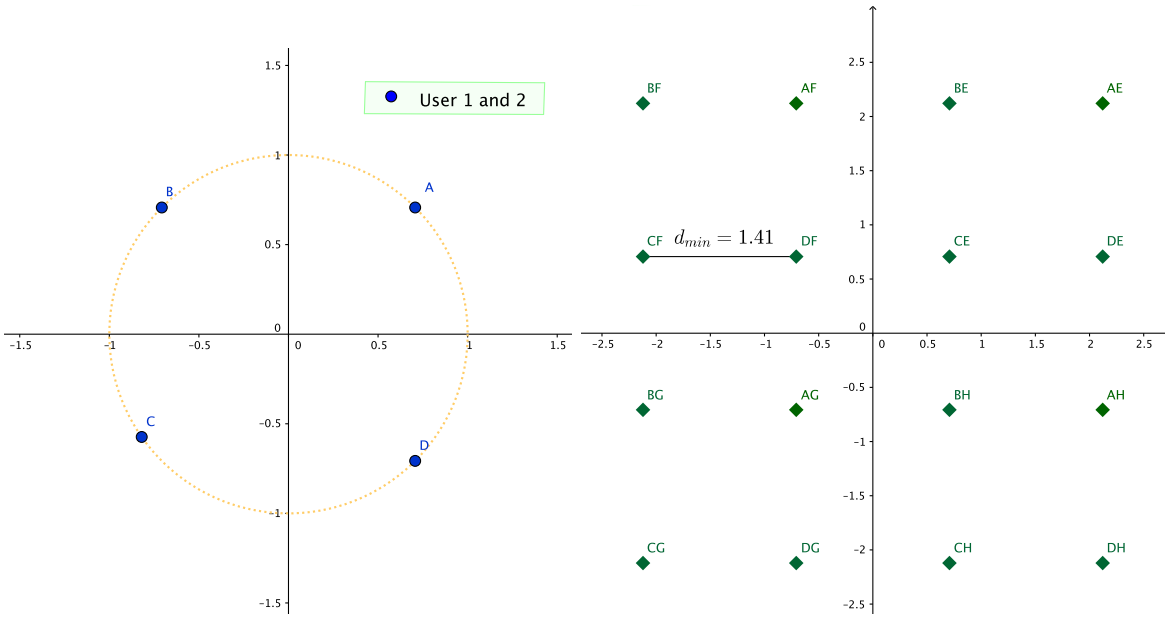

(a) User 1 $\mathfrak{M}_1^E$ and 2 $\mathfrak{M}_2^E$ (b) Joint constellation E

3.4.3 Performance for UEP designs

Let us analyze the proposed constellation schemes for the UEP case, whose classification is summarized in Table 3.2 on the basis of the MD and the power among users. The main objective in this analysis is to check the number of antennas R reached for a reasonable BER in these communication systems.

Minimum Distance (MD): d_{min}		**Average Power Lever**	
Individual Scheme	**Joint Scheme**	**Unequal**	**Equal**
Unequal MD	Unequal MD	A, B	-
	Equal MD	C	-
Equal MD	Unequal MD	-	D
	Equal MD	-	E

Table 3.2: Classification for proposed UEP designs.

The designs proposed were simulated following the system model in Chapter 2 without channel coding scheme. In Figure 3.9, the received constellation at the BS, corresponding to the joint constellation for the design A with $J = 2$ users and $M = 4$ symbols is shown, as representative of the UEP schems. In this simulation, we increase the SNR at the same time that R decreases. We can see as R has more influence on the received joint constellation than SNR to correct the channel phase. This is noted in Figure 3.9(b)-(c).

A low SNR is enough thanks to the energy efficiency of m-MIMO. By contrast, for UEP schemes, we need a high R to achieve the free-noise constellation in Figure 3.9(a).

Figure 3.9 Constellation A received for $J = 2$ users and M=4 symbols per user.

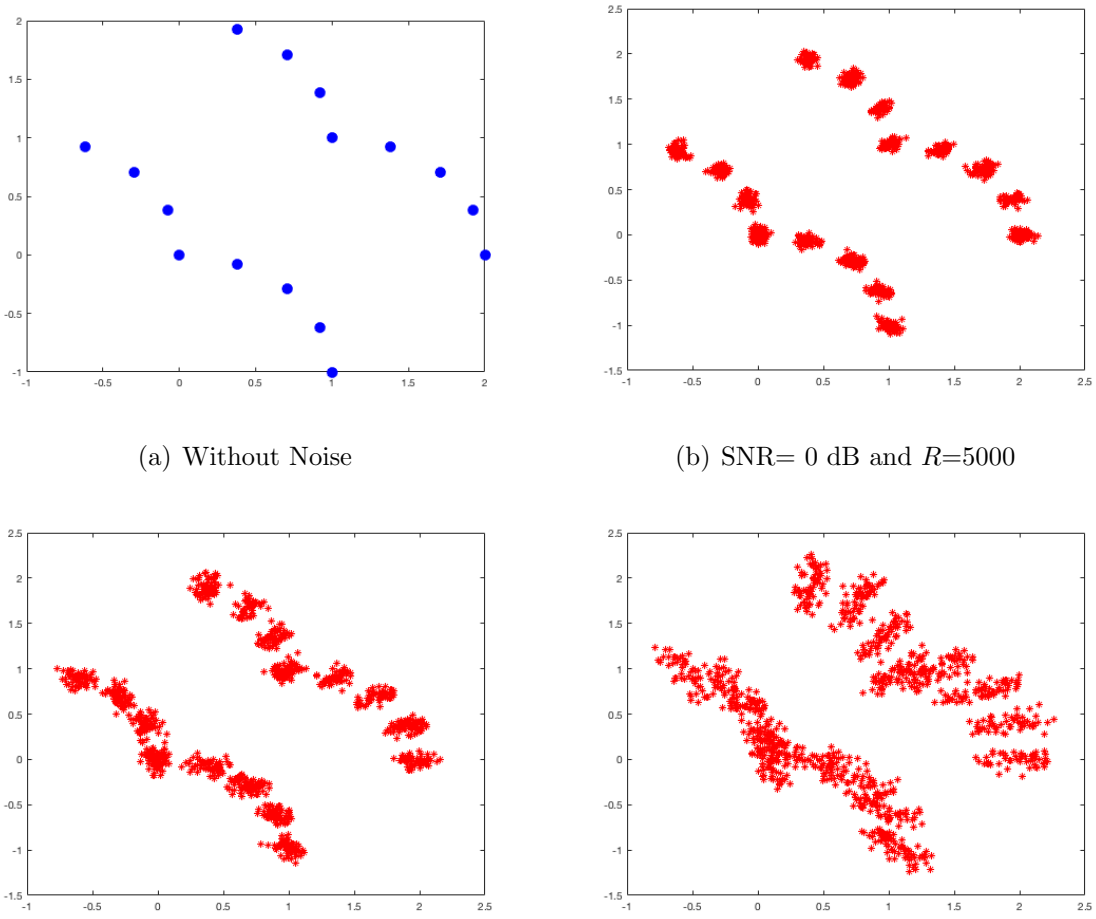

(a) Without Noise

(b) SNR= 0 dB and R=5000

(c) SNR= 3 dB and R=1000

(d) SNR= 10 dB and R=100

First, we validate the bounds obtained in Section 3.4 using the unequal designs. Figure 3.10 shows the performance of constellation D for DBPSK, DQPSK and 8-DPSK modulations with maximum NMD, where the accuracy of the bounds defined in Section 3.4 can be contrasted to the simulation results. We can see that the upper bound is tight. The lower bound, although looser, provides also a good approximation to the SEP. For higher SINR values both bounds become quite accurate.

For constellation design D with DQPSK the values that achieve the best SER for a given ρ are $\alpha_j = 2^{j-1}$ as was explained in Section 3.4. For this case, Figure 3.11 shows the SER performance given by the upper and lower bounds as J is increased. We can see that up to $J = 4$ simultaneous users can be supported by the same time and frequency resource at a ρ as low as 0 dB.

Figure 3.10 SER bounds with $J = 2$ users for DBPSK, DQPSK and 8-DPSK modulations using constellation A.

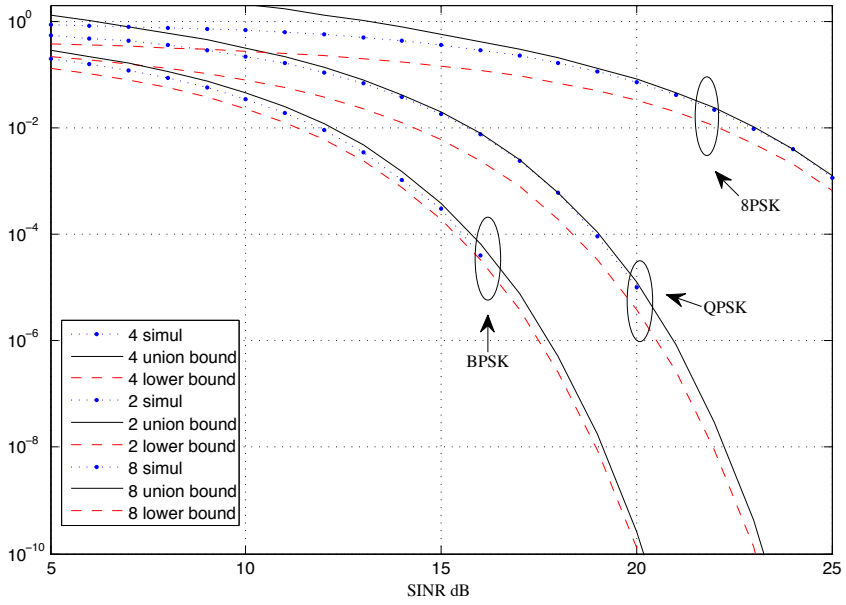

Figure 3.11 SER performance (UB: union bound, LB: lower bound) for J =1,2,3 and 4 users and DQPSK for $\rho = 0$ dB and constellation D.

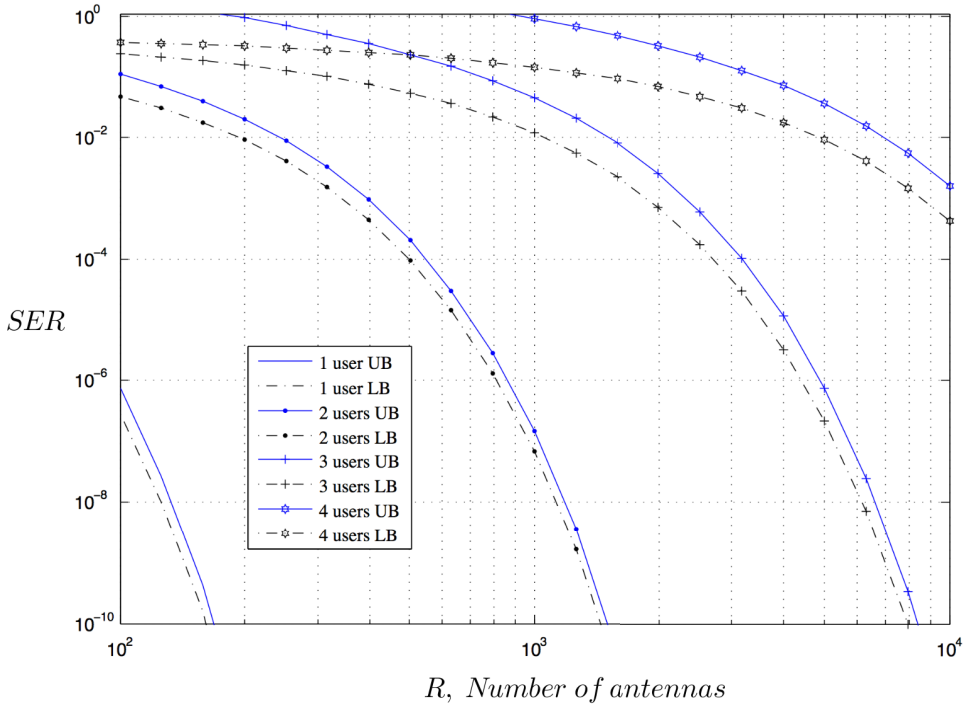

Figures 3.12 to 3.15 show the BER performance of the proposed UEP schemes. In Figure 3.12, the constellations A, B and C are compared for the case $\rho = 0$ dB, $J = 2$ users and $M = 4$ symbols. We can see that the performance is unequal between the two users for all schemes, being always better for user 1, since it has higher d_{min} than user

2. This difference between both users for BER= 10^{-3} is measured on the basis to R, obtaining 2000, 150 and 200 antennas extra for user 2 with respect to 1, for the A, B and C schemes, respectively. In the scheme B and C, we increase the MD for user 2 in the individual constellation, therefore the difference between both users is lower than for A scheme. In addition, for the scheme C, we achieve the same MD for all joint symbols, hence, we need a lower R to reach a lower BER than with the A and B schemes. However, since the difference between both users in B and C is approximately the same, the fact of achieving the same MD in C design among joint symbols does not help to obtain an equal performance between users.

Figure 3.12 BER comparison of A, B and C constellation designs for $\rho = 0$ dB, $J = 2$ users and M=4.

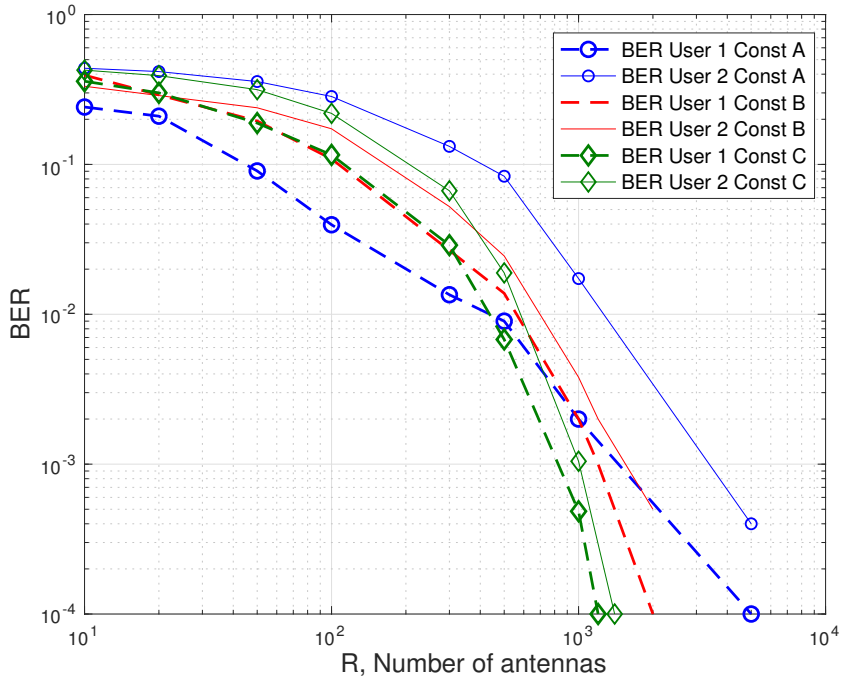

In Figure 3.13, increasing the SNR to 2 dB, the design B achieves to equal performance of both users. However, R is still very high to be considered in a practical system, even with m-MIMO. In Figure 3.14, we increase the size of constellation to $M = 8$ symbols. We can see that the design A gets worse, while B scheme remains the same. For a BER= 10^{-3}, A requires over 10^5 antennas, unacceptable even for m-MIMO. This is due to the MD for A in (3.49) is reduced more quickly than B in (3.52). However, note that increasing the size of constellation in both designs the number of antennas is quite high for a reasonable performance.

Figure 3.13 BER performance comparison of constellation designs A and B for $\rho = 2$ dB, $J = 2$ users and M=4.

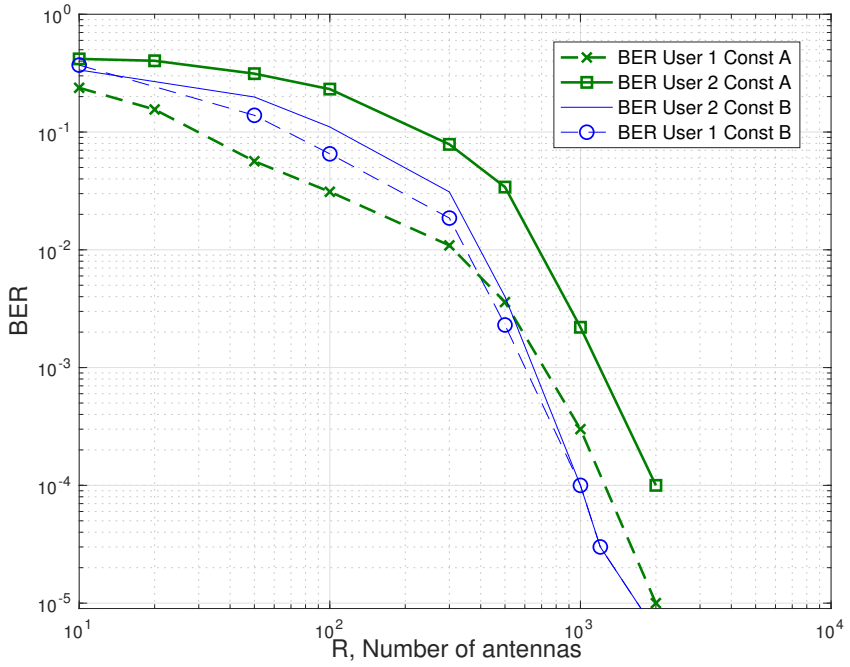

Figure 3.14 BER performance comparison of designs A and B for $\rho = 0$ dB, $J = 2$ users and M=8.

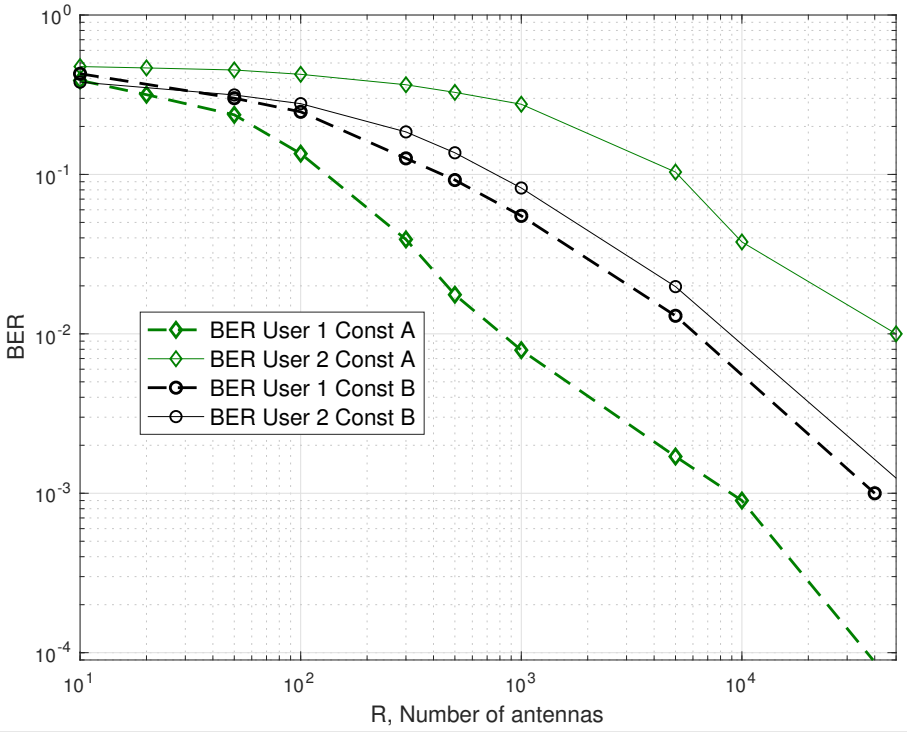

Now, we analyze the UEP cases with unequal power. In Figure 3.15, the designs D and E are shown for $\rho = 2$ dB, $J = 2$ users, M=4 and using $\alpha_2 = 2$ for user 2. These designs are compared to the B scheme, with $\alpha_2 = 1$ for user 2, corresponding to a

equal power. The evolution of the performance for D and E is similar, overcoming B for $R > 300$ antennas. The difference between D and E schemes lies in the joint constellation, resulting the same distance for all joint symbols in E. However, this feature does not affect on the performance, since only we have rotated the individual constellation. These results are consistent with that already discussed for A, B and C schemes in Figure 3.12. We conclude that the minimum distance for the bounds described in Section 2.3 is exclusively that found in the individual constellation for each user.

Figure 3.15 BER performance comparison of D and E with $\alpha_2 = 2$ and B ($\alpha_2 = 1$) constellation designs for $\rho = 0$ dB, $J = 2$ users and M=4.

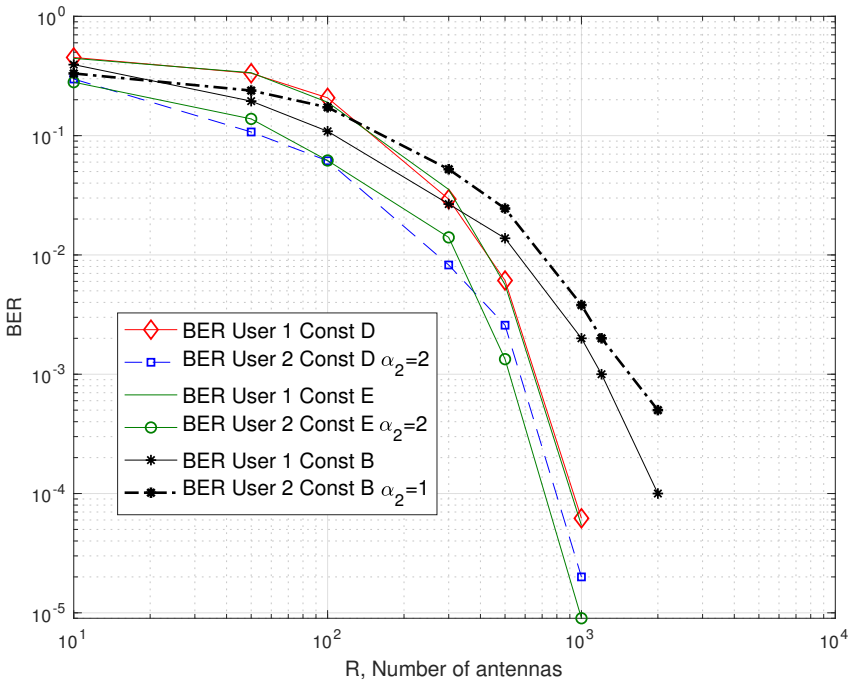

In Figure 3.16, we have represented the SER, in order to check the joint demodulation of both users. Note that the joint SER depends on the worst user, in this case the user 2. As with BER, the individual SER for design B is better than A due to the MD.

In Figure 3.17, we increase the number of users to $J = 4$ for a size of constellation of $M = 2$ and design A. We can see the unequal BER performance of the four user for $\rho = 0$ and 3 dB. However, increasing to $M = 4$, it is impossible to decode the user 4 as shown in Figure 3.18, even increasing the SNR to 5 dB. This result is consisting with that already discussed in Figure 3.9.

Figure 3.16 SER comparison of designs A and B for $\rho = 0$ dB, $J = 2$ users and M=4.

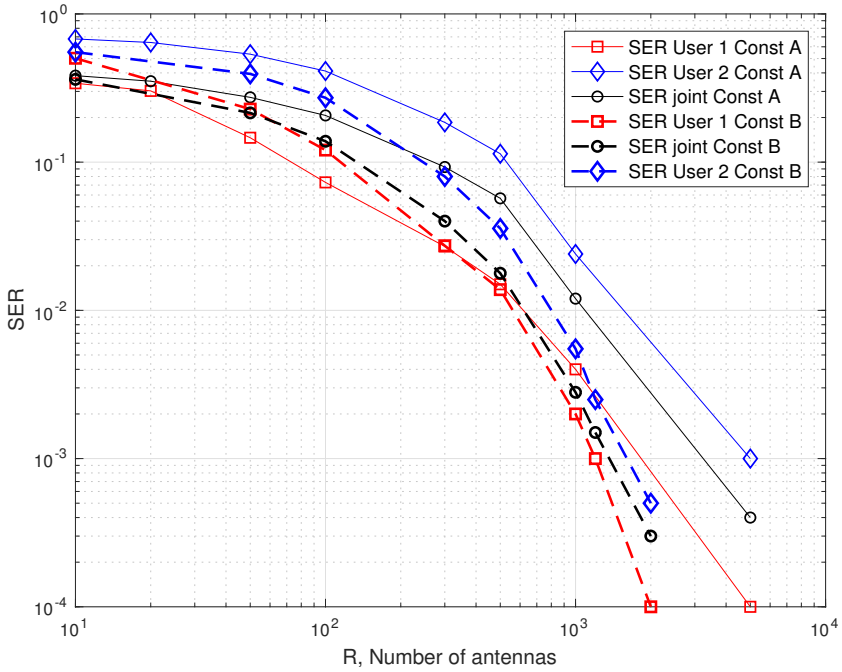

Figure 3.17 BER performance comparison of design A for $J = 4$ users and M=2.

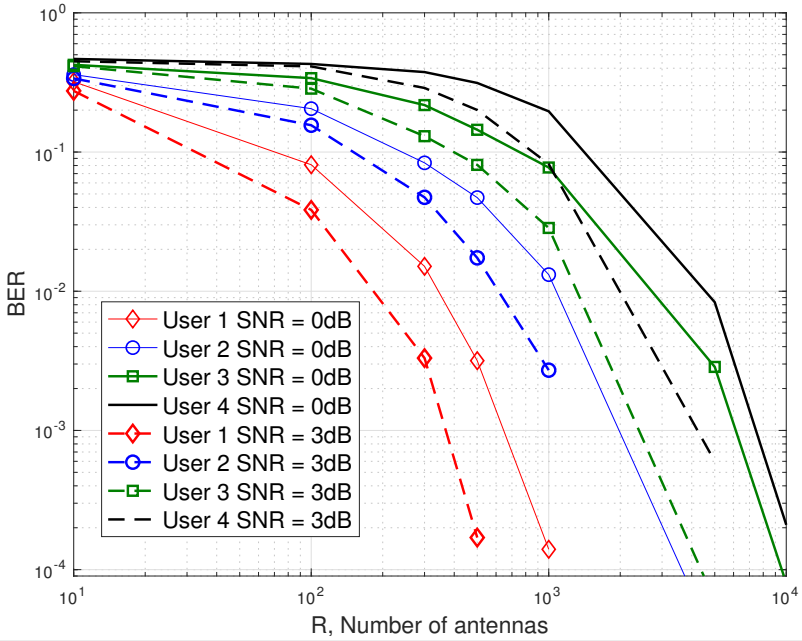

Figure 3.18 BER performance comparison of design A for $J = 4$ users, M=4 and ρ =5 dB.

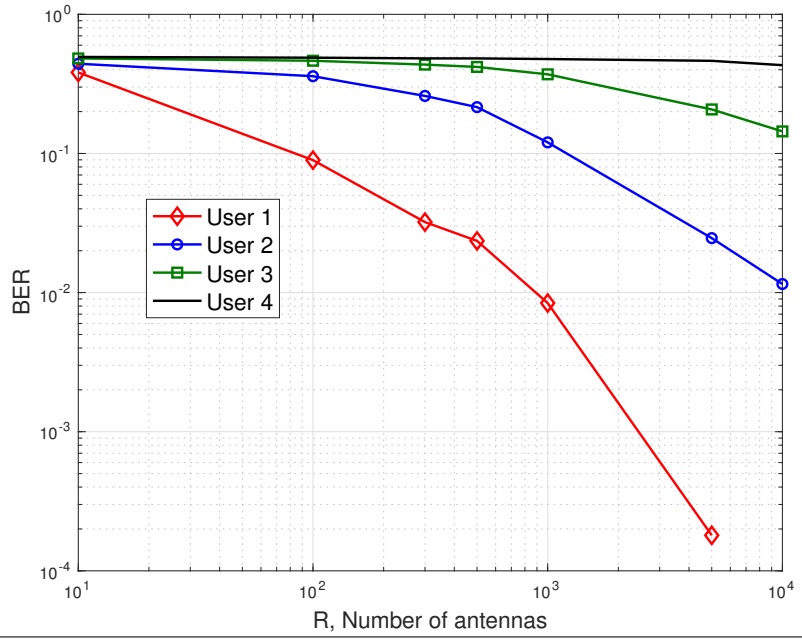

3.5 Design for Equal Error Performance (EEP)

In this section, we study how to achieve that every user experiences the same performance and we propose a constellation design for that, so-called EEP scheme. From the evaluation of the results in the previous design, we concluded that the MD in the joint constellation does not affect for having equal performance. By contrast, the symbols in the individual constellation have to be at the same distance, in turn, being this one the same for all users. This means that we can not have different MD among users.

Regarding the design criteria, we follow this separation: on the one hand for same average power level, and, on the other hand, each user transmits with different power level. For this latter, it is not a new proposal, but a combination of the UEP designs.

3.5.1 EEP design with equal power level per user

This design is based on placing all symbols for a given user at equal distance and also keeping the same distance between any two symbols for all users. In order to achieve these distance properties, the users are intercalated in the unit circle symbol by symbol, instead of inserting the full constellation for one user, as in some UEP designs. In this way, all users will obtain the same error performance. Hence, the constellation $\mathfrak{M}_j$ for user j is defined as

$$\mathfrak{M}_j^{EEP} = \left\{ \frac{2\pi}{JM}[(m+1)J - 1 + j], m = 0, 1, ..., M-1 \right\}, j = 1, ..., J \tag{3.57}$$

In Figure 3.19, an example of the user's constellation is shown for 2 users and a size of constellation of $M = 4$ symbols. The MD is $d_{min} = 0.59$ for joint symbols, which is lower than for UEP, as shown in Figure 3.19(d). The individual MD is the same for both users. This is the main reason for equal performance. In this case, the joint MD is decreased with respect to UEP ($d_{min}^{EEP} = 0.56 < d_{min}^{A} = 0.69$), with the corresponding slight degradation on the joint performance, in exchange for equaling this MD for both users. In Figure 3.19 (c) are illustrated both intercalated and individual constellation schemes in order to verify that all symbols are at the same distance before combining them in the joint symbol.

In Figure 3.20, a scheme for $J = 4$ users and $M = 4$ symbols is shown. Note the same distance among the symbols belonging to one user and, on the other hand the same distance among all users.

Figure 3.19 Constellation scheme for EEP design with $J = 2$ users and $M = 4$.

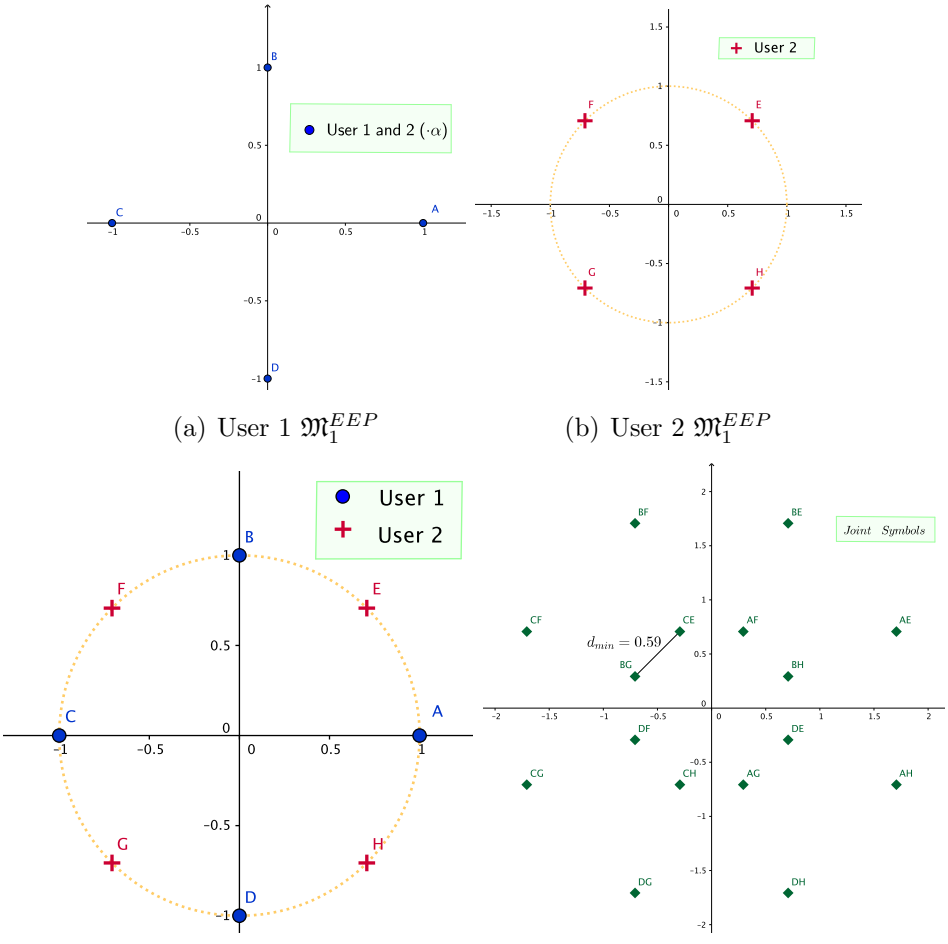

(a) User 1 $\mathfrak{M}_1^{EEP}$ (b) User 2 $\mathfrak{M}_1^{EEP}$

(c) User 1 and User 2 intercalated (d) Joint Constellation EEP

Figure 3.20 Constellation scheme for EEP design with $J = 4$ users and $M = 4$.

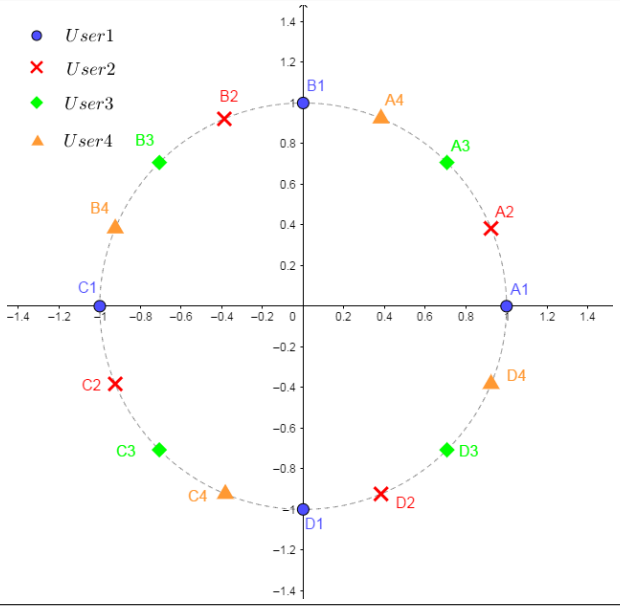

3.5.2 Performance for EEP designs

As in Section 3.4, now we analyze the performance for EEP designs. In Figure 3.21, the BER for $\rho = 0$ dB, $J = 2$ users and M=4 symbols is shown. Since the design is according to EEP, we can see that both users experience the same performance. Another way to achieve equal performance is using the UEP that were designed with equal power per user, but varying the power for user 2 until reaching the same performance as user 1. Here, experimentally we achieved it using $\alpha_2 = 2$ and UEP-A scheme to obtain a design which tends to EEP as R increases, as is shown in Figure 3.21. Another advantage for EEP noted in this figure is that it is better than UEP, even increasing the power for the user 2 in UEP scheme.

In Figure 3.22 we compare EEP design to UEP-A and C for the case of $\rho = 0$ dB, $J = 2$ users and M=4. In this case, note that the design C for user 1 is close to EEP scheme, reaching it both users for $R > 10^3$ antennas. This is due to the fact that the user 1 in both cases has the same MD. For the same conditions, the design A is worse than EEP, although for low R the user 1 in A achieves a lower BER.

In Figure 3.23 we compare the EEP scheme for $J = 4$ users and $M = 4$ to UEP using the proposal A for $\rho = 0$ dB. For EEP we have only shown two users of the total set, since the performance we can see that is the same. Note that increasing the number of users, the EEP design sacrifices the performance for some user, in this case the 1 and 3, in exchange to equal it. By contrast, UEP-A is not able to demodulate all users, while EEP does.

Figure 3.21 BER performance for EEP design, $\rho = 0$ dB, $J = 2$ users and $M = 4$.

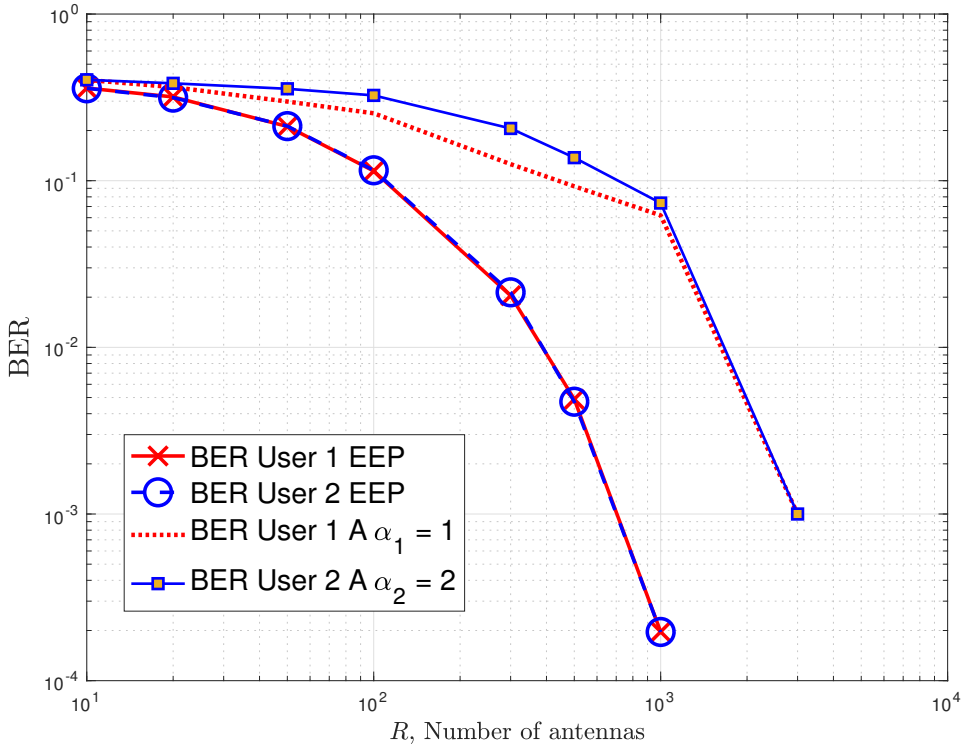

Figure 3.22 BER Comparison between EEP and UEP design, $\rho = 0$ dB, $J = 2$ users and M=4.

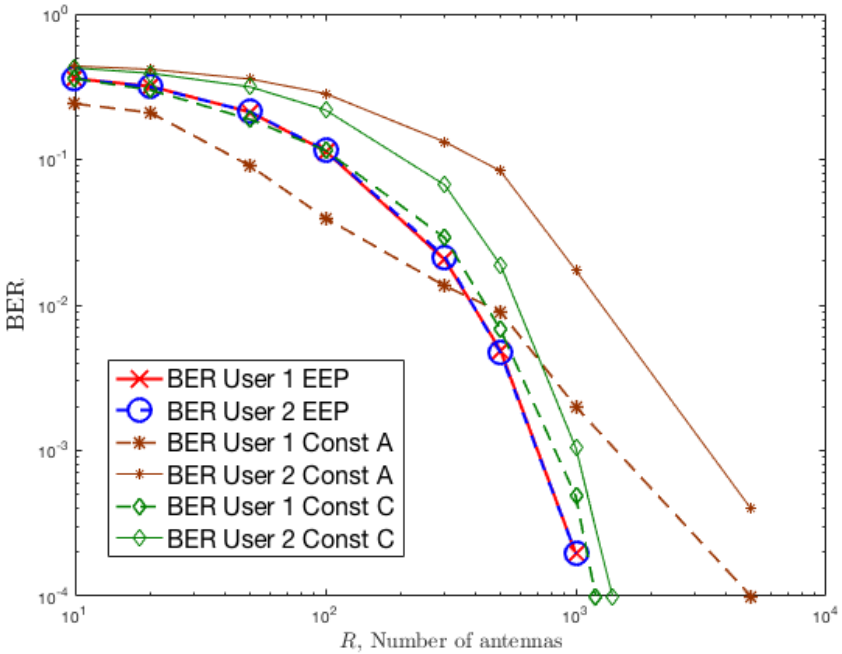

Figure 3.23 BER performance for EEP design, $\rho = 0$dB, $J = 4$ users and M=4.

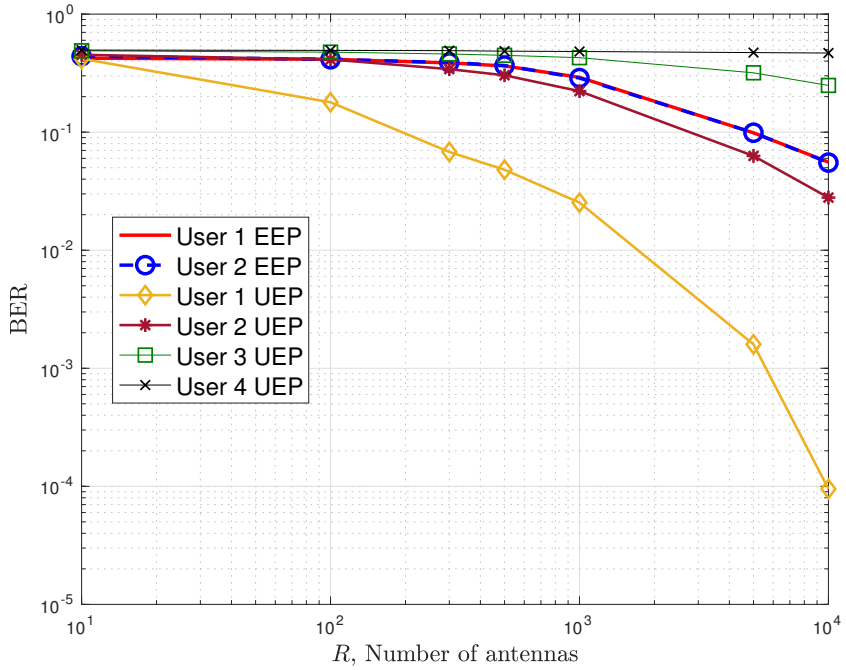

3.6 Comparison between coherent and non coherent schemes in Rayleigh fading

Since through this Thesis we intend to validate the NC schemes in m-MIMO as alternative for the future communication systems, we analyze how far our proposal is from its coherent counterpart. For that purpose, we also compare the performance relying on our EEP design to that achieved by a coherent Maximum Ratio Combining (MRC) receiver which is widely used in the literature for m-MIMO.

An MRC receiver normally works worse than ZF and MMSE. However, as power levels are reduced, the cross-talk introduced by the MRC receiver eventually falls below the noise level, and hence, becomes a viable and advisable option for large arrays of antennas.

The resulting signal in a coherent receiver which employs MRC can be expressed as follows

$$y_{MRC} = \frac{\sum_{r=1}^{R} \hat{h_r}^* y_r}{\sum_{r=1}^{R} |\hat{h_r}|^2}, \tag{3.58}$$

where $\hat{h_r}$ is the estimation of the channel in the r^{th} antenna. For this comparison, we assume that the CSI is estimated and, hence, it is subject to a realistic estimation error, which is assumed to be Gaussian. We generate these estimations as $\hat{h_r} = h_r + h_{error}$, where $h_{error} \sim CN(0, \sigma_e^2)$, being σ_e^2 the error variance.

Moreover, for a fair comparison we should take into account the effective throughput reduction due to the insertion of pilots for the channel estimation. In LTE this loss is

15% for a reduced number of antennas [123], while in [124] the optimum amount of pilots is shown to be 35%-40% for low SNR with $R = 16$ and an optimized number of users $J < M$. We will assume a rate-loss of 33% due to pilot overhead. This implies that for the same rate, we should compare non-coherent DQPSK to coherent 8-PSK.

In Figure 3.24 a comparison between a NC-m-MIMO for $J = 2$ users size of constellation of $M = 4$ and a coherent scheme is shown. We use the UEP design A, B and C and the EEP design for this comparison. We can see that for the same order of constellation, $M = 4$ the coherent system need 30 antennas less than the NC. However, considering a fair comparison our EEP scheme proposed reaches to the coherent with $M = 8$ increasing the SNR 2 dB. Note that the difference is lower than the classical 3 dB. By contrast, the UEP designs need more antennas or SNR to reach their coherent counterpart.

Figure 3.24 BER Performance for both NC and coherent detection.

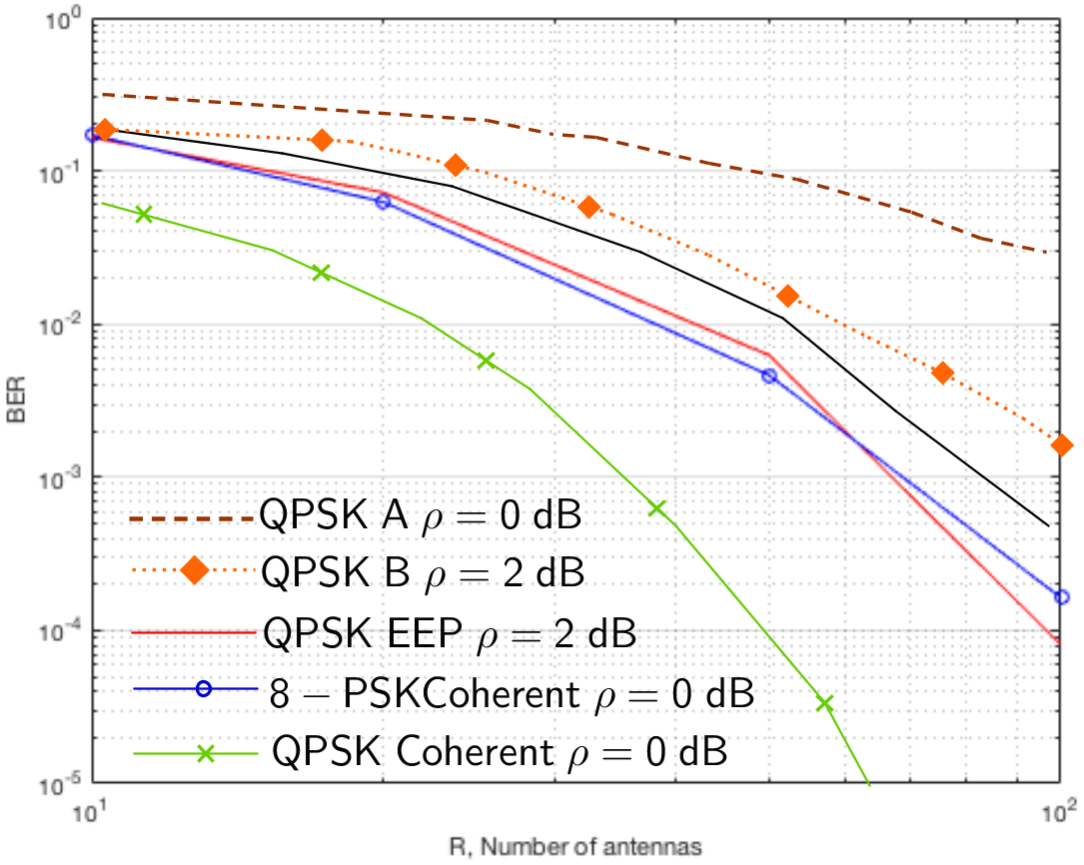

3.7 Comparison with other proposed constellations in m-MIMO

The most research for NC-m-MIMO are based on energy detection, as was shown in the state of the art. The ASK, APSK, DAPSK and DQAM, these three later combine in addition with the phase-detection, are the most prevalent constellation schemes. Therefore, in this section we analyse these schemes within the framework of the NC techniques, to compare them to our proposed design for differential phase-detection.

Let us start reviewing the features for these modulations to analyse the differences with our design. Particularly, they all have in common transmitting the total or part of the information on the amplitude (energy) of the signal.

3.7.1 Constellation for energy detection

The ASK scheme is the most commonly used model so far for the NC energy based detection schemes, although without making differential encoding. In this scheme, the information is conveyed in the signal amplitude and recovered by energy-based detection symbol-by-symbol, assuming known channel statistics. This NC detection is possible due to the high number of antennas.

The transmitter sends symbols belong to the constellation $\mathcal{P} = \{\sqrt{\mathfrak{p}_m},\ \ m = 1, \cdots, M\}$, being $\mathfrak{p}_m$ the energy levels. The signal received at the BS is as in (2.11), then, the decoder computes the average received power across all the antennas as $\frac{||y||^2}{R}$. From the Law of Large Numbers [41], it can be conclude the following decision statistic

$$\frac{||y||^2}{R} = \mathfrak{p} + \bar{\nu}. \tag{3.59}$$

In order to decide, the receiver divides the positive real axes into M non-intersecting intervals, so-called decoding regions, corresponding to each of the transmitted possible symbols, then, it chooses the symbol p_m related to the region or interval I_m to which $\frac{||y||^2}{R}$ belongs. To design the $\mathcal{P}$ constellation, we have to take into account that all available power levels p_m have to be transmitted with equal probability and there is an average power constraint specified as

$$\frac{1}{M}\sum_{m=1}^{M} \mathfrak{p}_m < 1. \tag{3.60}$$

This translates into

$$\begin{aligned} &\underset{P,\, I_m}{minimize}\ P_e \doteq \frac{1}{M}\sum_{m=1}^{M} P_e(\mathfrak{p}_m) \\ &subject\ to\ \frac{1}{M}\sum_{m=1}^{M}\mathfrak{p}_m = 1, 0 \leq \mathfrak{p}_m, \forall m, \end{aligned} \tag{3.61}$$

where P_e is the error probability.

To comply with the foregoing, the energy-designs consider also minimum distance decoding, deriving from (3.60) that the neighboring points in the individual constellation should be separated by

$$d_{min}^{ASK} = \frac{2}{M-1}. \tag{3.62}$$

This MD is bigger than that obtained by phase-designs. Using (3.62), the $\mathcal{P}$ constellation and its decoding intervals I are

$$\begin{aligned} &\left\{\mathfrak{p}_1 = 0, \mathfrak{p}_2 = \frac{2}{L-1}, \mathfrak{p}_m = \frac{2(m-1)}{M-1}, \mathfrak{p}_M = 2\right\} \\ &I_1 = [0, \frac{d_{min}}{2}), I_2 = [\frac{d_{min}}{2}, \frac{3d_{min}}{2}), \cdots, I_M = [2 - \frac{d_{min}}{2}, \infty). \end{aligned} \tag{3.63}$$

We compare a NC-ASK to our NC-DPSK aided m-MiMO system for single user, $\rho = 0$ dB and different sizes of constellation $M \in \{2, 4, 8, 16\}$ symbols. This analysis is shown in Figure 3.25. In all cases the required R for phase-detection (DPSK) is lower than for energy-detection, approximately 550 antennas less for $M = 4$, 1000 for $M = 8$ and over 10000 antennas less for $M = 16$. These results match with the expected ones, since DPSK has always been better than ASK from the single antenna case [43].

3.7.2 Combined constellations schemes

Now, let us compare DPSK to other schemes which include differential encoding and combine the energy detection with phase based detection. The DQAM scheme could also be regarded as a collection of designs which make differential encoding or only in the amplitude, or only in the phase or in both ones. These designs are based on a constellation scheme known as *star QAM*.

- **Star QAM:**

  This modulation is based on two concentric PSK constellations or rings, having two different amplitudes, a_0 and a_1 as shown in Figure 3.26. Star-QAM schemes having more than two PSK constellations are also referred to as Differential Amplitude and Phase-Shift Keying (DAPSK) schemes.

Figure 3.25 BER comparison between ASK and DPSK schemes for single user.

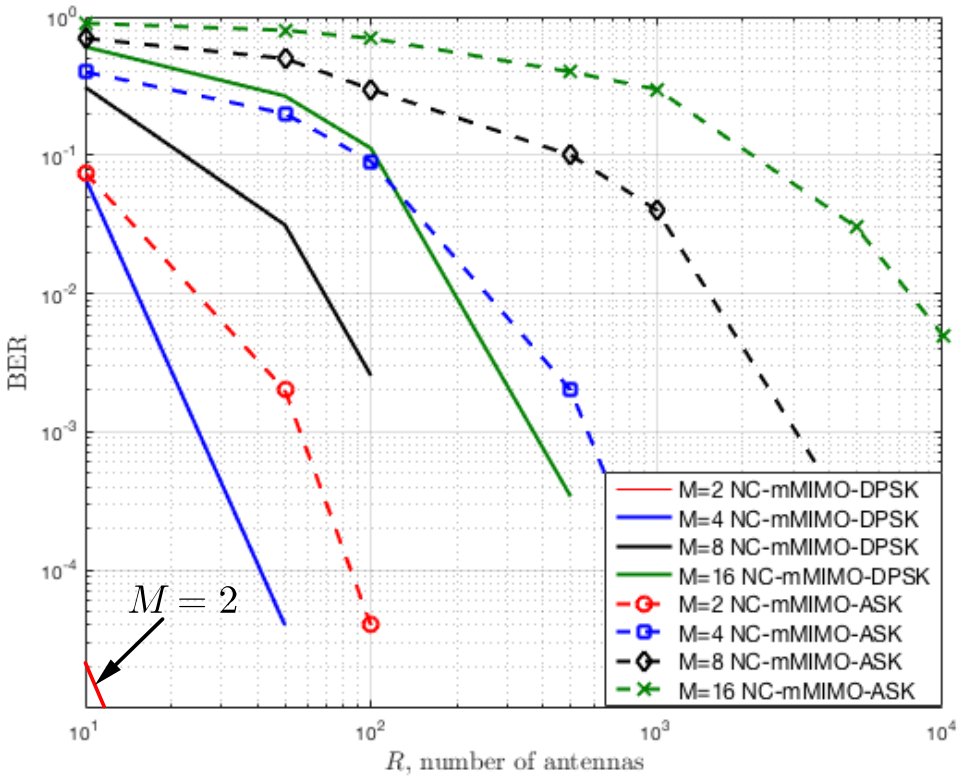

Figure 3.26 Constellation Star-QAM for $M=$ 16 symbols.

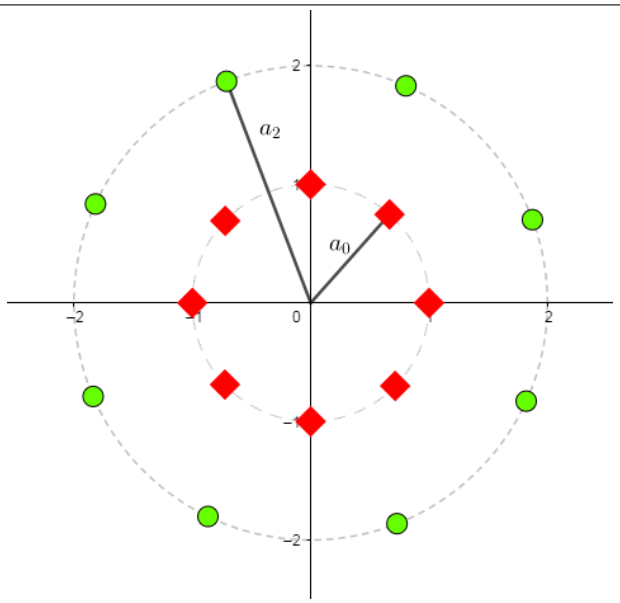

Similarly to any DPSK design, we have to insert a reference symbol at the beginning of each frame before transmitting a star-QAM symbol. Using as example a 16-star-QAM, we have two 8-PSK and we need four bits per symbol, b_0, b_1, b_2, b_3. The most significative bit (MSB) b_3 is used for selecting the amplitude of the PSK ring (a_0, a_1). If $b_3 = 0$ the amplitude remains the same as that of the previous symbol,

$a_n = a_{n-1}$, whilst for $b_3 = 1$ we have to switch to another ring. The phase is differentialy encoded as in (2.1). In this case, we have to make two detection: one for the amplitude and other one for the phase. First, we can detect the amplitude as

$$\frac{|y_n|}{|y_{n-1}|} \approx \frac{|a_n|}{|a_{n-1}|} \in \begin{Bmatrix} ring_0 = \frac{a_1}{a_1} \; or \; \frac{a_2}{a_2} = 1 \\ ring_1 = \frac{a_1}{a_2} \\ ring_2 = \frac{a_2}{a_1} \end{Bmatrix} \tag{3.64}$$

then, we detect the symbol received using PSK constellation corresponding to the ring selected in (3.64).

In star-QAM constellations, we may maximize the MD of the constellation by appropriately adjusting the ring ratios of the amplitude levels.

- **DQAM:**

  This scheme was first proposed by Weber [7] in 1978. We can achieve a DQAM scheme by applying the DPSK principle to the phases of Star QAM symbols, whereas the ring amplitudes of the Star QAM symbols are directly transmitted without differential encoding. This scheme was later denoted as absolute-amplitude DPSK (ADPSK) in [125] to distinguish it from those DQAM designs which make in addition differential encoding in the amplitude.

  As a result, the ADPSK receiver invokes a low-complexity NC detector, where the data-carrying phase is recovered by the CDD-DPSK techniques, which observes the phase changes between every pair of consecutive received samples determining the particular quadrant, and then the ring amplitude is demodulated by a quantizer within the detected quadrant.

  Star QAM constellations are preferred for DQAM design, since the phase angles of the square-QAM constellation points are not equispaced, which inevitably results in arbitrary phase rotations after differential encoding of the phase.

- **ADPSK or APSK**

  Absolute-Amplitude Differential Phase-Shift Keying only encodes the phase, being the amplitude transmitted without coding. In [125], a detector for m-MIMO using APSK is proposed. This is similar to that proposed here, but it has to consider the amplitude for the phase detection, which for the NC-m-MIMO-DPSK scheme is not needed reducing the complexity of the receiver. The detector proposed in [125] which we simulate is

$$(\hat{x}_{t-1}, \hat{x}_t) = arg \min_{x_{t-1}, x_t \in M} \left| \frac{r_t}{\alpha} - x_t x_{t-1}^* \right|. \tag{3.65}$$

- **DAPSK:**

  The DAPSK scheme is particularly advantageous for NC communications since its coherent QAM counterpart suffered from a realistic channel estimation error. In addition, it exhibits a benefit because of its low signal detection complexity as well. This is due to the fact that the separate detection of the amplitude and the phase of a received symbol exhibits lower complexity than jointly detecting the two terms. However, it was observed in [4] that the performance of CDD-DAPSK degrades, and eventually, an error floor is formed in Rayleigh fading channels, when the Doppler frequency f_D is increased. As we will see in Chapter 6, f_D does not have any effect on our NC proposal. To further improve the CDD performance, the classic DFDD presented in the state of the art for DPSK in [8] and [9] was further developed for DAPSK in [10]-[12].

Figure 3.27 BER comparison among APSK, DAPSK and DPSK for M= 16 and single user.

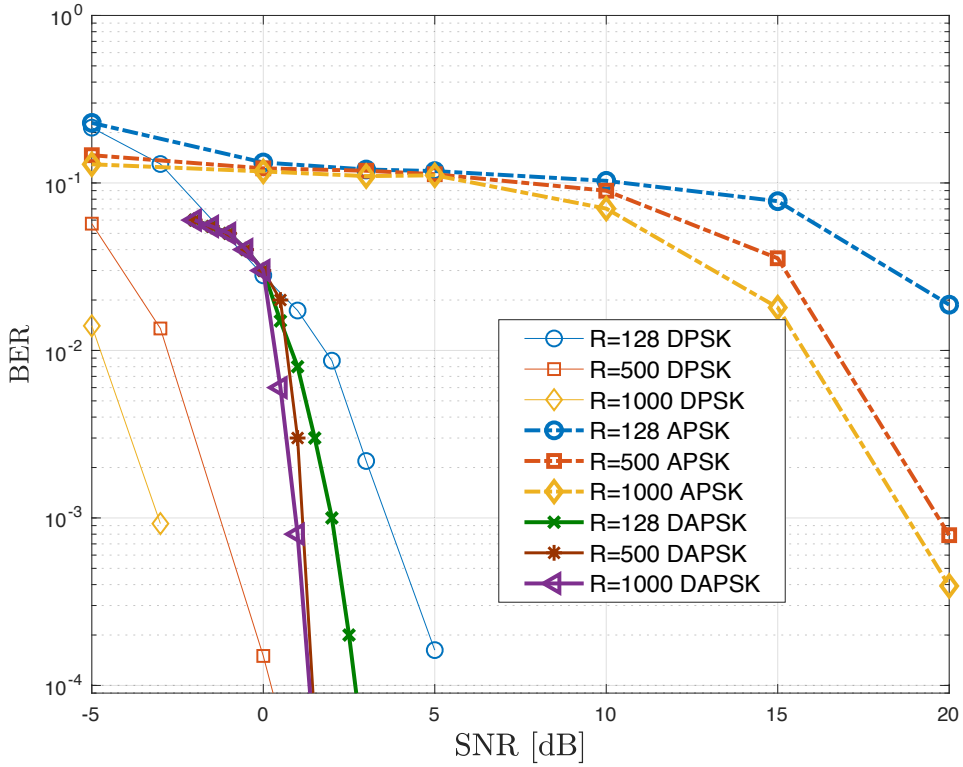

In Figure 3.27, a comparison among APSK, DAPSK and our DPSK proposal is shown for $M = 16$, $R = 128$, 500 and 1000 antennas and single user. We can see that for APSK scheme increasing over 500 antennas we do not have any improvement on the performance, mMIMO does not help. In addition, we need a high SNR with respect to DPSK to the same BER. By contrast, the difference between DPSK and DAPSK is not too abrupt. For $R = 128$ antennas, DAPSK shows a better performance than DPSK, conversely, similar

to APSK, DAPSK does not offer any improvement over 500 antennas. For low SNR, DAPSK solves the demodulation better than DPSK.

3.7.3 Analysis of the complexity

For each scheme we computed their complexity in terms of signal processing as the number of multiplications and comparison the receiver performs. In general, these numbers depend on the number of levels of amplitude M_A and number of phases M_P as $M = M_A M_P$. In the case for purely energy based detection, such as ASK schemes, $M_P = 1$ then the complexity is $M = M_A$, while for DPSK the complexity is $M = M_P$ with $M_A = 1$. These schemes do not perform $M = M_A M_P$ comparisons and no multiplication.

Although APSK shows worse performance due to the fact the amplitude is not encoded, it performs $M_A + M_P$ comparison and one multiplication for each received sample, less than DPSK schemes and the same as DAPSK. Another advantage over conventional QAM for practical implementation is that APSK presents a lower number of possible amplitude levels, resulting in fewer problems with non-linear amplifiers. Conversely, DPSK has only one power lever, not showing problems for the amplifier.

3.8 Conclusions

Novel constellation designs are proposed for a multiuser non coherent m-MIMO uplink scenario that allow us to separate the users' signals at the receiver thanks to a one-to-one correspondence between the constellation for each user and the joint constellation in the receiver. The designs consist in the multiplexing of users in the constellation, intercaling the symbols belonging to them. Two approaches are considered: in terms of BER, each user achieves a different performance and, on the other hand, the same performance is provided for all users.

For the UEP designs, in addition, the variation in the received power for different users allows us to set up uneven error correction schemes. In the EEP case, the design does not rely on strict power control and yet provides the same performance for all users. We have analyzed the number of antennas required by all designs. This number depends on the minimum distance between symbols in the individual constellation, not on the characteristics of the joint constellation. Also we probe that the number of antennas is more influential that the SNR on the performance. The UEP designs usually require more antennas than EEP schemes, taking into account that this number tends to the same value for both designs as the minimum distance in UEP approximates to the EEP one.

We have analyzed the interference and SINR for these designs. We derivate the error probability for NC-m-MIMO as a function of minimum distance, SINR and the total interference, providing some performance bounds for our designs.

We have shown that our proposal performs better than the benchmark of the designs based on energy detection [97,98,105,126] regarding BER. Conversely, they show a similar performance to other constellations which perform differential encoding, such as APSK, DAPSK. However, these designs are more susceptible to the noise since they use the amplitude to convey the information, whilst in DPSK only the phase is used. APSK gets worse performance than DAPSK and DPSK, whilst DPSK for high R is better than DAPSK, their performance tends to be the same as BER is lower. Other advantage for our designs is that they are able to operate in multiuser environment by multiplexing multiple users in the constellation, whilst the other designs, APSK, DAPSK or DQAM, are considered only for single user. This increases the capacity of the DPSK systems. In addition, our proposals are not far from the performance of an equivalent coherent system operating under realistic channel assumptions.

Chapter 4

Channel Coding Schemes for multiuser non coherent massive MIMO systems based on DPSK for Rayleigh Channels

In the previous chapter the performance for multi-user NC-m-MIMO systems based on DPSK without coding was shown for Rayleigh channels. The simulation results showed a good performance against their coherent counterparts, validating the non coherent detection in massive MIMO aided differential phase. In addition, these novel constellation designs outperformed the schemes based on energy detection. However, the number of antennas needed to achieve a reasonable performance is much too large for a feasible communication system. Therefore, in this chapter we propose a powerful encoding scheme based on the principle of bit-interleaved coded modulation and iterative decoding (BICM-ID) [127] as novelty for NC m-MIMO aided DPSK with the objective of reducing the number of antennas R by channel coding. We will design this encoding scheme based on EXIT-curves, providing a new approach for this tool in the non coherent m-MIMO field.

First, we review the concept and principles of BICM and iterative decoding and detection techniques. Then, we present the channel coding scheme proposed over the reference system model shown in Chapter 2. In order to exchange information in the iterative decoding procedure, we need soft information in form of *log-likelihood ratio (LLR)*, which are derived for non coherent detection. Consecutively, we present the new approach of the EXIT chart for our proposal. Finally, we analyse the performance and the capacity of a NC-m-MIMO system aided DPSK with channel coding.

4.1 Principles of BICM-ID coding schemes

Bit-interleaved coded modulation (BICM) technique was first introduced by Zehavi in [128]. This technique belongs to coded modulations group, which has as goal the joint design of coding and modulation. In coding, the diversity order of a code is defined as the minimum Hamming distance of the code, or equivalently, the number of different symbols between the shortest erroneous path and the correct path (error free event) in the decoding procedure. The difference with other coded modulations, such as trellis coded modulation (TCM) [129], is that BICM interprets the diversity order of a code equal to the smallest number of different bits, instead of the different symbols, by employing independent bit-based interleaving rather than symbol. The bit error probability is lower in Rayleigh fading channels than that of TCM that maximizes the euclidean distance, due to the fact that BICM scheme operates at bit-level. Thus, BICM maximizes the minimum Hamming distance.

As shown in Figure 4.1, a message vector **u** is encoded into a codeword **c**, interleaved by the random bit interleaver π generating **c'**. Then the stream **c'** is grouped by serial-parallel conversion and fed through the modulator, which includes a sophisticated mapping scheme to produce the symbols **x** to be transmitted.

Figure 4.1 BICM-ID system schematic.

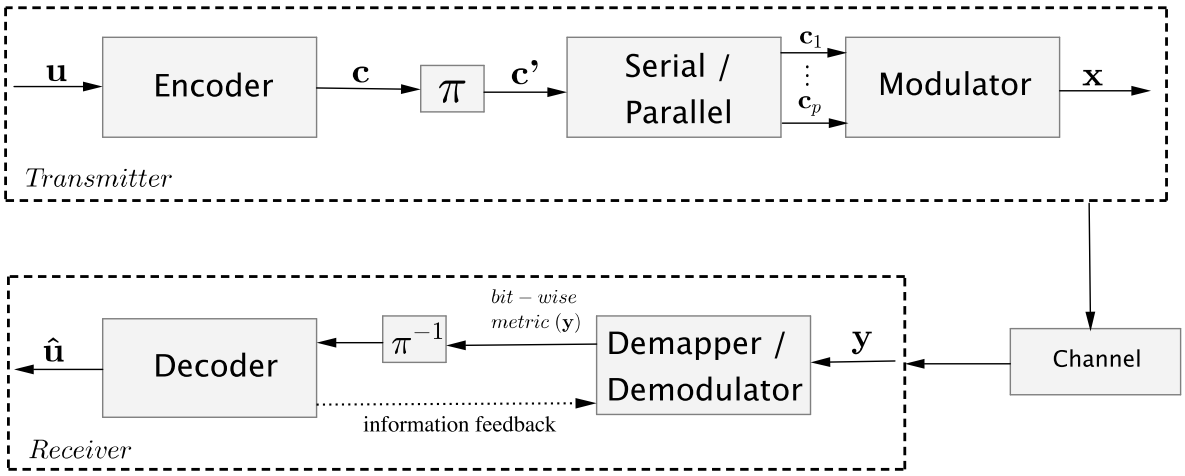

In the receiver we can have a significant performance gain including iterative decoding at the cost of increased complexity but still at reasonable level, also referred in the literature as "turbo principle". This technique consists in concatenating Recursive Systematic Convolutional codes with interleavers between the constituent encoders. First, they were placed in parallel [130] and then it was extended to serially concatenated convolutional codes [131]. BICM using Iterative Decoding (BICM-ID) was proposed by Li in [127] in order to further improve the BICM scheme. This improvement is achieved first with an

appropriate mapping scheme between the interleaved bits and the phasor constellation and, secondly, with an iterative information exchange between the decoder and the demodulator as illustrated in Figure 4.1, improving the reliability of the information passed from the channel decoder to the demodulator in each iteration. Hence, once the received stream $\mathbf{y}$ is demapped, in contrast to other coded modulation schemes, a bit-level metric is derived, deinterleaved by π^{-1} and passed to the decoder to generate the extrinsic information which is fed back to the demapper. In the last iteration, the decoder returns the estimated message vector $\hat{\mathbf{u}}$.

In Section 4.3 we calculate the metric for the baseline non coherent m-MIMO system based on DPSK proposed in this work. In Section 4.4, we design the BICM-ID scheme that best suits the constellations proposed in the Chapter 3 with the help of the EXIT chart tool and their performance will be evaluated for transmission over Rayleigh channels.

4.2 System model including the channel coding scheme

Having described the operating principles of a BICM-ID scheme in the previous section, the channel coding block in the baseline system proposed in Chapter 2 is replaced by a BICM-ID scheme as it is shown in Figure 4.2.

Figure 4.2 BICM-ID transmitter model for non coherent multi-user massive MIMO system with J users.

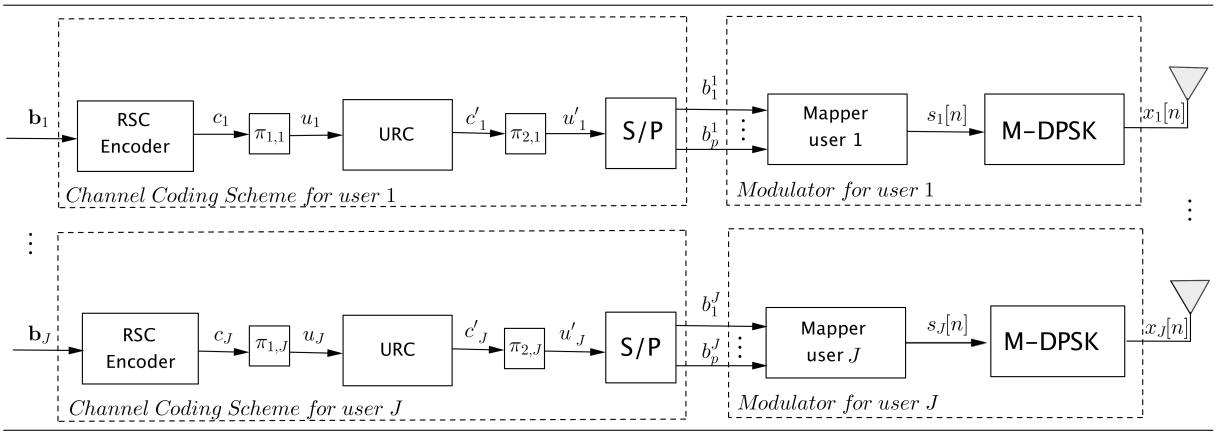

In this design we use a serial concatenation between encoders for the turbo-codes as shown in Figure 4.2. A block of bits $\mathbf{b}_j$ belong to user j is encoded by a Recursive Systematic Convolutional (RSC) code (outer encoder) generating the bit stream c_j, which is then interleaved by the first random bit interleaver $\pi_{1,j}$. The interleaved sequence u_j is then fed through the Unity-Rate Code (URC) encoder (inner encoder), where the coded bits c'_j at the output of the URC are interleaved by the second random bit interleaver $\pi_{2,j}$, producing the bit stream u'_j. The URC encoder is introduced for avoiding the bit error

rate (BER) floor because its infinite duration impulse response efficiently randomizes the extrinsic information provided for Bahl-Cocke-Jelinek-Raviv (BCJR) decoder [132]. The design details for outer encoder and inner encoder are presented in Subsection 4.4.2 and Subsection 4.4.4 respectively, where we argue about the importance and why we need both encoder types, in particular an URC encoder. After bit interleaving, the bits are grouped in sets of p bits, $\{b_1^j, b_2^j, ..., b_p^j\}$, by serial-parallel conversion to be mapped to symbols $s_j[n]$. These symbols are independent of each other and belong to an M-ary constellation $\mathfrak{M}_j$, which may in fact be different for each user, as we explained in previous chapters.

Figure 4.3 BICM-ID receiver model for non coherent multi-user massive MIMO system for J users

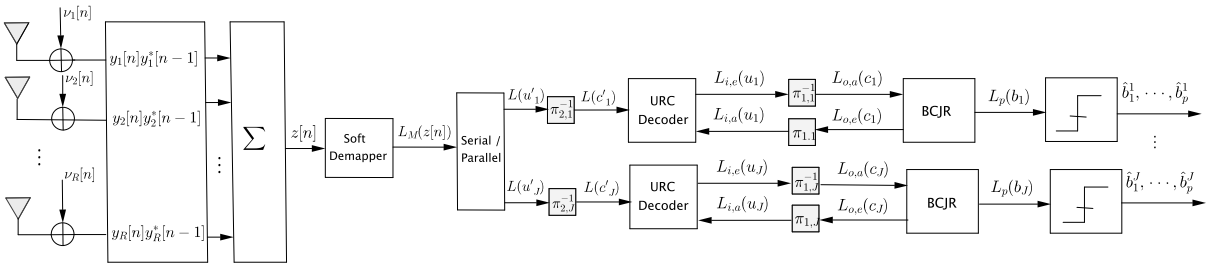

At the receiver of Figure 4.3 the non coherent detection, just like the case without coding in Chapter 3 is performed jointly for all users to obtain the decision variable $z[n]$ (3.1), which is delivered to the *soft-demapper block*. This block calculates, from the symbols $z[n]$, the soft information for each coded bit of the joint symbol ς, which is expressed in form of $L = LLR_q$ for the q^{th} bit[1]. Hence, from $z[n]$, the set $L_M = \{LLR_q\}_{q=0}^{l}$ is obtained where l is the number of LLR per joint symbol, $l = J \log_2 M$ and M is the order of the individual constellation $\mathfrak{M}_j$. Then the LLRs of each user $L(u'_K)$ are obtained from the set of l values in L_M by a serial-parallel conversion. This separation for each user and the details for non coherent derivation of LLRs are presented in Section 4.3.

After non coherent detection, the decoding process is carried out independently for each user. The URC decoder processes the information provided by the soft demapper, deinterleaved by $\pi_{2,j}^{-1}$, in conjunction with the *a priori* information $L_{i,a}(u_j)$ passed back to it from the RSC decoder, in order to generate the extrinsic LLRs $L_{i,e}(u_j)$. Then, the LLRs $L_{i,e}(u_j)$ are deinterleaved by a soft-bit deinterleaver $\pi_{1,j}^{-1}$, as seen in Figure 4.3. Next, the soft-bit values $L_{o,a}(c_j)$ are passed to the RSC decoder in order to compute the extrinsic LLRs $L_{o,e}(c_j)$. The RSC decoder invokes the BCJR algorithm [132]. During the last iteration, only the *a posteriori* LLR values, $L_p(b_j)$, of the original uncoded systematic information bits are required, which are passed to a hard decision decoder in order to determine the estimated transmitted source bits $\hat{\mathbf{b}}_j$.

[1]Hereinafter, L corresponds to LLR.

4.3 Derivation of LLR for NC schemes in m-MIMO and DPSK

The *soft-demapper block* in Figure 4.3 is responsible for calculating from the symbols $z[n]$ the soft information corresponding to each coded bit q of the joint symbol $\varsigma[n]$, meaning, the set $\{LLR_q\}_{q=0}^{l}$. The LLRs are defined as the logarithm of the ratio of the probabilities of the q^{th} bit assuming its two legitimate values conditioned to $z[n]$. According to [133], the LLRs can be defined as follows

$$LLR_q \triangleq \log \frac{P(q=0|z[n])}{P(q=1|z[n])} \tag{4.1}$$

where $P(q|z[n])$ is the conditional probability density function (pdf). Particularizing for the joint constellation $\mathfrak{M}$ each LLR can be written as follows

$$LLR_q = \log \frac{\sum_{\varsigma \in \mathfrak{M}_q^{(0)}} p(z[n]|\varsigma)}{\sum_{\varsigma \in \mathfrak{M}_q^{(1)}} p(z[n]|\varsigma)}, \tag{4.2}$$

where $\mathfrak{M}_q^{(b)}$ is the subset of $\mathfrak{M}$ with the q^{th} bit having the value of $b=0$ or $b=1$.

By using Bayes' rule we can obtain the conditional pdf $p(z[n]|\varsigma)$ from $P(q|z[n])$, which obeys the next Gaussian distribution

$$p(z[n]|\varsigma) = \frac{1}{2\pi\mathfrak{I}} \exp\left(\frac{-|z[n]-\varsigma|^2}{2\mathfrak{I}}\right), \tag{4.3}$$

where $\mathfrak{I}$ is the interference plus noise variance. As well, we use the max-log approximation formulated as

$$\ln(e^A + e^B) = max(A,B) + \ln(1 + e^{(-|A-B|)}) \approx max(A,B), \tag{4.4}$$

explained in [132] for BCJR algorithm in logarithm domain, for the sake of converting multiplications to additions. The losses stemming from max-log approximation are analyzed in [134]. With all this we can derive the LLR for bit q as follows

$$LLR_q = \log \frac{\underset{\varsigma \in \mathfrak{M}_q^{(0)}}{max}\ p(z[n]|\varsigma)}{\underset{\varsigma \in \mathfrak{M}_q^{(1)}}{max}\ p(z[n]|\varsigma)} = -\frac{1}{\mathfrak{I}}\left(\underset{\varsigma \in \mathfrak{M}_q^{(0)}}{min}|z[n]-\varsigma|^2 - \underset{\varsigma \in \mathfrak{M}_q^{(1)}}{min}|z[n]-\varsigma|^2\right). \tag{4.5}$$

We can observe that this metric is the same as for a coherent system with the advantage that channel information is not necessary because of the scaling laws of m-MIMO. where the channel effects have disappeared due to (2.18) (2.20) and (3.2).

Once we have the set of l LLRs values in L_M for each joint symbol ς, then the LLRs of each user $L(u'_J)$ are obtained by a serial-parallel conversion. This is done by grouping

l/J consecutive values for each user. This way of separating the individual symbols from the joint symbols is due to the labelling used in the mapping of the joint symbol in connection with each individual user's labelling at the transmitter. Remember from Section 2.4.2 that the joint labelling is formed by concatenating the individual labelling (an example for building the joint constellation was shown in that section).

From the point of view of the soft information, if we have J=3 users and M=4, where user 1 transmits the pair of consecutive bits $\{u_1^{'(1)}, u_1^{'(2)}\}$, the user 2 transmits $\{u_2^{'(1)}, u_2^{'(2)}\}$ and the user 3 transmits $\{u_3^{'(1)}, u_3^{'(2)}\}$, then the labelling of the joint symbol is the serial concatenation formulated as

$$\{u_1^{'(1)}, u_1^{'(2)}, u_2^{'(1)}, u_2^{'(2)}, u_3^{'(1)}, u_3^{'(2)}\}.$$

Then, when we have the soft-values $L_M = \text{“}\underbrace{LLR_1, LLR_2}_{user1}, \underbrace{LLR_3, LLR_4}_{user2}, \underbrace{LLR_5, LLR_6}_{user3}\text{”}$, the separation for each individual user gives $L(u_1^{'}) = \text{”}LLR_1, LLR_2\text{”}$, $L(u_2^{'}) = \text{“}LLR_3, LLR_4\text{”}$ and $L(u_3^{'}) = \text{”}LLR_5, LLR_6\text{”}$.

In order to employ the EXIT chart the pdf of the a priori LLR values has to be Gaussian, which depends on the interleaver length (Section 4.4.1). We simulate the system shown in Figure 4.2 and Figure 4.3. At each iteration, we plot the histogram of the LLRs for checking their distribution. As an example, we plot the distribution for an iteration in the decoding procedure in Figure 4.4, where we can see that the distribution for the a priori LLRs is Gaussian with zero mean.

Figure 4.4 Probability density function for *a priori LLR* values.

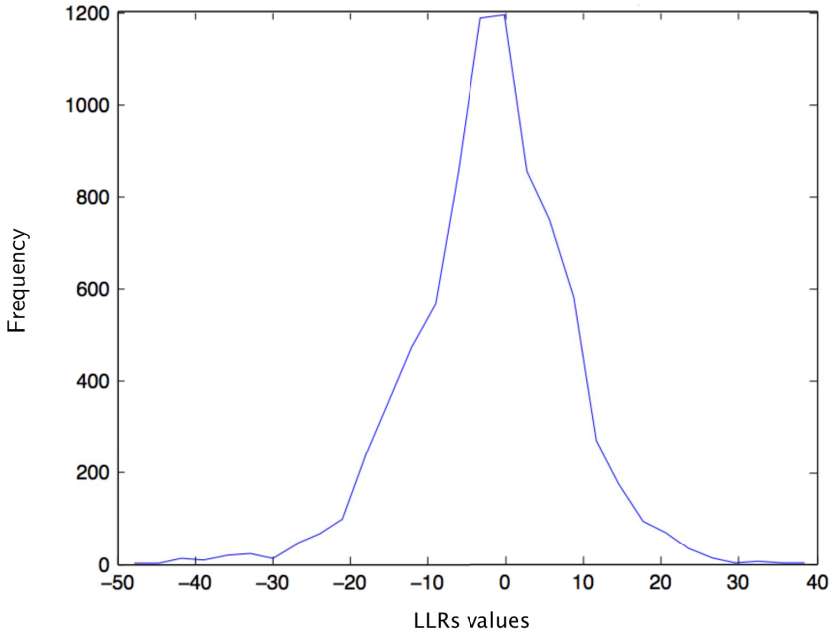

4.4 New approach of EXIT chart tool in massive MIMO

The EXtrinsic Information Transfer (EXIT) chart concept was first proposed by Stephan ten Brink in [135], which constitutes a powerful tool for designing and analyzing iteratively decoded systems. A comprehensive tutorial is provided in [133] on the design of systems based on EXIT-curves. However, in this work we present a new approach of EXIT tool focused for m-MIMO.

The purpose of using the EXIT charts is to predict the convergence behavior of the iterative decoder, composed of both parallel or serially concatenated encoders. This is achieved by examining the evolution of the input/output mutual information (MI) exchange between the constituent decoders in consecutive iterations. The average MI represents the average amount of source information X acquired per received symbol Y, defined by information theory in [136] as

$$I(X,Y) = \sum_{i,j} P(X_i, Y_j) \cdot \log_2 \left(\frac{P(X_i/Y_j)}{P(X_i)} \right) \quad bits/symbol, \tag{4.6}$$

where $P(X_i, Y_j)$ is the joint probability that X_i was transmitted and Y_j was received. $P(X_i)$ is the probability of transmitting X_i and $P(X_i/Y_j)$ is the conditional probability that the Y_j was received given that X_i was transmitted. In order to plot the EXIT chart, we have to derive the MI between the bit stream and its corresponding L soft-values. It was shown in [137] that the MI between the general equiprobable bits X and their respective LLRs L always obeys

$$\begin{aligned} I(X,L) &= 1 - \int_{-\infty}^{+\infty} p(L|X=+1) \cdot \log_2[1+e^{-L}]dL \\ &= 1 - E\{X=+1\}\log_2[1+e^{-L}], \end{aligned} \tag{4.7}$$

where $E\{X\}$ is the expected value of X. Henceforth, the bit stream X is associated with the coded bits $\mathbf{c}$ or $\mathbf{u}$ in Figure 4.2, depending on whether we are talking about outer or inner encoder, respectively. The L-values have to obey a symmetric distribution of $p(L|X=\pm 1)$ and to satisfy the consistency condition defined in [137]. The closer to 1 MI is, the more accurate the iterative decoding, then the lower BER is. There are two main methods to compute the MI in (4.7): the histogram based approximation [138, 139] and the method based on time averaging [137]. We employ in this work the time averaging method which has the advantage of not requiring any knowledge of the input bit sequence $\mathbf{b}$.

Thus far, the contributions which use EXIT tool to design iteratively decoded systems, built the EXIT-curves based on SNR. Conversely, in this thesis we propose a new approach

to build the EXIT-curve, this is based on the number of antennas R to measure and represent the nature of a m-MIMO system.

4.4.1 Construction of the EXIT chart for non coherent schemes in massive MIMO and DPSK

In order to obtain the EXIT chart, we have to develop two functions: one for the outer curve represented by the first channel encoder in the transmitter shown in Figure 4.2, corresponding RSC encoder family; and the other one for the inner curve formed by URC encoder in conjunction with mapper, both with their respective decoder shown in Figure 4.3.

In Figure 4.5 is shown an example of EXIT chart with the parameters which influence on the system design, which are: the two curves introduced before (inner and outer), the open tunnel and the decoding trajectory. In general, the inner curve depends on the channel and the SNR, however in this work as novel we built this curve without knowledge of the channel and for the number of antennas R, as will be detailed in Section 4.4.4. The open tunnel is a condition which must be fulfilled to decode the information. This condition entails that both encoder-curves can not be crossed each other. The colored area between both curves in Figure 4.5 represents the open tunnel. The decoding trajectory determines the number of iterations N_I which are required to achieve the BER convergence to infinitely low value. In the EXIT chart shown as example in Figure 4.5 we can see seven iterations, but due to the fact that both curves are close and the tunnel is very narrow in the final end, causing a large number of iterations making the iterative decoding difficult.

Figure 4.5 Design parameters in an example of EXIT chart.

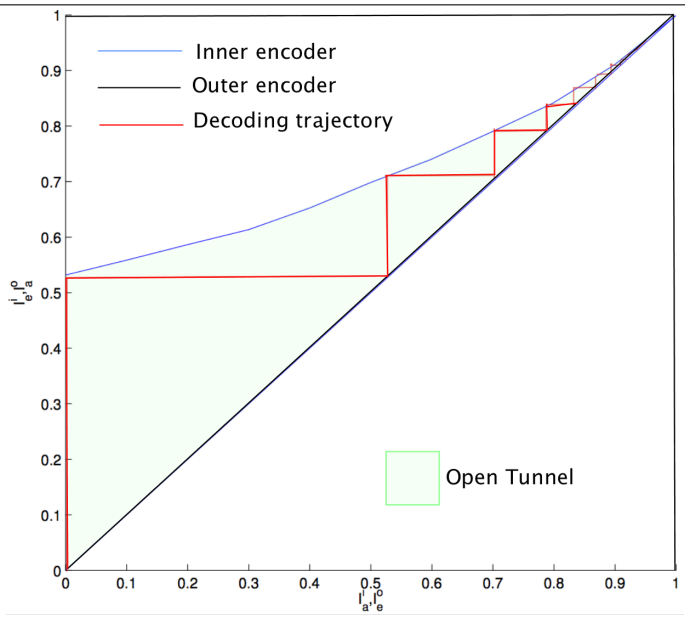

In addition, another parameter which we have to take into account is the depth of the interleaver between encoders. This parameter has relevance in the accuracy of the outer and inner curves as shown in Figure 4.6, since L-value distribution may be or not gaussian as explained Section 4.3.

Figure 4.6 Interleaver depth effect on EXIT curves for inner and outer decoder used by a transmission over Rayleigh m-MIMO channel.

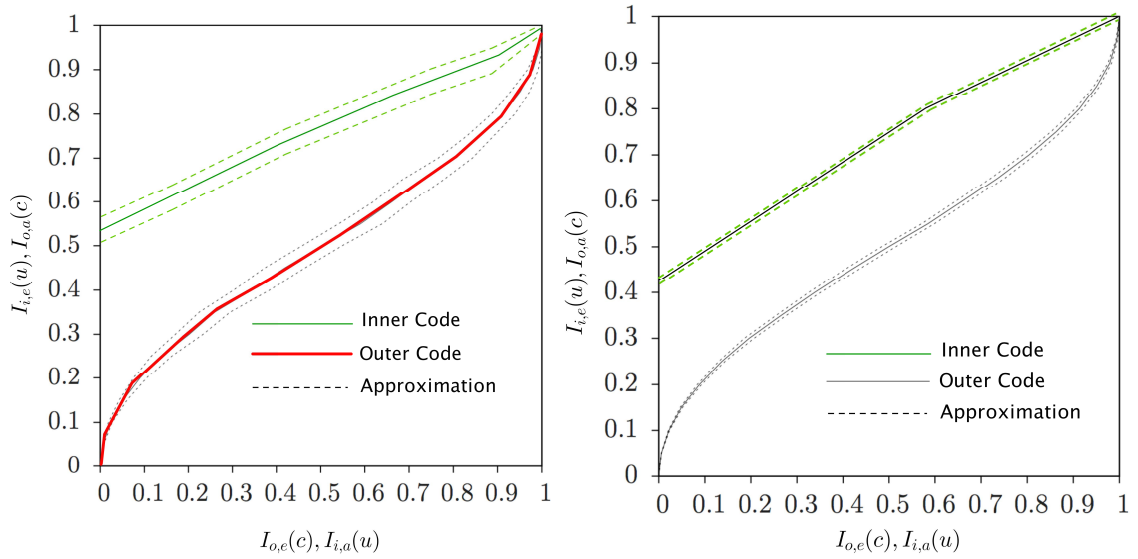

(a) 100 bits (b) 1000 bits

In the following, we give an explanation to build each curve in the EXIT chart dispensing with the CSI, corresponding to non coherent systems. We will now see the detailed description for each parameter of EXIT chart.

1) Transfer characteristics of the RSC decoder (outer, subindex o):

The EXIT characteristic of the RSC decoder in Figure 4.3, as outer function, describes the relationship between the RSC *a priori* input $L_{o,a}(\mathbf{c})$ and the RSC extrinsic output $L_{o,e}(\mathbf{c})$. In the full system shown in Figure 4.3, RSC decoder receives $L_{o,a}(\mathbf{c})$ by a single input from the URC decoder. Therefore, the EXIT characteristics of the outer channel decoder are independent of the reference SNR value, ρ, and hence may be written as

$$I_{o,e}(\mathbf{c}) = T_o[I_{o,a}(\mathbf{c})], \tag{4.8}$$

where $I_{o,a}(\mathbf{c}) = I[c; L_{o,a}(\mathbf{c})] \in [0,1]$ is the MI defined in (4.7) between the RSC coded bits $\mathbf{c}$ and the *a priori* L-values $L_{o,a}(\mathbf{c})$ and in the same way, $I_{o,e}(\mathbf{c}) = I[c; L_{o,e}(\mathbf{c})] \in [0,1]$ is the MI (4.7) between the RSC coded bits $\mathbf{c}$ and the extrinsic L-values $L_{o,e}(\mathbf{c})$. The EXIT

characteristic (4.8) is calculated for a specific $I_{o,a}$ using (4.7) as

$$\begin{aligned} I_{o,e}(\mathbf{c}) &= I[c; L_{o,e}(\mathbf{c})] \\ &= 1 - E\{\log_2[1 + e^{-L_{o,e}}]\} \\ &\approx 1 - \frac{1}{N}\sum_{n=1}^{N} \log_2[1 + e^{-c(n)\cdot L_{o,e}(n))}] \end{aligned} \tag{4.9}$$

where N is the number of bits forming an input message.

The schematic represented in Figure 4.7 is to plot and evaluate the EXIT curve of the outer RSC channel decoder in isolation. We generate sequences of a priori L, $L_{o,a}(\mathbf{c})$, using a set of MI $I_{o,a}(\mathbf{c}) \in [0, 1]$ which simulates the information from URC. The RSC decoder provides the extrinsic soft information $L_{o,e}(\mathbf{c})$ which is delivered for computing the MI in combination with coded bits $\mathbf{c}$ by (4.9) to get $I_{o,e}(\mathbf{c})$.

Figure 4.7 Schematic of EXIT chart for generating the outer curve (RSC decoder).

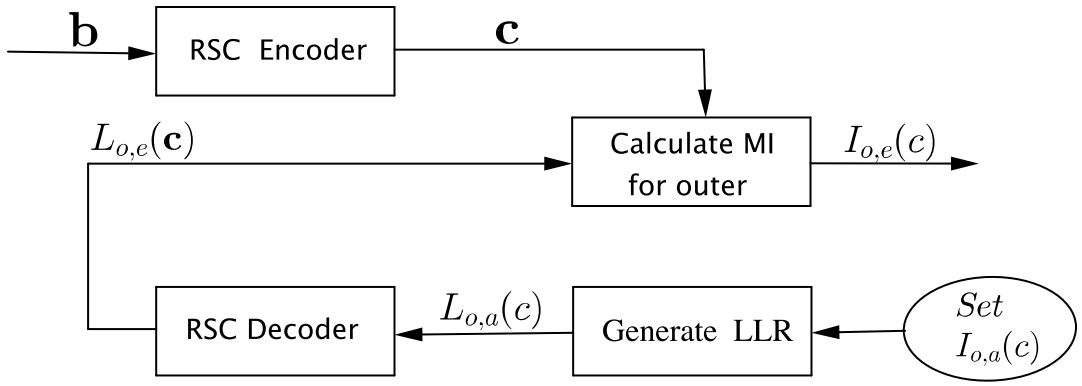

Finally, the EXIT chart for outer code is plotted with its input $I_{o,a}(\mathbf{c})$ on the horizontal axis and its output $I_{o,e}(\mathbf{c})$ on the vertical axis, as in example EXIT chart in Figure 4.5.

2) Transfer characteristics of the demapper (inner, subindex i):

Generally, the modulator block (mapper and MDPSK) serves as inner encoder/decoder without considering URC encoder. In order to quantify the information content of the outer code as well as interleaved bits $\mathbf{u}$ and the extrinsic LLR values $L_{i,e}(\mathbf{u})$ at the output of the demapper, the MI $I_{i,e}(\mathbf{u}) = I[U; L_{i,e}(\mathbf{u})]$ can be used. Based on this MI, the demapper's extrinsic information transfer characteristic is defined in [133] as

$$I_{i,e}(\mathbf{u}) = T_i[I_{i,a}(\mathbf{u}), E_b/N_0], \tag{4.10}$$

where reference E_b/N_0 was defined for the system model in (2.15) including the channel coding scheme. Note that the MI for the demapper is a function of both the *a priori* information $I_{i,a}(\mathbf{u})$ and the Eb/N_0. The latter is replaced by the SINR for our system,

which depends on the number of antennas R as defined in (3.36). Then, the function (4.10) for our particular m-MIMO system translates to

$$I_{i,e}(\mathbf{u}) = T_i[I_{i,a}(\mathbf{u}), SINR] = T_i[I_{i,a}(\mathbf{u}), R, \rho]. \tag{4.11}$$

Using again the time averaging method to compute the MI just like for the outer code, the extrinsic MI for the inner code is derive as follows

$$\begin{aligned} I_{i,e}(\mathbf{u}) &= I[u; L_{i,e}(\mathbf{c})] \\ &= 1 - E\{\log_2[1 + e^{-L_{i,e}}]\} \\ &\approx 1 - \frac{1}{N}\sum_{n=1}^{N} \log_2[1 + e^{-u(n)\cdot L_{i,e}(n))}] \end{aligned} \tag{4.12}$$

We can combine (2.14) and (3.36) to obtain the SINR as a function of the reference SNR as

$$SINR = \frac{R}{J^2}\frac{\rho^2}{\rho^2 + 2\rho + 1}, \tag{4.13}$$

which in turn depends on E_b/N_0 by (2.15). The exchange of extrinsic information in the system of Figure 4.3 can be visualized by plotting the EXIT characteristics of the inner demapper and the outer RSC decoder in an EXIT chart [140]. The outer RSC decoder's extrinsic output information $I_{o,e}(\mathbf{c})$ becomes the demapper's *a priori* input information $I_{i,a}(\mathbf{u})$. Similarly, we plot the demapper's extrinsic output information $I_{i,e}(\mathbf{u})$, which becomes the outer RSC decoder's *a priori* input information $I_{o,a}(\mathbf{c})$.

In the case that the EXIT curve of the inner demapper and the outer RSC decoder, explained in (4.8) are intersected before reaching the (1.0, 1.0) point of the perfect convergence, the error probability curve will not exhibit a steep turbo-cliff shape that we expect in a BICM-ID system. Therefore, we have to include an additional recursive inner encoder/decoder component in order to reach the point of the perfect convergence. In this way, an error probability as low as desired can be achieved. This new component is the URC encoder in Figure 4.2 and Figure 4.3. In the following sections, we will see in the performance analysis how an URC is necessary for our proposed NC system.

In order to plot and evaluate the EXIT characteristic represented in (4.11), we use the schematic illustrated in Figure 4.8. A random bit stream $\mathbf{u}$ is generated to simulate the bits from outer encoder and the first interleaver π_1. This bit stream continues the same process to be transmitted as that explained for the system model in Figure 4.2. Through m-MIMO channel we receive the symbols y which are non coherently detected and follow until being decoded by URC decoder. Unlike RSC encoder, an inner decoder (URC) has two inputs: the detected and demapped symbols in form of LLR, $L(c')$, and the L-values generated from *a priori* MI $I_{i,a}(u) \in [0, 1]$ for the inner code (which simulates the *a priori* information $L_{i,a}(u_j)$ passed back to it from the RSC decoder), in order to

Figure 4.8 Schematic of EXIT chart for generating the inner curve (URC decoder + demapper).

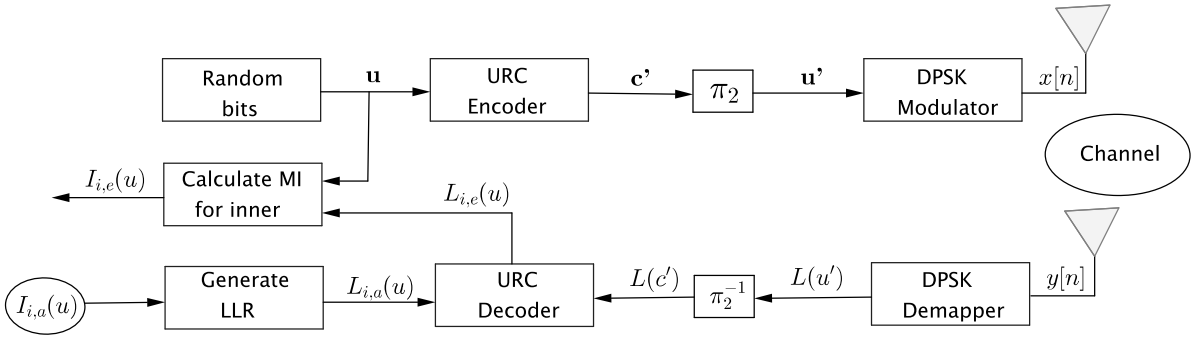

generate the extrinsic LLRs $L_{i,e}(u_j)$. Then, the MI $I_{i,e}(u)$ in (4.12) is obtained with the extrinsic L-values and the random initial bits.

Finally, the EXIT chart for inner code is plotted with its input $I_{i,e}(\mathbf{u})$ on the horizontal axis and its output $I_{i,a}(\mathbf{u})$ on the vertical axis. The a priori and extrinsic information is reversed with respect to the outer curve.

3) Decoding trajectory:

The predictions about the BER convergence that are made by using the EXIT chart can be verified looking at the iterative decoding trajectory. This represents the actual extrinsic information transfer between the inner and outer decoders. The open tunnel and the decoding trajectory are related: the narrower the tunnel, the more iterations are required for reaching the perfect convergence point. The more iterations are required to reach the perfect point (1,1), the more complexity in the receiver to decode the information. The perfect point implies that given $I_a = 1$, inner or outer, we have $I_e = 1$, then BER approaches the channel capacity.

Sometimes in order not to assume such complexity in the receiver it might be interesting to consider increasing the number of antennas R for the sake of broadening the open tunnel. Consequently decreasing R entails more iterations in the receiver. In the design we have to make a tradeoff for R and the N_I. Obviously, in turn these two parameters depend on the encoder chosen with the inner/outer curves.

4) Collecting three curves in EXIT chart:

Once we have plotted all curves in EXIT chart for the encoders of interest, we follow the flow shown in Figure 4.9 and explained in Algorithm 1 in order to select the best pair of encoders available for our proposal. In Figure 4.10, a series of EXIT functions are represented to illustrate the procedure of encoder selection for a reference $E_b/N_0 = 10$ dB. The first case in Figure 4.10(a) is for a $1/2 - rate$ CC as outer code and an URC

encoder[2] type 1 as inner code for which we plot the inner curve for an example mapping scheme ϕ_1 and $R = 50$ antennas. We can notice in Figure 4.10(a) that the (1,1) point is not reached, then we select another mapping scheme, ϕ_2, which achieves an open tunnel, hence we compute $N_I = 3$ iterations for $R = 50$ antennas. Although Figure 4.10(b) allows the decoding, we increase up to $R = 100$ antennas, reducing N_I to 1 iteration. In this point, we choose 100 antennas and less iterations, since this number of antennas it is still manageable for a practical array.

In the second case, Figure 4.10(b), we increase the coding rate using a $4/5 - rate$ CC outer code. The reduction of the channel coding involves an increase of R. Similarly to the above case, now for 50 antennas both curves reach to (1,1), but they are crossing, then we increase the number of antennas for the same mapping scheme. For $R = 90$, we have open tunnel, then we compute $N_I = 6$ iterations. Conversely, for 190 antennas, we have 3 iterations. In this case, we should assume the high complexity due to the number of iterations instead of high R due to the fact that 190 antennas are so many for a practical system.

On the other hand, we reduce the coding rate of the channel coding scheme in Figure 4.10(c) with a $1/10 - rate$ CC outer, consequently we can reduce R up to 10 antennas but the (1,1) point is not reached. The same happens with 45 antennas. We have to increase R up to 85 antennas with only $N_I = 1$ iteration to obtain curves that do not cross, though the (1,1) point is not reached, also. Then we can decode but we do not have a BER infinitely low.

The number of iterations N_I is obtained with the aid of the EXIT chart analysis. It indicates the number of iterations which are needed so that BER tends to an infinitesimally low value. We chose for each case the specific number of iterations which achieve the best BER.

[2]The candidates for URC encoder are explained in details in Section 4.4.3

Figure 4.9 Flow to plot a EXIT chart for CC, R, and ρ.

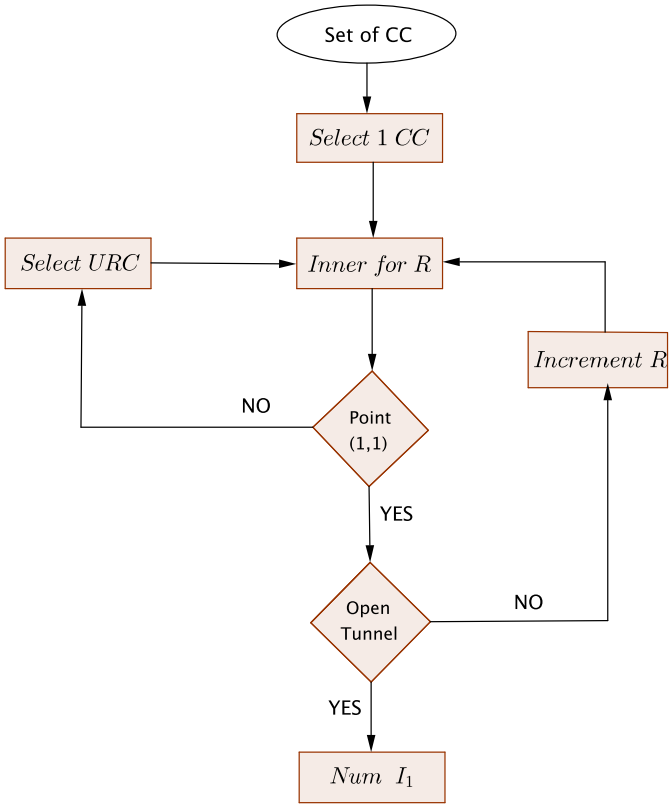

Algorithm 1 Select the best outer and inner codes based on R for NC-m-MIMO system.

Input Data: Set of convolutional codes (CC) + E_b/N_0
Step 1: select one CC of the set.
    Plotting the outer curve for selected CC
End
Step 2: for $R-$value, mapping scheme and URC encoder
    Plotting inner curve
if Both curves achieve the point (1,1) **then**
  if there is open tunnel **then**
    Plotting the trajectory to get I_1
  else
    Increment R and go step 2.
  end if
else
  Select other URC or mapping scheme and go step 2.
end if
Result: URC code, R and I

Figure 4.10 Example of EXIT charts for selecting the best pair encoders for the schemes in Figure 4.2-4.3 using Algorithm 1 and Figure 4.9 for a reference $E_b/N_0 = 0$dB.

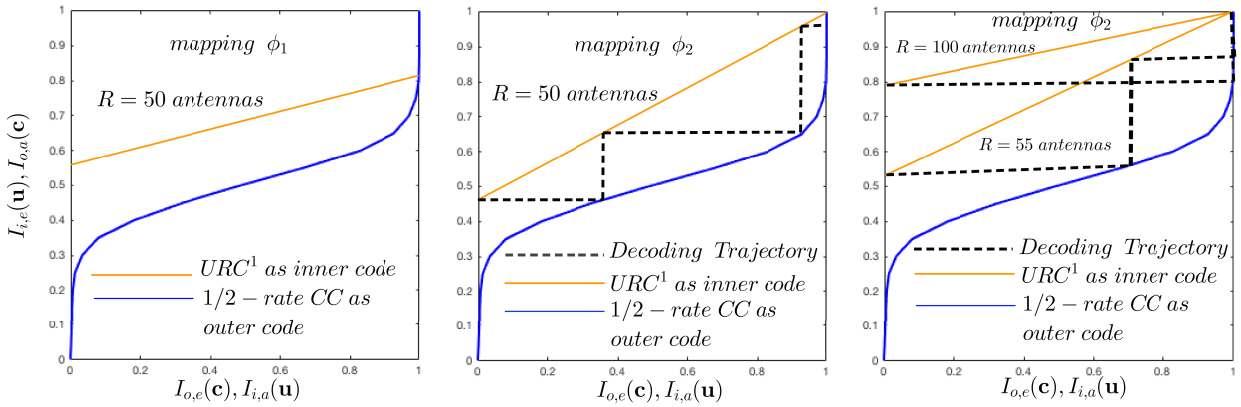

(a) EXIT functions for 1/2-rate CC encoder as outer and URC^1 encoder as inner.

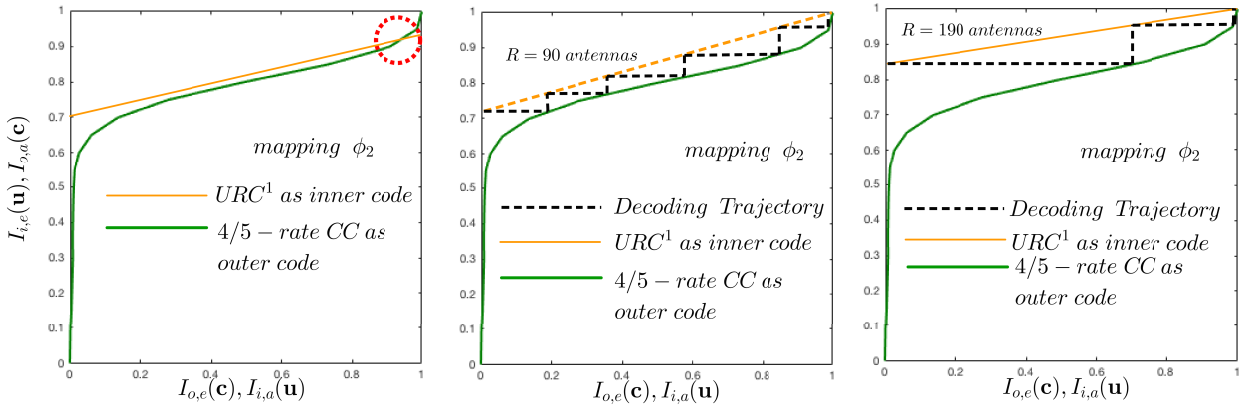

(b) EXIT functions for 4/5-rate CC encoder as outer and URC^1 encoder as inner.

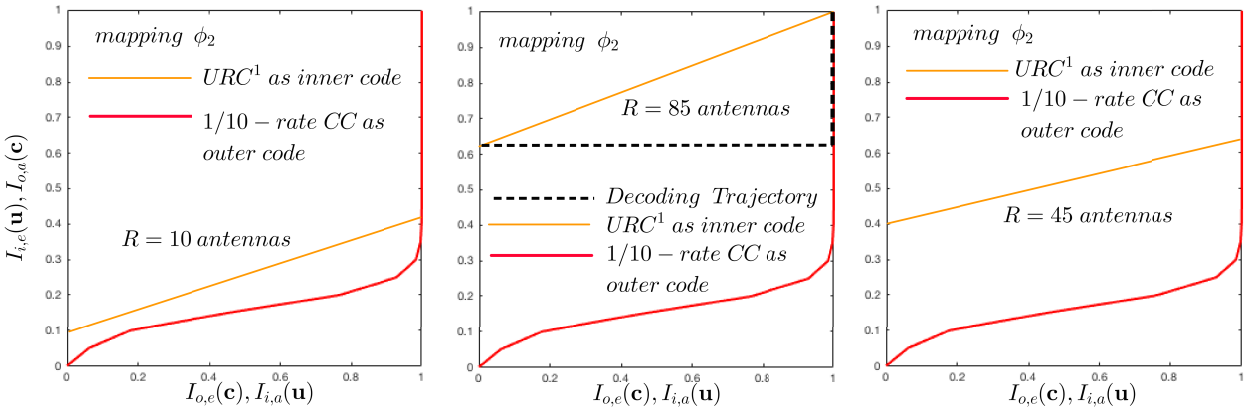

(c) EXIT functions for 1/10-rate CC encoder as outer and URC^1 encoder as inner.

4.4.2 Selecting the outer encoder for multiuser non coherent massive MIMO systems

Typically for the outer encoders are used convolutional codes (CC), however any arbitrary channel code family may be used for iterative decoding or turbo codes. In this work we decide to use CC. In Figure 4.11(a) a basic CC encoder is shown. As we can see, CC encodes $\mathfrak{n}_1$ input bits in $\mathfrak{n}_2$ output bits ($\mathfrak{n}_2 > \mathfrak{n}_1$), being coding rate $r = \frac{\mathfrak{n}_1}{\mathfrak{n}_2}$ and they are composed of memory registers D. For representing a CC, we use the output generator sequences represented by a polynomial g and in a more compact form as G=[g_1, $\cdots$ g_p] with p outputs.

Figure 4.11 General schematic for Convolutional Code (CC).

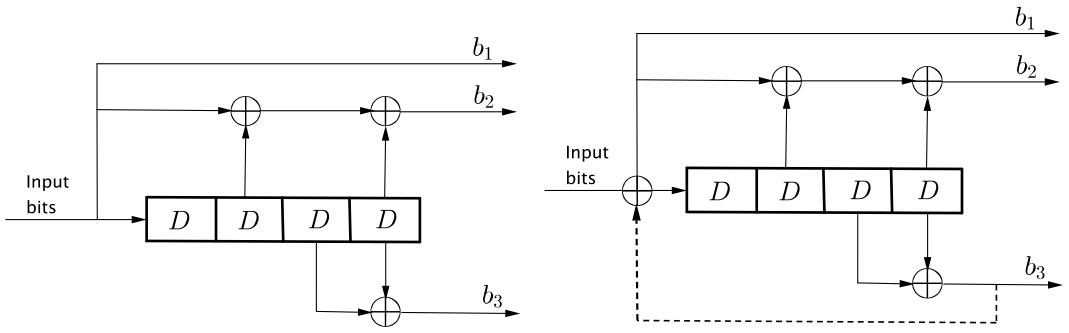

(a) Example for CC (b) Example for RSC

When output bits do not include the input bits these CC are called non-systematic (NSC). Conversely, if the input data are prevalent in the output are called systematic. In addition, if one of its encoded outputs is feeding back to its input, the CC is recursive, as shown in Figure 4.11(b). The recursive systematic convolutional (RSC) codes group have become more popular in Turbo Codes.

In order to achieve CC with different rates, Tuchler and Hagenauer proposed the usage of IRregular Convolutional Codes (IRCCs) in serial concatenated schemes [141,142], which are constituted from a basic RSC by puncturing, obtaining a subgroup of CC having different rates r, used in order to design a near-capacity system. The IRCC codes shape appropriately the EXIT curves minimizing the area within the open tunnel.

In [140], a family of 17 IRCC subcodes are proposed for using in EXIT chart as outer code. They are constructed from a systematic, rate r =1/2, memory-4 mother RSC code defined by the generator polynomial $g = 1/g_0 \cdot (g_0 g_1)$, where

$$\begin{aligned} g_0 &= 1 + D + D^4 \\ g_1 &= 1 + D^2 + D^3 + D^4. \end{aligned} \tag{4.14}$$

Since the rate for main RSC is 1/2, we employ puncturing in order to obtain higher rates ($r > 1/2$), while for lower rates ($r < 1/2$) we need to add more generator polynomials in

conjunction with puncturing technique. Only two new generators (g_2, g_3) are required for achieving lower r,

$$\begin{aligned} g_2 &= 1 + D + D^2 + D^4 \\ g_3 &= 1 + D + D^3 + D^4. \end{aligned} \tag{4.15}$$

Each of the 17 subcodes is identified by the tuples as follows [140],

$$\{r_k, (w_0, w_1, w_2, w_3), l_k, (p_0, p_1, p_2, p_3)\} \;\; for\ k = 1, \cdots, 17 \tag{4.16}$$

where w_i specifies how often g_i occurs in the generator g, l_k is the puncturing period, and p_i is the octal representation of the puncturing pattern associated to g_i. In summary, the 17 subcodes are collected in Table 4.1.

Table 4.1: Candidates for Outer Codes

r_k	(w_0,w_1,w_2,w_3)	l_k	(p_0,p_1,p_2,p_3)
0.1	(1,4,4,1)	1	(1,1,1,1)
0.15	(1,3,2,1)	3	(7,7,7,3)
0.2	(1,2,1,1)	1	(1,1,1,1)
0.25	(1,1,1,1)	1	(1,1,1,1)
0.3	(1,1,1,1)	3	(7,7,7,1)
0.35	(1,1,1)	7	(177177077)
0.4	(1,1,1)	2	(3,3,1)
0.45	(1,1,1)	9	(777777021)
0.5	(1,1)	1	(1,1)
0.55	(1,1)	11	(3777,2737)
0.6	(1,1)	3	(7,3)
0.65	(1,1)	13	(17777,05253)
0.7	(1,1)	7	(177025)
0.75	(1,1)	3	(7,1)
0.8	(1,1)	4	(17,1)
0.85	(1,1)	17	(377777010101)
0.9	(1,1)	9	(777,1)

For our proposal we avail of the set of subcodes in [140] as candidates for the outer code. Figure 4.12 shows the EXIT characteristics for the 17 subcodes, achieved using (4.8). Each CC in Figure 4.12 is associated with a bit rate which will be analyzed later considering the required number of antennas for each case. In general, the higher coding rate, the more unprotected the information is. Therefore, we need to increase R in the corresponding for the lower curves in EXIT chart shown in Figure 4.12. By contrast, the curve in up zone in EXIT chart, we need less antennas.

Figure 4.12 Set of 17 candidates IRCC for outer encoder in a NC-m-MIMO system.

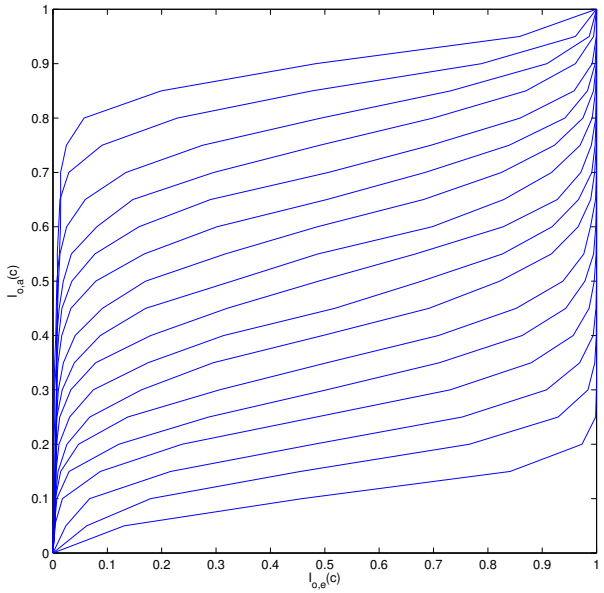

4.4.3 Mapping schemes for multiuser non coherent massive MIMO systems

The mapper block, formed by DPSK encoder in conjunction with bit-symbol mapping scheme (MS), act as inner encoder in our system. We denominate an MS as ϕ. We have to select the appropriate individual labelling for the constellation designs, which were proposed in Chapter 3, for mapping the individual constellation from joint constellation. At the moment, we analyze the channel coding scheme without the URC encoder, in order to demonstrate latter the necessity to include it as part of the inner encoder.

It is widely recognized [133] that Gray Mapping (GM) is not advisable for implementing iterative decoding since it does not produce any iteration gain upon increasing the MI at the demapper. Hence, it produces a poor BER performance without reaching the channel capacity.

In our system, we have to define two MS: one for the individual constellation $\mathfrak{M}$ and the other one for the joint constellation $\mathcal{M}$. The latter is which influences on the iterative decoding procedure. Actually, as it was explained in Chapter 2, the labelling for joint constellation depends on the concatenation of the individual labelling, hence the MS definition is only required for individual users and thus, joint MS never presents a GM even though the individual MS are GM. There is a large number of legitimate anti-Gray mappings (AGM) that can be created from the combination of the individual users constellation. Although, again, their impact on the attained performance is not significant. Nonetheless, we have analyzed a group of mappings, from which we select two examples for GM and other two for AGM as representative, summarizing them in Table

4.2 with a constellation size of $M = 4$ symbols for both.

Cases	**Mapping Scheme (MS) ϕ**	**Binary Labelling**	**Type**
1	ϕ_1	$[00, 01, 11, 10]$	GM
2	ϕ_2	$[10, 11, 01, 00]$	GM
3	ϕ_3	$[00, 01, 10, 11]$	AGM
4	ϕ_4	$[00, 10, 01, 11]$	AGM

Table 4.2: Proposed mapping schemes for individual users.

Based on the mappings defined in Table 4.2, we analyze the behavior of the system for three general cases. First, all users employ GM. Second, all users operate with AGM. The last one, some users using GM while the other ones AGM. In Table 4.3 the different combinations for the case of $J = 2$ users are shown.

Combinations	**User 1**	**User 2**	**Description**
1	ϕ_1	ϕ_1	Both users the same GM
2	ϕ_2	ϕ_2	Option 2: both users the same GM
3	ϕ_1	ϕ_2	Both users with GM, but different between them
4	ϕ_3	ϕ_3	Both users the same AGM
5	ϕ_4	ϕ_4	Option 2: both users the same AGM
6	ϕ_3	ϕ_4	Both users with AGM, but different between them
7	ϕ_1	ϕ_3	One user GM and the other one AGM

Table 4.3: Combinations for MS between the users.

For each of the considered combinations in Table 4.3, the inner function was obtained for a reference $E_b/N_0 = 0$ dB, $M = 4$, $J = 2$ users and $R = 20$ antennas. Let us now examine the performance of the MS combinations for both our EEP and UEP designs respectively. The first thing that attracts our attention is that none of the curves reach to the (1,1) point for perfect convergence. This is the main reason why we need to include an URC encoder.

Also, we can notice that the performance does not depend on neither the specific MS nor design philosophy (EEP or UEP), not even of the constellation design, solely whether there is GM or not. When at least one of the users employs GM there is a gain with respect to the rest of the combinations defined in Table 4.3. Nevertheless, we do not achieve the perfect point.

Figure 4.13 shows the EXIT chart of the BICM-ID non-coherent m-MIMO system of Figure 4.3 without taking into account the URC encoder. Several inner curves are plotted for different number of antennas, R =20, 40 and 60 employing the EEP constellation of Figure 3.57. As outer code, 1/2-rate RSC is selected corresponding to the code 9 of the family shown in Figure 4.12 which offers a rate of $r = 1/2$. Due to the fact that the EXIT curve of the inner demapper and the outer RSC decoder intersected before reaching the (1,1) point of the perfect convergence, the error probability curve will not exhibit the steep turbo-cliff shape that we expect in a BICM-ID system.

Figure 4.13 Inner curve only considering MS (without URC encoder).

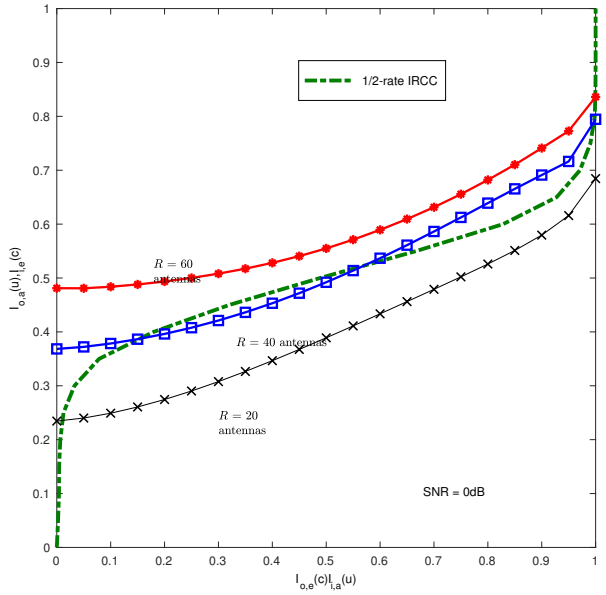

Finally, for the rest of the work, we have opted for the specific mapping ϕ_1 that provided the best BER for a given number of antennas among all the analyzed mappings.

4.4.4 Selecting the inner encoder for multiuser non coherent massive MIMO systems

A recursive *inner* encoder is needed in order to maximize the interleaved gain and to avoid the formation of a BER floor when we employ iterative decoding. In addition, it can be of great help for reaching the $(I_a, I_e) = (1, 1)$ point. It was shown in [140] that an URC encoder as inner code can be employed for designing low-complexity iterative detection aided schemes, suitable for bandwidth and power limited systems which have stringent error probability requirements. The URC encoder is a simple r-1 memory-1 accumulator as shown in Figure 4.14. Introducing URC only produces a slight complexity increase for the receiver, although still allowing a low-complexity iterative detection. Also, URC encoders have an Infinite Impulse Response (IIR) and hence, they randomize the

extrinsic information without increasing the interleaved delay and without reducing the throughput.

Figure 4.14 Schematic of the simplest URC encoder.

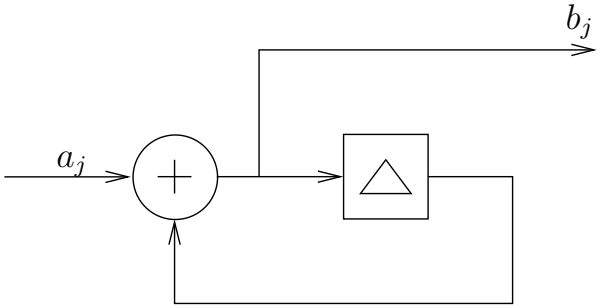

There are several possible URC codes in the literature summarized in Figure 4.15 from [143]. In Table 4.4, the polynomial generators of the each 10 candidate URC, $\{URC^i\}_{i=0}^{10}$, are shown. We select the first (URC^1), the fourth (URC^4) and the sixth (URC^6) because of the following reasons:

- We choose a representative for 1, 2 and 3 memory register.
- They offer some non-zero extrinsic mutual information $I_{i,e}$ even in the absence of any *a priori* mutual information $I_{i,a}$. This means, for $I_a = 0$, we have output information $I_e \neq 0$. This may be attributed to the presence of only a single non-zero coefficient within their polynomial generators. This feature allows us decoding the information in conjunction with the outer codes selected in previous section. Otherwise, with the remaining URC codes, not even increasing the number of antennas, we will not be able to obtain an open tunnel in our proposal.

Table 4.4: Generator Polynomials for the 10 URC from [143].

URC	URC^1	URC^2	URC^3	URC^4	URC^5	URC^6	URC^7	URC^8	URC^9	URC^{10}
(g,f)	(2,3)	(7,5)	(7,6)	(4,7)	(6,7)	(8,B)	(D,C)	(8,F)	(B,F)	(E,F)

In Figure 4.13 it was showed the EXIT chart of the BICM-ID non-coherent m-MIMO system of Figure 4.3 without taking into account the URC encoder. Now, considering an URC as inner code, the iterative detection is carried out by exchanging extrinsic information between the outer RSC decoder (represented by the set of IRCC subcodes) and the URC decoder, instead with the demapper. We repeat the inner curves of Figure 4.13 for R =20, 40 and 60 antennas and SNR= 0dB, employing the EEP constellation of Figure 3.19. As outer code, 1/2-rate IRCC corresponding to the code 9 in Figure 4.12. Note now that the convergence at the (1,1) point is researched, as it is shown in Figure 4.16.

Figure 4.15 List of candidates for URC encoder.

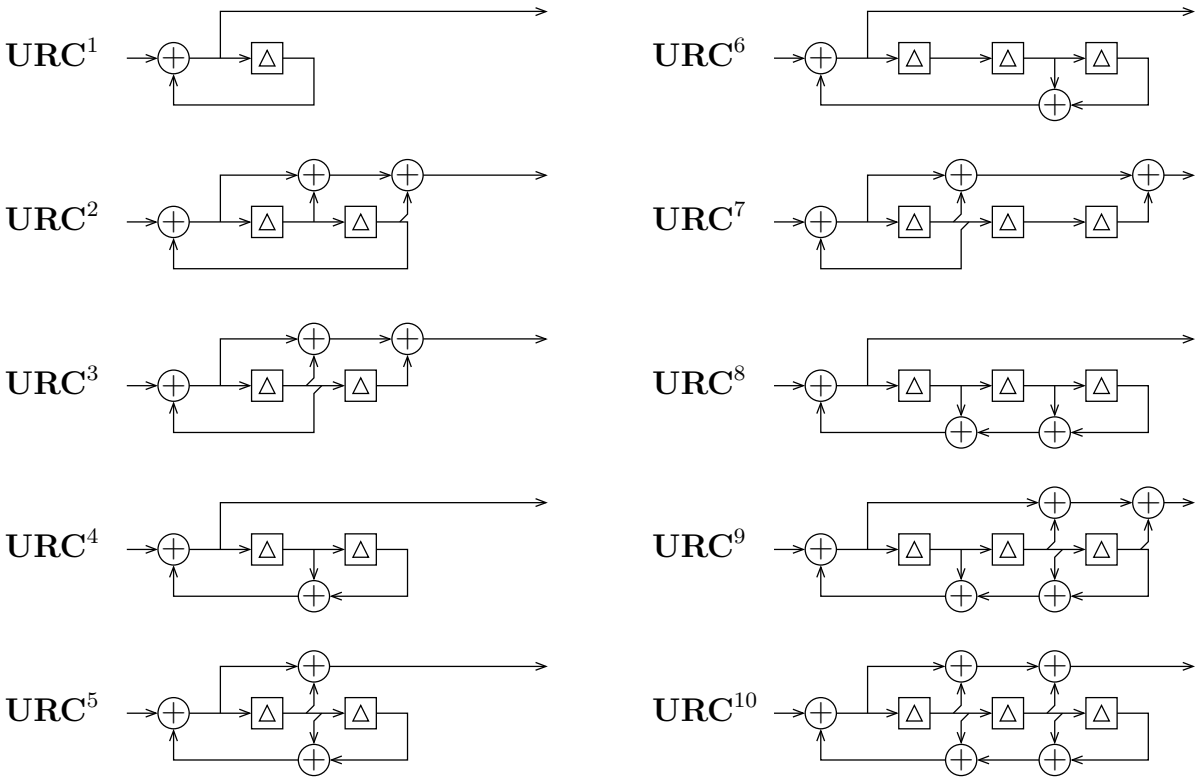

The insertion of the URC encoder does not reduce the throughput, but a modest increase in the required value of R is noticed for the same outer encoder. For the case with our URC, using $R = 60$ the decoding is possible but the BER does not converge to a very low value. However, in the case with URC, 60 antennas is not valid for $1/2-$rate IRCC because we do not have an open tunnel, both curves are crossed. We need to increase R up to 80 antennas in order to open the tunnel.

We plot the inner curve for reference SNR = -6 and 0 dB, several R and our selected URC $\{URC^1, URC^4, URC^6\}$ in Figure 4.17. The reference outer code continues being $1/2-$rate IRCC. For -6dB we can not decode, observing that URC^1 is the worse inner code. However, once we can decode for SNR=0 dB, URC^1 is the best option due to the fact that it requires a lower value of R or it throws lower area between both curves (open tunnel). The URC^4 and URC^6 for low a priori MI,$I_{i,a}$, require less R than URC^1, but they present a narrower tunnel which involves a higher number of iterations, thus, more complexity for the receiver. In general, taking into account the tradeoff between both encoders, our proposal URC^1 offers better performance, as we will see in the next sections.

Figure 4.16 Inner curve with URC encoder.

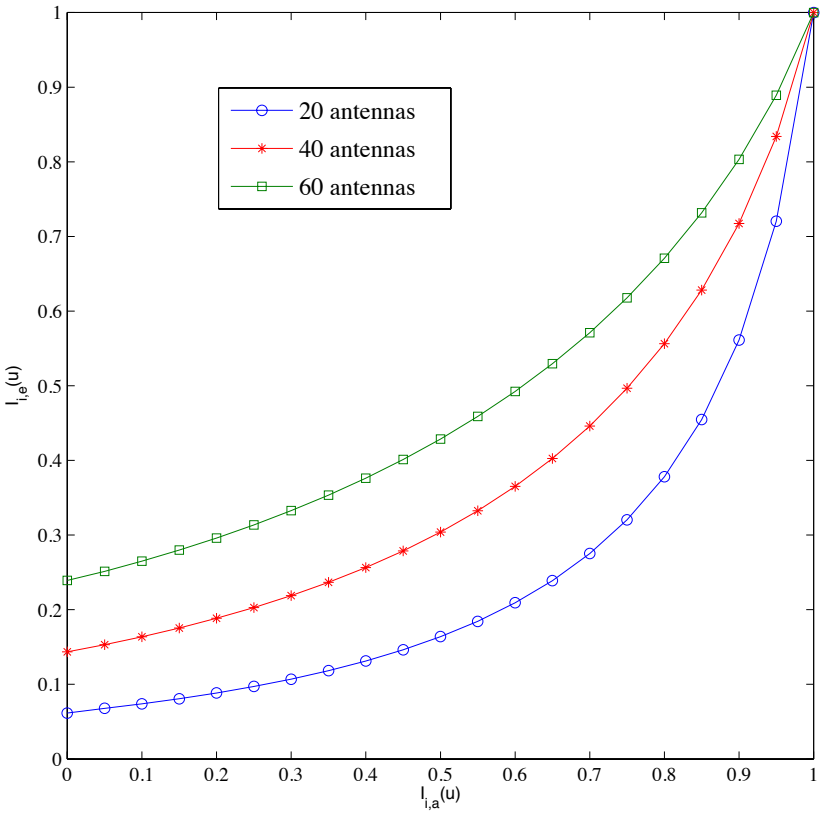

Figure 4.17 Comparison with different URC encoder for SNR=-6 dB and 0 dB.

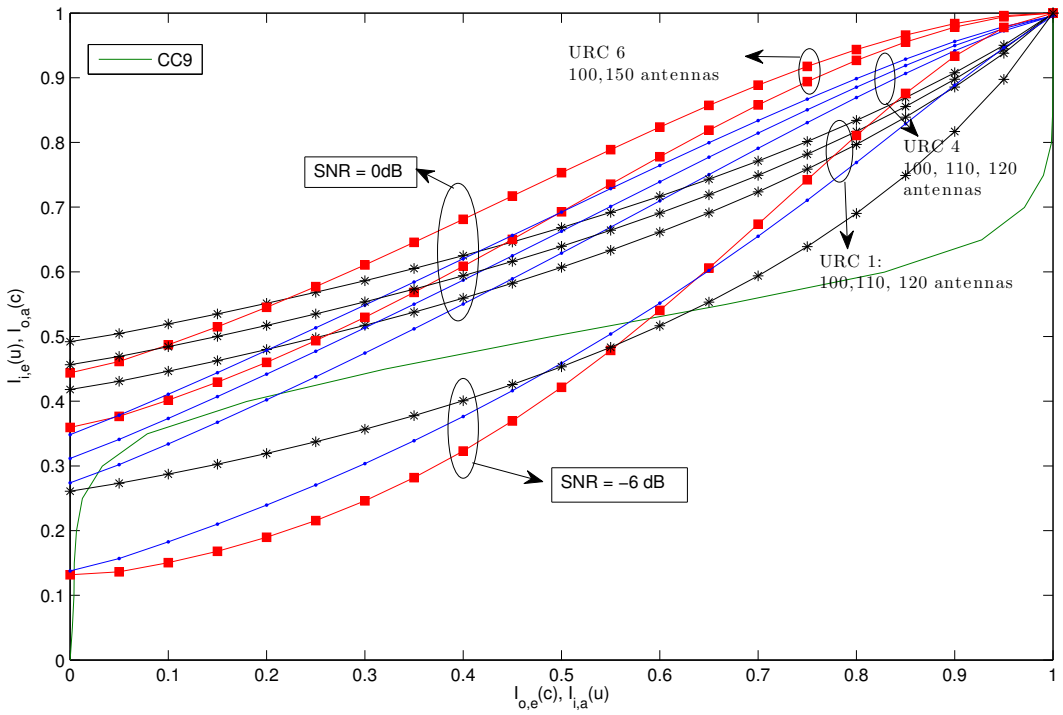

4.5 Performance of multiuser non coherent massive MIMO system based on DPSK with channel coding

Once each EXIT characteristic had been explained and discussed in the previous section, we analyse the performance for our NC m-MIMO proposal based on this tool. Specifically, we study the BER and SER in order to find the channel coding scheme that is better suited for our constellation designs, when communicating over uncorrelated Rayleigh fading channels with AWGN. The objective of this analysis is to optimize the value of R required in order to attain a good performance, since R should be a feasible number for a m-MIMO system. The simulations are carried out by Monte Carlo method. Block fading is assumed, where the channel's envelope remains constant during the transmission of a symbol burst, but it varies randomly between bursts. The effects due to the real nature of the wireless channels such as the time- or frequency-varying on the system performance are analyzed in Chapter 6. In order to ensure the Gaussian distribution of the LLRs, we use long interleavers with a depth of D_{int}=800,000 bits. The remaining simulation parameters are: the frame length of the modulator is set to 400,000 symbols, 10,000 frames are transmitted and a total of 1,000,000 information bits were transmitted during one simulation run. Finally, we set $\rho = 0$ dB, unless otherwise is stated.

The performance is analyzed for the UEP and EEP designs, both presented in Chapter 3, for the case with channel coding scheme. Now, we search the suitable $R-$value for these designs. Finally, we compare the results for NC-m-MIMO with those obtained without coding and for its coherent counterpart using MRC.

4.5.1 Performance for UEP designs

We select a reference SNR, following the Algorithm 1 and Figure 4.9 to plot for the set of 17 subcodes (outer, IRCC) in conjunction with the inner curves for a range of antennas from 20 up to 200 in steps of 10 antennas. From 200 antennas we increase the step to 20 antennas due to the fact that coding rate is lower in the high region. In this case, we plot from 220 up to 360 antennas as shown in Figure 4.18 as an example.

We associate the best inner curve attached to a given $R-$value with each IRCC curve of the 17 subcodes. The results are collected in Table 4.5 for the UEP-A constellation design, $\mathfrak{M}^A$, described in Section 3.4. This table shows the estimated resources required for that UEP design when we use the URC^1 and URC^4, which were shown in Figure 4.15, for a reference SNR ρ=0, 3 and 6 dB. For the UEP design we verify the fact that different users have a different performance, therefore it is necessary to show both users. The user

1 is better than user 2, so that lower R is needed for the same performance. This is because of the minimum distance among symbols for user 1 is bigger than the user 2. In addition, increasing the coding rate reduces the number of antennas for both URC, although for URC[1] the number of antennas R required is lower than for URC[4]. For high channel coding, increasing the reference SNR does not produce any gain over R.

Figure 4.18 EXIT Chart for $J = 2$ users , $M = 4$, URC 1 and UEP

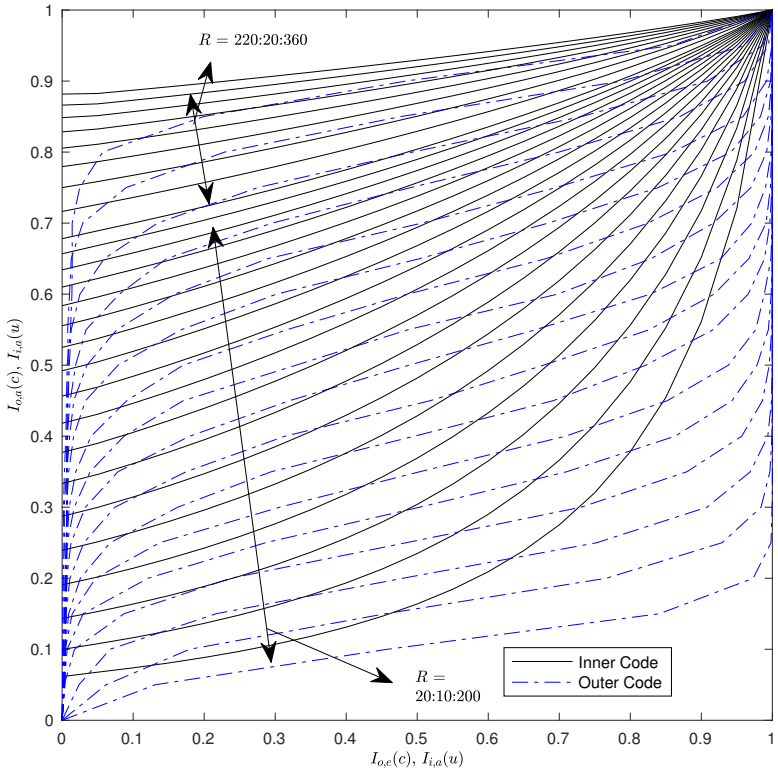

In order to predict the complexity that the receiver has, we need the decoding trajectory. In Figure 4.19 we show the EXIT chart for design A with $J = 2$ users, a reference SNR of 0 dB for both users separately, $M = 4$, URC[1] as inner code and the code 9 of 17 as outer, in conjunction with its trajectory for decoding. The complexity will be marked by the user 2 which requires more iterations to reach the (1,1) point. In this case, for R=370 antennas, the user 2 needs 5 iterations and the user 1 only needs 1 iteration.

The BER of the UEP-A design for $J = 2$ users, URC[1], $M = 4$ symbols and $r - 1/2$ IRCC is shown in Figure 4.20. Note that the user 1 has better performance than user 2, however both users need a reduced R compared to the results without coding, analyzed in Section 3.4. Also, Figure 4.20 verifies the decoding trajectory in Figure 4.19. The user 1 needs 3 iterations to converge when using 40 antennas, while the user 2 needs 5 iterations to converge with 370 antennas. Due to the fact that the number of antennas has to be the same for both users, the first user's performance is increased with respect to the second user.

	Outer RCS Conv. Code (CC)	User 1 Inner Code (URC 1) R for SNR			User 2 Inner Code (URC 1) R for SNR			User 1 URC 4 R for E_b/N_0			User 2 URC 4 R for SNR		
		0 dB	3 dB	6 dB	0 dB	3 dB	6 dB	0 dB	3 dB	6 dB	0dB	3 dB	6 dB
Coding rate in	1/10-CC1	20	20	20	100	60	40	20	20	20	150	90	60
	3/20-CC2	20	20	20	130	80	55	20	20	20	190	110	75
	1/5-CC3	20	20	20	170	95	65	25	20	20	220	130	90
	1/4-CC4	20	20	20	200	115	80	30	20	20	260	160	110
	3/10-CC5	30	20	20	230	130	90	30	20	20	290	180	120
	7/20-CC6	30	20	20	260	150	115	35	20	20	320	200	135
	2/5-CC7	30	20	20	290	170	130	40	20	20	360	220	150
	9/20-CC8	35	20	20	320	190	140	45	25	20	400	240	160
	1/2-CC9	40	25	20	360	210	155	50	30	20	430	260	175
	11/20-CC10	45	25	20	400	230	165	60	30	20	480	280	190
	3/5-CC11	50	30	20	440	260	175	65	35	25	530	300	210
	13/20-CC12	55	35	25	500	290	200	70	40	30	580	330	230
	7/10-CC13	65	40	25	550	320	220	80	50	35	630	360	250
	3/4-CC14	75	45	35	600	360	250	100	55	40	690	400	280
	4/5-CC15	100	55	40	640	420	280	120	70	50	750	450	310
	17/20-CC16	130	80	55	690	480	330	170	110	70	810	500	380
	9/10-CC17	190	120	85	740	530	380	250	140	100	860	550	430

Table 4.5: Performance Comparison for J =2 users with UEP-A constellation and different encoders.

Figure 4.19 EXIT Chart for ρ =0 dB, $J = 2$ users , $M = 4$, URC[1] and UEP design A.

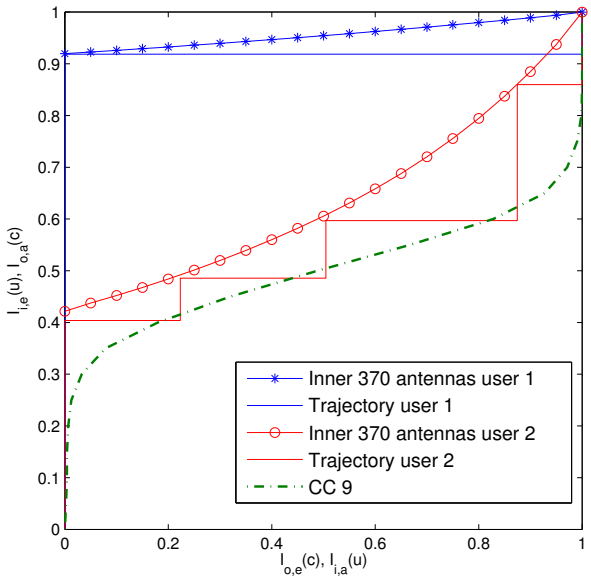

Figure 4.20 BER for $J = 2$ users UEP-A, $\rho = 0$ dB, URC^1 as inner encoder and CC9 as outer encoder

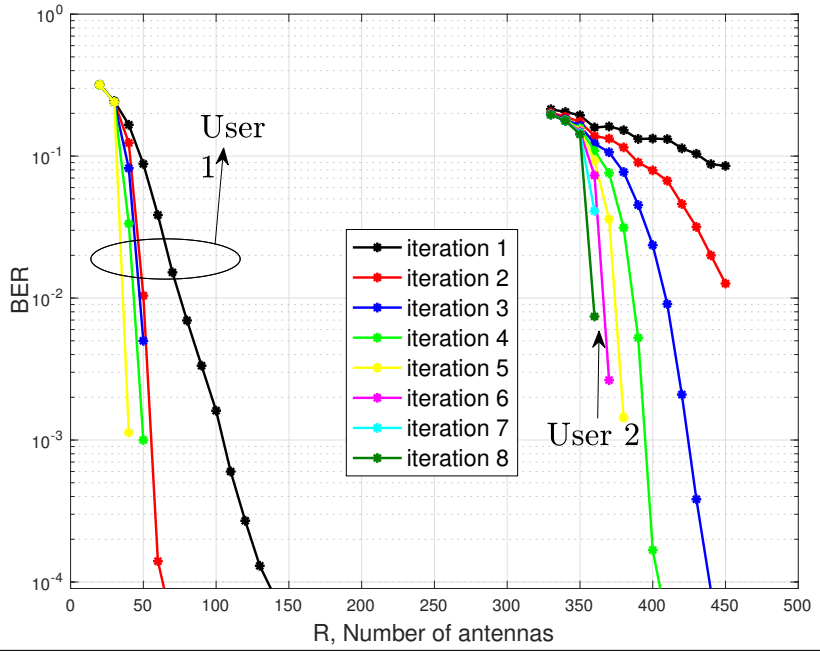

4.5.2 Performance for EEP designs

Let us now examine the performance for the EEP design explained in Section 3.5. First, we check that effectively the performance is the same for all users. In Figure 4.21, we plot the inner curve for J =2, 4 and 6 users. Indeed, all users experience the same EXIT chart, thus, they will have the same BER curve.

As for UEP designs, we estimate the antennas required for different reference SNR. Before, we analyze the influence of URC encoder type for EEP approach. We illustrated the decoding trajectories for URC^1 in Figure 4.22, for URC^4 in Figure 4.23 and for URC^6 in Figure 4.24, all of them for $M = 4$, $J = 2$ users and ρ=0 dB. We use as example a $1/2 - rate$ and $9/10 - rate$ IRCCs. In Figure 4.22, for 90 antennas the inner curve reaches perfect point after N_I =12 decoding iterations. In this case, the open tunnel between inner and outer encoder is very tight so we need more iterations to reach this point. We can assume a slight increase in R, with only 10 additional antennas, so then the performance converges with half the number of iterations. For 110 antennas we need N_I =6 too, then we select R =100 antennas to decode using the basic convolutional code 9 from set of 17 subcodes. In the case we want to increase the coding rate to 9/10 using the convolutional 17, we need to increase up to R =350 antennas. The user 2 presents the same results due to the equal error protection design.

Figure 4.21 Performance between multiple users for EEP design

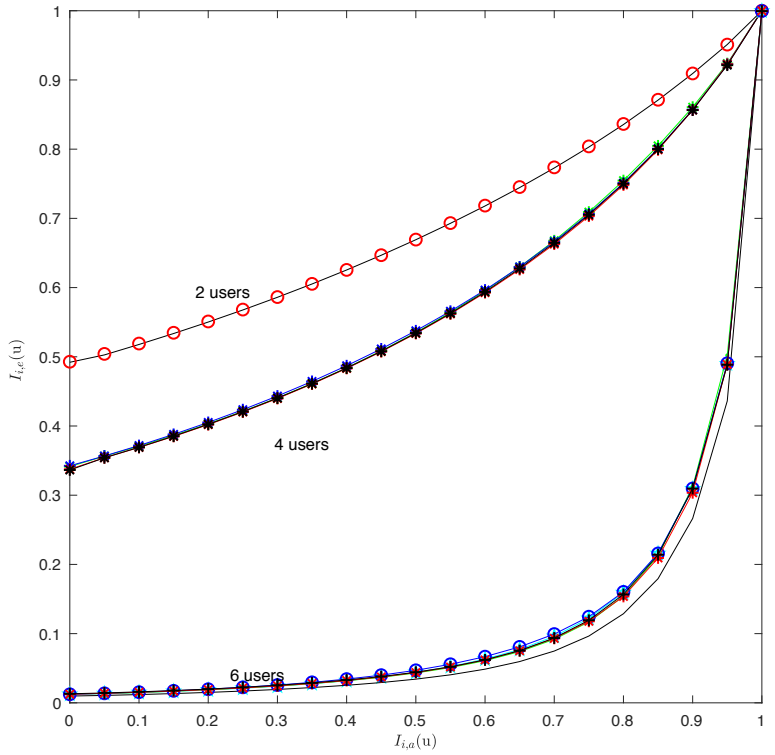

Figure 4.22 EXIT Chart for $J = 2$ users , $M = 4$, URC[1] and EEP

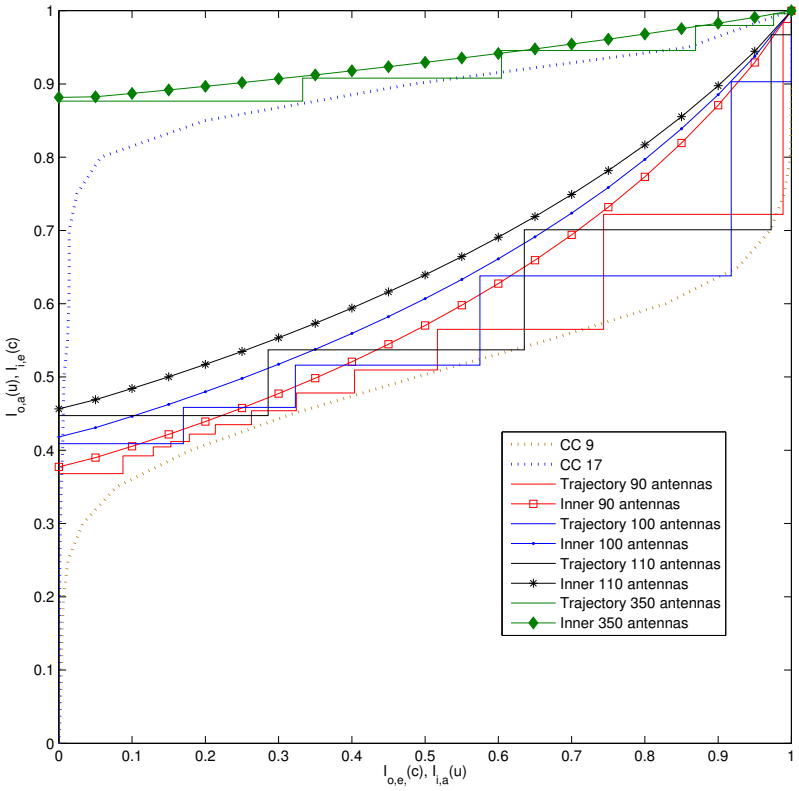

Figure 4.23 EXIT Chart for $J = 2$ users , $M = 4$, URC[4] and EEP

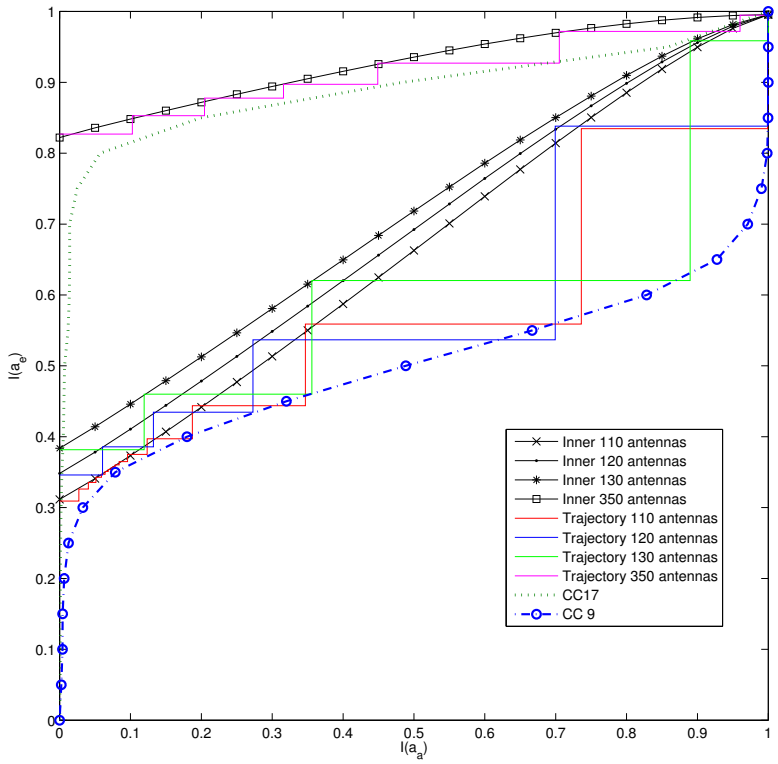

Figure 4.24 EXIT Chart for $J = 2$ users , $M = 4$, URC[6] and EEP

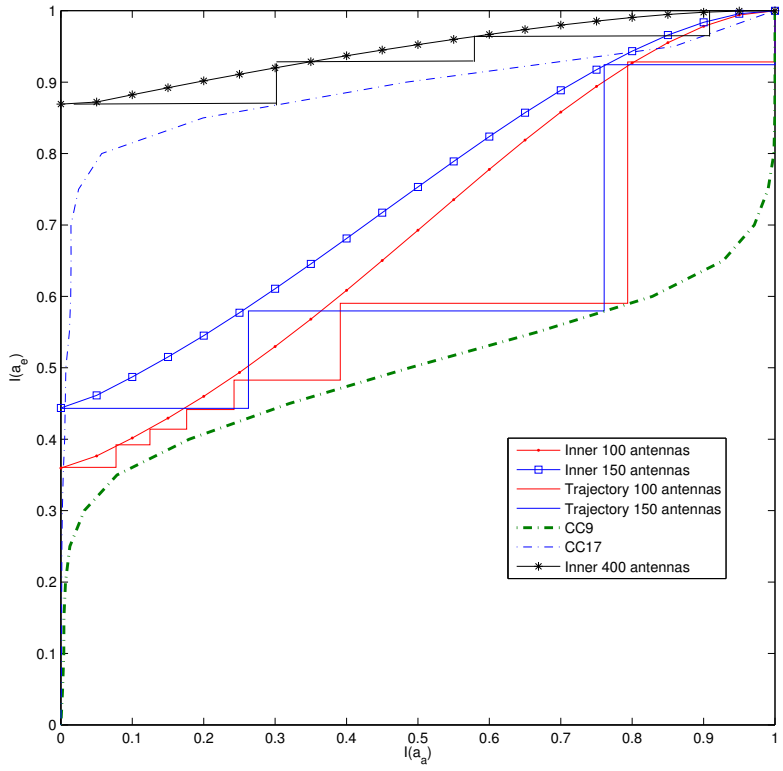

In Figure 4.23, we can see that for URC^4 with 1/2−CC, we need minimum 100 antennas for N_I =7 iteration, 10 antennas and one iteration more than with URC^1. The next inner curve goes up to 150 antennas, in exchange of reducing only 3 iterations. By contrast, for 9/10-CC R and N_I is kept.

In the case for URC^6 shown in Figure 4.24, note that R is increased up to 110 for 1/2-CC and up to 400 antennas for 9/10-CC. We compare the decoding trajectory for the EEP constellation design using URC^4 in Figure 4.23 and URC^6 in Figure 4.24. In both cases the number of iterations to reach the point (1,1) is larger than for URC^1.

In general, the URC^1 is which offers a better tradeoff between R-N_I. Therefore, we decided for the EEP designs to use also the URC^1, in addition, due to the fact that R is lower for a given coding rate. Hence, we plot for a range of antennas all the inner and outer curves using Algorithm 1 and flow chart, as the same way that UEP schemes. Table 4.6 provides a comparison of the estimated resources required for different combinations of inner and outer encoders using the EEP design. Only one user is shown since it is EEP approach.

	Outer (CC) Conv. Code	Inner Code (URC 1) R for SNR					Inner Code (URC 4) R for SNR				Inner Code (URC 6) R for SNR			
	(RCS)	0 dB	3 dB	6 dB	-3 dB	-6 dB	0 dB	3 dB	-3 dB	-6 dB	0 dB	3 dB	-3 dB	-6 dB
Coding rate	1/10-CC1	20	20	20	50	120	40	20	100	250	40	25	100	250
	3/20-CC2	30	20	20	70	180	45	25	100	300	50	30	125	300
	1/5-CC3	40	20	20	90	230	55	30	125	350	60	35	150	355
	1/4-CC4	50	25	20	110	280	65	35	150	400	70	40	175	450
	3/10-CC5	55	30	20	125	310	75	40	175	475	80	45	200	500
	7/20-CC6	60	35	25	140	370	85	45	200	500	90	50	200	550
	2/5-CC7	70	40	30	110	440	95	55	225	575	100	60	225	575
	9/20-CC8	80	45	30	170	500	105	60	250	650	110	60	250	600
	1/2-CC9	90	50	35	200	550	120	70	300	700	110	70	275	750
	11/20-CC10	100	60	40	250	650	130	75	350	850	120	80	300	875
	3/5-CC11	120	65	45	270	750	145	85	375	950	120	90	350	1000
	13/20-CC12	130	75	55	300	850	160	95	420	1050	125	100	400	1100
	7/10-CC13	150	90	60	350	1000	190	105	475	1200	130	110	425	1250
	3/4-CC14	180	100	70	400	1150	210	120	550	1300	135	120	475	1350
	4/5-CC15	210	120	85	500	1300	240	140	600	1400	140	140	550	1400
	17/20-CC16	260	150	100	600	1600	300	170	750	1700	150	170	700	1750
	9/10-CC17	350	180	130	750	1900	350	200	850	1950	160	200	825	1900

Table 4.6: Performance Comparison for $J = 2$ users with EEP Constellation and different encoders.

We can see that, as it may be expected, the higher the coding rate (less information is protected or coded, the higher R; and, conversely, we need more antennas to lower the coding rate. Note that the results are satisfactory with respect to the values of R. These results show a reduction compared to the previous work in [103] that did not include coding. Also, we can see in Table 4.6 that low R is required for low SNR. The lowest value we can propose is 20 antennas since for lower values the approximation (3.6) is not fulfilled. By comparing Table 4.5 and Table 4.6 we can see that there is an increase in R for the EEP design if we wish to guarantee that both users have the same performance. In any case, R is considerably lower than in [103]. For example, at millimeter-waves frequencies a 10x10 array having 100 antennas would require a coding rate of 3/4 at SNR=3dB according to Table 4.6 with EEP design.

Figure 4.25 shows the attainable performance for J=2 users relying on the EEP design. As it can be inferred by carefully comparing Figures 4.22-4.25, the BER of user 1 in Figure 4.25 becomes vanishingly low for 90 antennas after $N_I = 12$. Reducing the N_I to 4, upon using a 1/2-rate IRCC, we have reduced the value of R from 1,000 to 100 antennas compared to the uncoded case of Section 3.5. Alternatively, it can be observed in Figure 4.25 that we are able to reduce R to 350 antennas with respect to $R = 1{,}000$ for the uncoded case in conjunction with $N_I = 5$ using a 9/10-rate RSC as the outer code. Furthermore, we can compare both schemes for the same number of iterations, such as $N_I = 4$. In this case, the performance of the 9/10 rate code is slightly worse, as seen in Figure 4.22. Additionally, it is explicitly observed in Figure 4.25 that $N_I = 4$ is sufficient for the 1/2-rate IRCC to converge, while 9/10 requires one additional iteration.

As it was shown in Figure 4.22 and Table 4.6, we can save a 40% in coding rate when we use 350 antennas with a 9/10−coding rate. In Figure 4.26 BER for $\rho = 0$ dB, EEP, $J = 2$ but using a 9/10-rate IRCC (CC17) is shown. Note that for this value the BER converges for 5 iterations in Figure 4.26. As we can see by studying Table 4.6, Figure 4.22 and Figure 4.26 the BER thresholds are accurately predicted by the EXIT chart analysis. The results predicted by the EXIT chart analysis closely match the actual results observed in the BER curve for ρ=0dB.

Figure 4.27 shows the BER for J=4 users, the EEP design, URC[1] and CC9 for ρ=0 dB. There is a sudden drop in the BER for 3,500 antennas after 8 iterations. This result drastically reduces R as compared to [103] where R>15,000 antennas were required to support 4 users.

Figure 4.25 BER for $J = 2$ users EEP, $\rho = 0$ dB, URC as inner encoder and 1/2, 9/10-rate RSC as outer encoder

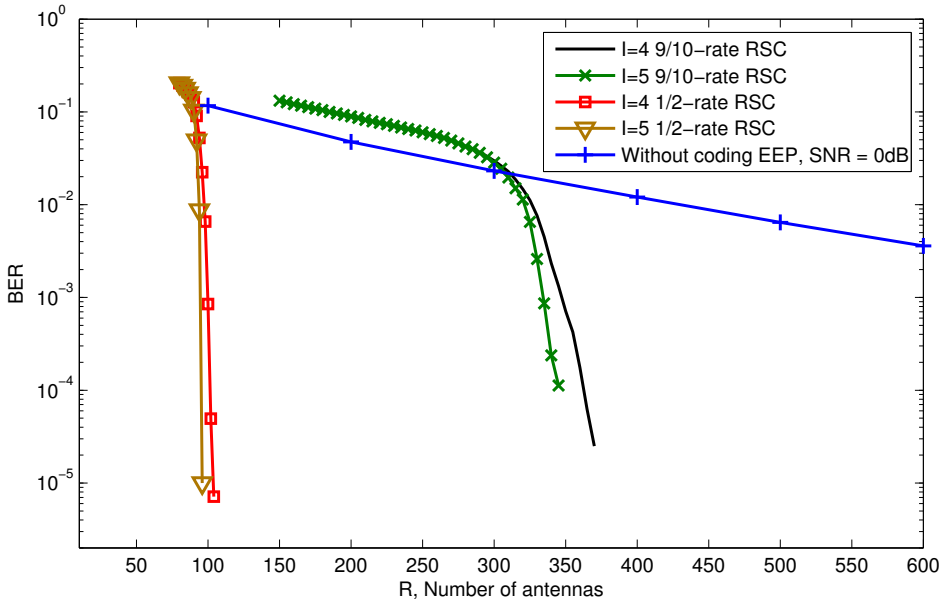

Figure 4.26 BER for $J = 2$ users EEP, $\rho = 0$ dB, URC 1 as inner encoder and CC17 as outer encoder

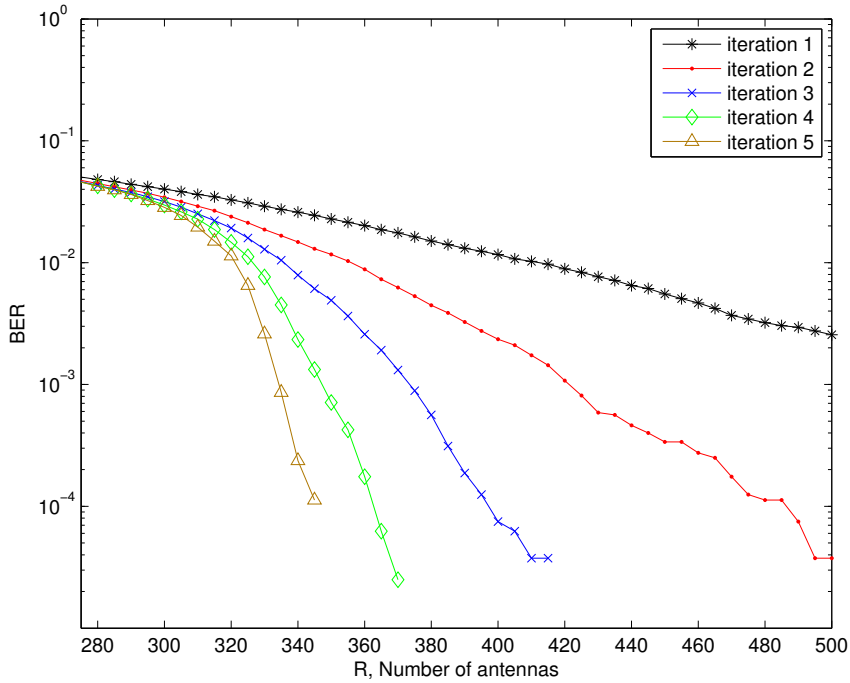

4.5.3 Performance comparison between different schemes with channel coding

Figure 4.28 provides an example of the results shown in Table 4.5, where R = 50 and a code rate of 1/10 are fixed, while varying the E_b/N_0. The difference between EEP and

Figure 4.27 BER for $J = 4$ users EEP, $\rho = 0$ dB, URC 1 as inner encoder and CC9 as outer encoder

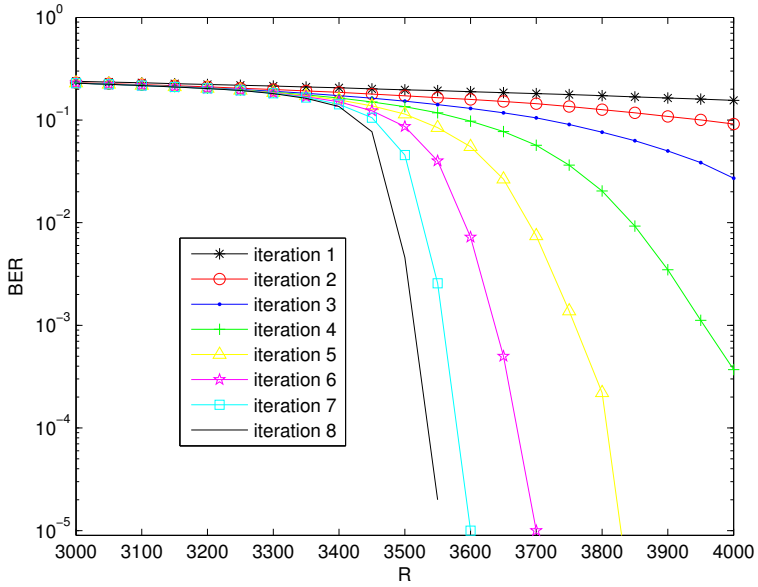

UEP can be explicitly observed. For the second user of the UEP scheme to reach the same performance as user relying on the EEP scheme, we have to increase the number of antennas to 250, as shown in Figure 4.28. This extra number of antennas compensates for an E_b/N_0 difference of 8 dB, equivalently evaluated for the effective ρ.

In order to compare the performance to previous work [105] we use now the SER. This probability is dominated by the worst distance, so that it is minimized when all users have a similar distance which means similar error probability (EEP design). Figure 4.29 shows the SER for both the UEP and EEP schemes as well as for [105]. For the same performance, our system needs a lower number of antennas than [105] for SER=10^{-3} and more than 3 orders of magnitude lower for SER=10^{-5}, which is an explicit benefit of iterative decoding.

Figure 4.28 NC performance comparison for $J = 2$ users, EEP and UEP designs.

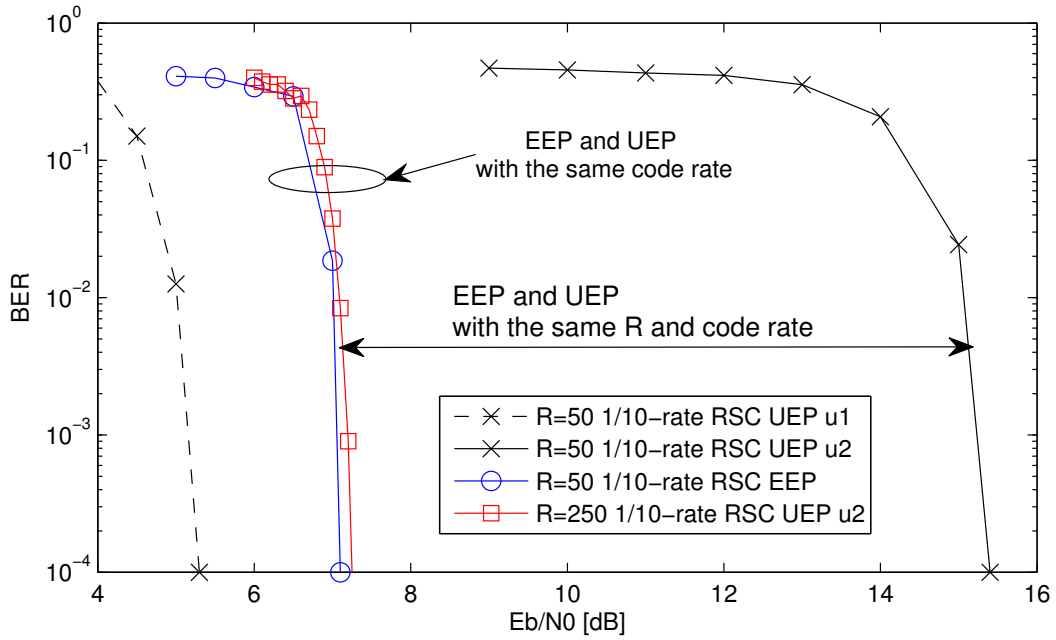

Figure 4.29 SER comparison with [105] for $J = 2$ users EEP, $\rho = 0$ dB, URC , 1/2-rate RSC

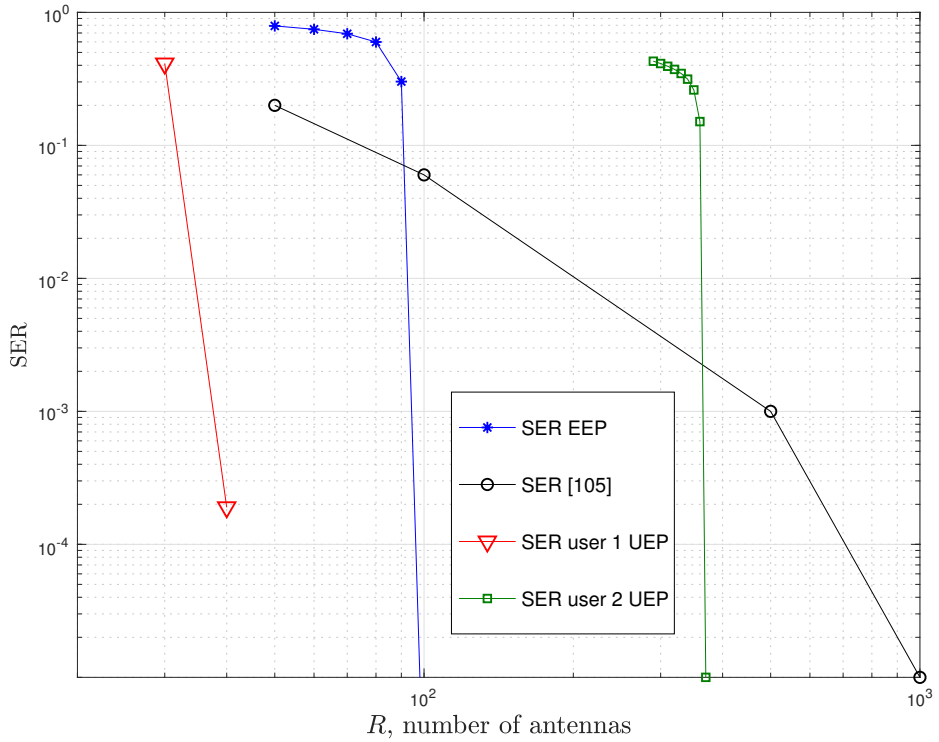

4.5.4 Performance comparison between coherent and non coherent schemes with channel coding

We also compare the performance of J=2 users relying on our EEP design to that achieved by a MRC receiver. For this comparison we assume that the CSI is estimated and hence it is subject to a realistic estimation error, which is assumed to be Gaussian. Moreover, for a fair comparison we should take into account the effective throughput reduction due to the insertion of pilots for channel estimation. We will assume a rate-loss of 33% as detailed in Section 3.6. In Figure 4.30 for $R = 90$, the NC scheme using a 1/5-rate is compared to its coherent counterpart associated with a 3/10-rate, so they have the same effective rate. We can see that for the target of BER= 10^{-4} the E_b/N_0 difference is 2 dB, the same that was found without coding [103]. This difference can be overcome by increasing R in the NC scheme. As shown in the figure, for $R = 110$ antennas the difference is approximately 0.5 dB. If we target a lower BER, the difference between the NC and the coherent scheme is reduced to 1 dB, which is compensated by having only 20 additional antennas. For even lower BER, the two schemes are equivalent. The authors of [5] and [19] have also found the same asymptotic relationship between the coherent and NC schemes. Moreover, the fact that for low E_b/N_0 the use of CSI can result in a waste of resources has already been pointed out in [5].

Figure 4.30 Performance comparison between the non-coherent and coherent schemes for $J = 2$ users for the EEP design.

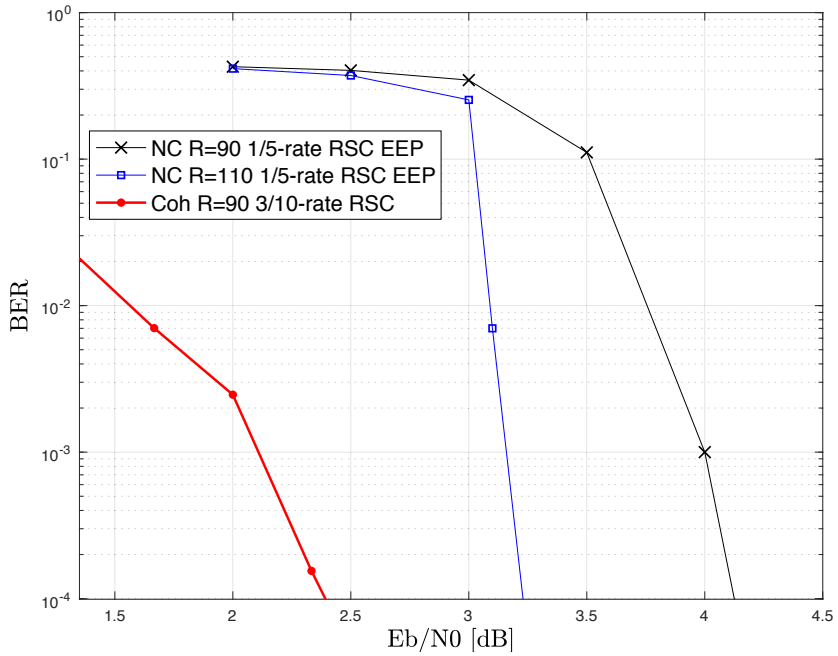

4.6 Conclusions

We have proposed a multi-user BICM-ID scheme for a non-coherent massive MIMO system based on M-ary DPSK with the objective of reducing the number of antennas required for a target performance. We have analyzed and proposed the EXIT chart as a useful tool for finding the best schemes for m-MIMO saving simulation. We propose an approach for EXIT curves based on the number of antennas for m-MIMO. Based on this model, we design a coding scheme suited for the constellation designs proposed in Chapter 3. The EEP design offers better performance than the UEP, although both schemes perform better than previous work. Also, including coding, we improve the design for unequal error protection, that may also be interesting to support multiple applications with different QoS requirements. We have shown that the number of users served by the BS can be increased with a 70% reduction in the number of antennas with respect to previous work. In particular, we show that with 100 antennas for the EEP design and a coding rate of $1/2$ we achieve the minimum probability of error. We have seen that R is allowed to decrease about two orders of magnitude with respect to the systems without coding presented in Chapter 3 and in [103]. Using iterative decoding also improves the performance compared to [104].

We parameterized the EXIT curves by the number of antennas that were used to optimize both UEP and EPP designs. We demonstrated that a feasible number of $R = 100$ antennas are sufficient for several situations. We have seen that R may be reduced from 1,000 to 100 with respect to the system operating without coding presented in Chapter 3. Moreover, using iterative decoding also improves the performance compared to other coded schemes [104]. The number of users that can be supported by the BS can increase at the cost of a higher number of antennas R. We show the importance of the mapping scheme, focusing on the mapping for individual constellation. However, an optimized mapping for the joint constellation is subject of future research.

The number of users that can be multiplexed together may be further increased with the aid of other coding schemes chosen as outer code, which are also left for further research.

Chapter 5

New Constellation based on DPSK for Rice Channels

In the previous chapters, we focused on the constellation scheme designs for channels with Rayleigh fading. In addition, these designs present a reasonable number of antennas even for m-MIMO thanks to the power channel coding schemes incorporated.

In this chapter, we redesign the previous constellations to consider a Rician fading that is likely to be found in the new scenarios in the future communication systems.

5.1 Introduction

The current scenarios such as rural or suburban environments, backhaul wireless systems [107], and even new D2D communications [34] can have a predominant line-of-sight (LOS) component, so that they are better modeled by Rician fading [108], [109]. The same happens when using higher frequencies, looking for wider spectrum availability, such as in millimeter frequency bands considered recently for 5G or even the emerging communications in the terahertz frequencies band [144].

For multi-user scenarios with Rician fading, the designs in [103] and those proposed in this thesis in Chapter 2-4, (published in [115, 116, 118]), originally proposed for Rayleigh fading, are no longer valid when we consider Rician fading due to the fact that the LOS component generates inter user interference (IUI) and inter symbol interference (ISI) when these designs are used under such propagation conditions. Therefore, the constellation scheme has to be redesigned in order to counteract as much as possible these effects of the LOS channel component. [111], [145] analyze the behavior of coherent massive MIMO in Rician channels and stress the importance of considering these specific propagation characteristics that may happen in realistic scenarios. The issues raised in these works

are for coherent systems. Now, in this chapter we consider them for the non-coherent systems.

In the area of the NC detection, often the correlation between the phase distortions experienced by the consecutively transmitted symbols is exploited by jointly processing the received multiple symbols in order to improve the system performance [9]. The authors in [146] presented a multiple symbol differential detector for m-SIMO which is not valid neither for Rician fading channels nor multi-user systems as we will show. Here, we will demonstrate that a multiple-symbol detection is not enough to compensate the interference unless we carefully select a new constellation design. In addition, the large number of antennas is not sufficient to cancel the IUI and ISI with the resources proposed in [115]. Therefore, we have to find an algorithm to cancel these terms.

5.2 Non coherent detection procedure in channels with Rician fading

We start from the decision variable $z[n]$ in (2.16). In respect of the channel, in this chapter we use the model defined in Chapter 2 for Rician fading. First, we analyse the full terms for the single user case, outlining the advantages of our design based on DPSK against energy-based detection.

5.2.1 Single user non coherent detection in Rician channel

We assume that our system has only one user ($J = 1$). The resulting received symbol from $z[n]$ is extended as follows

$$\begin{aligned} z[n] =&(\frac{1}{R}\sum_{r=1}^{R}|h_{r1}|^2 + \frac{2\mu}{R}\sum_{r=1}^{R}Re\{h_{r1}\} + \mu^2)s_1[n] \\ &+ \frac{1}{R}\sum_{r=1}^{R}h_{r1}x_1[n]v_r^*[n-1] + \frac{1}{R}\sum_{r=1}^{R}h_{r1}^*x_1^*[n-1]v_r[n] \\ &+ \frac{\mu}{R}[\sum_{j=1}^{R}x_1^*[n-1]v_r[n] + \sum_{r=1}^{R}x_1[n]v_r^*[n-1]] \\ &+ \frac{1}{R}\sum_{r=1}^{R}v_r[n]v_r^*[n-1]. \end{aligned} \tag{5.1}$$

As with the Rayleigh case, using the Law of Large Numbers [41] for the new terms we have that

$$\frac{1}{R}\sum_{r=1}^{R}|h_{r1}|^2 \overset{R\to\infty}{=} \sigma_h^2, \tag{5.2}$$

$$\frac{1}{R}\sum_{r=1}^{R} Re\{h_{r1}\} \overset{R\to\infty}{=} 0, \tag{5.3}$$

$$\frac{\mu}{R}[\sum_{r=1}^{R} x_1^*[n-1]v_r[n] + \sum_{r=1}^{R} x_1[n]v_r^*[n-1]] \overset{R\to\infty}{=} 0, \tag{5.4}$$

almost surely. Taking into account $(\sigma_h^2 + \mu^2) = 1$, we have

$$z[n] \overset{R\to\infty}{=} s[n] + i[n], \tag{5.5}$$

then we can calculate an estimation of $s[n]$ from $z[n]$ as (3.8). The noise plus interference term $i[n]$ is again extended for this case as follows

$$i[n] = z[n] - s_1[n] = \underbrace{s_1[n](\frac{1}{R}\sum_{r=1}^{R}|h_{r1}|^2 + \frac{2\mu}{R}\sum_{r=1}^{R} Re\{h_{r1}\} + \mu^2 - 1)}_{i_1[n]} + \underbrace{\frac{1}{R}\sum_{r=1}^{R}\nu_r^*[n-1]\nu_r[n]}_{i_4[n]}$$
$$\underbrace{\frac{1}{R}\sum_{r=1}^{R} h_{r1}x_1[n]v_r^*[n-1] + \frac{1}{R}\sum_{r=1}^{R} h_{r1}^* x_1^*[n-1]v_r[n]}_{i_2[n]} + \underbrace{\frac{\mu}{R}[\sum_{r=1}^{R} x_1^*[n-1]v_r[n] + \sum_{r=1}^{R} x_1[n]v_r^*[n-1]]}_{i_3[n]} \tag{5.6}$$

The four terms $i_1[n]$, $i_2[n]$, $i_3[n]$ and $i_4[n]$ are independent because the channel and noise are independent and uncorrelated. This assumption is demonstrated, as done for the Rayleigh case in Chapter 3, knowing that the covariance between any two interference terms is zero as

$$\begin{gathered} Cov(i_j, i_k) = E\{i_j[n]i_k[n]\} - E\{i_j[n]\}E\{i_k[n]\} = 0 \\ E\{i_j[n]i_k[n]\} = E\{i_j[n]\}E\{i_k[n]\}. \end{gathered} \tag{5.7}$$

Let us obtain the expectation for each term:

$$\begin{aligned} E\{i_1[n]\} =& E\{s_1[n](\frac{1}{R}\sum_{r=1}^{R}|h_{r1}|^2 + \frac{2\mu}{R}\sum_{r=1}^{R} Re\{h_{r1}\} + \mu^2 - 1)\} \\ =& \sigma_h^2 + \mu^2 - 1 \end{aligned} \tag{5.8}$$

as $(\sigma_h^2 + \mu^2) = 1$, then $E\{i_1[n]\} = 0$. On the other hand, the expectations for each term are

$$E\{i_2[n]\} = -\frac{1}{R}\sum_{r=1}^{R} E\{\nu_r^*[n-1]\}E\{h_{r1}x[n]\} - \frac{1}{R}\sum_{r=1}^{R} E\{\nu_r[n]\}E\{h_{r1}^* x^*[n-1]\} \tag{5.9}$$

$$E\{i_3[n]\} = \frac{\mu}{R}\left[\sum_{r=1}^{R} E\{x_1^*[n-1]\}E\{v_r[n]\} + \sum_{r=1}^{R} E\{x_1[n]\}E\{v_r^*[n-1]\}\right] \tag{5.10}$$

$$E\{i_4[n]\} = \frac{1}{R}\sum_{r=1}^{R} E\{v_r^*[n-1]\}E\{v_r[n]\} \tag{5.11}$$

as $E\{v_r[n]\} = 0$ then (5.9), (5.10) and (5.11) are 0.

Regarding the cross expectations $E\{i_j[n]i_k[n]\}$, since all terms include the expectation of the noise, $E\{v_r[n]\} = 0$, these terms cancel each other, giving $E\{i_j[n]i_k[n]\} = 0$ for any j and k in (5.7). For all that, we can add independently the power of the interference terms as $\mathfrak{I}_{Rice\ Single} = I_1 + I_2 + I_3 + I_4$. Then, the new individual interference terms in a NC-m-MIMO system with Rice fading for the single user case are formulated as follows

$$I_1 = \frac{(\sigma_h^2 + \mu^2)^2}{R} = \frac{1}{R} \tag{5.12}$$

$$I_2 = \frac{2\sigma_h^2\sigma^2}{R} \tag{5.13}$$

$$I_3 = \frac{2\mu^2\sigma^2}{R} \tag{5.14}$$

$$I_4 = \frac{1}{R}\sigma^4. \tag{5.15}$$

Therefore, the SINR obeys

$$SINR = \frac{E\{|s|^2\}}{\mathfrak{I}_{Rice\ Single}} = \frac{R}{1 + 2\sigma^2(\sigma_h^2 + \mu^2) + \sigma^4} = \frac{R}{1 + 2\sigma^2 + \sigma^4}. \tag{5.16}$$

As we can see in (5.16), the interference is independent of the Rician factor K, resulting that both Rice and Rayleigh channels are equivalent for $J = 1$ user.

5.2.2 Performance for single user non coherent m-MIMO system in Rician channels

In this section, numerical results by simulations are presented to assess the performance of the DPSK m-MIMO design. We assume a block fading, where during the transmission of a long symbol burst, *e.g.* 100,000 bits, the channels stay invariant, varying randomly between bursts.

In Figure 5.1 we plot the bit error rate (BER) for SNR=-8, -5 and 0 dB with a constellation size of $M = 4$ and $M = 16$ symbols. For $M = 4$, we compare the performance in two different Rician channels ($K = 10$ and $K = 100$) and Rayleigh channel ($K = 0$). As observed the K-factor does not influence in the performance when we use the DPSK design. Therefore, in contrast to previous works [126], we would not need to know the statistics of the channel. This is an advantage over energy-detection-based constellation designs. We can also see that an increase of the constellation order is possible at the expense of a higher number of antennas. In Figure 5.2, we analyse the BER versus the

reference SNR of the 32−DPSK scheme with regard to different R at the BS under Rician propagation. The receiving number of antennas is set to $R = 500$, 256 and 128. We can verify that the K-factor does not change the results with respect to the Rayleigh case. With this figure we show that it is feasible to increase the constellation order, by increasing the SNR or R.

Figure 5.1 Performance of 4-DPSK and 16-DPSK for several SNR and different K factors.

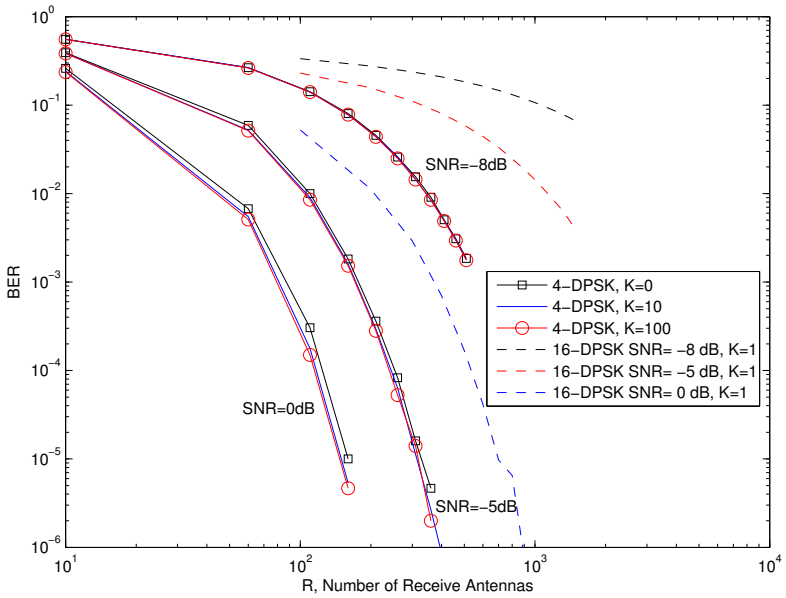

Figure 5.2 Performance of 32-DPSK for different R.

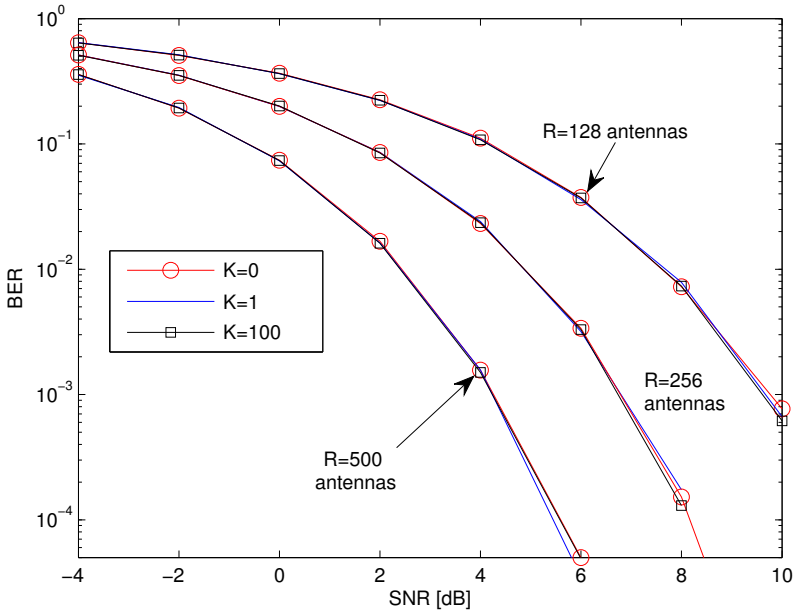

In order to compare the performance to previous work [126] we plot now the symbol error rate (SER) in Figure 5.3. It shows a performance comparison between the DPSK scheme and the energy detection scheme [126], both with $M = 8$ under Rician channels. We can see that the DPSK scheme exhibits better SER performance than the energy detection. In order to obtain the same performance as [126] with K=1 and SNR=10dB, our system requires an SNR of -1 dB. This means that we have an SNR gain of 11 dB for K=1. Similarly, we have 9 dB gain for $K = 10$ and 8.5 dB in the case of $K = 100$.

Figure 5.3 SER comparison of DPSK constellation with energy based design in m-MIMO.

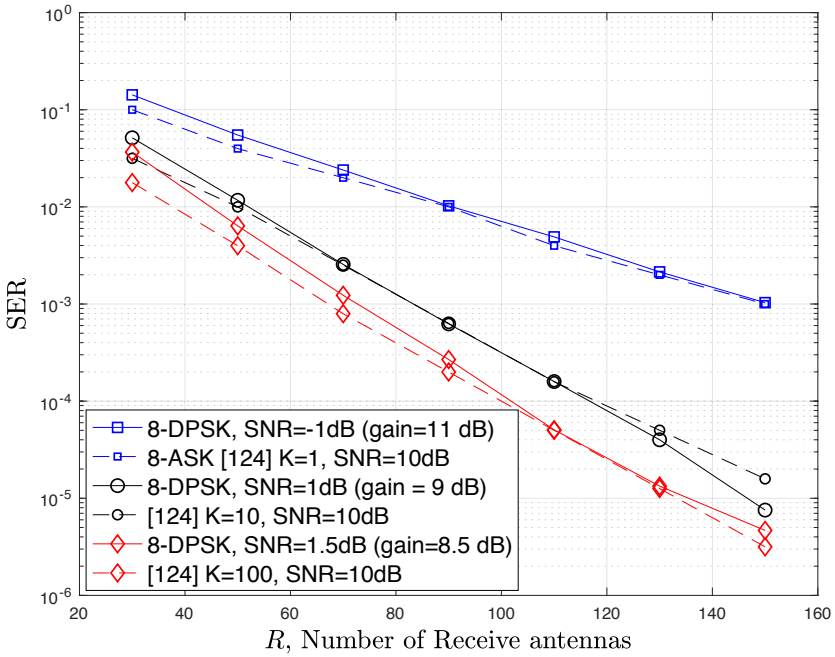

In Figure 5.4 we compare our proposed system to [126] for the same SNR = 10 dB and $M = 8$, where we show the performance of higher order DPSK modulation. Comparing the curves of DPSK and energy detection with $K = 1$ and for a target SER = 10^{-3}, we can see that with DPSK we can reduce in 140 the required number of antennas. If we wish to obtain the same performance with the same number of antennas, we can increase the order of constellation up to $M = 32$. The reduction in R is lower for higher K factor, because the energy detection of [126] works better for high K. Consequently our system can increase the spectral efficiency. In the case if we increase the K-factor to 10, our system reduces the required R in 80 antennas for a BER= 10^{-3}, while for $K = 100$ the reduction is 50 antennas.

Figure 5.5 shows the minimum required number of antennas R needed in order to achieve a target SER of 10^{-4} using different constellation size. We can see that the DPSK scheme with SNR=1dB is equivalent in performance to energy detection with SNR = 10 dB. Then we have an improvement of 9dB in SNR. For the same SNR = 10 dB, DPSK

allows us to save approximately 100 antennas when $M = 8$. The reduction is even larger for higher constellation size. If we fix a number of antennas, DPSK can increase the spectral efficiency. For example, for R=20 we have M=3 with [126] and M=8 for DPSK.

Figure 5.4 SER performance versus number of antennas.

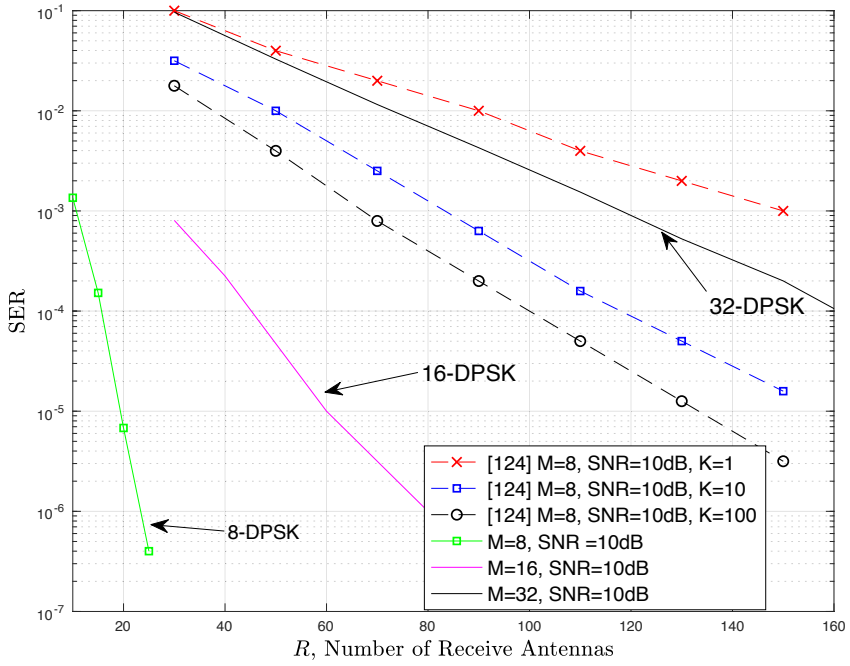

Figure 5.5 Minimum number of receive antennas R for a target SER= 10^{-4} performance for two different constellation designs.

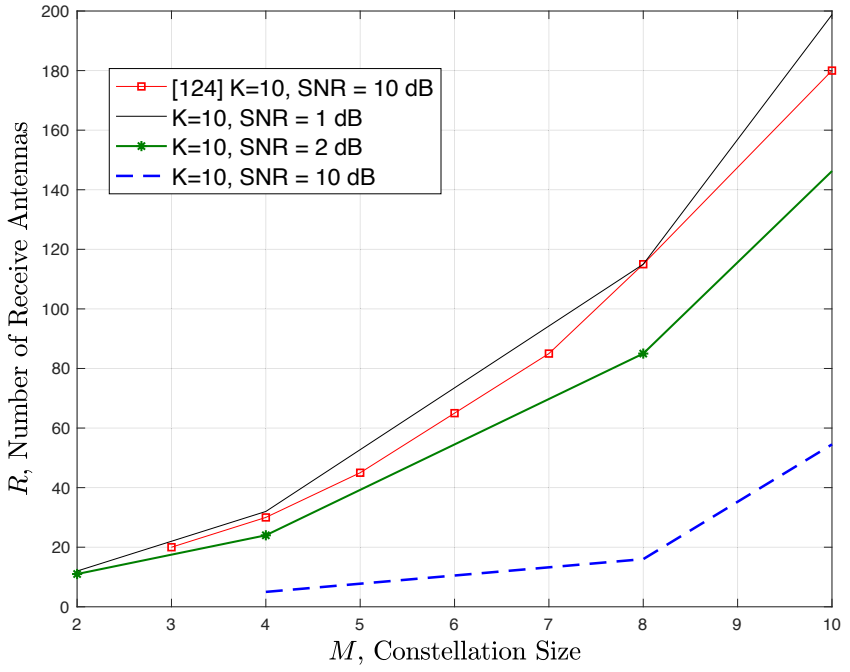

5.2.3 Problems for the multiuser systems

Having studied the single user case, it is the turn of MU case when we have Rician channel. In order to identify the effect of the LOS component we have to expand the different terms in the received signal $z[n]$ in (2.16), obtained after the NC detection procedure in the system model without channel coding scheme. Then, we can compute it for the channel statistics in (2.6) and (2.7) for the channel model in Section 2.3. Thus, the decision variable for Rician channel is as follows

$$z[n] = \frac{1}{R}\sum_{j=1}^{J}\sum_{r=1}^{R}[|h_{rj}|^2 + 2\mu\Re\{h_{rj}\} + \mu^2]s_j[n] + \underbrace{\mu^2\sum_{j=1}^{J}\sum_{\substack{k=1\\k\neq j}}^{J} x_j[n]x_k^*[n-1]}_{\substack{\textit{term not dependent on } R,\ (UIT)\\ \textit{due to the LOS component}}}$$

$$+ \underbrace{\frac{1}{R}\sum_{r=1}^{R}\sum_{j=1}^{J}\left\{\sum_{\substack{k=1\\k\neq j}}^{J} h_{rj}h_{rk}^* x_j[n]x_k^*[n-1] + h_{rj}x_j[n]v_r^*[n-1] + h_{rj}^* x_j^*[n-1]v_r[n] + v_r[n]v_r^*[n-1]\right\}}_{\textit{old terms also present in the Rayleigh case}}$$

$$+ \underbrace{\frac{1}{R}\sum_{r=1}^{R}\sum_{j=1}^{J}\left\{\sum_{\substack{k=1\\k\neq j}}^{J}\mu h_{rj}x_j[n]x_k^*[n-1] + \sum_{\substack{k=1\\k\neq j}}^{J}\mu h_{rj}^* x_j^*[n-1]x_k[n] + \mu[x_j[n]v_r^*[n-1] + x_j^*[n-1]v_r[n]]\right\}}_{\textit{new terms due to the LOS component}}. \tag{5.17}$$

In (5.17) we can see old terms which are also present in the solely Rayleigh case. Since the channel variance changes due to the K-factor, these terms are now as follows

$$\frac{1}{R}\sum_{r=1}^{R}|h_{rj}|^2 \overset{R\to\infty}{=} \sigma_h^2, \tag{5.18}$$

$$\frac{1}{R}\sum_{r=1}^{R}\Re\{h_{rj}\} \overset{R\to\infty}{=} 0. \tag{5.19}$$

Moreover, extracting the mean μ from channel coefficients we can notice the new terms in (5.17) which are related to the LOS component. For Rayleigh case, since $K = 0$, then $\mu = 0$, consequently these terms are zero. By contrast, here the new terms obey

$$\frac{1}{R}\sum_{r=1}^{R}\sum_{j=1}^{J}\sum_{\substack{k=1\\k\neq j}}^{J}\mu h_{rj}x_j[n]x_k^*[n-1] \overset{R\to\infty}{=} 0, \tag{5.20}$$

$$\frac{\mu}{R}[\sum_{r=1}^{R} x_j^*[n-1]v_r[n] + \sum_{r=1}^{R} x_j[n]v_r^*[n-1]] \overset{R\to\infty}{=} 0. \tag{5.21}$$

Due to the law of Large Numbers all new terms are canceled except one, which does not depend on R. This term, caused by the LOS component, is called *useful interfering term* (UIT) and is defined as

$$UIT[n] = \sum_{j=1}^{J} \sum_{\substack{k=1 \\ k\neq j}}^{J} x_j[n]x_k^*[n-1]. \tag{5.22}$$

The UIT increases the number of interfering terms which cause IUI with respect to the Rayleigh case. Here, we find the main issue for NC-m-MIMO based on DPSK in a multiuser environment with Rician fading. The apparent difficulty is the cancellation of this term which does not depend on R, so increasing the number of antennas does not involve any effect on the UIT.

Consequently, we analyse this term because we will be able to convert part of the IUI into a useful term for the non-coherent detection. In Section 5.3 , we will show how to consider the characteristics of the UIT in the constellation design in order to improve the performance in the Rice channels with respect to Rayleigh channels. Based on this new design which accounts for the UIT, the receiver in Figure 2.7 is modified as shown in Figure 5.6. The output of the NC detection procedure is feed through the Joint Symbol Detection (JDS) block which can obtain an estimate of $\varsigma[n]$ from $z[n]$, as will be explained in Section 5.6 and efficiently recover the users data $s_j[n]$ from the jointly detected symbol $\hat{\varsigma}[n]$.

Figure 5.6 Receiver Model for multiuser NC-m-MIMO in Rice fading case.

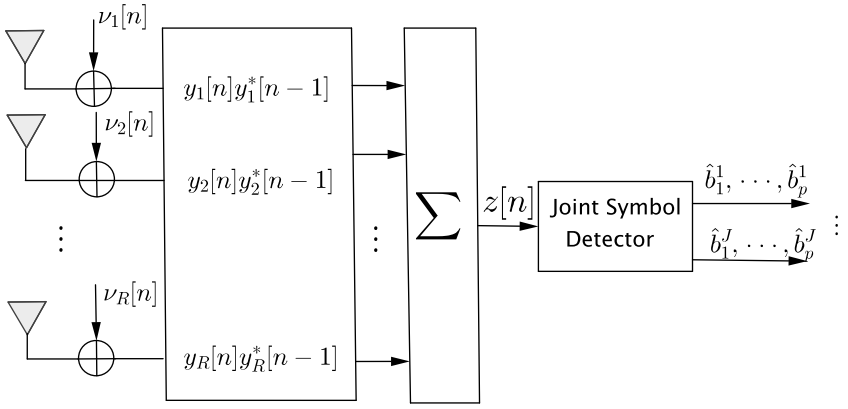

5.3 New constellation design for Rician fading

Our previous designs (published in [115]) achieved a good performance with a reasonable number of antennas in Rayleigh fading, as was described in Chapter 3-4. When we have Rician channel, our designs remain valid in single user systems as was explained in Section 5.2.1 (published in [116]), but they are not applicable when we have a multi-user system due to the new IUI terms introduced by the LOS component, as we will show next.

As it was done in [110], for energy detection, when the channel is Rice we need to redesign the constellation based on DPSK. Here we propose a new design and we provide some general guidelines for further designs.

5.3.1 Previous design: influence of UIT on constellation design

In Section 3.5, an EEP design was proposed with the objective that all users have the same error performance. In that design, the users symbols were intercalated in the unit circle, keeping equal distance among them. When that design is applied to a Rice channel, in the constellation which was shown in Figure 3.57 for Rayleigh, new terms that appear due to the IUI, bring forth the constellation shown in Figure 5.7

Figure 5.7 shows for $M = 2$ and $J = 2$ the received constellation with UIT and neglecting the interference terms that vanish with increasing R. The red stars denote the position of the joint symbol plus interference computed from (2.18) and (5.22) as:

$$\varsigma[n] + UIT[n] = \varsigma[n] + \mu^2\varsigma[n] = (1 \pm \mu^2)\varsigma[n]. \tag{5.23}$$

The UIT defined in (5.22) depends on the information symbols transmitted by each user:

- The UIT coincides with the joint symbol ς when both users transmit the same or opposite symbol in two consecutive time instants resulting in a positive sign $(+\mu^2)$ in (5.23):

$$UIT[n] = \varsigma[n] \quad when \quad \begin{cases} s_j[n] = s_j[n-1] & or \\ s_j[n] = -s_j[n-1] & \forall j \end{cases} \tag{5.24}$$

- The UIT is opposite to the joint symbol $(-\varsigma)$ when one user transmits the same symbol and the other user transmits opposite symbol in two consecutive time instants resulting in a negative sign in (5.23), $(-\mu^2)$:

$$UIT[n] = -\varsigma[n] \quad when \quad \begin{cases} s_j[n] = s_j[n-1] & and \\ s_k[n] = -s_k[n-1] & j \neq k \end{cases} \tag{5.25}$$

The issue in the design shown in Figure 5.7 is that we have double symmetry with respect to the coordinate axes. Hence, in the case that the UIT is opposite to the joint symbol $(-\varsigma)$ the amplitud of the received joint symbol is reduced an amount of $1-\mu^2$, more reduced as the LOS increases. Therefore ς plus UIT converges to zero as $(\mu \to 1)$, making impossible to decode the users information.

Figure 5.7 Constellation for J =2 users and $M = 2$ valid for Rayleigh case but not for Rice case.

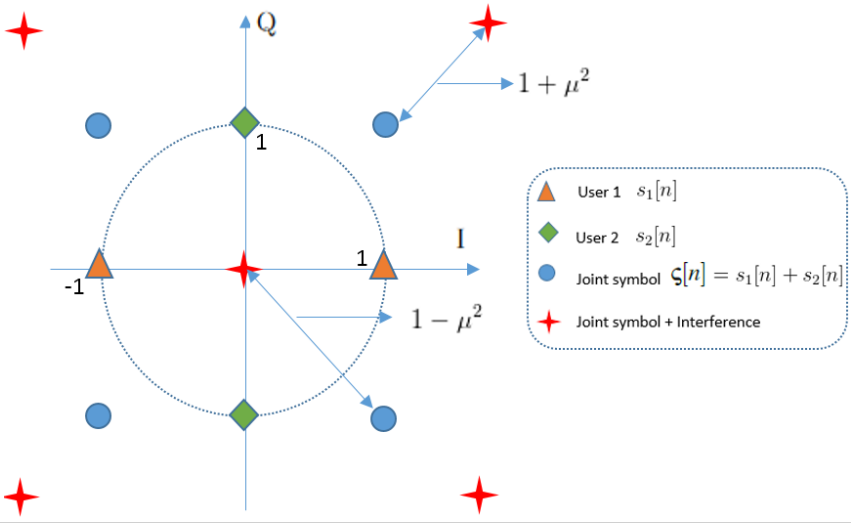

5.3.2 New constellation design for Rician channel

In order to solve the problem of interference due to the LOS component we present a new design. In Figure 5.8 an example is shown for $J = 2$ users and $M = 2$. The full constellation for one user (*e.g.* green diamond in Figure 5.8 (a)) is intertwined with another user (orange triangles in Figure 5.8 (a)), instead of inserting each symbol one by one as in Figure 5.7. More users $(J > 2)$ can be interspersed throughout in the unit circle. The blue circles represent the ideal joint constellation as in the Rayleigh case $(K = 0)$, but when we consider the effect of μ, the red stars appear in Figure 5.8 (b). This is due to the UIT in (5.17) that is not cancelled by increasing R, but merely moves the joint symbol ς towards zero. Unlike in the constellation in Figure 5.7, we have an unambiguous relation between users symbols and the joint symbols despite the UIT. In addition, extra symbols appear that help us for a more reliable decision since they give us information about the channel effects, that we will use in the detection algorithms. This is due to the fact that we remove the double symmetry showed Figure 5.7.

We can note that in the first received symbol $(l = 1)$ the UIT term is always known. In the particular case of two users $(J = 2)$, $x_j[0] = 1$ and considering differential encoding in (2.5) we have

$$\begin{aligned} UIT(1) &= x_1[1]x_2^*[0] + x_2[1]x_1^*[0] \\ &= s_1[1]x_1^*[0]x_2^*[0] + s_2[1]x_2^*[0]x_1^*[0] \\ &= s_1[1] + s_2[1] = \varsigma[1] \end{aligned} \tag{5.26}$$

Then, the first received symbol has no IUI but is just amplified, case $(1+\mu^2)\varsigma$ in (5.23). We will make use of this property in the proposed detection algorithm in Section 5.6.

Figure 5.8 New Constellation Design for J =2 users and $M = 2$. (a) For Rayleigh case. (b) For Rice case.

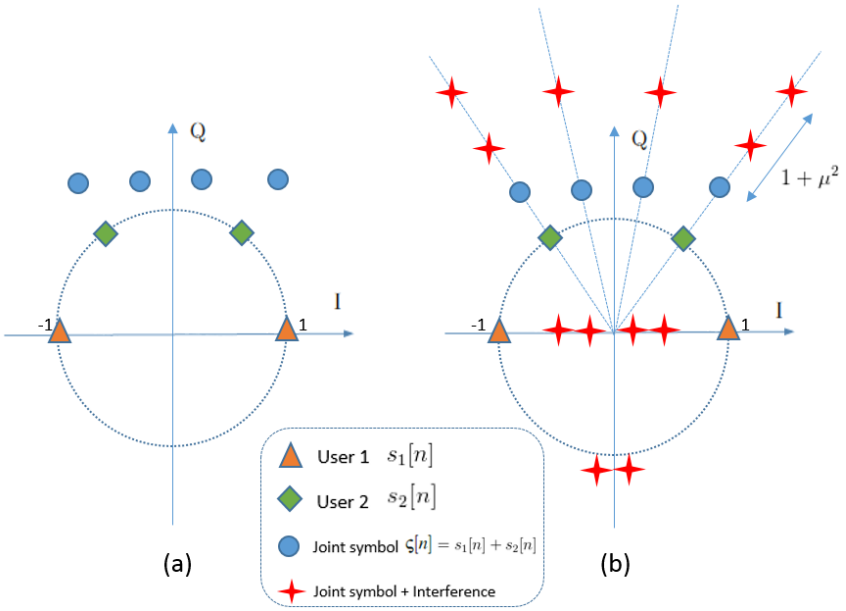

5.3.3 Considerations for MU NC m-MIMO

After an in-depth analysis on the constellation design and the issues detected, we can offer several considerations which have to be taken into account when designing a different constellation to work with a Rician fading.

1. In general, all individual constellations $\mathfrak{M}_j$ must be designed so that their symbols do not overlap after adding the transmitted signals from all users at the BS, in order to separate the users' signals.

2. The joint constellation can not display a double symmetry with respect to the coordinate axes. One possible option is intercalating the symbols of a given user between two symbols of the previous user to avoid the symmetry.

3. The best solution is obtained with the same distance among the symbols of the same users (maximizing the minimum distance).

4. Using the half plane for allocating each user is more recommendable because the joint symbols are better distributed and remain unambiguously detectable even with the interference.

In addition, we must bear in mind that the interference created by the LOS component is in general harmful, since it can cause that several different transmit symbols collapse to the same one at reception, making then impossible to detect. Therefore, by constellation design, the LOS component can be used to cause several different joint symbols corresponding to the same transmitted one, which helps us to make a more reliable decision, because it provides information about the interference itself.

5.4 Analysis of Signal to Interference plus Noise Ratio for Rician fading

In this section, we extend the analysis of the power of the different terms of the interference performed for Rayleigh channel in Chapter 3 to the Rice case. We further demonstrate that all interfering terms $i[n]$ are keeping independent among them, so the total interference power I is the sum of the individual powers. Here, a novelty is the presence of UIT which does not depend on R, contrary to the others that in general decrease with R. Therefore, we study the SINR for the following different cases.

5.4.1 SINR with unknown UIT

In order not to increase the complexity in the receiver with respect to the Rayleigh case, we consider the UIT is totally unknown in the detection procedure. Since it can not be removed by increasing the number of antennas R, the total interference will be increased due to the lack of knowledge of this term. We consider this case as a worst performance bound. Consequently, we will have to include the power of UIT (I_{UIT}) in the total interference. By exploiting the properties of Gaussian and Wishart matrices, the expectation of the power of the different terms of $i[n]$ can be obtained. The first four terms have been already obtained in Section 3.2. However, the value of some of them is

different because here $\sigma_h^2 \neq 1$. They are as follows

$$
\begin{aligned}
i[n] = z[n] - \varsigma[n] = & \underbrace{\frac{1}{R}\sum_{j=1}^{J}(\sum_{r=1}^{R}[|h_{rj}|^2 + 2\mu\Re\{h_{rj}\} + \mu^2] - 1)s_j[n]}_{i_0[n]} \\
& + \underbrace{\frac{1}{R}\sum_{r=1}^{R}\sum_{j=1}^{J}\sum_{\substack{k=1 \\ k\neq j}}^{J} h_{rj}h_{rk}^{*}x_j[n]x_k^{*}[n-1]}_{i_1[n]} + \underbrace{\frac{1}{R}\sum_{j=1}^{J}\sum_{r=1}^{R}[h_{rj}x_j[n]v_r^{*}[n-1] + h_{rj}^{*}x_j^{*}[n-1]v_r[n]]}_{i_2[n]} \\
& + \underbrace{\frac{1}{R}\sum_{r=1}^{R} v_r[n]v_r^{*}[n-1]}_{i_3[n]} + \underbrace{\frac{\mu}{R}\sum_{r=1}^{R}\sum_{j=1}^{J}\sum_{\substack{k=1 \\ k\neq j}}^{J}[h_{rj}x_j[n]x_k^{*}[n-1] + h_{rj}^{*}x_j^{*}[n-1]x_k[n]]}_{i_4[n]} \\
& + \underbrace{\frac{\mu}{R}[\sum_{r=1}^{R}\sum_{j=1}^{J} x_j[n]v_r^{*}[n-1] + \sum_{r=1}^{R}\sum_{j=1}^{J} x_j^{*}[n-1]v_r[n]]}_{i_5[n]} + \underbrace{\sum_{j=1}^{J}\sum_{\substack{k=1 \\ k\neq j}}^{J}\mu^2 x_j[n]x_k^{*}[n-1]}_{(useful)\ interference\ term}
\end{aligned}
\tag{5.27}
$$

$$I_0 = \frac{J^2\sigma_h^2\mu}{R} \tag{5.28}$$

$$I_1 = \frac{\sigma_h^4 J}{R} \tag{5.29}$$

$$I_2 = \frac{2\sigma_h^2\sigma^2 J}{R} \tag{5.30}$$

$$I_3 = \frac{\sigma^4}{R}. \tag{5.31}$$

The power of the new terms, which appear due to the non-zero mean of the channel, are

$$I_4 = \frac{2\mu^2 J(J-1)\sigma_h^2}{R} \tag{5.32}$$

$$I_5 = \frac{2\mu^2\sigma^2 J}{R}. \tag{5.33}$$

Similarly, the interfering power due to the UIT is

$$I_{UIT} = J(J-1)\mu^4, \tag{5.34}$$

then the total interference is formulated as

$$I_{total}^{worst} = \sum_{i=0}^{5} I_i + I_{UIT}, \tag{5.35}$$

and the SINR that we can achieve is

$$SINR_{worst} = \frac{E\{||\widetilde{\mathbf{H}}x||^2\}}{I_{total}^{worst}} = \frac{(\mu^2+\sigma_h^2)JR}{J(J-1)\mu^4R + J\sigma_h^2(J\mu+\sigma_h^2+2\mu^2(J-1)) + 2\sigma^2J(\mu^2+\sigma^2)+\sigma^4} \tag{5.36}$$

since $(\mu^2+\sigma_h^2)=1$, then the SINR for the worst case can be reduced to

$$SINR_{worst} = \frac{JR}{J(J-1)\mu^4R + J\sigma_h^2(J\mu+\sigma_h^2+2\mu^2(J-1)) + 2\sigma^2J+\sigma^4} \tag{5.37}$$

We can now propose two approximations for the low and high SNR regimes, that is when either the self-interference or the AWGN noise contributions are dominant. For high SNR we have that only I_{UIT} is significant and constant (independently of R), so that

$$SINR_{worst}^{H} = \frac{1}{(J-1)\mu}, \tag{5.38}$$

while for low SNR (5.39), the main dominant term is I_5 which does not depend on the Rice factor K, matching with the Rayleigh case.

$$SINR_{worst}^{L} = \frac{RJ}{\sigma^4}. \tag{5.39}$$

Since we are interested in the low SNR regime, we can see that our system is independent of the channel statistics for low ρ.

As we can see in Figure 5.9, the SINR when we can not estimate the UIT matches the theoretical expression in (5.37) for $R = 100$ and 1000 antennas. Note that as ρ increases the SINR is limited by the UIT value which depends on the Rician factor K but not on the number of antennas. Also the bounds for high and low K are shown.

5.4.2 SINR with perfectly known UIT

In this case, we consider that the UIT is correctly estimated using the best detection algorithm at the cost of an increased receiver complexity. This is just considered in this subsection for obtaining a performance bound that we will try to achieve with our designs (Figure 5.8). Consequently, we can ignore that term to derive the total interference as $I_{total}^{ideal} = \sum_{i=1}^{5} I_i$. Then the SINR obeys

$$SINR_{ideal} = \frac{E\{||\widetilde{\mathbf{H}}x||^2\}}{I_{total}^{ideal}} = \frac{JR}{J\sigma_h^2(J\mu+\sigma_h^2+2\mu^2(J-1)) + 2\sigma^2J+\sigma^4} \tag{5.40}$$

We propose two approximations for the low and high SNR regimes as well. For high SNR we have that only I_0 is significant, so that

$$SINR_{ideal}^{H} = \frac{R}{J\mu\sigma_h^2}, \tag{5.41}$$

Figure 5.9 SINR for unknown UIT case (worst case).

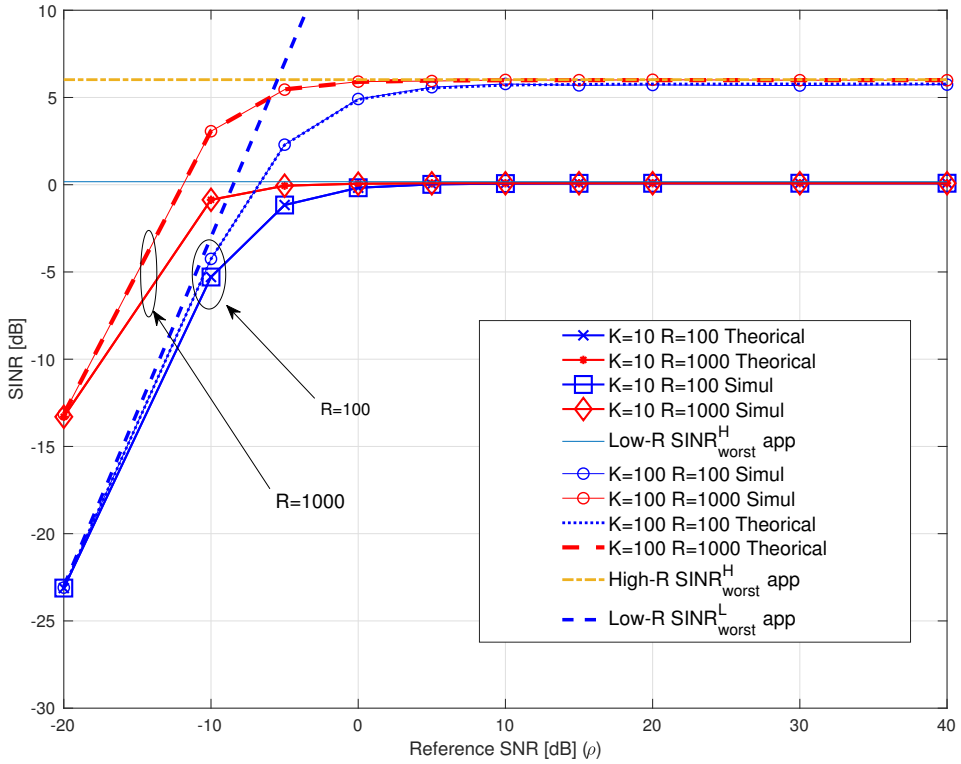

while for low SNR (5.42), the main dominant term is I_3 which does not depend on the Rice factor K, matching with the Rayleigh case and the worst case previously explained. Again, we can see as our system is independent of the channel statistics for low ρ.

$$SINR^{L}_{ideal} = \frac{RJ}{\sigma^4}. \tag{5.42}$$

From equations (5.40)-(5.42) we can see that, increasing the number of antennas at the BS, the SINR increases in the same proportion. That is, the energy efficiency scales as R, the same scaling law as for coherent systems with perfect CSI, while for coherent systems with non-perfect CSI the energy efficiency scales as $\sqrt{R}$ [39].

Figure 5.10 shows the SINR obtained by simulation along with the theoretical values for $J = 2$ users, K =10, 100 and 1000, where we can see the perfect agreement with (5.40) and the approximations (5.41) and (5.42). Again we can see that Rice and Rayleigh cases are identical for low SNR. Conversely, we are in the high SNR regime when $\sigma^4 << J^2\sigma_h^2\mu$, applying $\mu\sigma_h^2 = 1/K$, then $\sigma^4 << J^2/K$. According to (2.14) this happens when the reference $SNR >> K$. In this case we have a gain with respect to Rayleigh propagation thanks to the UIT is correctly estimated.

Figure 5.10 SINR for perfectly Known UIT case.

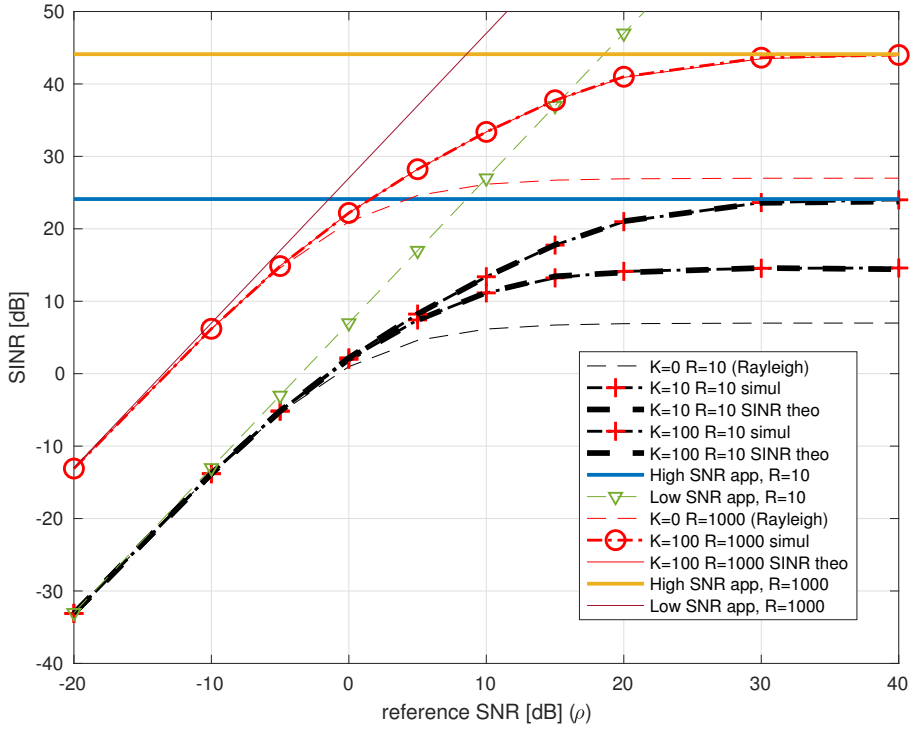

5.5 Classical Algorithm for multiuser detection

In this section, we review classical algorithms which are well known in the literature and have been proposed to decode frames of L symbols ($l = 1, \cdots, L$) for non-coherent multi-user schemes. We assume a frame is made of one reference symbol followed by L information symbols, then we have $L + 1$ symbols per frame. In Table 5.1 we collect some examples for the spectral efficiency corresponding to different values of L. The classical algorithms have some drawbacks when we talk about NC-m-MIMO in Rician channels. Their complexity grows exponentially with L and they can not compensate the interference caused by Rician fading. Therefore, we will propose in the following section a new algorithm to compensate this interference and even improve the performance with respect to the Rayleigh case.

Table 5.1: Spectral Efficiency reduction due to the insertion of a reference symbol

	$L = 2$	$L = 5$	$L = 10$
Useful Rate	2/3	5/6	10/11

5.5.1 Detection by L-symbol sequences

This technique consists in decoding sequences formed by multiple symbols instead of symbol-by-symbol, to reduce the effect of the UIT. However, independently of the chosen constellation, due to the fact that different combinations of user symbols may collapse to the same UIT after non-coherent combination at the receiver, we may get the same sequence in reception for different transmitted symbols. Increasing L does not help, because it creates even higher probability of having some repeated sequences. Therefore, this detection technique does not offer a good performance in Rician channels for our NC system.

5.5.2 Detection by double Minimum Distance

Another method is using a MD detector twice: one detector for the joint symbol, $\hat{\varsigma}_j$ and another MD detector for the UIT. Then we choose the minimum distance solution jointly as follows: for each received joint symbol, we choose a feasible value of UIT originating from the constellation in Figure 5.8. Then, each UIT is subtracted to the received symbol ($z[n]$). In order to make a minimum distance detection we compare the obtained symbol with the joint constellation $\mathfrak{M}$, obtaining a distance d_k, where the subindex k indexes the set of UIT values. We repeat this procedure for all possible UIT values. Finally, we select the estimated joint symbol corresponding to the minimum d_k. For the case $K = 0$, we do not have the UIT term, therefore the decoding procedure boils down to the one in Section 3.2. The main problem is the error propagation (EP), because we are doing symbol-by-symbol detection, taking a decision based on the previous symbol.

5.6 Algorithm proposal for non coherent detection in Rician fading: *Joint Symbol Detection*

It is noticed from (3.1) that non-coherent differential detection causes extra interfering terms with respect to the Rayleigh case. It was not possible to cancel such terms using classical algorithms. Therefore, we avail of the new joint constellation of Figure 5.8 to improve the decision. Recall that Figure 5.8 shows an extended constellation that considers all possible received points due to all possible experienced UIT values. Hence, by using this constellation, the originally transmitted symbols are detected without knowing the actual UIT that took place.

5.6.1 Stages of the proposed algorithm

The first two symbols of each sequence of L, rely on the decision of $l = 1$ to improve the decision of $l = 2$. With these decisions, we provide a reduction of the possible received sequences, avoiding their repetition. By analyzing how this UIT progresses as the users transmit information symbols, we have decided to restrict the detection of UIT for the first two symbols. Extending it to $l = 3$ would increase seriously the complexity and errors may propagate from the decision $l = 2$ to $l = 3$, since differential encoding is employed. In order to avoid the effect of the EP, a decision can be based on a number of consecutive symbols just like in [9] with multi-symbol differential detector, once we have avoided the repetition of sequences with the decision of the first two symbols. Thus, the number of symbols which are used in the detection is L. The new algorithm consists in the next steps:

1. The first symbol ($l = 1$) can be obtained directly by dividing the received symbol by $1 + \mu^2$, followed by a minimum distance detection using the constellation in Figure 5.8 (a) since there is not IUI yet.

2. For $l = 2$, we take a decision according to:

   2.1 Select the sequence with minimum distance among all possible resulting sequences of any $L = 2$ symbols of the extended joint constellation (Figure 5.8 (b)).

   2.2 We compare the symbol corresponding for $l = 1$ in the selected sequence in 2.1 with the step before.

   a) In the case the symbol for $l = 1$ coincides with the decoded one in step 1: the selected sequence for $l = 2$ is correct.

   b) In the case the symbol for $l = 1$ does not coincide with step 1: select those sequences for $L = 2$ symbols matching with the decision for symbol $l = 1$ in step 1. Repeat a minimum distance based decision among all the sequences of the subset.

3. For $l > 2$, select the sequences whose $l = 1$ and $l = 2$ fit with those selected in step 1 and 2. Make a minimum distance decision with the subset of resulting sequences.

In Algorithm 1 a pseudocode is shown for the proposed non-coherent detection algorithm.

Algorithm 2 Non-coherent detection of sequences with $L > 2$ symbols for JSD Algorithm.

Input Data: received L symbols: $z[1], ..., z[L]$
Result: $b_1^j, ..., b_p^j$ for j=1, ..., J
Initialization
Step 1: decoding symbol 1 **is**
    $z[1]/(1+\mu^2)$
    MD using constellation Figure 5.8(a)
    return $\hat{s}_j[1]$
end
Step 2: decoding symbol 2 **is**
    MD using constellation Figure 5.8(b) **return** $s_j^*[1], s_j^*[2]$
if $s_j^*[1] = s_j[1]$ **then**
  sequence correct
  $\hat{s}_j[1] = s_j^*[1]$ and $\hat{s}_j[2] = s_j^*[2]$
else
  subset: sequences of $L = 2$ symbols with $s_j[1]$ **from** step1
  multiple-sequence MD with subset using constellation Figure 5.8 (b) $\hat{s}_j[1]$ = step 1 and $\hat{s}_j[2] = s_j^*[2]$
end if
    return$\hat{s}_j[1]$ and $\hat{s}_j[2]$
end
Step 3: decoding symbol $l > 2$ **is**
    subset: sequences of L with $\{s_j[1]$,$s_j[2]\}$ **from** step2;
    MD using constellation Figure 5.8(b)
    return $\{\hat{s}_j[1], ..., \hat{s}_j[L]\}$
end
Binary Conversion : $\hat{s}_j[n] \rightarrow \hat{b}_1^j, ..., \hat{b}_p^j$

5.6.2 Simulation results

In this section we examine the performance of our design in a two-user ($J = 2$) uplink scenario with frequency-flat Rician fading, where a random channel is generated at each iteration following the model explained in Chapter 2 and it is kept constant for L consecutive transmitted symbols (block fading), for a minimum of 100,000 iterations. The channels corresponding to the transmission for each of the two users are uncorrelated and they have the same K factor (with values 0, 1, 5, 10, 50 and 100) following equations (2) and (3). The constellation order of the users signals M varies from 2 to 8 and the number of antennas at the BS is changed between $R = 10$ and $R = 10000$.

Firstly, we analyze the SER obtained by the previous classical algorithms. In the case of detection by L-symbol sequences, Figure 5.11 shows that the detection is possible only for sequences of $L = 2$ symbols and increasing the K factor helps to improve the performance. However, when L increases there is a number of antennas R from which the performance worsens when K increases, that is the detection by sequences does not help when we have a Rice fading. In particular, we can see in Figure 5.11 that for $L \geq 10$ and $R > 100$ the performance for $K = 10$ is worse than for Rayleigh propagation ($K = 0$) in [115]. Alternatively, we can use MD, as shown in Figure 5.11. In this case, the SER for the case of $J = 2$ users and a Rician factor of $K = 10$ is shown. We can see a strong degradation in the performance as L increases, remaining the same from $L \geq 8$, due to the fact that the EP increases for longer frames. Again, this technique does not offer a good performance for Rician channels.

Figure 5.11 Comparison of SER in classical algorithms for $J = 2$ users, $\rho = 0$ and $M = 2$ as L and K values.

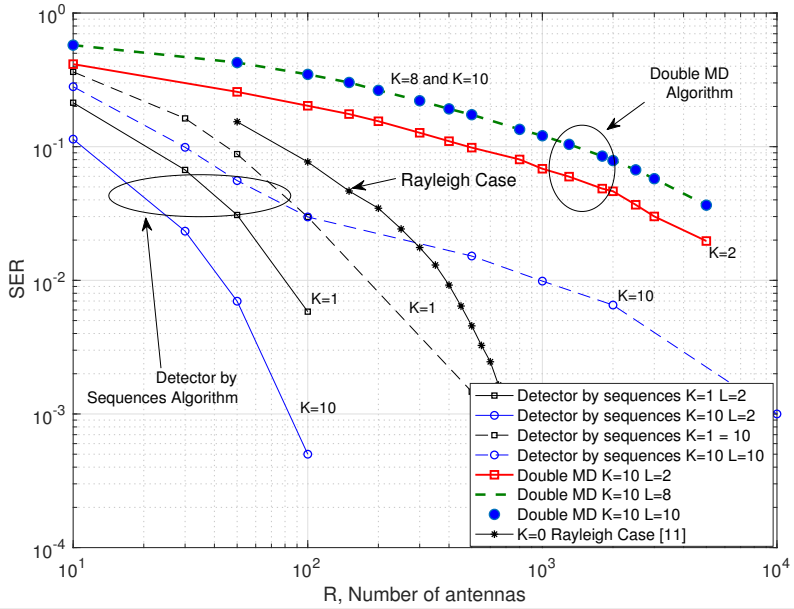

Now, we examine the performance of the proposed JSD algorithm with the new constellation. First we verify the accuracy of the detection of the first two symbols, since the remaining ones depend on them. In Figure 5.12 the SER when only decoding the first symbol ($l = 1$) is shown, corresponding to the first step in JSD algorithm. $R = 50$ antennas is used for three constellation sizes ($M = 2, 4$ and 8-DPSK) and different fading factors. We can see that even for very low SNR, we can correctly detect the first symbol. Moreover, the performance improves when increasing K factor up to $K = 5$ where it saturates. Hence the IUI does not affect the detection in this first step due to the fact that the UIT coincides with the first transmitted symbol.

Figure 5.12 SER for first symbol, J=2 users, R=50 antennas and M=2, 4 and 8.

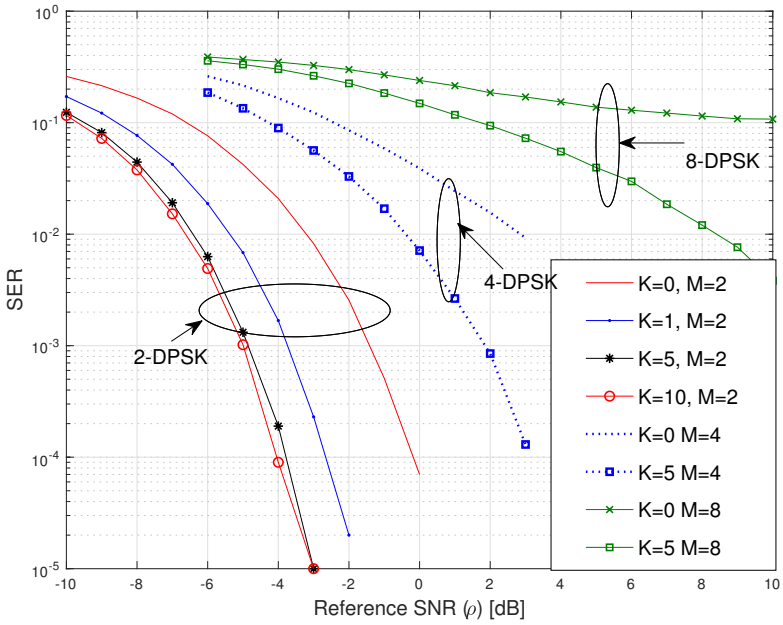

Next, we validate in Figure 5.13 the second step in the JSD algorithm, that is detecting the second symbol ($l = 2$), by means of the SER. We can see that using the knowledge of the first symbol helps us to detect the second one. Again, the performance improves when increasing K factor up to $K = 10$ where it saturates in this case. This contrasts with the performance of [110] where a value of $K > 100$ is needed to obtain an advantage with respect to Rayleigh propagation.

Figure 5.13 SER for second symbol detected, $J = 2$ users, $\rho = 0$ dB, $M = 2$.

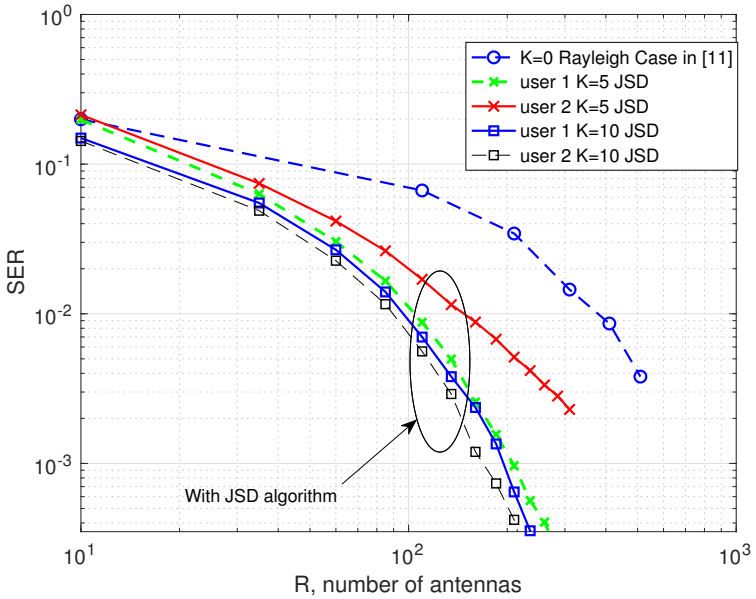

Once we have validated the detection of the first two symbols, we present in Fig-

ure 5.14 the SER when detecting the complete sequence of $L = 5$ symbols for $K = 1$ and $SNR = 0$ dB. We can see that JSD offers a better performance than the two conventional algorithms as R increases. In this figure we also show the theoretical SER corresponding to considering UIT as interference (the worst case defined in Section 5.4.1), that is, using the SINR of (25) in (33) and the theoretical SER obtained when UIT is perfectly known (the ideal case presented in Section 5.4.2), that is, using the SINR of (29). We can see that with JSD we practically approach the bound defined by (29).

Figure 5.15 shows the SER and its bounds for $K = 10$ and $SNR = 0$ dB. Again, we can see that our scheme outperforms the conventional ones. The performance improves when L increases in our JSD algorithm, unlike in classical algorithms. In particular, for $L = 2$ we have a performance that is slightly worse than the theoretical bound of (29), for $L = 5$ it is practically approaching the bound (29), while with $L = 10$ we even outperform this bound, meaning that we are able to not only cancel but make use of the UIT to improve the performance.

The performance in Rayleigh and Rice channels is further examined in Figure 5.16 where we plot the SER of (33) with SINR (29), that is, when UIT is perfectly known. In this figure $\rho = -3$ dB and 3 dB, $J = 2$ users and a higher order constellation, $M = 4$ is used. We can see that for very low SNR the K factor does not influence the performance, as we anticipated in Figure 5.10. When we increase the SNR, the Rician propagation helps to improve the performance.

Figure 5.14 SER for $K = 1$ with $J = 2$ users, $\rho = 0$ dB, $M = 2$ and $L = 5$.

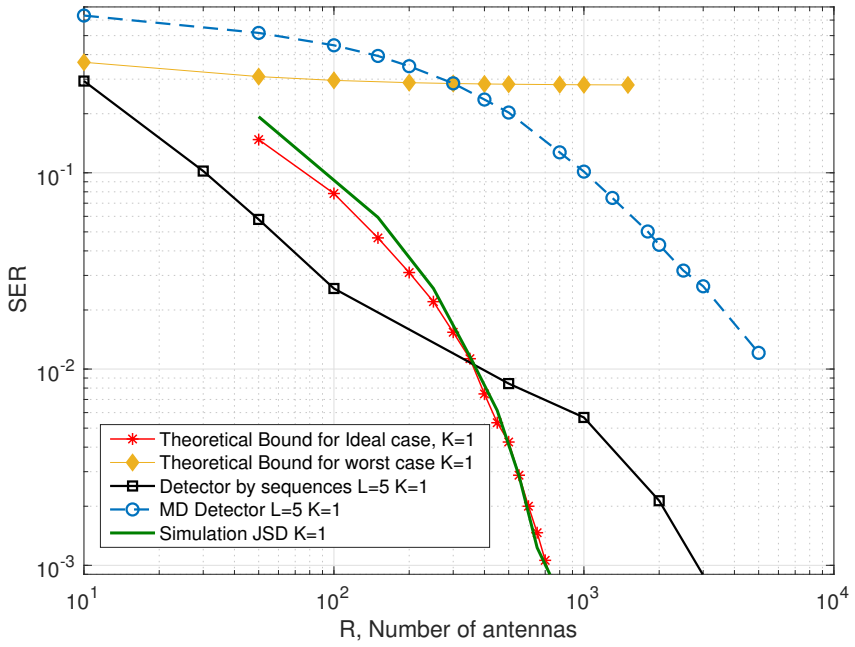

Figure 5.15 SER for $K = 10$ with $J = 2$ users, $\rho = 0$ dB, $M = 2$ and $L = 5$.

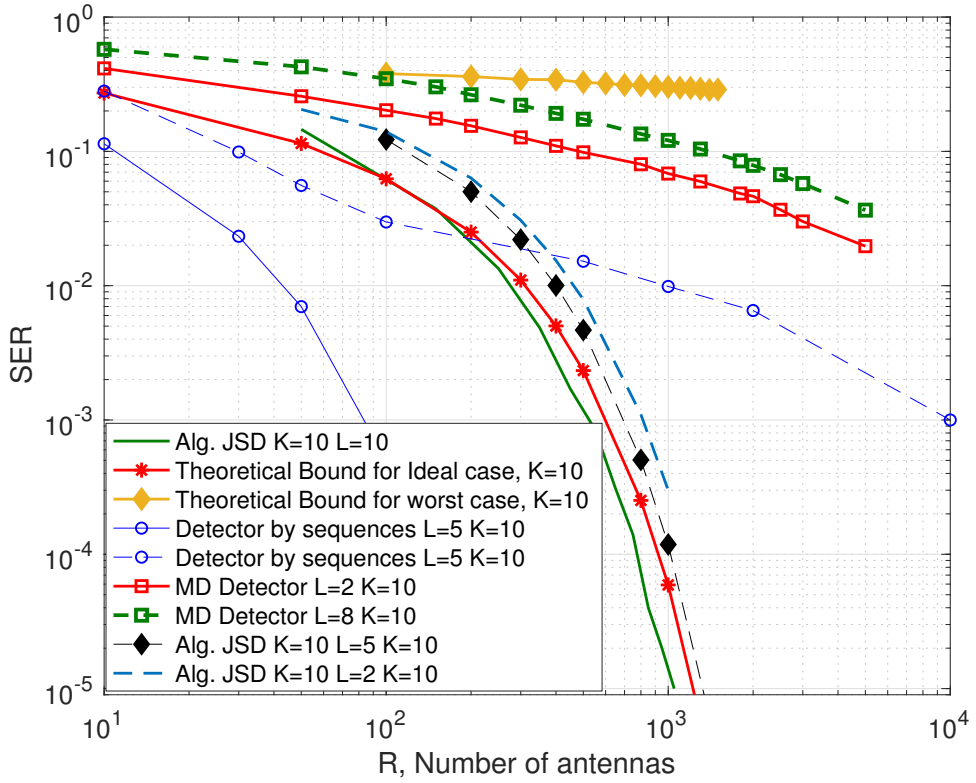

Figure 5.16 SER for perfectly known UIT (ideal case) with $J = 2$ users, $M = 4$.

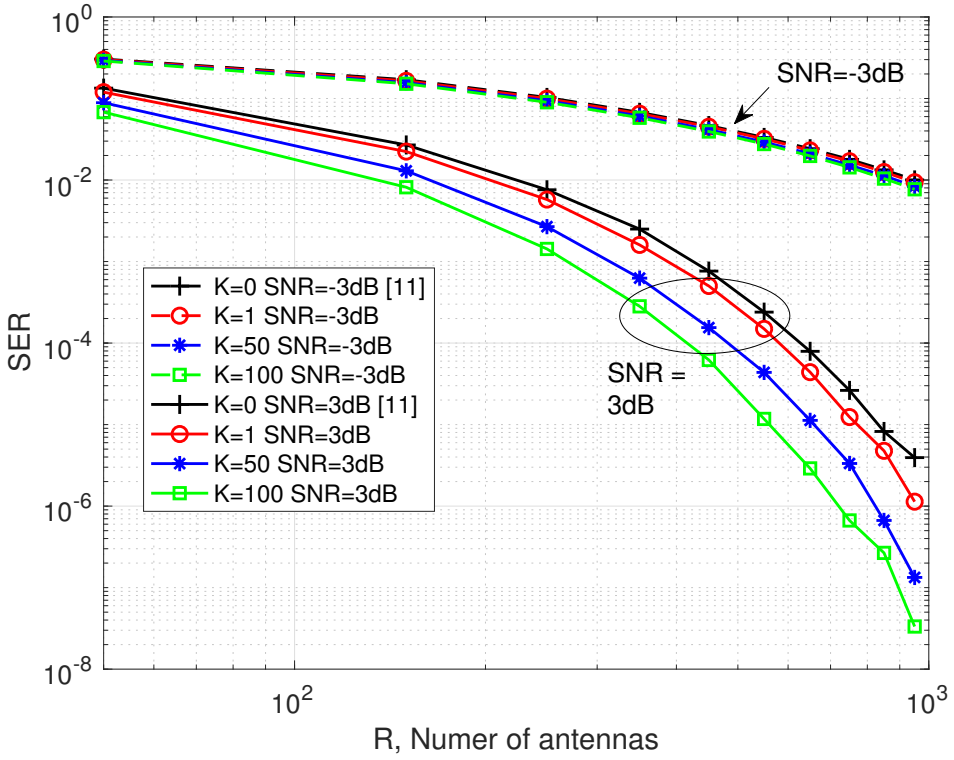

5.7 Complexity Analysis

We compare the computational complexity of our proposed algorithm with those of conventional algorithms. We study the complexity dependency with the number of symbols per frame (L), the order of the constellation (M), and the number of users (J). For these parameters of the system, we calculate the number of comparisons that must be performed between each received frame of symbols with all possible transmitted sequences.

For the first classical algorithm, detection by L-symbol sequences, the number of comparisons required is M^{JL}. For the classical second algorithm, the complexity is $M^{J(l+1)}$ for the l^{th}-symbol and the complexity required to detect the total L received symbols is $M^J + \sum_{l=2}^{L} M^{J(l+1)}$.

The complexity of our proposed JSD algorithm is calculated in 2 phases: first for $l = 2$ it is the same as for the detection by L-symbol sequences since we have to compare with all the possible symbols of the new constellation, this is M^{2J}. In the second phase, once the symbols 1 and 2 are detected, we make $M^{J(L-2)}$ comparisons with the remaining subset. Then the complexity is $M^{2J} + M^{J(L-2)}$. Compared to the first detection algorithm we obtain a reduction of 92% in calculations. Compared to the detection by double MD algorithm we obtain the reduction of 98%. For example: when we receive a sequence of $L = 5$ symbols for $M = 2$ and $J = 2$, our proposed JSD algorithm makes 80 comparisons against 1024 and 5444 comparisons in the $L-$symbol algorithm and MD respectively.

5.8 Conclusions

In this chapter, we have analyzed the issues arising as a result of the multiuser non coherent detection in Rician channel. We have presented a new constellation for a multi-user non-coherent massive MIMO system with M-DPSK that can be used in Rician channels. This constellation allows an unambiguous detection of the transmitting symbols despite the interference caused by the LOS component. This proposal is presented as pioneer for multiuser NC m-MIMO in Rician fading against the rest of designs in the literature shown for single users scenarios. Furthermore, we have proposed a detection algorithm based on the multi-symbol joint decision enhanced with the knowledge of the new constellation and the effect of interference. The SINR and SER have been theoretically analyzed showing a good match with the simulations. We have analyzed the performance of the system showing an improvement with respect to classical non-coherent detection techniques. With the proposed constellation and detection algorithm we are able to leverage the LOS component of the Rician propagation, obtaining a better performance than with Rayleigh channels. This better performance translates to a decrease of the required number of

antennas. Furthermore, we have seen that the designs based on M-DPSK outperform those based on energy detection [110] and [39] also in Rician propagation.

Chapter 6

Practical issues of a multiuser non coherent massive MIMO system based on DPSK

In order to carry out the implementation of NC-m-MIMO in real communication systems we have to handle several practical issues emerging from the nature of the real channels and scenarios. First, in Chapter 3 and Chapter 5 we have presented designs for NC m-MIMO systems in Rayleigh and Rice channels independently of each other, respectively. We showed that for single user case, the design under a Rayleigh fading attained the same performance as Rice. However, the constellation design optimized for Rayleigh fading in a multiuser environment is not valid for the Rician channels due to the inter user interference. On the other hand, the design optimized for Rice channel had to be only considered for two users and short frames of symbols due to the high complexity regarding the number of operations at the receiver side that the algorithm requires. The issue is that the scenarios for 5G may be subject to heterogeneous fading conditions. Hence, we analyse the combination of users which experience a pure Rayleigh fading with the ones with a pure Rice channel. In addition, this grouping between users can help to improve the performance and reduce the complexity compared to the scenarios with only Rician fading.

Second, throughout this work, we normally assume that the channel stays time-invariant during the transmission of two consecutive symbols, meaning that $h[n] = h[n-1]$. In contrast, in an uplink scenario in mobile communications, as proposed in this thesis, at least one of the communication endpoints may be in motion. Hence, the channel effectively varies randomly with time. In terms of the carrier frequency, the use of mmWave frequencies is becoming increasingly more popular in conjunction with m-MIMO systems [38], which is motivated for two reasons: the compact nature of the large-scale antennas as well

as by the promise of abundant spectrum above 10 GHz. Additionally, communication in the Terahertz band is considered for satisfying the high traffic demands [144]. Hence, the use of these high frequencies as well as the support of high-speed vehicular communications implies that the channel is time-variant and the above assumption for the channel does not necessarily hold. All these reasons motivate the analysis of our proposed scheme under time varying channels characterized by short coherence times.

Another drawback towards implementing m-MIMO is the enormous amount of RF hardware which transceivers need for the MIMO channel in a massive environment. The solution is using spatial modulation, one of the new radio technologies proposed for 5G and presented in the introduction. We propose a multiuser differential spatial modulation scheme for our NC-m-MIMO to address this problem. With all these issues appearing when implementations in real communications systems are considered, in the next sections we explain several improvements in our NC-m-MIMO design and analyze their behavior in such conditions, showing that our proposal is able to overcome all these drawbacks.

6.1 User Grouping with heterogeneous propagation conditions

In this section, we analyse the SINR and the performance in terms of symbol error rate (SER) of NC DPSK-based massive MIMO in heterogeneous scenarios with Rayleigh and Rice fading. We also quantify the advantage of the mixed-propagation user grouping in terms of complexity.

6.1.1 Changes in the system model

The reference model introduced in Chapter 2, is reorganized in Figure 6.1. In the transmitter side, the users are grouped like this: the signals transmitted from J_1 of J users experience Rayleigh fading (we refer to that circumstance in the following as the Rayleigh case), while the signals transmitted from the other $J_2 = J - J_1$ users follow a Rician fading (Rician case). Each of the user signals are differentially encoded from $s_j[n]$ as (2.5) and the signals from all users are grouped into the $(J \times 1)$-element vector $\mathbf{x}$, as explained in Chapter 2. The user symbols belong to the optimum constellation $\mathfrak{M}_j^{EEP}$ (3.57) defined in Chapter 3, which is also now valid for Rician fading due to the user grouping as will be seen in the following sections.

For the channel, we use in this case the two models explained in Chapter 2. In Rayleigh case, the m-MIMO wireless channel is modeled by the $(R \times J_1)$-element matrix $\mathbf{H}$, whose elements $h_{rj} \sim CN(0, 1)$ represent the propagation between user j and the r-th antenna

at the BS for the user group whose signals experience a Rayleigh fading. On the other hand, for the case of the user group whose signals follow a Rician fading, the channel is modeled by a matrix $\widetilde{\mathbf{G}} = \mathbf{G} + \boldsymbol{\mu}$ of size $(R \times J_2)$. Its elements are defined as $\widetilde{g}_{rj} = g_{rj} + \mu_j$, where $g_{rj} \sim CN(0, \sigma_{gj}^2)$. The parameters of the channel for the Rician case are defined as (2.6) and (2.7), where for this analysis we consider different K-factor by the pair (μ_j, σ_{gj}^2) for user j.

Figure 6.1 Schematic for a Non Coherent Multi-user Massive MIMO system for J users in heterogeneous scenarios.

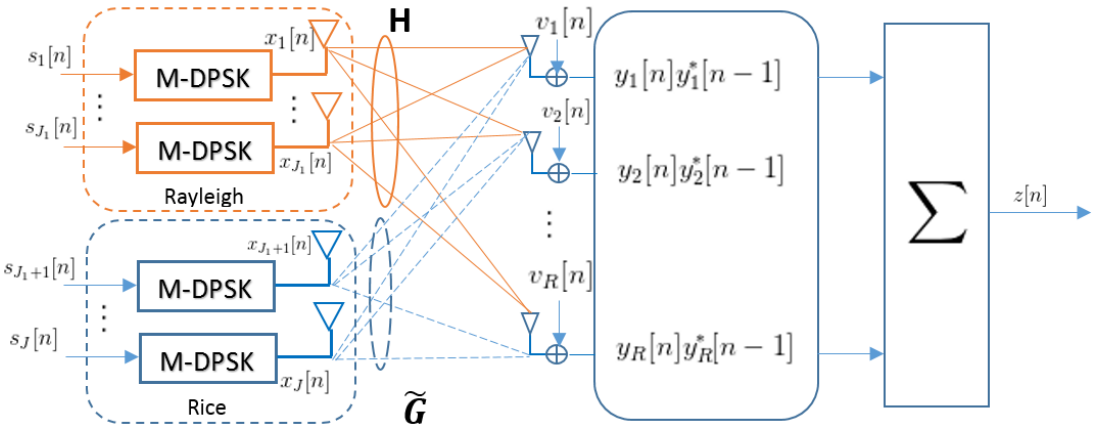

The $(R \times 1)$-element vector $\mathbf{y}[n]$ groups the signals received in each of the BS antennas at time instant n. Then, $\mathbf{y}[n]$ is obtained as follows

$$\mathbf{y} = [\mathbf{H} \;\; \widetilde{\mathbf{G}}]\mathbf{x} + \nu. \tag{6.1}$$

The AWGN is represented by the $(R \times 1)$-element vector $\nu \sim CN(0, \sigma^2)$. In this section, we assume all users experience the same power level ($\alpha_j = 1 \; \forall j$), then the power of the signal received at each antenna is

$$E\left\{\left\|[\mathbf{H} \; \widetilde{\mathbf{G}}]\mathbf{x}\right\|^2\right\} = \sum_{j=1}^{J_1} |s_j|^2 + \sum_{j=J_1+1}^{J} |s_j|^2(\sigma_{gj}^2 + \mu_j^2) = J_1 + J_2 = J, \tag{6.2}$$

as $|s_j|^2 = 1$ and $(\sigma_{gj}^2 + \mu_j^2) = 1$, maintaining the reference SNR as (2.14). We still keep our assumption that the channel stays time-invariant for two consecutive symbols for both cases, meaning that $h_{rj}[n-1] = h_{rj}[n] = h_{rj}$ for $r = 1, ..., R$ and $j = 1, ..., J_1$ and in the same way $g_{rj}[n-1] = g_{rj}[n] = g_{rj}$, for $r = 1, ..., R$ and $j = J_1 + 1, ..., J$. Hence, the phase difference is non-coherently detected as was explained in Chapter 2. The resulting $z[n]$

as in (2.16) is now extended as follows

$$z[n] = \underbrace{\frac{1}{R}\sum_{r=1}^{R}\sum_{j=1}^{J_1}|h_{rj}|^2 s_j[n] + \sum_{j=J_1+1}^{J}[|g_{rj}|^2 + 2\mu_j\Re\{g_{rj}\} + \mu_j^2]s_j[n]}_{joint\ symbol} + \underbrace{\frac{1}{R}\sum_{r=1}^{R} v_r[n]v_r^*[n-1]}_{noise\ terms}$$

$$+ \underbrace{\frac{1}{R}\sum_{r=1}^{R}\left[\sum_{j=1}^{J_1}\left(\sum_{\substack{k=1\\k\neq j}}^{J_1} h_{rj}h_{rk}^* x_j[n]x_k^*[n-1] + h_{rj}x_j[n]v_r^*[n-1] + h_{rj}^* x_j^*[n-1]v_r[n]\right)\right]}_{terms\ \ due\ to\ Rayleigh\ fading} + \underbrace{\sum_{j=1}^{J_2}\sum_{\substack{k=1\\k\neq j}}^{J_2}\mu_j x_j[n]\mu_k x^*[n-1]}_{new\ UIT}$$

$$+ \underbrace{\frac{1}{R}\sum_{r=1}^{R}\sum_{j=J_1+1}^{J}\left[x_j[n]v_r^*[n-1] + x_j^*[n-1]v_r[n]\right] + \frac{1}{R}\sum_{r=1}^{R}\sum_{j=J_1+1}^{J}\sum_{\substack{k=1\\k\neq j}}^{J}\left(\mu_j g_{rj}x_j[n]x_k^*[n-1] + \mu_k g_{rj}^* x_j^*[n-1]x_k[n]\right)}_{terms\ \ due\ to\ Rician\ fading}$$

$$+ \underbrace{\frac{1}{R}\sum_{r=1}^{R}\sum_{j=J_1+1}^{J}\sum_{\substack{k=1\\k\neq j}}^{J}\left(g_{rj}g_{rk}^* x_j[n]x_k^*[n-1] + g_{rj}x_j[n]v_r^*[n-1] + g_{rj}^* x_j^*[n-1]v_r[n]\right)}_{terms\ \ due\ to\ Rician\ fading}$$

$$+ \underbrace{\frac{1}{R}\sum_{r=1}^{R}\sum_{j=1}^{J_1}\sum_{k=J_1+1}^{J}\mu_j\left[h_{rj}x_j[n]x_j^*[n-1] + h_{rj}^* x_j^*[n-1]x_j[n]\right] + \mu_k\left[h_{rj}g_{rk}^* x_j[n]x_k^*[n-1] + h_{rj}^* g_{rk}x_j^*[n-1]x_k[n]\right]}_{terms\ due\ to\ the\ mixture\ of\ fading\ types}.$$

(6.3)

In order to analyze the trend of the terms in (6.3) using the Law of Large Numbers [41], we can consider the same asymptotic behavior for all users

$$\begin{aligned}\text{Rayleigh case: } j = 1, ..., J_1 &\rightarrow \tfrac{1}{R}\textstyle\sum_{r=1}^{R}|h_{rj}|^2 \overset{R\to\infty}{=} 1,\\ \text{Rician case: } j = J_1+1, ..., J &\rightarrow \tfrac{1}{R}\textstyle\sum_{r=1}^{R}|g_{rj}|^2 \overset{R\to\infty}{=} \sigma_g^2,\end{aligned} \tag{6.4}$$

$$\frac{1}{R}\sum_{r=1}^{R}\sum_{j=1}^{J_1}\sum_{\substack{k=1\\k\neq j}}^{J_1}\mu h_{rj}x_j[n]x_k^*[n-1] \overset{R\to\infty}{=} 0, \tag{6.5}$$

$$\frac{\mu}{R}[\sum_{r=1}^{R}x_j^*[n-1]v_r[n] + \sum_{r=1}^{R}x_j[n]v_r^*[n-1]] \overset{R\to\infty}{=} 0, \tag{6.6}$$

and the new terms due to the mixture of both types of channel fading obey

$$\frac{\mu}{R}\sum_{r=1}^{R}\sum_{j=1}^{J_1}\sum_{p=J_1+1}^{J}\left[h_{rj}x_j[n]x_p^*[n-1] + h_{rj}^* x_j^*[n-1]x_p[n]\right] \overset{R\to\infty}{=} 0, \tag{6.7}$$

$$\frac{1}{R}\sum_{r=1}^{R}\sum_{j=1}^{J_1}\sum_{p=J_1+1}^{J}\left[h_{rj}g_{rp}^* x_j[n]x_p^*[n-1]+\right] \overset{R\to\infty}{=} 0. \tag{6.8}$$

According to this, since interference terms vanish, making a minimum distance detection with the joint symbol (2.18), as it was shown in Chapter 3, we retrieve the user symbols $s_j[n]$. However, we have a new UIT in (6.8) which is different to that shown in Chapter 3 for a Rice pure mode due to the fact that each user experiences a difference K-factor. This fact leads us to a new extended joint constellation at the BS with more possible joint symbols; hence, in order to carry out the detection we need to know how is this new received constellation. Starting with an EEP constellation scheme for individual users, the received constellation is extended as shown in Figure 6.2 for the different K-factor case. In this figure the constellation for $J = 4$ users and $M = 2$ is shown, where 2 users experience a Rayleigh fading while the other two users a Rician fading, the four users with EEP individual design. In the Rice group, one user has $K = 1$ and the other one $K = 50$. The circles represent the joint constellation as with Chapter 3. Having different K-factor, the circles are moved towards the diamond symbols. Conversely to pure Rice, the decision regions at the receiver caused by LOS component are not overlapped allowing the user detection. In addition, we can see more symbols related to only one point of the joint constellation of Chapter 3, which helps us for more a feasible decision. In the case that all users experience the same mean (μ), the constellation scheme in Figure 6.2 is still valid but we have less extra symbols to decide. This is, with different means each circle is related with more diamonds, but when we have the same μ, not all circles make redundant diamonds available, in each region there will be only one diamond per circle.

Figure 6.2 Constellation Scheme for different K-factor.

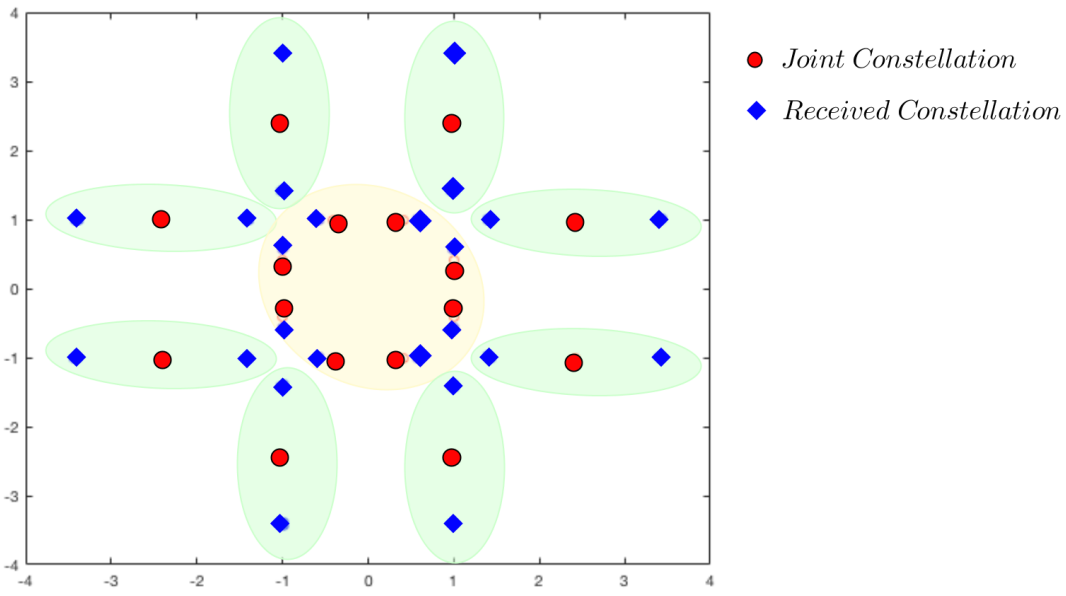

6.1.2 Derivation of the total interference power and SINR

When detecting ς from $z[n]$, just like in the independent fading cases, the interference plus noise arises from the interfering terms $i[n]$ in (2.20). We show the interference terms in (6.9) and group these terms in interference caused by Rayleigh fading, the interference caused by the Rician fading and the terms which appear due to AWGN noise.

$$
\begin{aligned}
i[n] = z[n] - \varsigma[n] = & \underbrace{\frac{1}{R}\sum_{r=1}^{R}\sum_{j=1}^{J_1}|h_{rj}|^2 s_j[n] + \frac{1}{R}\sum_{r=1}^{R}\sum_{j=J_1+1}^{J}[|g_{rj}|^2 + 2\mu\Re\{g_{rj}\} + \mu^2]s_j[n] - \sum_{j=1}^{J_1} s_j[n] - \sum_{j=J_1+1}^{J} s_j[n]}_{i_0[n]} \\
& + \underbrace{\frac{1}{R}\sum_{r=1}^{R}\left[\sum_{j=1}^{J_1}\left(\sum_{\substack{k=1\\k\neq j}}^{J_1} h_{rj}h_{rk}^* x_j[n]x_k^*[n-1] + h_{rj}x_j[n]v_r^*[n-1] + h_{rj}^* x_j^*[n-1]v_r[n]\right)\right]}_{i_{rayleigh}[n]\ \ due\ to\ Rayleigh\ fading} + \underbrace{\frac{1}{R}\sum_{r=1}^{R} v_r[n]v_r^*[n-1]}_{i_{noise}[n],\ \ noise\ terms} \\
& + \underbrace{\frac{1}{R}\sum_{r=1}^{R}\sum_{j=J_1+1}^{J}\sum_{\substack{k=1\\k\neq j}}^{J}\left(g_{rj}g_{rk}^* x_j[n]x_k^*[n-1] + g_{rj}x_j[n]v_r^*[n-1] + g_{rj}^* x_j^*[n-1]v_r[n]\right)}_{i_{rice}[n],\ \ due\ to\ Rician\ fading} \\
& + \underbrace{\frac{1}{R}\sum_{r=1}^{R}\sum_{j=J_1+1}^{J}\sum_{\substack{k=1\\k\neq j}}^{J}\mu\left(g_{rj}x_j[n]x_k^*[n-1] + g_{rj}^* x_j^*[n-1]x_k[n]\right)}_{i_{rice}[n],\ \ due\ to\ Rician\ fading} \\
& + \underbrace{\frac{\mu}{R}\sum_{r=1}^{R}\sum_{j=1}^{J_1}\sum_{j=J_1+1}^{J}[h_{rj}x_j[n]x_j^*[n-1] + h_{rj}^* x_j^*[n-1]x_j[n] + h_{rj}g_{rj}^* x_j[n]x_j^*[n-1] + h_{rj}^* g_{rj}x_j^*[n-1]x_j[n]]}_{i_{mixture}[n],\ \ terms\ due\ to\ the\ mixture\ of\ fading\ types}
\end{aligned}
\tag{6.9}
$$

We use the SINR for pure Rayleigh and pure Rician fading defined in Section 3.2 and Section 5.4, respectively, as a reference to compare with the mixed mode. We define the following

$$I^0_{Rayleigh} = \frac{J_1^2}{R} \quad and \quad I^0_{Rice} = \frac{J_2^2\sigma_g^2\mu}{R} \tag{6.10}$$

$$I_{Rayleigh} = \frac{J_1(1+2\sigma^2)}{R} \tag{6.11}$$

$$I_{Rice} = \frac{(\sigma_g^4 + 2\sigma_g^2\sigma^2 + 2\mu^2(J_2-2)\sigma_g^2 + 2\mu^2\sigma^2)(J_2-1)}{R} \tag{6.12}$$

$$I_{noise} = \frac{\sigma^4}{R}. \tag{6.13}$$

The new interfering terms due to the combined fading are obtained as $E\{|i_{mixture}[n]|^2\}$ resulting in

$$I_{mixture} = \frac{2\mu^2 + 2\sigma_g^2}{R} \tag{6.14}$$

and because of the mixture of fading types the first term also changes to $I^0 = I^0_{Rayleigh} + I^0_{Rice}$. Then the total SINR for a heterogeneous scenario obeys (6.15).

$$SINR = \frac{RJ}{\sigma_g^4 + \sigma^4 + \sigma^2(2J_1 + 2\sigma_g^2 J_2 + 2\mu^2 J_2) + \sigma_g^2(J_2^2\mu + 2\mu^2 J_2(J_2 - 1) + 1J_1J_2) + J_1(2\mu^2 J_2 + J_1 + 1)} \tag{6.15}$$

In Figure 6.3 it is shown that (6.15) matches with the simulations for $R = 100$ antennas. The reference "pure" SINR is obtained for $J_1 = 2$ users experiencing both Rayleigh fading as (3.36) and $J_2 = 2$ users experiencing both Rician fading ($K = 5$) as (5.40). We compare these SINR curves to (6.15) for a scenario where the same number of total users that experience different fading (Rayleigh and Rician) are scheduled together ($J_1 = J_2 = 1$). We can see that the new SINR when we combine users improves, and to the SINR for the mixture is very close to the Rayleigh SINR. The curve for ideal pure Rice is a bound which can only be obtained when the LOS component is perfectly estimated. Grouping together users with different type of fading we get closer to this bound without the need for any complex detection algorithm in the receiver.

6.1.3 Performance evaluation in heterogeneous networks

In this section we examine the performance of our NC-m-MIMO when users experiencing Rayleigh and Rician fading are scheduled together. For the simulations, a random channel is generated at each iteration (minimum 100,000 iterations) following the model explained in Section 6.1.1 and it is kept constant for 1,000 symbols. For this example, in the case for Rice fading, the users' channels have the same $K = 5$ factor following equations (2.6) and (2.7). The propagation channels of all the different users are uncorrelated.

We compare in Figure 6.4 a combined scenario with $J = 2$ users ($J_1 = J_2 = 1$), for $M = 4$ and $\rho = 0$ dB to pure Rayleigh ($J_1 = 2$) and pure Rice ($J_2 = 2$) cases. We can see how combining 2 users with different fading, the user with Rayleigh propagation does not experience any changes, while the performance of the Rician-faded user improves with respect to the case of being multiplexed with another Rician-faded user. In addition, the constellation used in the mixed mode for both users is the same, that was defined

Figure 6.3 Comparison of the SINR for pure Rayleigh and Rice mode with a fading mixture with $R = 100$ antennas.

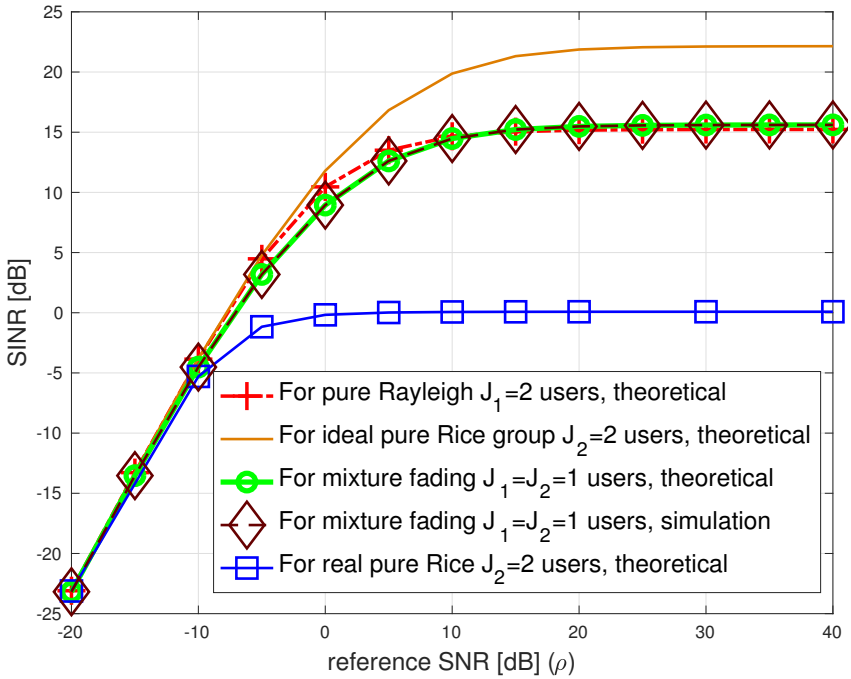

in (3.57), while for pure Rician propagation the one in Figure 5.8 has to be used, which offers a worse performance.

In Figure 6.5 the error performance is shown for three cases with $J = 4$ users with $M = 2$, $K = 5$ and $\rho = 0$ dB. First case is for one Rician-faded user and 3 users experience Rayleigh fading, this is $J_1 = 3$ and $J_2 = 1$. The Rician-faded user also experiences the same performance as the other three ones that have Rayleigh propagation. Second and third, 2 users with Rician fading and the other two with a Rayleigh fading, one case for the same μ between users where Rician users get worse with respect to Rayleigh users due to the fact that we do not use the constellation optimized for Rice case, but by contrast the pure Rice, we achieve to demodulate them using the same constellation as pure Rayleigh case. The other care, when the Rice users have different μ ($K = 5$ and $K = 50$), having more symbols to make decision, we can see in Figure 6.5 as Rice performance improves as μ increases with respect to Rayleigh case.

6.1.4 Analysis of complexity

We use the number of comparisons that must be performed between each symbol with all possible transmitted symbols in the detection process as a measure of the computational complexity of the system. Then the complexity is reduced from $M^J(M^2 + 1)$ to M^J for detecting all users by this adequate user grouping. In addition, the user detection is

performed symbol by symbol now, avoiding the delay caused when the detection is done per frame.

Figure 6.4 SER for $\rho = 0$ dB, $J = 2$ users, $M = 4$, and $K = 5$.

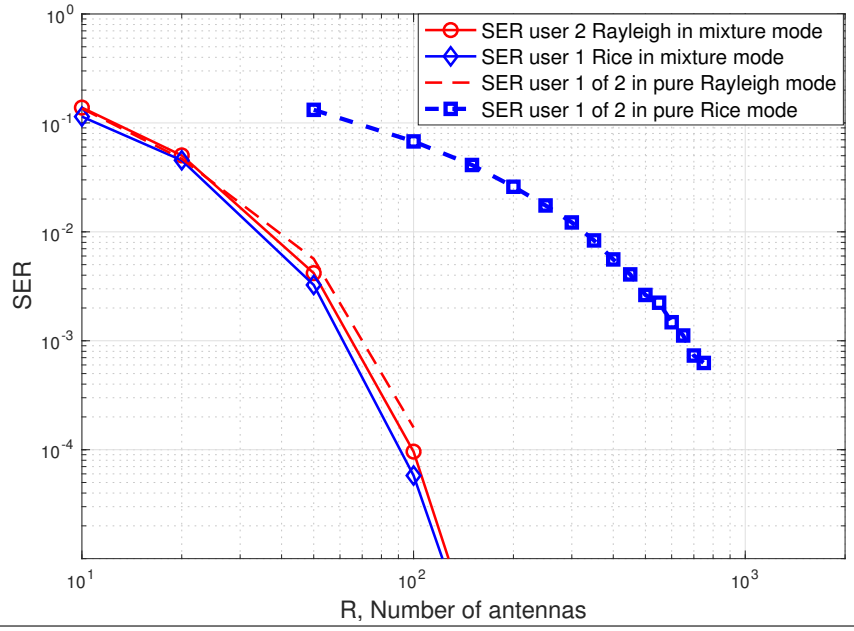

Figure 6.5 SER for $\rho = 0$ dB, $J = 4$ users, $M = 4$, and $K = 5$.

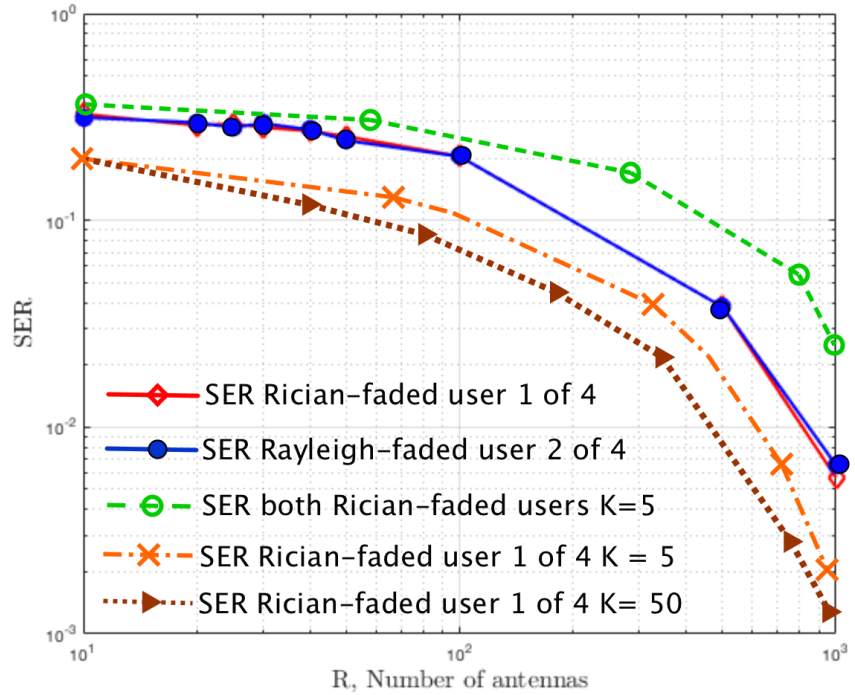

6.2 Performance in practical channels

In this section, we analyze the effect of time-varying channels on the attainable performance of our non-coherent system based on DPSK and BICM-ID using a high number of antennas. We define a novel metric in Chapter 2 for this purpose and then we analyse its values for the current standards and new scenarios proposed in 5G.

6.2.1 EXIT chart based on a new metric β

With the aim of preserving the target number of antennas R as little as possible, we use the channel coding system shown in Chapter 4. Thereby, we will use the EXIT chart tool for analyzing the constellation design and for finding the best coding scheme for our system based on R when we have a practical channel. Based on the interference analysis in Section 3.2 and (3.35), we can express the SINR as a function of ρ and R as follows

$$SINR = \frac{R}{J}\frac{\rho^2}{\rho^2 + 2\rho + 1}, \tag{6.16}$$

where it is considered the same average power level for all users, this is $\alpha_j = 1\ \forall j$. In addition, from the EXIT curves explained in Chapter 4, the inner curve is which includes the behavior of the channel, hence, we have included the dependence on β in the inner curve. In contrast to Chapter 4, here we draw an inner curve for each value of β, fixing R. Then, the demapper's extrinsic information transfer defined in (4.11) for our particular m-MIMO system depends now on β, apart from the *a priori* information, R and the SINR, which is formulated as

$$I_{i,e}(\mathbf{u}) = T[I_{i,a}(\mathbf{u}), R, \rho, \beta]. \tag{6.17}$$

For the outer decoder, we employ the set of 17 convolutional subcodes[1] explained in previous chapter for designing the channel coding scheme, whose coding rate spans the range [1/10-9/10]. Now, we have not only to select the number of antennas R, but we have to find the available value pairs (R, β) for ensuring an open EXIT tunnel with one of the 17 subcodes, ensuring an infinitesimally low BER.

6.2.2 Analysis of time-variability for NC massive MIMO

The objective of this analysis is to find the minimum value of R required to attain a specific target performance, such as a BER of 10^{-4} or below, when considering a time-varying channel. We also seek for the value of β, where the effect of the channel's time variation becomes negligible in terms of NC detection performance. For that purpose,

[1] We can refer to them, indistinctly, as IRCC or CC.

we draw a set of the inner curves as (6.17) which covers a range of values for β, fixing a $R-$value.

The EXIT characteristics of the NC-m-MIMO system associated with ρ =0 dB, R=100 antennas, size of the constellation M=4 symbols and β values ranging from 1.5 to 6 by steps of 0.5 are shown in Figure 6.6. The encoders used are a 1/2−rate RSC (number 9 of the set CC) as outer code and an URC[1] as inner code. We can see that for $\beta < 6$ there is not open tunnel, hence the iterative decoding is not possible. Instead, for $\beta = 6$, the tunnel is open for 1/2−rate code, but it is very narrow, which means that we need a lot of iterations to reach the perfect converge point. On the other hand, we draw the inner curve for a value of β of 10, which already coincides with the constant channel. Then, for $\beta \in$ [6,10] with 100 antennas, we are able to guarantee the NC detection assuming a time-variant channel. In addition, we have plotted the inner curve for a very high value, $\beta = 15000$, which also matches with the constant channel curve, validating that the curves for real channels can not exceed the curve of constant channel. In Section 6.2.4 we analyse practical values for these β-values corresponding to real systems.

Figure 6.6 EXIT Chart of a NC-m-MIMO system with $J = 2$ users, $\rho = 0$ dB, $M = 4$ and R= 100 antennas for β-values from 1.5 to 6 by steps of 0.5.

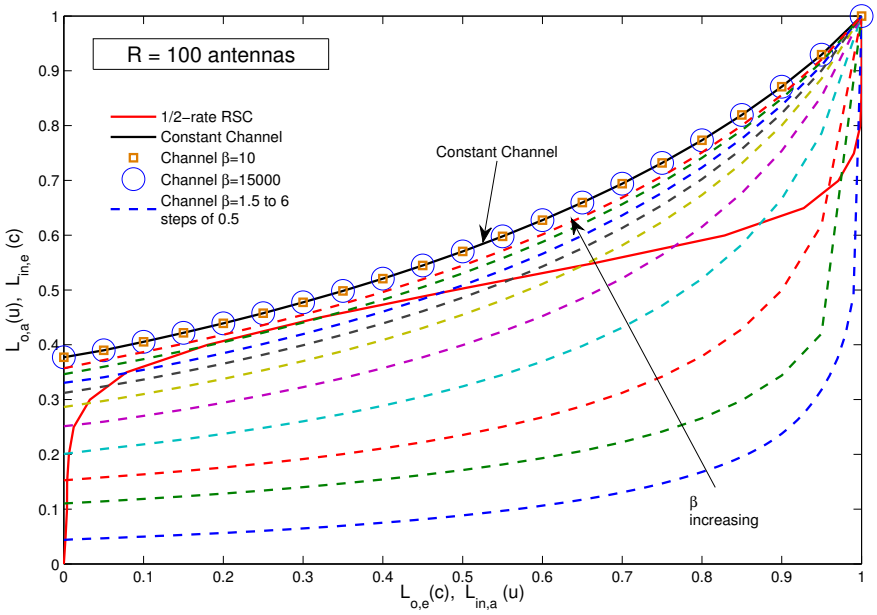

In the case that we want a value of β below 6 in the system shown in Figure 6.6, we have to increase the number of antennas, keeping the rate of the outer code. For the same conditions defined previously regarding SNR, number of users and constellation, we show the EXIT-curve for R = 300 antennas with β =3 and for R = 140 using β =5 in Figure 6.7, in conjunction with their decoding trajectories, where the energy efficiency

attained by our m-SIMO is clearly evidenced by the fact that a low ρ is sufficient for having an open EXIT tunnel. We can see that this condition is fulfilled with 4 iterations for $\beta = 5$ and 3 iterations for $\beta = 3$. This latter needs less N_I at the expense of increasing R.

Figure 6.7 EXIT Chart for $J = 2$ users, $\rho = 0$ dB, $M = 4$, (β, R)=(3,300) and (β, R)=(5,140).

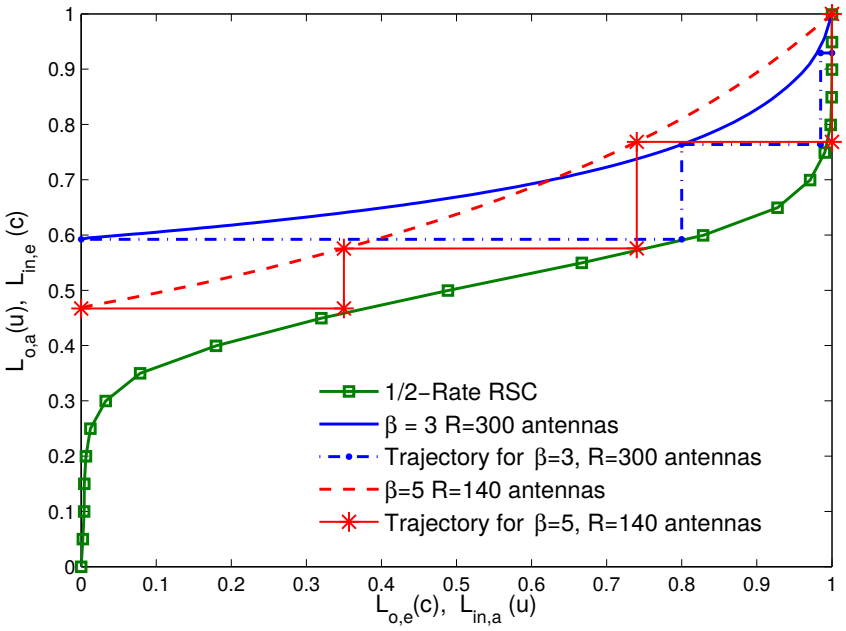

In Figure 6.8 we show the BER for J =2 users, $\rho = 0$ dB, M=4. We only plot the last iteration for each case previously noted in the EXIT chart in Figure 6.7. In this case, we evaluate the effect of the time varying channel on the BER performance. Having an infinitesimally low BER at R= 140 antennas for β=5 (achieved in the fourth iteration) and R=300 antennas for β=3 (achieved in the third iteration), an increment of 50 and 200 antennas, respectively, is required with respect to the constant channel. This result matches with the EXIT chart predictions in Figure 6.7.

On the other hand, in case that the number of antennas has to be lower, for a target β, we have to change the outer code. In Figure 6.9, EXIT chart for $R = 50$ antennas and a 1/4−rate RSC outer code is shown. Just like for 100 antennas, we need $\beta > 6$ for decoding. However, a large number of iterations is required for ensuring that the performance becomes equivalent to that of the constant channel, since the EXIT-tunnel is narrower than for $\beta \geq$10. The system exhibits a similar performance to the constant channel for $\beta \geq$10.

Once we have studied the effect of β, shown in Figures 6.6-6.9, with some specific cases, we analyse the number of antennas required for attaining an open EXIT tunnel over

Figure 6.8 BER performance for $J = 2$ users, $\rho = 0$ dB, $M = 4$, URC, EEP and $\beta = 3$ and $\beta = 5$

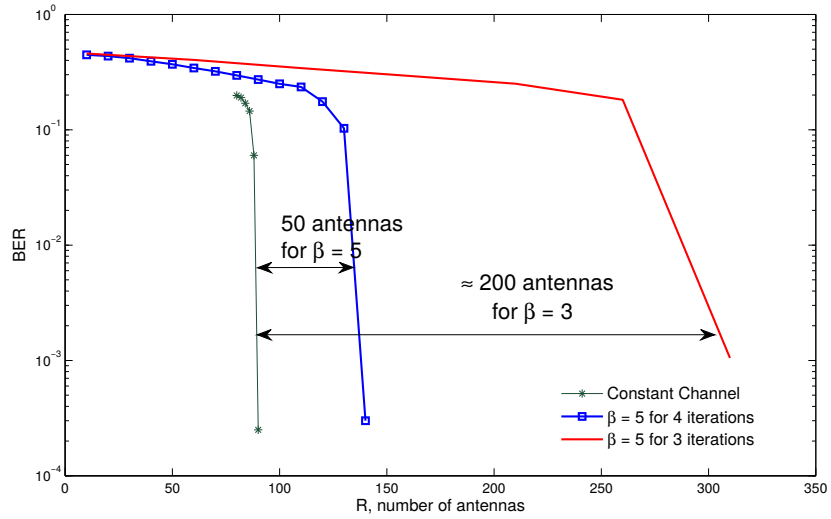

Figure 6.9 EXIT Chart with $J = 2$ users, $\rho = 0$ dB, $M = 4$ and R= 50 antennas for β from 1.5 to 6 by steps of 0.5.

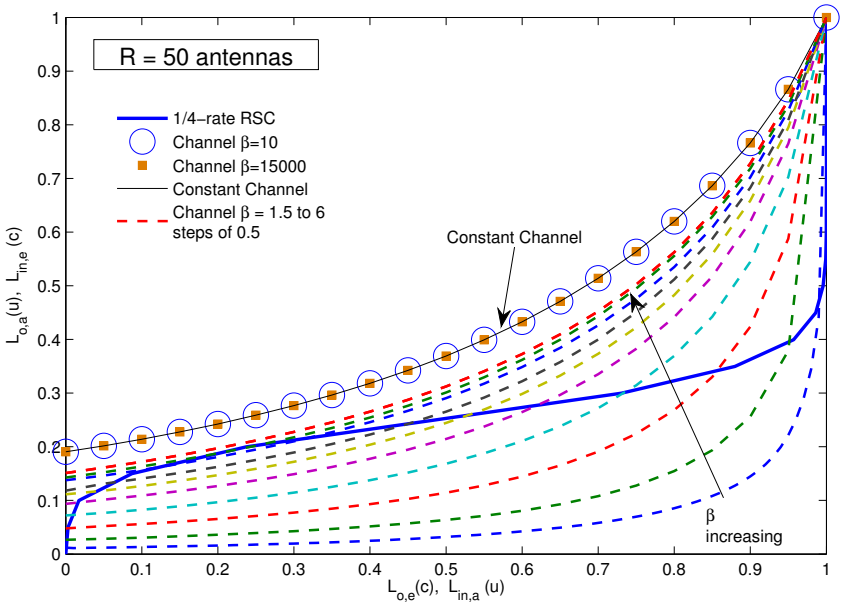

different reference SNR, when considering a constant channel and also for different degrees of channel variability β. We list the resulting R-values in Table 6.1. For selecting the R-values, we follow the Algorithm 4.9 proposed in Section 4.4.1. These values sometimes require a high number of iterations, when the open EXIT tunnel is narrow. As β decreases, which results in more violent channel time variation, the R required for achieving the same performance as that of the constant channel increases. We can maintain the same R as

for the constant channel at the expense of a reduced throughput by using a lower channel coding rate. When the coding rate is low, increasing the reference SNR ρ, the effect of time variations is less visible. This is not, however, the case for high coding rates. Also, for ρ=0 dB and $\beta = 3$ there are certain coding rates that do not have an open tunnel for any R. For instance, in order to decode a 1/2−rate RSC code with a channel characterized by $\beta = 3$ we have to increase R from 90 to 180 antennas, or to 110 antennas for the case $\beta = 5$, to keep the same performance as the constant channel, as shown in Table 6.1.

Additionally, for R=50 antennas we can decode using a 1/4−rate IRCC when the channel is constant. However, when β increases, the required R for practical channels changes from 50 to 90 antennas for β=3 and to 55 antennas for β=5 as shown in Table 6.1.

	Outer IRCC	Required R for each SNR:											
		Constant Channel			β=3			β=5			β=10		
		0 dB	3 dB	6 dB	0 dB	3 dB	6 dB	0 dB	3 dB	6 dB	0 dB	3 dB	6 dB
Coding rate	1/10	20	20	20	40	25	20	25	20	20	20	20	20
	3/20	30	20	20	60	35	25	35	20	20	30	20	20
	1/5	40	20	20	70	40	30	45	25	20	40	20	20
	1/4	50	90	20	90	50	35	55	35	25	50	90	20
	3/10	55	30	20	100	60	35	65	40	25	55	30	20
	7/20	60	35	25	120	65	45	75	45	30	60	35	25
	2/5	70	40	30	140	80	55	85	50	35	70	40	30
	9/20	80	45	30	150	90	65	95	55	40	80	45	30
	1/2	90	50	35	180	105	75	110	60	45	110	60	45
	11/20	100	60	40	210	120	85	120	70	50	100	60	40
	3/5	120	65	45	240	145	100	140	80	60	120	65	45
	13/20	130	75	55	280	170	120	160	90	70	130	75	55
	7/10	150	90	60	320	200	140	180	105	80	150	90	60
	3/4	180	100	70	450	240	180	210	120	90	180	100	70
	4/5	210	120	85	500	300	210	250	140	100	210	120	85
	17/20	260	150	100	X	400	270	350	170	120	260	150	100
	9/10	350	180	130	X	500	310	360	210	150	350	180	130

Table 6.1: Performance for $J = 2$ and EEP design for different IRCC encoders and β .

From these results, we note that the time variations affect the required R when we consider a practical channel. The system exhibits a similar performance to the constant channel for $\beta \geq$10, therefore the same number of antennas is required for that case. Hence, we note that our system is capable of withstanding f_D close to the channel's bandwidth as (2.10).

6.2.3 Achievable bit rate on a NC massive MIMO system with channel coding

In addition to predicting the behavior of the iterative decoding, the EXIT chart can be also used to compute the capacity of the system or maximum achievable rate (MAR), as discussed in [133]. The area beneath the inner EXIT curve corresponds to the channel capacity, while the area beneath the curve created by the outer code is the coding rate. The larger the SNR is, the higher the EXIT curves of the outer code are. Therefore, the higher capacity can be achieved. In our proposal, we have the same results increasing the number of antennas instead of SNR.

In this section, we characterize the MAR of our non-coherent m-MIMO-DPSK-BICM-ID scheme. Remember that the inner code is represented by the URC encoder and the mapper shown in Figures 4.2-4.3. Here, we translate the expression in [133] to evaluate the MAR as a function of the number of antennas R, since we parametrize the EXIT curve as a function of R rather than SNR. The area A is calculated for different R values, denoted as A_R, then the MAR η_{max} may be defined in terms of R as follows

$$\eta_{max}(R) = \log_2(M) \cdot A_R. \tag{6.18}$$

Then, in order to obtain the MAR of (6.18) that our system can support, for each ρ, R and a candidate constellation we chose the EXIT curve that has an open tunnel. If there is indeed an EXIT chart that has an open tunnel, this means that this modulation order M is decodable with a vanishingly low BER. In order to keep a feasible value of R, we select the modulation order from the set $\mathfrak{M} = \{2, 4, 8, 16\}$, since higher values of M require a significantly higher number of antennas. Then, the practical MAR for NC-m-MIMO is given by the maximum modulation order that we found to be decodable multiplied by the coding rate as follows:

$$\eta_p(R, \beta, M_i) = \log_2(M_i) \cdot rate \tag{6.19}$$

where *rate* is the original outer code rate.

For a given ρ and R value, we can draw an EXIT chart for each possible value of the constellation order M_i, following the same procedure described in Figure 4.9 to select the coding scheme. With the aid of each of these EXIT charts we can select the coding scheme that produces an open tunnel at the lowest value of the outer code rate.

In Table 6.2 we collect the practically MAR achieved for $J = 2$ users with EEP design and $\beta = 3$ as example. We follow a similar procedure to obtain $\beta = 5$ and 10.

		R, Number of antennas											
SNR [dB]	M	100		300		500		1000		5000		10000	
		IRCC	rate	IRCC	rate	IRCC	rate	IRCC	rate	IRCC	rate	IRCC	rate
0	2	17	0.9	17	0.9	17	0.9	17	0.9	17	0.9	17	0.9
	4	5	0.6	12	1.3	14	1.5	17	1.8	17	1.8	17	1.8
	8	X	-	3	0.6	6	1.05	11	1.87	16	2.55	17	2.7
	16	X	-	X	-	1	0.4	3	0.8	12	2.6	14	3
3	2	17	0.9	17	0.9	17	0.9	17	0.9	17	0.9	17	0.9
	4	9	1	14	1.5	17	1.8	17	1.8	17	1.8	17	1.8
	8	1	0.3	7	1.2	10	1.65	13	2.1	17	2.7	17	2.7
	16	X	-	X	-	3	0.8	7	1.6	14	3	15	3.2
6	2	17	0.9	17	0.9	17	0.9	17	0.9	17	0.9	17	0.9
	4	11	1.2	16	1.7	17	1.8	17	1.8	17	1.8	17	1.8
	8	3	0.6	9	1.5	2	1.85	15	2.4	17	2.7	17	2.7
	16	X	-	X	-	5	1.2	9	2	15	3.2	16	3.4
9	2	17	0.9	17	0.9	17	0.9	17	0.9	17	0.9	17	0.9
	4	12	1.3	16	1.7	17	1.8	17	1.8	17	1.8	17	1.8
	8	4	0.9	10	1.65	13	2.1	16	2.55	17	2.7	17	2.7
	16	X	-	X	-	6	1.4	10	2.2	15	3.2	17	3.4
12	2	17	0.9	17	0.9	17	0.9	17	0.9	17	0.9	17	0.9
	4	13	1.4	17	1.8	17	1.8	17	1.8	17	1.8	17	1.8
	8	5	1.05	11	1.8	13	2.1	15	2.4	17	2.7	17	2.7
	16	X	-	X	-	7	1.6	12	2.6	16	3.4	17	3.6

Table 6.2: Rate achieved for J =2, EEP design and $\beta = 3$.

In Figure 6.10 we show the achievable rate of the m-MIMO-DPSK-BICM-ID system, when R =100 antennas, as a function of the SNR ρ. In Figure 6.10, we show the constellation order $M_i \in \mathfrak{M}$ that provides this lower outer code rate value and the achieved η_p according to (6.19). The dotted line in Figure 6.10 is the MAR provided by the EXIT chart and represents the upper bound of MAR for our system. The solid lines are obtained for different β values. We note that the difference between the theoretical MAR and the practically achieved MAR is small for $\beta \geq$10, while for smaller β there is a noticeable degradation.

In Figure 6.11 the η_p for the β-value close to constant channel, $\beta = 10$, is shown as a function of R for $M = 8$ and 0 dB. We can see that for 1000 antennas the MAR is close to the channel capacity. From results of Figure 6.11, we calculate the MAR for R=1000 antennas in function of SNR. Note that there is a much smaller difference between β =3 and β=5, which means that the system is less affected by the time variability when the number of antennas is very high. Again, for $\beta \geq$10, the practical achievable MAR is very close to the upper bound provided by EXIT chart.

Figure 6.10 Maximum Achievable Rate for R=100 antennas.

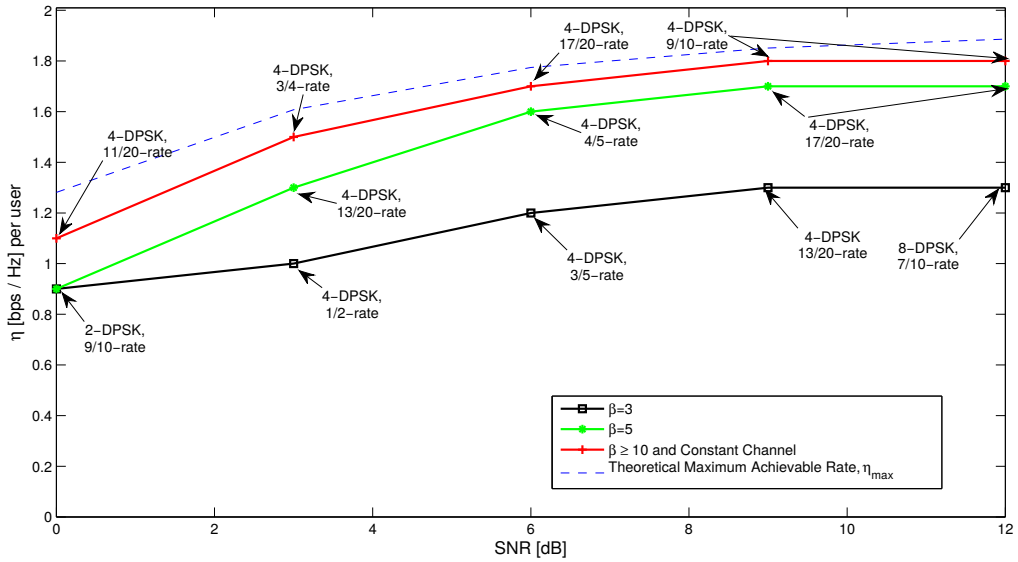

Figure 6.11 Achievable rate for $\beta = 10$

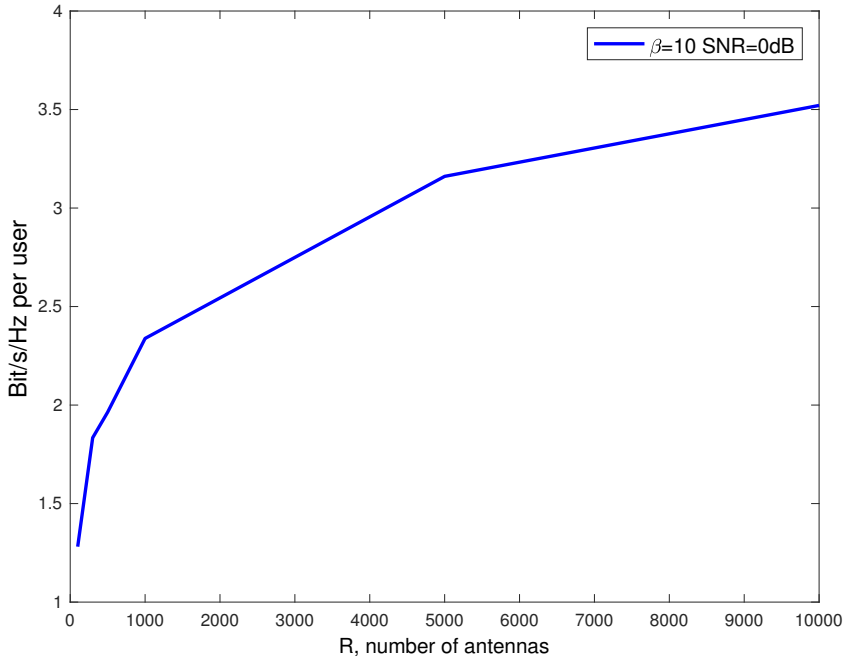

Figure 6.12 shows the maximum achievable rate for R=1000 antennas. These results confirm those commented in Figure 7.7

Additionally, we can fix the SNR and for each R look for the combination of M_i and *rate* that maximize η_p

Figure 6.12 Maximum Achievable Rate for R=1000 antennas.

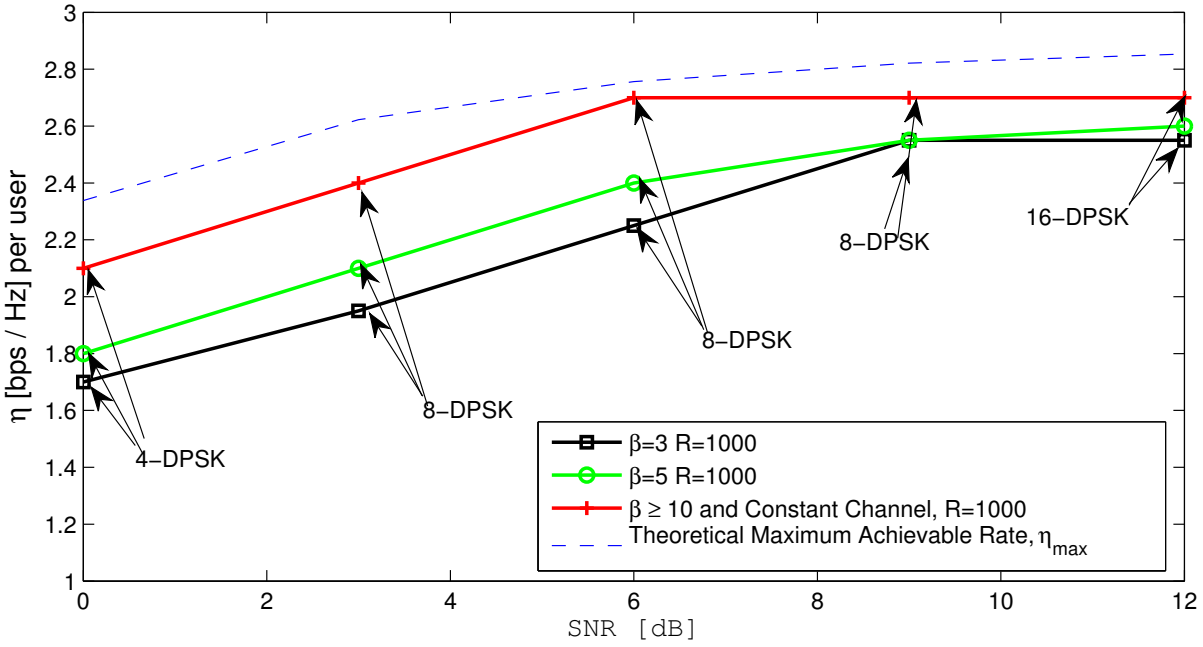

Figure 6.13 Maximum Achievable Rate for ρ=0dB.

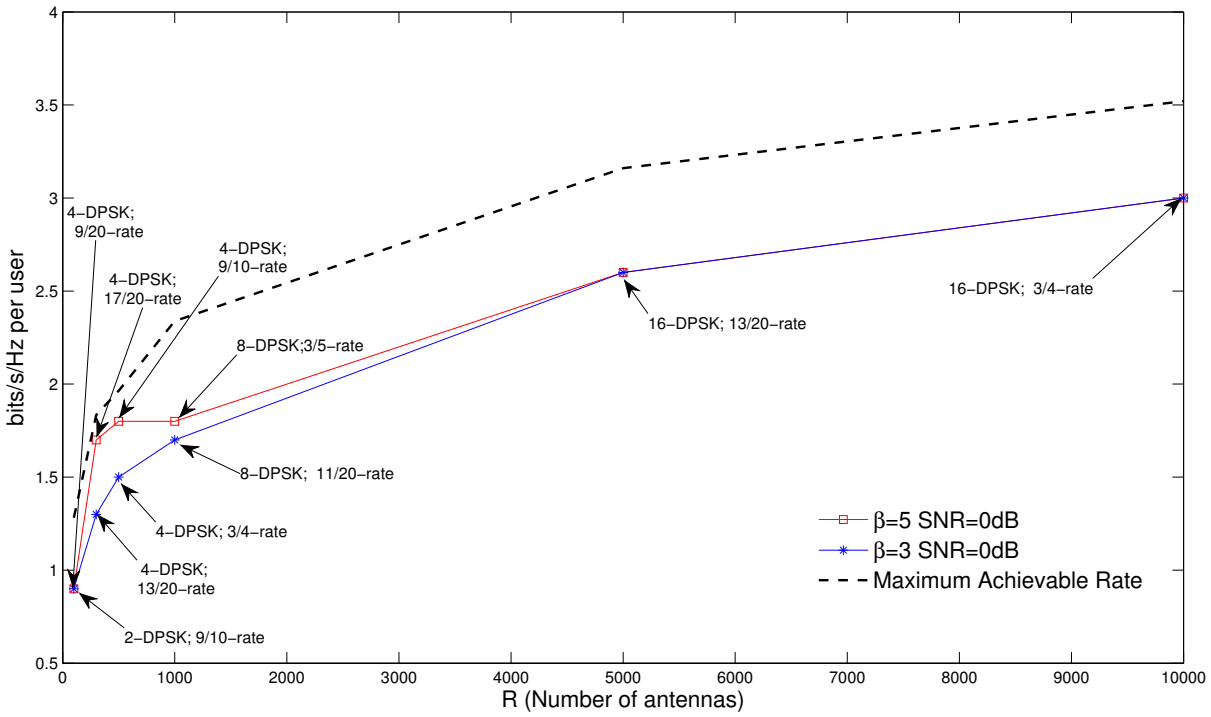

In Figure 6.13 we show the practically attainable MAR η_p versus the number of antennas when considering SNR of 0 dB. Here we can see that as R increases the performance losses due to a very small β becomes less noticeable.

6.2.4 Analysis on β for new requirements of 5G

We examine the typical value of β for the requirements of the future communications networks, such as 5G, for which the schemes proposed in this Thesis are foreseen. Nevertheless, we also analyze the β-values in the current wireless standards such as LTE, for which NC-m-MIMO can provide high benefits and serve as an evolution towards 5G.

- **LTE Standard** in [123]: we have typically $f_c = 2.6$ GHz, a BW of 20 MHz and a mobile velocity of $v = 120$ Km/h, we get a value of $f_D = v/\lambda = 290$ Hz. Then, according to (2.10) we have $\beta = 68,970$. Additionally, when we have $f_D = 200$ Hz and $v = 83$ Km/h, we obtain $\beta = 10^5$. In both cases β is very high, ensuring that we achieve the same performance as in the constant channel scenario.

- **LTE for high speed railway systems:** these environments are characterized by a high Doppler spread or short coherence time T_c and high speed. For example, with $f_c = 2.6$ and $v = 500$ Km/h we have a $f_D = 1.2$ KHz and $\beta = 16,615$, which again guarantees the same performance as for the constant channel.

- **mmWaves links:** due to the high f_c, the Doppler shift is also high. These links are foreseen to be used because of the high available bandwidth. For instance, employing BW= 100 MHz at f_c= 60 GHz, considering v=120 Km/h we have f_D= 6.7 KHz, we get β=15,000. According to the specifications in TR 38.913 by the 3rd Generation Partnership Project (3GPP) for 5G [10], for mmWave with $f_c > 6$ GHz the BW has to be over 400 MHz. Then, we obtain $f_D = 667$ Hz for 120 Km/h resulting in $\beta < 10^6$. With these values we have again the same performance as for the constant channel scenario.

- **THz Communications:** in this new area, the links use carrier frequencies which begin in the range of 0.1 THz, proposed for metropolitan areas. Here, for high speed and BW=10 GHz we can achieve $\beta = 7.16$. In this case, since β is lower than 10, we notice the effect of time variability. By contrast, for low speeds, we have again constant channel condition.

In the aeronautical sector, the 3GPP is developing LTE Advanced Pro in conjunction with 5G for supporting V2X communications. In these scenarios, an aircraft may reach a speed of 1000 Km/h, resulting in LTE frequency f_c =26 GHz $f_D = 0.024$ Hz, meaning a high β and constant channel condition.

We also consider the mobile satellite communication systems which employ fast-moving satellites with f_d variable in the [147] range [-25.5 KHz, 25.5 KHz]. For this Doppler spread, we have $\beta > 10$.

From the point of view of services, 5G will include massive machine type communications and ultra reliable low latency communications (URLLC) under the technologies of Internet of Things (IoT). For these services, we need high BW which gives high values of β.

With these examples, we can deduce that our system is very robust to the temporal variations of the channel in any use case that we can foresee.

6.3 Spatial Modulation for non coherent massive MIMO based on DPSK

For the implementation in real systems, not only we have to consider the effects of the channel and to have a feasible number of antennas, but also we have to take into account that a high R requires a lot hardware components. As we presented in the introduction of this Thesis, spatial modulation (SM) is a promising technique for new RAN considered for 5G, in which the number of RF chains is reduced exploiting the space and modulation domain. Compared to the traditional MIMO technology, SM improves the energy efficiency, avoids the inter-channel interference and antenna synchronization problems, all of them retaining the spectral efficiency. Severals works have been proposed for SM in coherent systems [32, 148, 149]. However, we still have a huge CSI estimation problem aggrieved by m-MIMO. Hence, due to the advantage shown by SM, we analyze this technique for our NC-m-MIMO proposal in this Thesis.

In this section, we consider a system model with differential SM (DSM) which modifies the baseline model shown in Chapter 2, increasing the number of antennas in the transmitter side to include the SM in our NC-m-MIMO, as shown in Figure 6.14. Now, in our uplink model, the transmitter side is equipped with R_t antennas and the BS with R_r, being R_t much smaller than R_r.

Figure 6.14 Schematic for NC Spatial Modulation in m-MIMO based on DPSK.

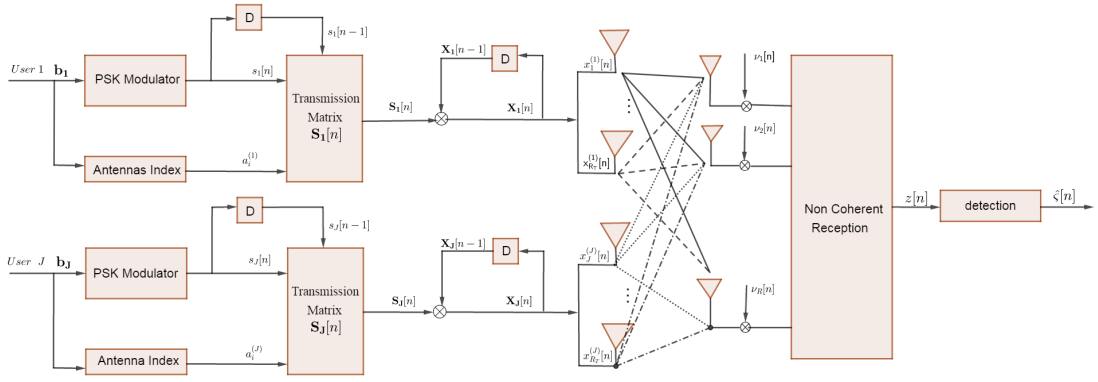

In our proposed SM-NC-m-MIMO, now the block $\mathbf{b}_j$ is composed of B bits, being $B = \lfloor \log_2 R_t! \rfloor + \log_2 M$, which is separated into two substreams, $\mathbf{b}_{ANT} = \{b_1, \cdots, b_a\}$ and $\mathbf{b}_{PSK} = \{b_1, \cdots, b_p\}$, where $a = \lfloor \log_2 R_t! \rfloor$ and p is our size of constellation as well as in the rest of the work. The first substream selects the antenna index a_i, which indicates the transmitting antenna among the available R_t antennas. The second substream selects the PSK symbol $s_j[n]$ to be sent by antenna a_i. This bit-grouping is shown in Figure 6.15. In order to perform SM, avoiding the channel estimation, we need to transmit the same

Figure 6.15 Bit grouping for Spatial Modulation.

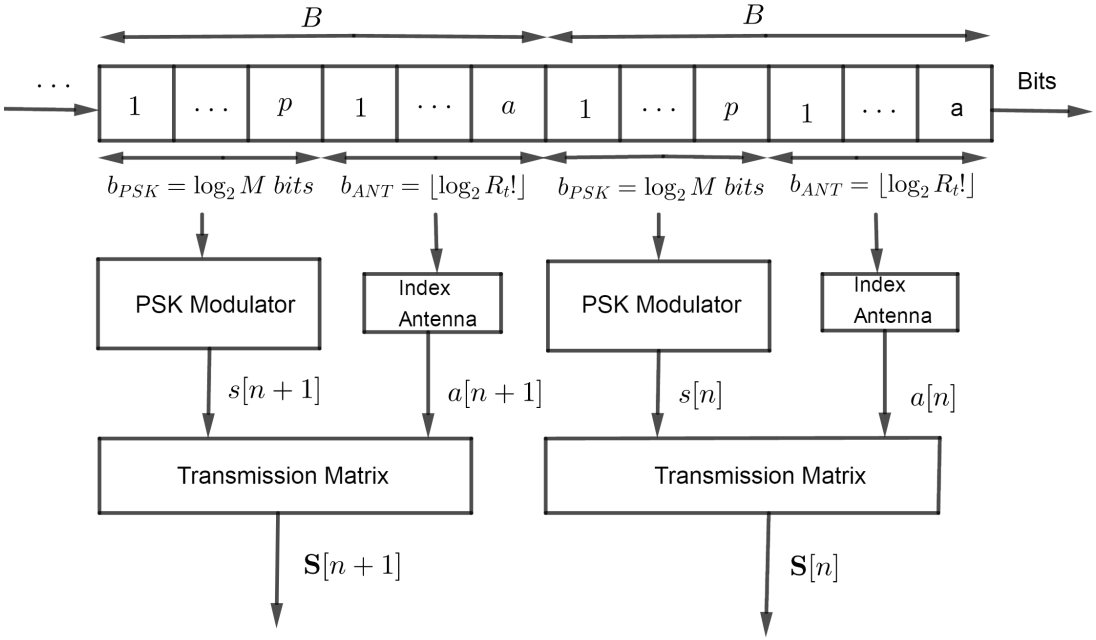

number of consecutive symbols as transmitting antennas, this is, we perform the differential encoding each R_t symbols. We collect a vector $R_t \times 1$ of consecutive symbols $s_j[n]$. This vector in conjunction with the antenna index a_i are delivered for composing the transmission matrix $(R_t \times R_t)$-$\mathbf{S}_j$ for user j, as shown in Figure 6.15. The $(a, n)^{th}$ entry of $\mathbf{S}_j$ denotes the symbol $s_j[n]$ transmitted via antenna a from user j at the instant n. The matrix $\mathbf{S}_j$ must satisfy the next conditions:

1. Only one antenna from R_t available can transmit at each time instant. This means that only one entry in any column of $\mathbf{S}_j$ is non-zero.

2. Each antenna is activated once and only once in the R_t successive time instants which shape $\mathbf{S}_j$. This is only one non-zero entry in any row of $\mathbf{S}_j$.

For example, in the case of $R_t = 4$ transmitting antennas, we need 4 consecutive symbols for the user j, this is the vector $s = \{s_j[1], s_j[2], s_j[3], s_j[4]\}$, and for an index vector

$a = \{1, 3, 4, 2\}$, then an example of possible transmit matrix is

$$\begin{bmatrix} s_j[1] & 0 & 0 & 0 \\ 0 & 0 & 0 & s_j[4] \\ 0 & s_j[2] & 0 & 0 \\ 0 & 0 & s_j[3] & 0 \end{bmatrix}. \tag{6.20}$$

Once we have $\mathbf{S}$, we perform the differential encoding in (2.5) in matrix format as follows

$$\mathbf{X}_j[n] = \mathbf{X}_j[n-1]\mathbf{S}_j[n],\ n > 1. \tag{6.21}$$

At the receiver, the n^{th} received block $\mathbf{Y}[n]$ may be expressed as

$$\mathbf{Y}[n] = \mathbf{H}\mathbf{X}[n] + \mathbf{V}[n], \tag{6.22}$$

where we kept the assumption on the channel $\mathbf{H}$ for NC detection $\mathbf{H}[n] = \mathbf{H}[n-1]$. The transmission is over Rayleigh channel. Note that for NC-SM as (6.21), the detection will depend on the previously demodulated transmission block, since the differential operation is by block, instead of symbol-by-symbol.

The new NC detection block in Figure 6.14, instead of $y[n]y^*[n-1]$, performs the following matrix operation in each receiving antenna

$$Z[n] = \underset{\forall \mathbf{X}}{arg\ min} \left\{ trace(\Re \left\{ \mathbf{Y}[n-1]^H \mathbf{Y}[n] \mathbf{X} \right\}) \right\}, \tag{6.23}$$

resulting our decision variable $z[n]$ used throughout this Thesis in matrix format.

Finally, we detect the vector of R_t joint symbols from $\mathbf{Z}[n]$ by ML detection using the joint constellation. For DSM, we have to extend the joint constellation explained in Chapter 2 to spatial joint constellation characterized by a matrix space, as detailed for single user in Section 6.3.1 and for multiuser in Section 6.3.2.

6.3.1 Single User NC Spatial Modulation

In the single user case, one user transmits symbols that belong to our individual constellations $\mathfrak{M}$, proposed in Chapter 3. Each R_t symbols are accumulated in a vector, which in conjuntion with the index vector a generates a block from the matrix space $\mathcal{X}$. This space for single user coincides with the joint matrix space defined for the reception. For example, in the case for $M = 2$ and $R_t = 2$ antennas, the matrix space generated to transmit is

$$\mathcal{X} = \left\{ \begin{bmatrix} s_1 & 0 \\ 0 & s_1 \end{bmatrix}, \begin{bmatrix} s_1 & 0 \\ 0 & s_2 \end{bmatrix}, \begin{bmatrix} s_2 & 0 \\ 0 & s_1 \end{bmatrix}, \begin{bmatrix} s_2 & 0 \\ 0 & s_2 \end{bmatrix}, \right. \\ \left. \begin{bmatrix} 0 & s_1 \\ s_1 & 0 \end{bmatrix}, \begin{bmatrix} 0 & s_1 \\ s_2 & 0 \end{bmatrix}, \begin{bmatrix} 0 & s_2 \\ s_1 & 0 \end{bmatrix}, \begin{bmatrix} 0 & s_2 \\ s_2 & 0 \end{bmatrix} \right\}. \tag{6.24}$$

We can see in (6.24) 8 combinations for $R_t = 2$, therefore we need only one bit to choose between the two possible transmitting antennas, giving the index vector $a = [1\ 2]$. Note that for $R_t > 2$, the antenna index indicate the combinations among antennas. In general, this number is $\lfloor \log_2 R_t! \rfloor$, resulting that the size of joint constellation is

$$\lfloor \log_2 R_t! \rfloor \cdot M^{R_t}. \tag{6.25}$$

In the literature, all proposals for DSM are considered for single user so far. Therefore, let us examine the performance of our NC system for single user environment ($J = 1$) and compare it to existing works. In the next section, we propose our SM-NC-m-MIMO as a pioneer multiuser DSM.

In Figure 6.16 BER performance for a size of constellation of $M = \{2, 4, 8\}$ and SNR=$\{-5, -3, 0\}$ dB is shown for $R_t = 2$. We can see that using DSM we can sustain the energy-efficiency of m-MIMO with NC detection.

Figure 6.16 BER performance for SM-NC-m-MIMO with $J = 1$ and $R_t = 4$.

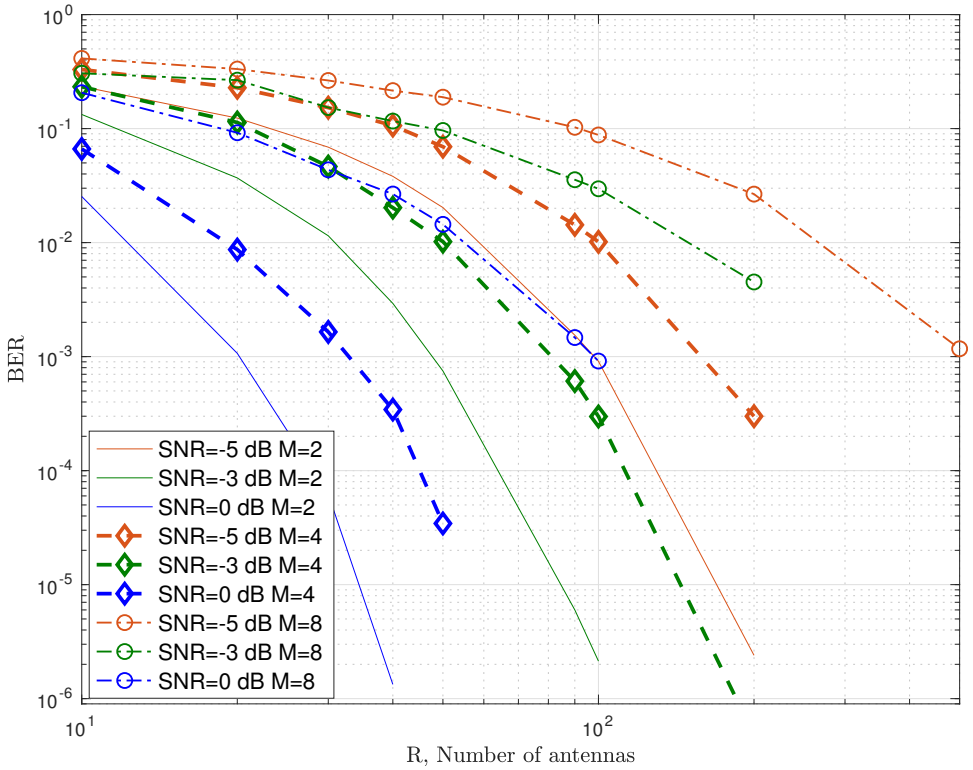

In Figure 6.17 we compare the three following detection methods: differential detection performed so far without considering the SM (CDD), the second one using SM combined with NC (NC-SM) and finally, its coherent counterparts with SM (Coh-SM). To make a fair comparison, we use a QPSK for the NC cases and the 8-PSK for the coherent one. This way we have to take into account the throughput looses due to the pilot signals. We can

see that the NC schemes using SM require 3 dB more to achieve the same performance as coherent scheme well known. In addition, note that NC schemes get the same performance with and without SM. This corresponds to a null gain in the R for SM-NC with respect to CDD.

In Figure 6.18 we compare the same methods as Figure 6.16 as a function of SNR, achieving a gain equal to 2 dB for the NC-SM scheme with respect to CDD. Also, we can see a degradation of the Coherent-SM for low R compared to NC.

Figure 6.17 Performance comparison based on R among NC-SM (QPSK), Coherent-SM (8-PSK) and CDD (QPSK) for m-MIMO using R_t=2.

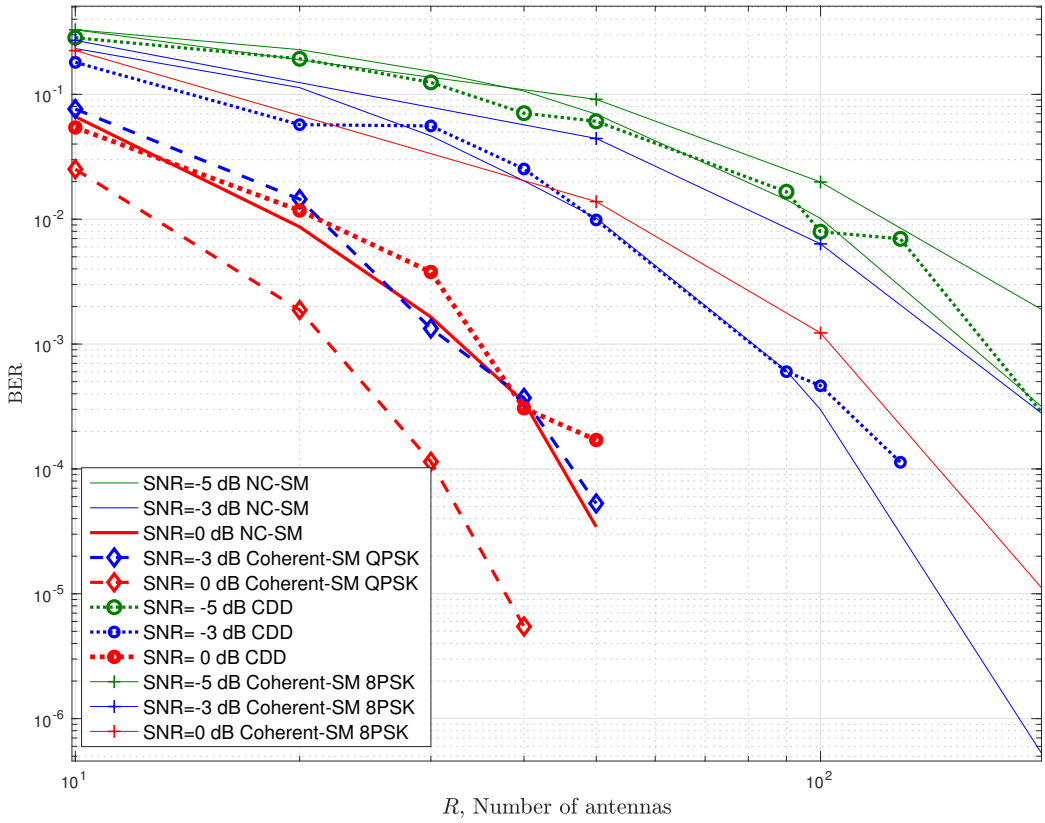

In Figure 6.19, BER performance for NC-SM is compared to CDD for $R_t = 4$ in function of SNR. In this case, we can see that the SNR gap is 2.5 dB.

Figure 6.18 Performance comparison based on SNR among NC-SM (QPSK), Coherent-SM (8-PSK) and CDD (QPSK) for m-MIMO using $R_t = 2$.

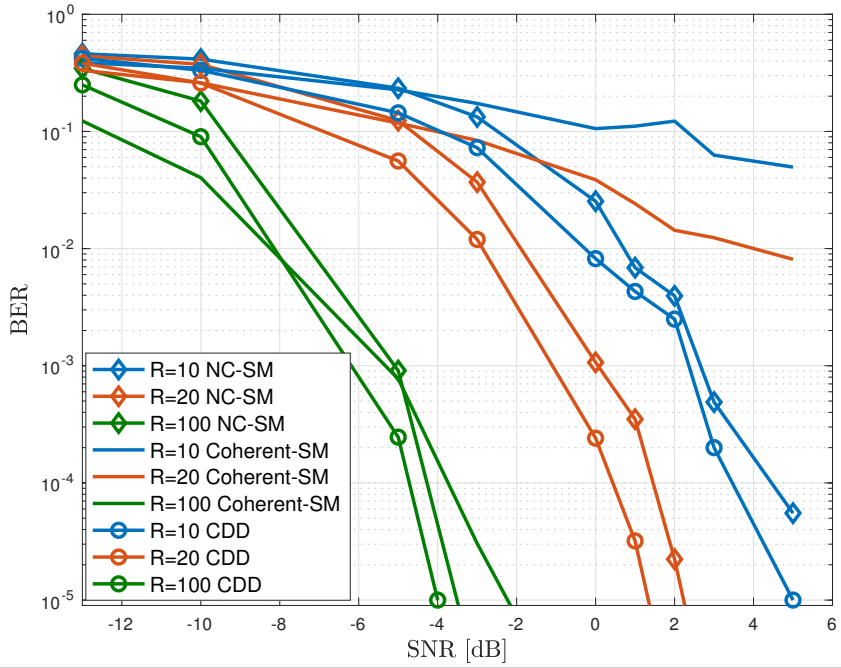

Figure 6.19 Performance comparison based on SNR among NC-SM (QPSK) and CDD (QPSK) for m-MIMO using $R_t = 4$.

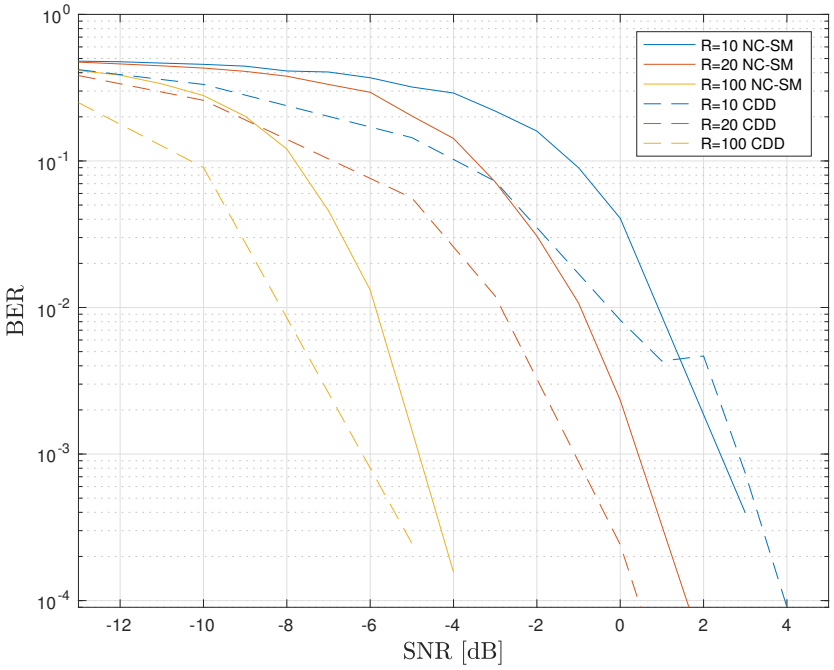

6.3.2 MultiUser NC Spatial Modulation

In the case of multiuser communications, the received joint constellation is extended with respect to the NC conventional transmission which was analyzed in Chapter 3. We have the two following cases depending on what transmitting antenna to be used:

1. Both users transmit using the same antenna index vector a: In this situation, the joint matrices space in the receiver side is composed by the diagonal matrices whose elements belong to the simple joint constellation $\mathcal{M}$ defined in Chapter 3. This space is for $R_t = 2s$

$$\mathcal{G}_1 = \left\{ \begin{bmatrix} \varsigma_j & 0 \\ 0 & \varsigma_j \end{bmatrix}, \begin{bmatrix} \varsigma_j & 0 \\ 0 & \varsigma_k \end{bmatrix}, \begin{bmatrix} 0 & \varsigma_j \\ \varsigma_j & 0 \end{bmatrix}, \begin{bmatrix} 0 & \varsigma_j \\ \varsigma_k & 0 \end{bmatrix} \right\}, \ \varsigma \in \mathcal{M}, \ with \ j,k = 1, \cdots, \mathfrak{K} \tag{6.26}$$

2. Each user employs a different antenna index vector a: the received blocks are composed by the individual symbols for each user without combining them in the joint symbol in the position as placed by a. In this case, the combinations are

$$\mathcal{G}_2 = \left\{ \begin{bmatrix} s_j^1 & s_j^2 \\ s_j^2 & s_j^1 \end{bmatrix}, \begin{bmatrix} s_j^1 & s_k^2 \\ s_j^2 & s_j^1 \end{bmatrix}, \begin{bmatrix} s_j^1 & s_j^2 \\ s_j^2 & s_k^1 \end{bmatrix}, \begin{bmatrix} s_j^1 & s_j^2 \\ s_k^2 & s_j^1 \end{bmatrix} \begin{bmatrix} s_j^1 & s_k^2 \\ s_j^2 & s_k^1 \end{bmatrix} \right\}, \ s_j^{(1)}, s_k^{(1)}, s_j^{(2)}, s_k^{(2)} \in \mathfrak{M}_j \tag{6.27}$$

Finally, the joint constellation for non coherent SM is composed by all possible matrices as follows

$$\mathcal{G} = \{\mathcal{G}_1, \ \mathcal{G}_2\}. \tag{6.28}$$

The total number of combinations for multiuser case is

$$\lfloor \log_2 R_t! \rfloor \cdot M^{R_t J}. \tag{6.29}$$

In Figure 6.20 an example of received joint constellation is shown for $M = 2$, $J = 2$ users, $R_t = 2$, $R_r = 500$ and a reference SNR=0 dB. Note that from all received symbols (blue), we have separated those belonging to the basic joint constellation ($\mathcal{G}_1$) as just the CDD, marked by red point. On the other hand, we have received the individual constellation for the user 1 and 2, corresponding to the cases when each user transmits with a different antenna index vector ($\mathcal{G}_2$). In addition, we have symbols at zero due to the idle antennas.

In Figure 6.21 the BER performance for $J = 2$ users and $R_t = 2$ is shown. We compare to conventional differential detection when we use EEP design. We check that both users have the same performance, corresponding to equal approach. In addition, as we see in the single user case (Section 6.3.1), we need the same number of antennas than CDD case. We obtain the same performance in NC-SM compared to its coherent counterpart, while we are saving hardware resources.

Figure 6.20 Received Joint Constellation in SM-NC-m-MIMO for $J = 2$.

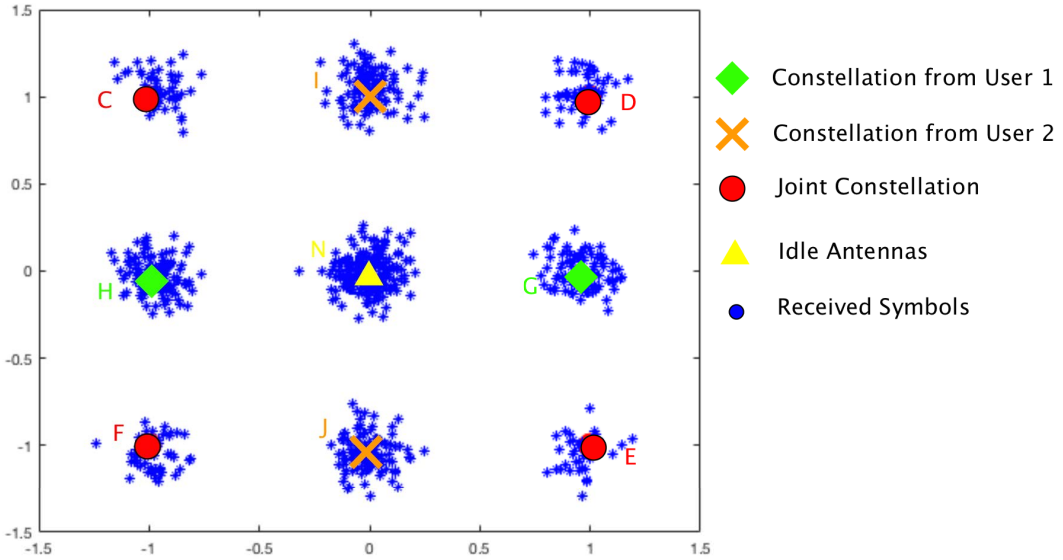

Figure 6.21 BER for $J = 2$ users, $R_t = 2$, $\rho = 0$ dB and $M = 4$ using EEP design.

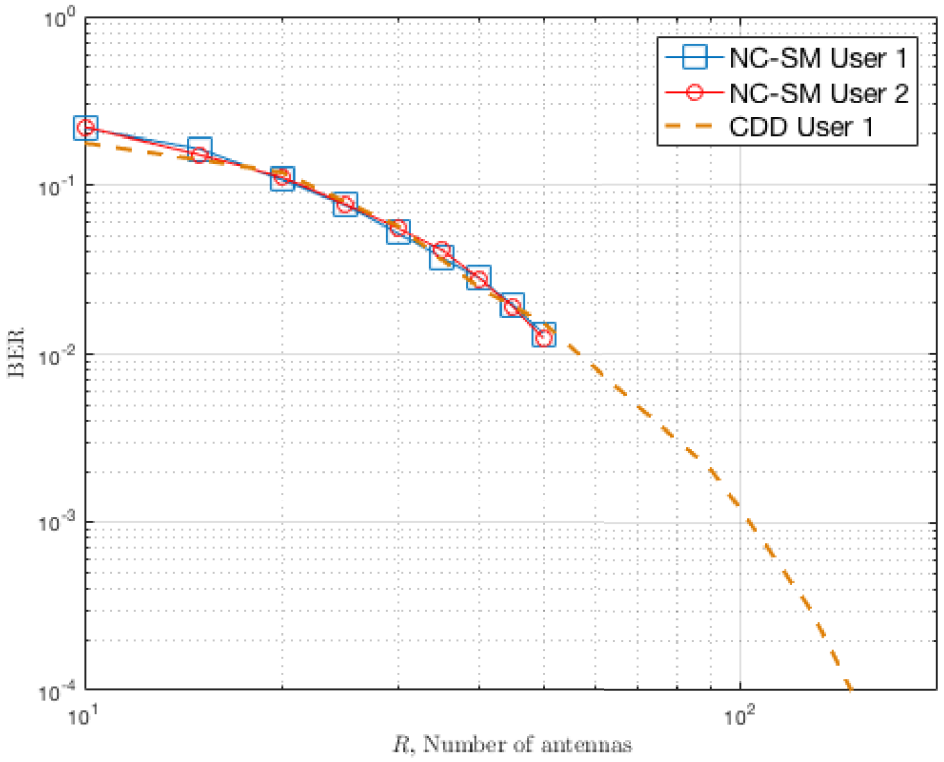

6.4 Conclusions

We have proposed grouping users which experience a Rayleigh fading with those with Rician fading, analyzing the SINR and the performance of such combination in a multi-user NC m-MIMO system based on *M*-DPSK. The adequate user grouping allows unifying the constellation for both groups of users and the detection algorithm, reducing the complexity of the receiver. Also, the number of users that may be multiplexed may be further increased thanks to the improved performance.

We have analyzed our non-coherent massive MIMO system relying on M-DPSK and BICM-ID operating in time-varying channels. We have used a metric to model the time-varying characteristics of the channel so that the analysis can be applied to any wireless communication standard. We have employed EXIT charts as a powerful technique of analyzing and designing iteratively decoded systems. The analysis based on EXIT chart allows us to obtain an estimate of the degradation of the system's performance imposed by realistic channels. Hence, we have shown that our proposed system is robust to temporal variations. From these results, we assess the integration of our NC-m-MIMO proposal in the future communication standards such as 5G.

On the other hand, we have shown that the practically achievable rate relying on the considered modulation and coding schemes approaches the theoretically achievable rate of M-DPSK combined with BICM-ID.

In addition, we have analyzed by simulation the frequency-selectivity and inclusion of an OFDM scheme in NC-m-MIMO based on DPSK. The results reveal an increment in the number of antennas compared to the basic system without OFDM.

Furthermore, we propose incorporating differential spatial modulation to facilitate its implementation, reducing the number of hardware resources required in terms of RF chains. We present and analyze a novel multiuser scheme for NC-m-MIMO combined with SM. We can see that the number of antennas is not affected by the incorporation of SM, even we have an improvement on the performance with respect to the coherent case.

Chapter 7

Suitability of the users multiplexing in non coherent massive MIMO systems based on DPSK

In order to increase the capacity of the system, the communication networks multiplex the users' access on different orthogonal resources. Typically, the networks use the time or frequency to carry out this separation among users. The most popular techniques are time division multiple access (TDMA) for time domain and frequency division multiplex access (FDMA) for frequency domain. With the 3G networks, the usage of code domain entailed the appearance of code division multiple access (CDMA) and the 4G introduced OFDM for multiplexing on orthogonal frequencies. However, the highly increasing demand for multimedia services has prompted the shortage for orthogonal resources offered by all these techniques, giving rise to new proposals based in non-orthogonal techniques known as NOMA [27].

The constellation designs proposed in this Thesis for m-MIMO systems with differential encoding and NC detection can be considered as a non-orthogonal multiplexing technique, where the users are multiplexed in the constellation and separated using the advantage of having a large number of antennas at the BS. The drawback is that, as the number of users increases, the number of the antennas required for a feasible performance becomes too high. Therefore, the multiplexing of the users in the constellation is more difficult. In addition, for the channels which experience a Rician fading presented in Chapter 5 for the new scenarios in 5G, the LOS component of the channel damages even more the performance, making impossible the detection. This issue required redesigning the constellation, involving more complexity in the receiver. Conversely, for the single user NC-m-MIMO based on DPSK, the performance is very promising, outperforming that achieved by its coherent counterpart and the NC designs based on energy detection,

as analyzed in Chapter 3, even for Rician fading (Section 5.2.1). Some previous designs presented in Section 3.5 for Rayleigh channel are still able to demodulate correctly two users multiplexed in constellation, and even up to four users employing the suitable channel coding scheme which reduces the number of antennas required. However, this scheme increases the complexity of the receiver.

Against this background and the results obtained so far, both for taking advantage of the opportunity of m-MIMO and handling the multiplexing of more users for the future communication systems, we analyze the appropriateness of performing a novel multiplexing in constellation combined with classical orthogonal techniques such as TDMA.

7.1 Analysis of the NC-m-MIMO behavior using BLER

Throughout this work we have used the BER or SER as metrics to assess the performance as a function of SNR or the necessary number of antennas in m-MIMO. The BER or SER measure the number of erroneous bits or symbols in a transmission, respectively, and have allowed us to verify the demodulation of the users in a NC-m-MIMO system from a simulation perspective. This means that we send a large frame of bits and we check if we are able to decode each of them. However, the transmission of information along networks is performed by data bit-packets. These packets are organized in sets of bits which assume different roles, for example, routing the information through the network or application information. Therefore, one packet with at least one erroneous bit must be discarded or retransmitted, since the functionality is compromised. The BER and SER metrics do not characterize uniquely the transmission performance, since they do not show how these errors are distributed in the packet. This is, a set of erroneous bits can appear all of them in only one packet or they can be scattered randomly among different packets. Then, in the first case, only one packet is discarded, whilst, in the second, all the packets with one or several erroneous bits are discarded. Hence, for two systems with the same BER, one can be discarding all data packets, whilst the other one is able to decode the information even having errors. This is even more important when the information moves upwards through higher layer protocols such as transport control protocol (TCP), for which the number of erroneous packets is an indicator of the performance. Therefore, the BER or SER are not enough to analyze the behavior of the communication systems. By contrast, the block error rate (BLER) and, related to it, the throughput are more meaningful metrics to describe this behavior.

We started assuming that the channel is invariant in the time, this is $h[n] = h[n+1]$, so the system performance does not depend on the temporal variability of the channel, as was validated in Section 6.1.3. Therefore, we can transmit very long frames of symbols

without significantly affecting the capabilities of the system. However, as was mentioned, this is not entirely correct since it depends on the error localizations. Now, we have to consider a length of packet or transmission frame which determines the efficiency of the system to deliver packets.

With this purpose, the parameters for a transmission based on frames or packets, which verify the usability of our proposal in a communication network, are:

- L is the number of symbols per frame or packet, being l the symbol position within an L-symbol packet.
- The total number of packets transmitted per simulation is F.
- In our designs, $p = \log_2 M$ is the number of bits per symbol for our user's constellations M, then the total number of bits per packet transmitted is pL and for a transmission of size pLF.
- The number of erroneous bits is denoted as e.

Then, we define the probability of having more than e erroneous bits in a packet as follows

$$P(e, pL) = \sum_{n=e+1}^{pL} \binom{pL}{n} P_b^n (1 - P_b)^{pL-n}, \tag{7.1}$$

being P_b the probability of bit error or BER. The probability of erroneous packets is measured by the BLER. As introduced, a packet is erroneous and thus discarded, if at least one bit is erroneous. Using (7.1), we can calculate the probability of having zero errors in a packet as follows

$$P(e = 0) = P(0, pL) = \binom{pL}{0} P_b^0 (1 - P_b)^{pL} = (1 - P_b)^{pL}. \tag{7.2}$$

Then, we calculate the probability of having an erroneous packet, and thus the BLER, as the probability of having any non-zero number of errors per packet as follows

$$BLER = 1 - P(e = 0) = 1 - (1 - P_b)^{pL} = 1 - (1 - BER)^{pL}. \tag{7.3}$$

We can use the bounds defined in Section 3.3 to derive from them the BLER for our NC-m-MIMO scheme. These bounds were calculated for SER. Therefore, we can define the BLER at symbol level, instead of bit level, obtaining the erroneous symbols per packet. In this case, the BLER is

$$BLER_s = 1 - (1 - P_s)^L = 1 - (1 - SER)^L, \tag{7.4}$$

where P_s is the probability of symbol error or SER. However, the communication standards define commonly the BLER in function of BER, instead of SER. Therefore, first we have to translate the SER to BER to calculate the BLER at bit level.

We consider that one symbol which contains p bits is erroneous if at the least one bit is received erroneously. As with the packets, we use (7.1) to determine the relation between SER and BER as follows

$$SER = 1 - (1 - BER)^p \rightarrow BER = 1 - \sqrt[p]{(1 - SER)}. \tag{7.5}$$

We can differenciate two cases depending on the L value for the new scenarios in 5G. In M2M communication, it is typically transmitting short packets. A short block length is assumed when the number of bits in a block is relatively small (i.e. less than 20). By contrast, long block length, high L values, can be considered from 100 bits for a packet. In Figure 7.1 we check (7.5) for high L and for low value of L with several SER and BER obtained by simulation for a single user system and $M = 4$ as functions of SNR. So, from

Figure 7.1 Validating expression (7.5) for different L.

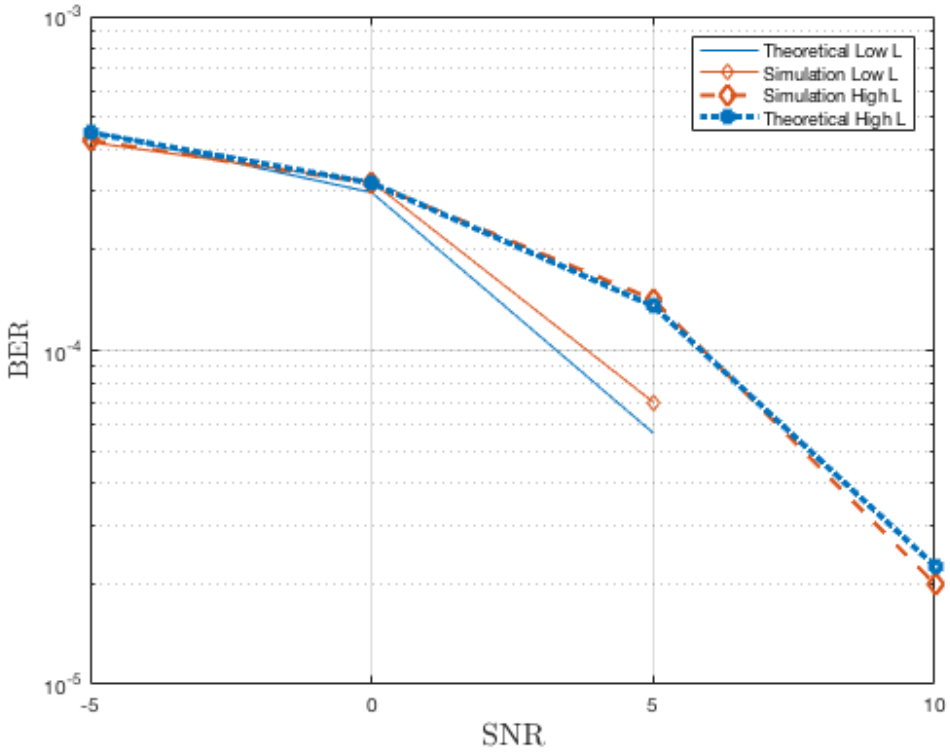

the previous test, we can define BLER interchangeably from SER or BER as follows

$$BLER = 1 - (1 - BER)^{pL} = 1 - (\sqrt[p]{1 - SER})^{pL} = 1 - (1 - SER)^L. \tag{7.6}$$

In Figure 7.2 we calculate the BLER for L=$\{10, 50, 100\}$ symbols per packet. We simulate the transmission of $F = 1,000,000$ packets for a reference SNR $\rho = \{-3, 0, 3\}$ dB. We can see that the higher L is (more symbols per packet are transmitted), the higher BLER is and, thus we need more antennas. This confirms that although our NC-m-MIMO scheme is very robust to the temporal variability, allowing us to transmit large frames of symbols, actually we have to limit the number of symbols transmitted per packet to reduce the probability of having an erroneous symbol.

Figure 7.2 BLER comparison for different L values.

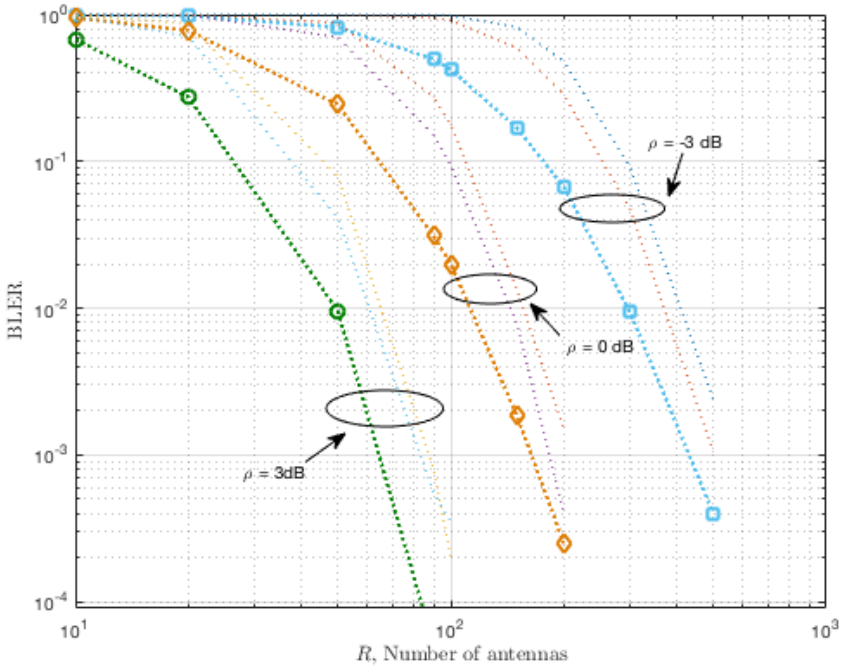

In the remaining simulation for this section, we use $L = 10$, unless otherwise stated. This value is chosen due to the fact that it is the maximum number of symbols demodulated using the Algorithm 2 (Section 5.5) for Rician channel. In addition, a low L is recommended in M2M scenarios, an interesting application of our NC schemes in 5G context.

In Figure 7.3 we show the BLER as a function of the number of antennas for a single user system, $\rho \in \{-3, 0, 3\}$ dB and $M = 4$ ($p = 2$ bits/symbol). We calculate the BER for a simulation of F =1,000,000 packets of $L = 10$ symbols. Then, we obtain also the BLER by simulation and we compare with (7.3). We can see that BLER matches perfectly with the theoretical expression.

In Figure 7.4 we perform the same procedure as for Figure 7.3, but in this case we calculate the SER by simulation and then we obtain the BLER using (7.6) for low L in order to compare to that obtained by simulation. Also in this case, BLER matches

perfectly with the theoretical expression.

Figure 7.3 BLER validation at bit level for single user for $M = 4$, $F = 1{,}000{,}000$ and L=10.

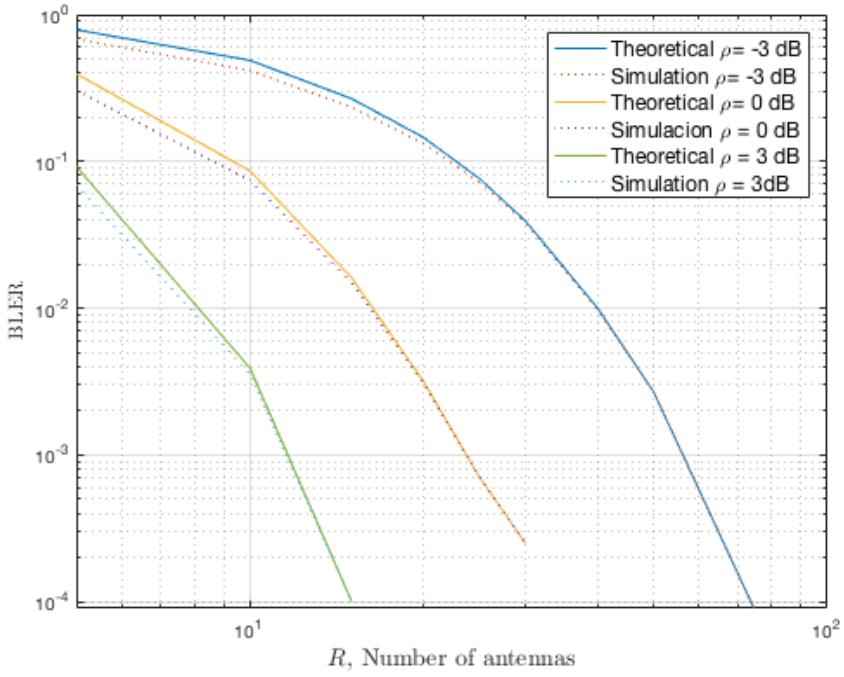

Figure 7.4 BLER validation at symbol level for single user for $M = 8$, $F = 1{,}000{,}000$ and L=10.

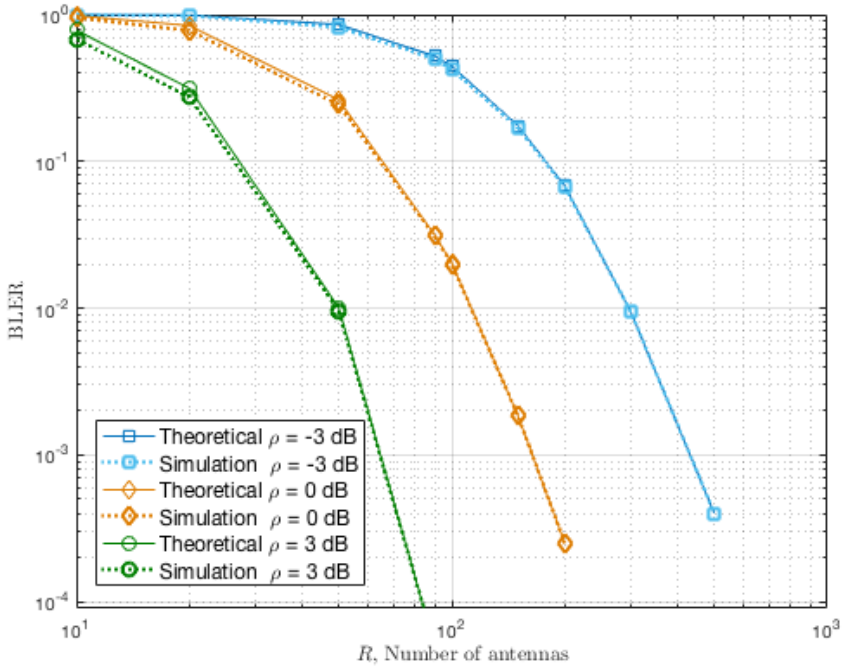

In Figure 7.4 we obtain the BLER for a different size of constellation, $M = 8$. We can see that the BLER coincides to (7.6) too.

7.2 Constellation or TDMA multiplexing

In this section, we compare two forms of multiplexing users in NC-m-MIMO: non orthogonaly using the constellation as proposed in this Thesis, denoted as *Constellation Multiplexing Scheme* (CMS) against multiplexing orthogonally users in the time, denoted here as TDMA Multiplexing Scheme (TMS). In CMS we are introducing IUI due to the non orthogonality among users, but J users can individually make use of the fully available bandwidth. Conversely, in TMS the interference is suppressed at the expense of reducing the BW for each user, which is shared among them. However, due to the high degradation that performance suffers when we increase the number of users in CMS, we can consider switching to TMS and sharing BW from a certain number of users or for certain R. Hence, the objective of this analysis is finding the number of antennas and users for which CMS is more recommended than TMS.

For this purpose, we can use the throughput which measures the rate of successful packets delivery in bit per channel use (bpcu). In order to consider that a transmission is successful we have to overcome the maximum number of erroneous packets. Therefore, we calculate the throughput on the basis of the BLER for each multiplexing proposal as follows

$$Throughput_{CMS}\,[bpcu] = \begin{cases} 0 & BLER_{MU} > BLER_0 \\ (1 - BLER_{MU}) \log_2 M & BLER_{MU} < BLER_0 \end{cases} \tag{7.7}$$

$$Throughput_{TMS}\,[bpcu] = \begin{cases} 0 & BLER_{SU} > BLER_0 \\ \dfrac{(1 - BLER_{SU}) \log_2 M}{J} & BLER_{SU} < BLER_0 \end{cases} \tag{7.8}$$

We can see in (7.7) and (7.8) that using a simplification the throughput will be zero if we do not overcome certain number of erroneous packets. This number is $BLER_0$, which is marked by the standards or depending on the application. For example, in LTE is assumed a threshold of $BLER_0 = 10\%$. Meanwhile, for URLL communications this value can be more restrictive due to the high security which require this type of applications. In case we include a channel coding scheme, we can reduce this constraint. In addition, note that for the same BLER, the throughput achieved by TMS is lower than that achieved by CMS due to the BW sharing. However, the high interference in CMS increases BLER faster than in TMS, thus crossing both schemes. We are interested in this crossing point.

In order to carry out the comparison, we have two schemes as shown in Figure 7.5. In this figure, a CMS and a TMS for $J = 2$ users is illustrated.

1. For CMS, J users transmit simultaneously multiplexed in the constellation requiring only one time slot.

2. For TMS, J users transmit consecutively sharing one time slot as corresponding to TDMA. In this case, the BW in each time slot is divided by J users, acquiring each user BW/J.

Figure 7.5 Schematic for multiplexing $J = 2$ users.

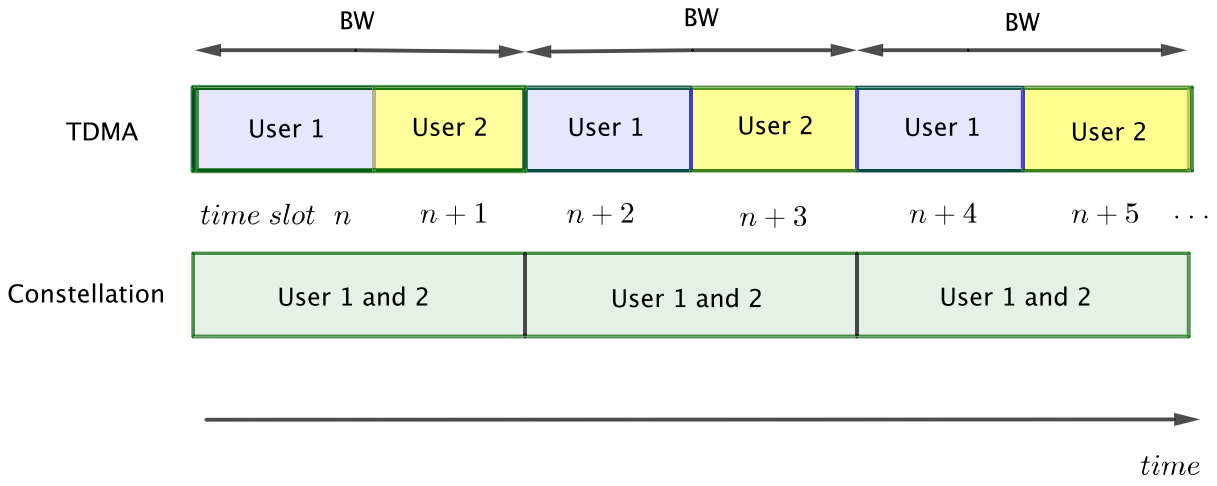

The multiplexing may be performed the same way for the frequency domain or code domain instead of the time domain. We have chosen the time domain as an illustrative example for the analysis.

7.2.1 Individual multiplexing

First, we analyze the BLER and the throughput which each user achieves individually inside a multiuser environment when we use CMS and, on the other hand with TMS. We simulate a NC-m-MIMO-DPSK system with $J = 2$ users and several SNR, varying the number of antennas.

For the CMS case, we multiplex two users ($J = 2$) by constellation with the EEP designed in Section 3.5. In this constellation, all users experience the same performance, thus the same BLER. We calculate the throughput for one user of the two, since it is the same, from BLER using (7.7). On the other hand, in TMS case we can analyze the performance for one user in its corresponding time instant, this is equivalent to single user with less BW. Once we have the BLER for TMS, we calculate the throughput using (7.8). Then, both curves are compared. In Figure 7.6 the throughput for CMS and TMS with 2 users is shown. The simulation is carried out over $F = 20,000$ packets and a size of the constellation of $M = 2$. We can see that we need to use in TMS 5 antennas at the BS

with $\rho = 3$ dB, 15 with $\rho = 0$ and 40 with $\rho = -3$ dB in order to receive correctly packets. By contrast, in CMS we need 10, 50 and 100 antennas for $\rho \in \{-3, 0, 3\}$ dB. In this case, for $M = 2$, in TMS each user achieves maximum throughput of 0.5 bit per channel use in 10, 20 and 50 antennas. For the same throughput, CMS needs more antennas than TMS, however CMS achieves a higher throughput, reaching 1 bpcu. For low R, we can demodulate the users before using TMS than CMS. This makes sense, because we do not have m-MIMO conditions yet. From Figure 7.6 we conclude that for low M, multiplexing in constellation is recommended against time because we achieve higher throughput with an affordable number of antennas when we employ m-MIMO, highlighting our proposed design in this Thesis, in the two users case.

Figure 7.6 Comparison Throughput of 2 users in TMS and CMS for $M = 2$, L=10 and F =20000.

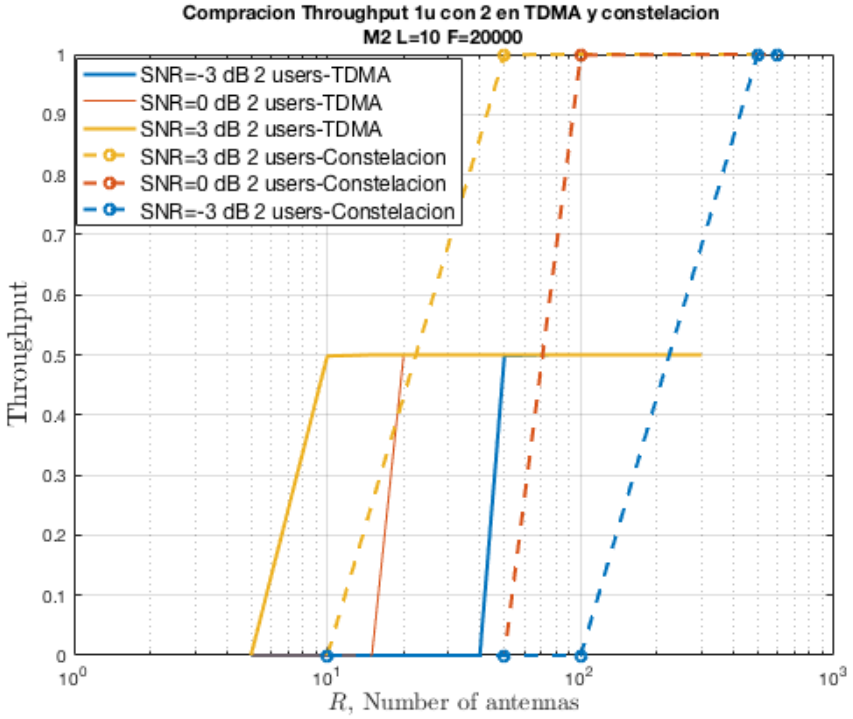

Now, we analyze what happens when we increase the number of users J. In Figure 7.7 CMS and TMS for 2, 4, 6, 8 and 10 users are shown. We can see that all users in CMS always achieve the maximum throughput for a given M. Instead, TMS reduces the throughput for each user as J increases. However, TMS is able to demodulate all users with the same R from the beginning, whilst CMS needs 30 antennas for 2 users, 550 antennas for $J = 4$ users and, for more users, over 1000 antennas are needed, which implies that increasing the size of constellation culminates in an excessive R. In this case, we may prefer using TMS instead of CMS.

We have seen in the first case that CMS is better than TMS, whilst in other case, TMS

Figure 7.7 Comparison Throughput of multiuser system in TMS and CMS for $M = 2$, L=10 and F =20000.

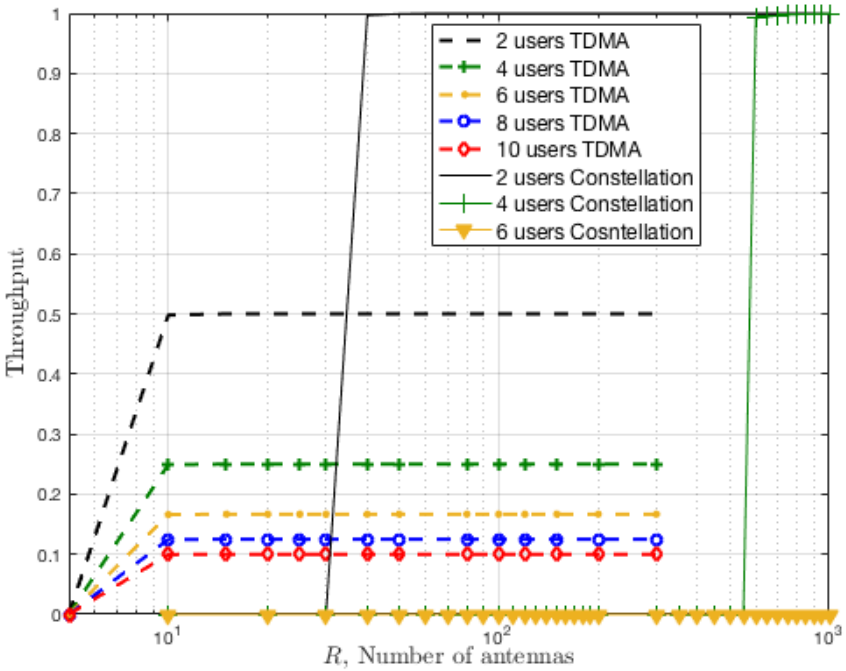

is shown as best option against CMS. Therefore, we propose to combine both schemes in the next section.

7.2.2 Scheduling TDMA combined with non coherently constellation multiplexing

In order to achieve the maximum possible throughput and, at the same time, the minimum R, we propose to schedule users by combining TDS with CMS. In Figure 7.8 the throughput for $J = 4$ and $M = 2$ is shown. We simulate three options of distributing users between TMS and CMS. First, the four users are multiplexed in the time (pure TMS); second, four users are multiplexed in constellation (pure CMS); the last one, we schedule 2 users in constellation and the other two in the time as shown in Figure 7.9. We can see that in mixed option we achieve an intermediate throughput between pure modes, in addition, the number of antennas required to start the reception of correct packets is reduced from 550 to 30 antennas, with the corresponding throughput reduction. However, this reduction is lower compared to the R reduction in pure CMS.

In Figure 7.10 we show the throughput for $J = 8$ users for the three combinations shown in Figure 7.11. The first option is scheduling four users grouped in CMS (4-CMS) and, in turn two groups in TMS (2-TMS). The second option for 8 users is 2 users

Figure 7.8 TMS combined with CMS for $J = 4$ users, $M = 2$ and $\rho = 3$ dB.

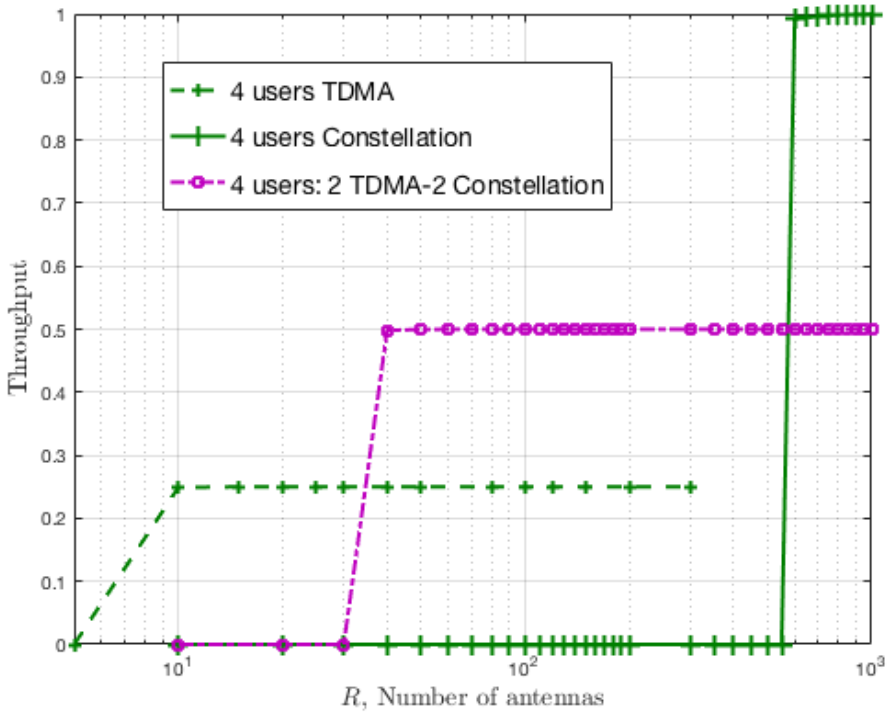

Figure 7.9 Schematic for multiplexing $J = 4$ users combined in TMS-CMS.

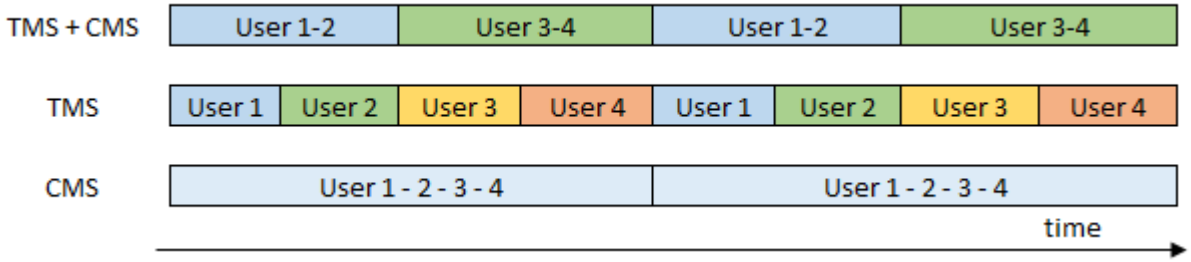

multiplexed in constellation (2-CMS) resulting in 4 groups in time (4-TMS). The third option is the 8 users multiplexed in time (8-TMS). We can see that for a R of 30 antennas which is suitable for m-MIMO we achieve twice the throughput. However, if we include more users in constellation than TDMA, this number of antennas is too high even for m-MIMO. It is preferable when combining both schemes introducing more users in TDMA than in the constellation.

Figure 7.10 TMS combined with CMS for $J = 8$ users, $M = 2$ and $\rho = 3$ dB. (Rev.)

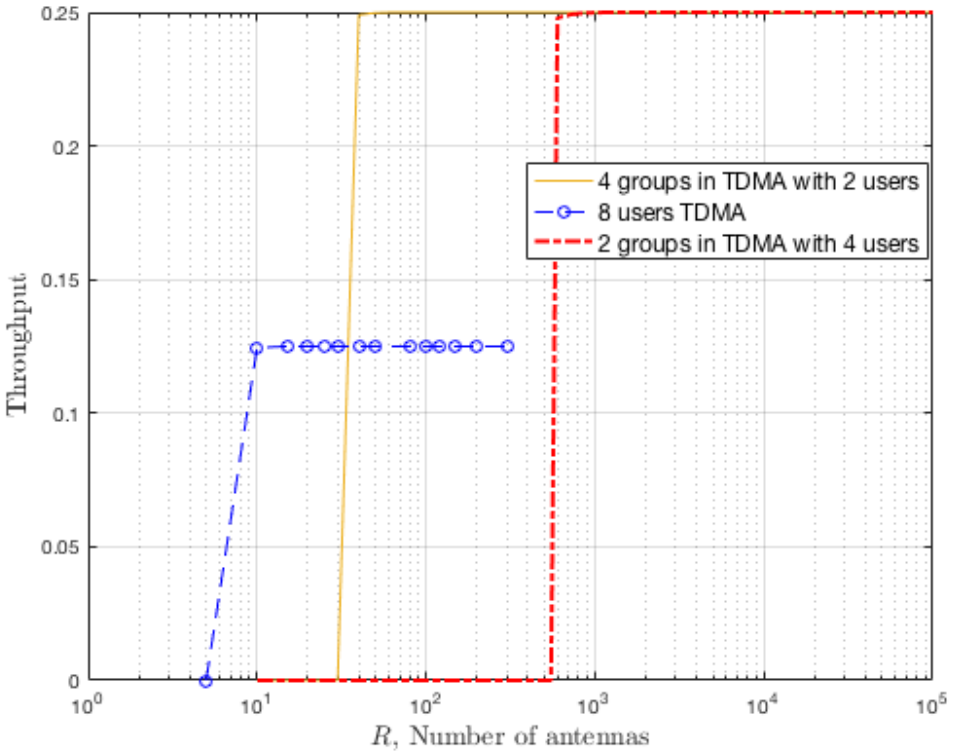

Figure 7.11 Schematic for multiplexing $J = 8$ users combined in TMS-CMS.

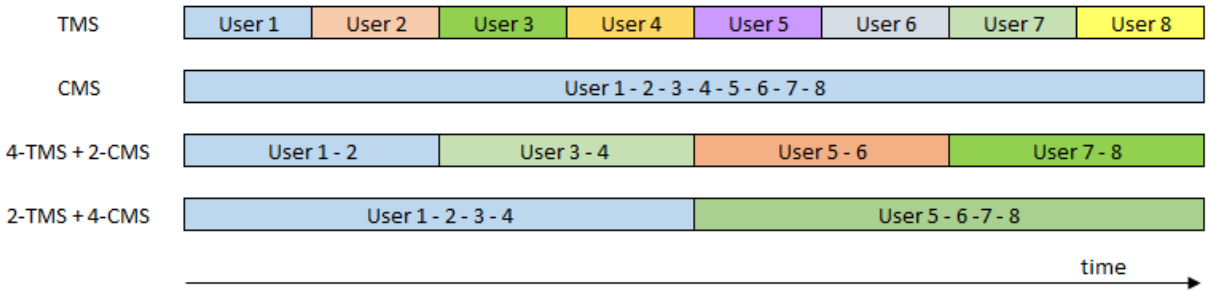

In Figure 7.12 we show the throughput for $L = 1000$. We can see that the R required for demodulation is higher than for $L = 10$ due to the fact that the probability of having errors in the packet is higher.

Figure 7.12 Comparison Throughput of MU system in TMS and CMS for M=2 and L=1000.

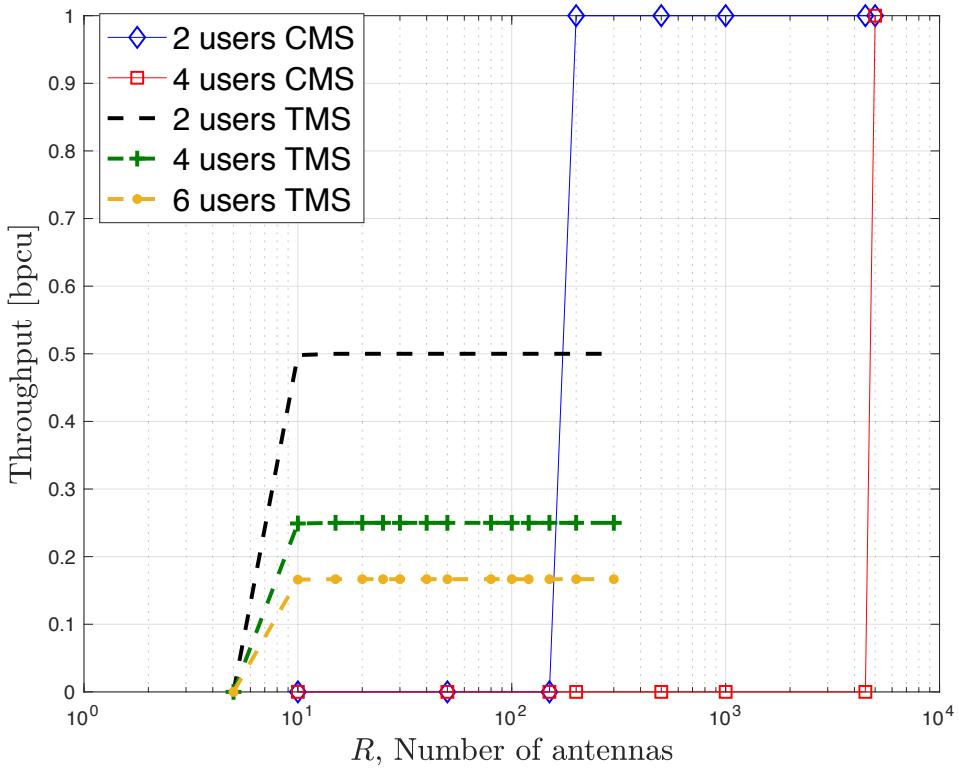

7.3 Limiting number of antennas for multiplexing in constellation

As it has been concluded in the sections above, there is a number of antennas for which CMS is better than TMS and vice versa, depending on the number of users and the size of the constellation. In order to calculate the BLER, we use the bounds for SER defined in Section 3.3 and from them we can optimize the throughput. The two main bounds, upper and lower, which we need in this section are the following

$$SER \leq (\mathfrak{K}-1)\, Q\left(\sqrt{\frac{d_{min}^2}{2\mathfrak{J}}}\right), \tag{7.9}$$

$$SER \geq \frac{1}{\mathfrak{K}} \sum_{m=0}^{\mathfrak{K}-1} Q\left(\frac{d_{min}^m}{\sqrt{2\mathfrak{J}}}\right). \tag{7.10}$$

For the purpose to optimize R, J and M, we use an approximation for the Gaussian-Q function used in the error bounds. We have analyzed several proposals in the literature

[150–161]. We selected the following approximation

$$Q(x) \approx \frac{(1-\exp^{-\frac{Ax}{\sqrt{2}}})\exp^{-x^2/2}}{B\sqrt{2\pi}x}, \tag{7.11}$$

where the best values for A and B are 1.98 and 1.134, respectively, resulting (7.9) in

$$\begin{aligned} SER &\approx (\mathfrak{K}-1)\frac{\left(1-\exp^{-\frac{A}{\sqrt{2}}\sqrt{\frac{d_{min}^2}{2\mathfrak{I}}}}\right)\exp^{-\frac{d_{min}^2}{4\mathfrak{I}}}}{B\sqrt{\pi\frac{d_{min}^2}{\mathfrak{I}}}} \\ &= \frac{(\mathfrak{K}-1)}{Bd_{min}}\sqrt{\frac{\mathfrak{I}}{\pi}}\left(\exp^{-\frac{d_{min}^2}{4\mathfrak{I}}} - \exp^{-\frac{d_{min}^2 A\sqrt{4\mathfrak{I}}}{4\mathfrak{I}}}\right), \end{aligned} \tag{7.12}$$

and (7.10) in

$$SER \approx \frac{1}{\mathfrak{K}}\sum_{m=0}^{\mathfrak{K}-1}\frac{(1-\exp^{-\frac{Ad_{min}^m}{\sqrt{2\mathfrak{I}}}})\exp^{-\frac{d_{min}^{2m}}{2\sqrt{4\mathfrak{I}}}}}{B\sqrt{\frac{\pi}{\mathfrak{I}}}d_{min}^m} \tag{7.13}$$

However, the approximation in (7.11) was optimized for a coherent system. In [161], we find an approximation generalized and improved, which reduces the number of exponentials. This is known as Chernoff bound, defined as

$$Q(x) \approx \frac{1}{2}\exp^{-x^2/2}, \tag{7.14}$$

then the SER belongs to upper bound in (7.9) is expressed as follows

$$SER \approx \frac{(\mathfrak{K}-1)}{2}\exp^{-\frac{d_{min}}{2\mathfrak{I}}}, \tag{7.15}$$

whilst for lower bound in (7.10) is formulated as follows

$$SER \approx \frac{1}{2\mathfrak{K}}\sum_{m=0}^{\mathfrak{K}-1}\exp^{-\frac{(d^m)^2}{4\mathfrak{I}}} \tag{7.16}$$

We include (7.15) in (7.6), and the resulting expression is included in throughput formulation (7.7) for low packet length, resulting for CMS case that

$$Throughput_{CMS} \approx p\left(1-\frac{(\mathfrak{K}-1)}{2}\exp^{-\frac{d_{min}}{2\mathfrak{I}_{MU}}}\right)^L, \tag{7.17}$$

where $\mathfrak{I}_{MU}$ is the multiuser interference caused by J users multiplexed in the constellation,

$$\mathfrak{I}_{MU} = \frac{J^2+2\sigma^2 J+\sigma^4}{R}. \tag{7.18}$$

On the other hand, we have the throughput resulting for the TMS case as

$$Throughput_{TMS} \approx \frac{p}{J}\left(1-\frac{(M-1)}{2}\exp^{-\frac{d_{min}}{2\Im_{SU}}}\right)^{L}, \tag{7.19}$$

where in this case there is only noise due to the fact there is one user transmitting, being this as follows

$$\Im_{SU} = \frac{1+2\sigma^2+\sigma^4}{R}. \tag{7.20}$$

We can remember the derivation of the interference in Chapter 3.

In order to optimize the number of antennas, we include (7.18) in (7.17) and (7.19) in (7.20), we set the L value and the size of the constellation M, which determines p. Then we get a function for the throughput obtained in CMS (7.21) and TMS (7.22) to be optimized which depend on R and the number of users J. The minimum distance will depend on the constellation design chosen. In this analysis, we employ the EEP schemes which gives $d_{min} = 0.56$ (Chapter 3).

$$f_{CMS}(R,J) = p\left(1-\frac{(\aleph-1)}{2}\exp^{-\frac{Rd_{min}}{2J^2+4\sigma^2J+2\sigma^4}}\right)^{L} \tag{7.21}$$

$$f_{TMS}(R,J) = \frac{p}{J}\left(1-\frac{(M-1)}{2}\exp^{-\frac{Rd_{min}}{2+4\sigma^2+2\sigma^4}}\right)^{L}. \tag{7.22}$$

In order to find the threshold where the CMS scheme is better than TMS scheme, we have to equate (7.21) and (7.22), this is $f_{CMS}(R,J) = f_{TMS}(R,J)$.

$$p\left(1-\frac{(\aleph-1)}{2}\exp^{-\frac{Rd_{min}}{2J^2+4\sigma^2J+2\sigma^4}}\right)^{L} = \frac{p}{J}\left(1-\frac{(M-1)}{2}\exp^{-\frac{Rd_{min}}{2+4\sigma^2+2\sigma^4}}\right)^{L} \tag{7.23}$$

For example, the threshold obtained for $J = 4$ users, $L = 10$, $M = 2$ and $\rho = 0$ dB ($\sigma = 1$) is 70 antennas, which match the result obtained by simulation in Figure 7.6. In the case we want to know the minimum R to start to demodulate the users with CMS, we have to optimize (7.21) as $\frac{df_{CMS}(R,J)}{dR} = 0$.

7.4 Conclusions

In this chapter, we analyzed the BLER and the throughput. These metrics have allowed us to validate the behavior of the proposed multiuser NC-m-MIMO system based on DPSK from the point of view of a communication network where packets are transmitted. The results obtained in previous chapters so far did not show the scope of multiplexing users in the constellation against other classical techniques such as TDMA. This way of sharing the resources among the users influences obviously in the performance and behavior of the network. Therefore, we have to compare the multiplexing of users in the constellation (CMS) against the multiplexing schemes in time (TMS).

The CMS needs to incorporate more antennas at the BS than TMS, although CMS provides a higher throughput than TMS. However, in some cases, the demodulation of multiple users in the constellation could require an excessively large number of antennas compared to TMS. Therefore, it is necessary to properly manage the tradeoff between throughout and the number of antennas, to reach an optimal operational point.

In order to take advantage of increasing the throughput with CMS, while we may reduce the number of antennas with TDS, we have proposed combining both schemes. We have achieved for 8 users, using only 30 antennas, to multiply by two the throughput with respect to orthogonal multiplexing. In addition, we conclude that it is preferable to have more groups multiplexed in time with a few users in constellation than all users in pure CMS or TMS, finding a good tradeoff between the number of antennas and the throughput.

Finally, we have proposed a function which allows optimizing the throughput as function of R, J and M.

Chapter 8

Conclusions and Future Work

In this chapter, we outline the contributions of this thesis, analyze the results obtained and we contemplate future research lines.

8.1 Summary

In this Ph.D. Thesis we have analyzed the use of massive MIMO systems with differential encoding and non coherent detection in multiuser environments. The contributions that can be outlined from this work range from new constellation designs and detection algorithms to the analysis of the effects and requirements of its implementation in future practical communication systems and technologies, such as 5G.

First, we consider the use of NC-m-MIMO systems based on DPSK for channels which experience Rayleigh fading. We have proposed several constellation schemes that have allowed us to separate the users' signals at the receiver thanks to the benefit of having a large number of antennas at the BS. Two approaches were considered in terms of error performance: each user achieves a different performance, so-called unequal error performance (UEP) and, on the other hand, the same performance is provided for all users known as equal error performance (EEP). The first one may be interesting to support multiple applications with different QoS requirements, such is the case for video applications. The second one, EEP designs may be more interesting for voice applications where all users require the same capabilities, and hence the same requirements. Other advantage for EEP is that it does not rely on strict power control, making it easier and interesting for m-MIMO. We have analyzed the number of antennas required by all designs. This number depends on the minimum distance between symbols in the individual constellation, not on the characteristics of the joint constellation in the receiver side. Also we have proved that the number of antennas is more influential that the SNR on the per-

formance. The UEP designs usually require more antennas than EEP schemes, taking into account that this number tends to the same value for both designs as the minimum distance in UEP approximates to that of the EEP one. For all these designs, we have analyzed the interference and SINR in order to obtain the error probability bounds for NC-m-MIMO, which depend also on the minimum distance, the number of antennas and the total interference.

After analyzing our non coherent proposals, UEP and EEP, we compare them to other constellation schemes proposed in the literature, some for m-MIMO but other proposed only for differential encoding and that is why is interesting the comparison with our scheme. We have shown that our proposal performs better than the benchmark of the designs based on energy detection [97,98,105,126] regarding BER. Conversely, they show a similar performance as other constellations which perform differential encoding, such as APSK, DAPSK or DQAM, extending our designs for multiuser cases taking advantage of the large number of antennas. In addition, our proposals are not far from the performance of an equivalent coherent system operating under realistic channel assumptions. We were able to reduce the difference between NC and coherent schemes to SNR 2 dB, instead of the classical 3 dB, being both systems equivalent for high number of antennas.

The initial designs proposed for Rayleigh channels required an excessive number of antennas for a target bit error probability. In consequence, a channel coding scheme is included with the objective of reducing the number of antennas required. For this purpose, we have proposed the combination of BICM scheme and iterative decoding with a multi-user NC-m-MIMO system based on M-ary DPSK

Additionally, we have analyzed and proposed the EXIT chart as a useful tool for finding the best channel coding scheme for m-MIMO saving simulation time. We propose an approach for EXIT curves based on the number of antennas for m-MIMO. Based on this model, we designed a channel coding scheme suited for the constellation designs proposed previously for Rayleigh fading in Chapter 3. The EEP design offers better performance than the UEP, although both schemes perform better than previous work and compared to the case without coding. Also, including coding, we improve the UEP designs. We have shown that the number of users served by the BS can be increased with a 70% reduction in the number of antennas with respect to previous work. In particular, we show that with 100 antennas for the EEP design with $J = 2$ users and a coding rate of $1/2$ we achieve the minimum probability of error. We have demonstrated that a feasible number of $R = 100$ antennas are sufficient for several situations. We have seen that R may be reduced from 1,000 to 100 with respect to the system operating without coding presented in Chapter 3. Moreover, using iterative decoding also improves the performance compared to other coded schemes [104] based on energy detection. We have seen that R is allowed to decrease about two orders of magnitude with respect to the systems without coding

presented in Chapter 3 and in [103]. The number of users that can be supported by the BS can increase at the cost of a higher number of antennas R. We show the importance of the mapping scheme, focusing on the mapping for the individual constellations.

In this point, we analyzed the proposed constellation for channels which experience Rician fading, since it is foreseen that the new environments emerging with 5G may be modeled by Rician channels. In the single user case, our NC-m-MIMO proposal in a Rice scheme is equivalent to Rayleigh channel regarding performance, achieving a better BER than energy detection based schemes in Rician channel. However, the line of sight (LOS) component of the channel generates an interference arising as a result of the multiuser non coherent detection in Rician channel, making impossible the demodulation of the users when there are more than one. Therefore, we had to redesign the constellation. The new constellation has allowed an unambiguous detection of the transmitted symbols despite the interference caused by the LOS component. This proposal is presented as a novel design for multiuser NC m-MIMO in Rician fading against the rest of designs in the literature shown for single user scenarios. Furthermore, we have proposed a detection algorithm based on the multi-symbol joint decision enhanced with the knowledge of the new constellation and the effect of interference. The SINR and SER have been theoretically analyzed showing a good match with the simulations. We have analyzed the performance of the system showing an improvement with respect to classical non-coherent detection techniques. With the proposed constellation and detection algorithm we are able to leverage the LOS component of the Rician propagation, obtaining a better performance than with Rayleigh channels for the newly designed constellation. This better performance translates to a decrease of the required number of antennas. Furthermore, we have seen that the designs based on M-DPSK outperform those based on energy detection [110] and [39] also in Rician propagation.

Another solution for addressing the interference caused by LOS component was grouping users which experience a Rayleigh fading with those with Rician fading, analyzing the SINR and the performance of such combination in a multi-user NC m-SIMO system based on M-DPSK. The adequate user grouping allows unifying the constellation for both groups of users and the detection algorithm, reducing the complexity of the receiver. Thanks to this grouping, the number of users that may be multiplexed may be further increased.

In addition to the analysis for Rayleigh and Rice channels, we study the behavior of our system depending on the real limitations in practical channel. The temporal variability is the main limitation for the non coherent detection. In principle, it may seem that we require a coherence time large enough to consider that the channel coefficients remain constant over a long transmission of symbols. Now, we started analysing our NC-m-MIMO system relying on M-DPSK and BICM-ID operating in time-varying channels. We have used a metric β to model the time-varying characteristics of the channel so that

the analysis can be applied to any wireless communication standard. As β decreases, which means a more severe channel time variation, the R required for achieving the same performance as that of the constant (time invariant) channel increases. We can maintain the same R as for the constant channel at the expense of a reduced throughput by using a lower channel coding rate. We employed EXIT charts again to obtain an estimation of the degradation of the system's performance imposed by realistic channels. The results showed that we need $6 < \beta < 10$ in order to be able to decode the information, whilst for $\beta > 10$ the effects of the temporal variability are negligible, being our system able to withstand high Doppler spread. Hence, we have shown that our proposed system is robust to temporal variations. We have also analyzed the β-values in the current wireless standards such as LTE, for which NC-m-MIMO can provide high benefits and serve as an evolution towards 5G. These values are higher than 10, ensuring that we achieve the same performance as in the constant channel scenario. From this results, we assess the integration of our NC-m-MIMO proposal in the future communication standards such as 5G and beyond. Moreover, we have shown for time-varying channels that the practically achievable rate relying on the considered modulation and coding schemes approaches the theoretically achievable rate of M-DPSK combined with BICM-ID.

Furthermore, we have proposed incorporating differential spatial modulation (SM) to facilitate its implementation in practical m-MIMO systems, reducing the number of hardware resources required in terms of RF chains. We have presented and analyzed a novel multiuser scheme for NC-m-MIMO combined with SM. We can see that the number of antennas is not affected by the incorporation of SM, even we have an improvement on the performance with respect to the coherent case.

Finally, in order to complete the study of NC-m-MIMO systems based on DPSK schemes, we have presented an evaluation of the BLER and the throughput to fully characterize the behavior of our proposal in a real packet-based communication network. This has allowed us to assess the scope of multiplexing users in the constellation (CMS) against other classical techniques such as TDMA (TMS). The results showed that the CMS needs to incorporate more antennas at the BS than TMS, although CMS provides a higher throughput than TMS. In some cases, the demodulation of multiple users in the constellation could require an excessively large number of antennas as compared with TMS, even considering m-MIMO. Therefore, it is necessary to properly manage the tradeoff between the throughput and the number of antennas, to reach an optimal operational point.

In order to take advantage of increasing the throughput with CMS, while we may reduce the number of antennas with TDS, we have proposed combining both schemes. We have achieved for 8 users, using only 30 antennas, to multiply by 2 the throughput with respect to orthogonal multiplexing. In addition, we conclude that it is preferable to have more groups multiplexed in time with a few users in constellation than all users in

pure CMS or TMS, finding a suitable tradeoff between the number of antennas and the throughput.

8.2 Future Directions

We briefly present some of the ideas for future research arising from these conclusions.

Optimization of the constellation. The constellation designs developed in this dissertation are based on heuristic methods which seek the minimum distance between user symbols with the purpose of demodulating the users, achieving a good performance. However, an optimal constellation scheme for non coherent massive MIMO based on phase detection is still an open issue.

New channel coding schemes. Another channel coding schemes can be developed not only for reducing the number of antennas, but for increasing the number of users multiplexed in the constellation. In this sense, future work focuses on analyzing the performance of LDPC codes or polar codes, considered recently for M2M communication inside the use cases for 5G. Also, it would be interesting the usage of different coding schemes between users. In addition, to improve the performance, other via is optimizing a mapping scheme for the joint constellation that is subject of further research.

Visible light communication channel. The electromagnetic spectrum crisis encourages the usage of the visible light to transmit the information. Therefore, the interaction of the non coherent m-MIMO and VLC network is an open research. In addition, the deployment of VLC implies that the network will be extremely heterogeneous, then future works would consider the non coherent detection in heterogeneous networks.

Channel model for mmWave and beam-forming. The usage of the millimeter frequency band is demanded for new scenarios or use cases in 5G. These frequencies in m-MIMO are conducted to perform beam-forming techniques, which require the knowledge of some type of channel state information. The implementation of these techniques for a non coherent system, which does not make CSI available is an opportunity for future research.

List of Symbols

General notation

- The superscript * is used to indicate complex conjugation. Therefore, x^* represents the complex conjugate of the variable x.
- The superscript ^{H} is used to indicate complex conjugate transpose operation. Therefore, $\mathbf{X}^H$ represents the complex conjugate transpose of the matrix $\mathbf{X}$.
- The superscript ^{T} is used to indicate matrix transpose operation. Therefore, $\mathbf{X}^T$ represents the transpose of the matrix $\mathbf{X}$.
- The notation $*$ denotes the convolutional process. Therefore, $x * y$ represents the convolution between variables x and y.
- The notation $\hat{x}$ represents the estimate of x.
- The notation $E\{\cdot\}$ is used to indicate the expectation operation. Therefore, $E\{x\}$ is the expected value of x.
- The notation $CN(\mu, \sigma^2)$ represents a μ-mean circularly symmetric complex Gaussian distribution with variance σ^2.
- The notation $\Re\{\cdot\}$ denotes the real part of a complex number. Therefore, $\Re\{x\}$ represents the real part of x.
- The notation $x!$ denotes the factorial of the number x.
- $P(x)$ denotes the function of probability of x.
- $P(x, y)$ denotes the function of joint probability of x and y.
- $P(x/y)$ denotes the function of conditional probability for the variable x given y.
- $Q-$Function defined as $Q(x) = \frac{1}{\sqrt{2\pi}} \int_{-\infty}^{x} \exp \frac{t^2}{2}\, dt$

Special symbols

A_R: Area under EXIT chart curve as function of R.

b_p: The p^{th} bits transmitted by an user within the bit vector $\boldsymbol{b}$.

$\boldsymbol{b}$: A bit combination representing one of the possible transmitted bit sequence.

c_n: The coded symbol of the encoder at instance n.

d_{min}: The minimum Euclidean distance.

$\bar{d}_{min}$: The normalized minimum Euclidean distance.

D: Delay between consecutive symbols.

D_{int}: Interleaver depth.

E_b: Bit energy.

E_b/N_0: Ratio of bit energy to noise power spectral density.

E_s: Symbol energy.

E_s/N_0: Ratio of symbol energy to noise power spectral density.

f_c: Central frequency of a communication system.

f_D: The Doppler shift.

$G(D)$: The generator polynomials matrix for Convolutional codes.

G: The $(R \times J)$-element channel matrix for a Rice distribution.

h_{rj}: Components of H which represent the propagation from the user j-th to the r-th antenna.

H: The $(R \times J)$-element channel matrix for a Rayleigh distribution.

$\widetilde{\mathbf{H}}$: The $(R \times J)$-element channel matrix for a Rayleigh distribution.

$i[n]$: The interference term in the time instant n.

$\mathcal{I}$: The total interference power, $\mathcal{I} = E\{|i[n]^2|\}$.

I: Detection intervals for ASK constellation.

$I_{j,a}$: The a priori information for the user j^{th}.

$I_{j,e}$: The extrinsic information for the user j^{th}.

J: The number of users.

K: The Rician fading parameter.

k: The possible values of a joint symbol of the joint constellation, $\mathcal{M}$.

$\mathfrak{K}$: The joint constellation dimensionality.

l: The symbol position within an L-symbols frame.

L: The number of symbols in each transmission interval, or the number of symbols per frame (or block).

L: The number of symbols intercalated in the UEP constellation design.

LLR_q: The log-likelihood ratio for the q^{th} bit.

L_M: The set of LLR for each $z[n]$. $L_M = \gamma(z[n])$

$L_{i,a}(u_j)$: The soft-bit values for input a priori information of user j^{th}.

$L_{i,e}(u_j)$: The soft-bit values for input extrinsic information of user j^{th}.

$L_{o,a}(c_j)$: The soft-bit values for output a priori information of user j^{th}.

$L_{o,e}(c_j)$: The soft-bit values for output extrinsic information of user j^{th}.

L_p: The a posteriori LLR values.

m:

m: The possible values of a source symbol of an user constellation, $\mathfrak{M}_j$.

M: The number of levels of a multi-level modulation scheme: DPSK, PSK, ASK or QAM.

$\mathfrak{M}_j$: Individual constellation for each user.

M_o: The number of modulation modes in an adaptive modulation scheme.

$\mathcal{M}$: Joint Constellation.

n: Time instants.

$\mathfrak{n}$: Number of bits input CC.

N: Number of bits.

N_I: Number if iterations.

N_0: Single-sided power spectral density of white noise.

p: The number of bits in a modulated user symbol.

$\mathfrak{p}$: Power level for ASK constellation.

P_b: Bit error probability.

P_s: Symbol error probability.

q: The number of bits in a joint symbol.

r: Coding rate.

R: Number of antennas.

S: The number of simulated channels.

$s[n]$: The transmitted user symbol at time instant n belonging to $\mathfrak{M}$.

T_c: The coherence time.

T_j: The mutual information transfer function for user j.

u_n: The input symbol to the encoder at instance n.

$\nu[n]$: AWGN added to the transmitted signal.

$\mathbf{v}$: Velocity.

$x[n]$: The transmitted differential symbol at instance n.

$y[n]$: The received symbol at instance n.

α: The relative power gain of the rest of users with respect to user 1.

β: The metric relates the bandwidth with shift Doppler.

λ: The wavelength.

ρ: The reference SNR at the input of the antennas.

η_{max}: Maximum achievable rate (MAR).

ς: The joint symbol belonging to joint constellation $\mathcal{M}$.

σ^2: The complex noise's variance.

σ_h^2: The complex channel's variance.

σ_s^2: The complex signal's variance.

π: Interleaver.

π^{-1}: Deinterleaver.

τ: The symbol-interleaver size in terms of the number of symbols.

Glossary

AGM: Anti-Gray mapping

APSK: Amplitude Phase Shift Keying

APP: Approximation

ASK: Amplitude Shift Keying

AWGN: Additive White Gaussian Noise

BBU: BaseBand Unit

BER: Bit error rate

BICM: Bit-Interleaved Coded Modulation

BICM-ID: Bit-Interleaved Coded Modulation-Iterative Decoding

BJCR: Bahl-Cocke-Jelinek-Raviv

BLER: Block error rate

bpcu: Bits per channel use

BPSK: Binary Phase Shift Keying

BS: Base Station

BW: Bandwidth

CC: Convolutional Code

CDD: Conventional Differential Detection

CDMA: Code Division Multiple Access

CMS: Constellation Multiplexing Scheme

CPFSK: Continuous Phase FSK

CSI: Channel State Information

D2D: Device to Device

DAPK: Differential Amplitude Phase Keying

DAPSK: Differential Amplitude Phase Shift Keying

DE: Differential Encoding

DFDD: Differential Feedback Decision Detection

DL: Downlink

DPSK: Differential Phase Shift Keying

DQAM: Differential Quadrature Amplitude Modulation

DQPSK: Differential Quaternary Phase Shift Keying

DSM: Differential Spatial Modulation

DSSS: Direct-Sequence Spread-Spectrum

DUSTM: Differential Unitary Space-Time Modulation

EEP: Equal Error Protection

EP: Error Propagation

EXIT: Extrinsic Information Transfer

FBMC: FilteBank Multi-Carrier

FD: Frequency Domain

FDMA: Frequency Division Multiple Access

FFT: Fast Fourier Transform

FM: Frequency Modulation

FP: Favorable Propagation

FSK: Frequency Shift Keying

GC: Grassmannian Constellations

GLRT: General Likelihood Ratio Test

GM: Gray Mapping

GSM: Generalized Spatial Modulation

IDD: Iterative Decoding and Demodulation

IDMA: Interleaver Division Multiple Access

IFFT: Inverse Fast Fourier Transform

IIR: Infinitive Impulse Response

IoT: Internet of Things

I/Q: Phase - Quadrature

IR-UWB: Impulse Radio-Ultra Wide Band

IRCCs: Irregular Convolutional Codes

ISI: Inter Symbol Interference

IUI: Inter User Interference

JSD: Joint Symbol Detection

LED: Light Emisor Diode

LiFi: Light Fidelity

LLR: Log Likelihood Ratio

LOS: Line of Sight

LTE: Long Term Evolution

m-MIMO: massive MIMO

m-SIMO: massive SIMO

M2M: Machine to Machine

MAR: Maximum Achievable Rate

MD: Minimum Distance

MFSK: M-ary Frequency Shift Keying

MI: Mutual Information

MIMO: Multiple-Input Multiple-Output

ML: Maximum Likelihood

MMSE: Minimum Mean Square Error

mmWaves: millimeter waves

MRC: Maximum Ratio Combining

MS: Mapping Scheme

MSB: Most significative bit

MSDD: Multiple Symbol Differential Detection

MSs: Mobile Stations

MU: Multi User

MU-MIMO: Multiuser-MIMO

MUD: Multiuser Detection

NC: Non Coherent

NC-m-MIMO: No Coherent massive MIMO

NC-m-MIMO-DPSK: No Coherent massive MIMO based on DPSK

NC-MIMO: No Coherent MIMO

NC-MUD: No Coherent Multiuser Detection

NC-SM: No Coherent Spatial Modulation

NMD: Normalized Minimum Distance

NOMA: Non Orthogonal Multiple Access

NSC: Non Systematic Code

OFDM: Orthogonal Frequency Division Multiple

OOK: On-Off Keying

PCMF: Pulse-Compressor Matched Filter

PLL: Phase-Locked Loops

post-NC-MUD: posteriori non coherent multiuser detection

prior-NC-MUD: a priori non coherent multiuser detection

PSK: Phase Shift Keying

QAM: Quadrature Amplitude Modulation

QoS: Quality of Service

RA: Receive Antennas

RAN: Radio Access Network

RF: Radio Frequency

RMT: Random Matrix Theory

RSC: Recursive Systematic Code

SCMA: Sparse Code Multiple Access

SEP: Symbol Error Probability

SER: Symbol error rate

SIMO: Single Input Multiple Output

SINR: Signal to Interference plus Noise Ratio

SISO: Single-Input Single-Output

SM: Spatial Modulation

SNR: Signal to Noise Ratio

SSK: Space Shift Keying

ST: Space-Time

SU: Single User

TCM: Trellis Coded Modulation

TCP: Transport Control Protocol

TD: Time domain

TDD: Time Division Duplex

TDMA: Time Division Multiple Access

TH/MC: Time-Hopping/Multi-Carrier

TMS: TDMA Multiplexing Scheme

TPC: Transmit Pre-Coding

UEP: Unequal Error Protection

UFMC: Universal Filtered Multi-Carrier

UIT: Useful Interference Term

UL: Uplink

URC: Unitary Recursive Code

URLLC: Ultra Reliable Low Latency Communications

V2X: Vehicle to anything

VLC: Visible Light Communications

Wifi: Wireless Fidelity

ZF: Zero Forcing

1G: First Generation

2G: Second Generation

3G: Third Generation

3GPP: 3rd Generation Partnership Project

4G: Fourth Generation

5G: Fifth Generation

List of Figures

List of Tables

Bibliography

[1] M. Tolstrup, *Overview of Cellular Systems*. Wiley, 2015.

[2] M. Sauter, *Evolution from 2G over 3G to 4G*. Wiley, 2013.

[3] A. Kukushkin, *Third Generation Network (3G), UMTS*, pp. 121–172. Wiley, 2018.

[4] M. Rumney, *Air Interface Concepts*. Wiley, 2013.

[5] M. Rumney, *Looking Towards 4G: LTE-Advanced*. Wiley, 2013.

[6] J. Zhang, B. Zhang, S. Chen, X. Mu, M. El-Hajjar, and L. Hanzo, "Pilot contamination elimination for large-scale multiple-antenna aided ofdm systems," *IEEE Journal of Selected Topics in Signal Processing*, vol. 8, no. 5, pp. 759–772, 2014.

[7] W. T. Webb, L. Hanzo, and R. Steele, "Bandwidth efficient qam schemes for rayleigh fading channels," *IEE Proceedings I - Communications, Speech and Vision*, vol. 138, pp. 169–175, June 1991.

[8] L. Wang and L. Hanzo, "Dispensing with channel estimation: Differentially modulated cooperative wireless communications," *IEEE Communications Surveys Tutorials*, vol. 14, pp. 836–857, Third 2012.

[9] C. X. D. L. S. X. L. Wang, L. Li and L. Hanzo, "Multiple-symbol joint signal processing for differentially encoded single- and multi-carrier communications: Principles, designs and applications," *IEEE Communications Survey Tutorials*, vol. 16, no. 2, pp. 689–712, 2014.

[10] A. Al-Dulaimi, X. Wang, and C.-L. I, *Standardization: The Road to 5G*. IEEE, 2018.

[11] M. Shafi, A. F. Molisch, P. J. Smith, T. Haustein, P. Zhu, P. D. Silva, F. Tufvesson, A. Benjebbour, and G. Wunder, "5g: A tutorial overview of standards, trials, challenges, deployment, and practice," *IEEE Journal on Selected Areas in Communications*, vol. 35, pp. 1201–1221, June 2017.

[12] A. Gupta and R. K. Jha, "A survey of 5g network: Architecture and emerging technologies," *IEEE Access*, vol. 3, pp. 1206–1232, 2015.

[13] M. Jaber, M. A. Imran, R. Tafazolli, and A. Tukmanov, "5g backhaul challenges and emerging research directions: A survey," *IEEE Access*, vol. 4, pp. 1743–1766, 2016.

[14] *Massive MIMO Networks: Spectral, Energy, and Hardware Efficiency*. now, 2017.

[15] R. Vannithamby and S. Talwar, *Massive MIMO Communications*. Wiley, 2017.

[16] F. T. E.G. Larsson, O. Edfors and T. Marzetta, "Massive mimo for next generation wireless systems," *IEEE Communication Magazine*, vol. 52, pp. 186–195, Feb 2014.

[17] E. G. L. E. Bjornson and T. L. Marzetta, "Massive mimo: ten myths and one critical question," *IEEE Communication Magazine*, vol. 54, no. 2, pp. 114–123, 2016.

[18] S. G. Glisic, *Massive MIMO*. Wiley, 2016.

[19] Y. W. D. Qiao and Y. Chen, "Massive mimo architecture for 5g networks: Co-located, or distributed?,," in *1th ISWCS*, vol. 1, (Barcelona, Spain), pp. 192–197, 2014.

[20] P. van Genderen and W. J. H. Meijer, "Non coherent integration in a medium prf radar," in *Proceedings International Radar Conference*, pp. 91–94, May 1995.

[21] I. Bekkerman and J. Tabrikian, "Target detection and localization using mimo radars and sonars," *IEEE Transactions on Signal Processing*, vol. 54, pp. 3873–3883, Oct 2006.

[22] T. L. Marzetta, "Noncooperative cellular wireless with unlimited numbers of base station antennas," *IEEE Transactions on Wireless Communications*, vol. 9, pp. 3590–3600, November 2010.

[23] L. Lu, G. Y. Li, A. L. Swindlehurst, A. Ashikhmin, and R. Zhang, "An overview of massive mimo: Benefits and challenges," *IEEE Journal of Selected Topics in Signal Processing*, vol. 8, pp. 742–758, Oct 2014.

[24] Y. Cai, Z. Qin, F. Cui, G. Y. Li, and J. A. McCann, "Modulation and multiple access for 5g networks," *IEEE Communications Surveys Tutorials*, vol. 20, pp. 629–646, Firstquarter 2018.

[25] A. Sahin, I. Guvenc, and H. Arslan, "A survey on multicarrier communications: Prototype filters, lattice structures, and implementation aspects," *IEEE Communications Surveys Tutorials*, vol. 16, pp. 1312–1338, Third 2014.

[26] J. Wen, J. Hua, W. Lu, Y. Zhang, and D. Wang, "Design of waveform shaping filter in the ufmc system," *IEEE Access*, vol. 6, pp. 32300–32309, 2018.

[27] Z. Ding, X. Lei, G. K. Karagiannidis, R. Schober, J. Yuan, and V. K. Bhargava, "A survey on non-orthogonal multiple access for 5g networks: Research challenges and future trends," *IEEE Journal on Selected Areas in Communications*, vol. 35, pp. 2181–2195, Oct 2017.

[28] A. Al-Dulaimi, X. Wang, and C.-L. I, *Nonorthogonal Multiple Access for 5G*. IEEE, 2018.

[29] M. D. Renzo, H. Haas, and P. M. Grant, "Spatial modulation for multiple-antenna wireless systems: a survey," *IEEE Communications Magazine*, vol. 49, pp. 182–191, December 2011.

[30] R. Y. Mesleh, H. Haas, S. Sinanovic, C. W. Ahn, and S. Yun, "Spatial modulation," *IEEE Transactions on Vehicular Technology*, vol. 57, pp. 2228–2241, July 2008.

[31] M. D. Renzo, H. Haas, A. Ghrayeb, S. Sugiura, and L. Hanzo, "Spatial modulation for generalized mimo: Challenges, opportunities, and implementation," *Proceedings of the IEEE*, vol. 102, pp. 56–103, Jan 2014.

[32] J. Wang, S. Jia, and J. Song, "Generalised spatial modulation system with multiple active transmit antennas and low complexity detection scheme," *IEEE Transactions on Wireless Communications*, vol. 11, pp. 1605–1615, April 2012.

[33] A. Bana, M. Angjelichinoski, E. d. Carvalho, and P. Popovski, "Massive mimo for ultra-reliable communications with constellations for dual coherent-noncoherent detection," in *WSA 2018; 22nd International ITG Workshop on Smart Antennas*, pp. 1–4, March 2018.

[34] Y. L. H. Zhang and L. Song, "D2d-u: Device-to-device communications in unlicensed bands for 5g system," *IEEE Transactions on Wireless Communications*, vol. 16, pp. 3507–3519, Mar 2017.

[35] O. N. T. B. M. Uysal, F. Miramirkhani and E. Panayirci, "Ieee 802.15.7r1 reference channel models for visible light communications," *IEEE Communication Magazine*, vol. 55, pp. 212–217, 2017.

[36] H. Haas, L. Yin, Y. Wang, and C. Chen, "What is lifi?," *Journal of Lightwave Technology*, vol. 34, pp. 1533–1544, March 2016.

[37] F. B. . R. W. H. . A. L. . T. L. M. . P. Popovski, "Five disruptive technology directions for 5g," *IEEE Communications Magazine*, vol. 52, pp. 74–80, 2014.

[38] T. S. Rappaport, S. Sun, R. Mayzus, H. Zhao, Y. Azar, K. Wang, G. N. Wong, J. K. Schulz, M. Samimi, and F. Gutierrez, "Millimeter wave mobile communications for 5g cellular: It will work!," *IEEE Access*, vol. 1, pp. 335–349, 2013.

[39] H. Q. Ngo, E. G. Larsson, and T. L. Marzetta, "Energy and spectral efficiency of very large multiuser mimo systems," *IEEE Transactions on Communications*, vol. 61, pp. 1436–1449, April 2013.

[40] F. Rusek, D. Persson, B. K. Lau, E. G. Larsson, T. L. Marzetta, O. Edfors, and F. Tufvesson, "Scaling up mimo: Opportunities and challenges with very large arrays," *IEEE Signal Processing Magazine*, vol. 30, pp. 40–60, Jan 2013.

[41] A. M. Tulino and S. Verdú, "Random matrix theory and wireless communications," *Foundations and Trends® in Communications and Information Theory*, vol. 1, no. 1, pp. 1–182, 2004.

[42] R. Corvaja and A. G. Armada, "Phase noise degradation in massive mimo downlink with zero-forcing and maximum ratio transmission precoding," *IEEE Transactions on Vehicular Technology*, vol. 65, pp. 8052–8059, Oct 2016.

[43] Proakis, *Digital Communications 5th Edition*. McGraw Hill, 2007.

[44] C. Xu, J. Zhang, T. Bai, S. P. Botsinis, R. G. Maunder, R. Zhang, and L. Hanzo, "Adaptive coherent/non-coherent single/multiple-antenna aided channel coded ground-to-air aeronautical communication," *IEEE Transactions on Communications*, pp. 1–1, 2018.

[45] C. Abou-Rjeily, N. Daniele, and J. Belfiore, "On the decode-and-forward cooperative diversity with coherent and non-coherent uwb systems," in *2006 IEEE International Conference on Ultra-Wideband*, pp. 435–440, Sep. 2006.

[46] S. Sugiura, S. Chen, and L. Hanzo, "Coherent and differential space-time shift keying: A dispersion matrix approach," *IEEE Transactions on Communications*, vol. 58, pp. 3219–3230, November 2010.

[47] S. Sugiura, "Coherent versus non-coherent reconfigurable antenna aided virtual mimo systems," *IEEE Signal Processing Letters*, vol. 21, pp. 390–394, April 2014.

[48] S. Sugiura, C. Xu, S. X. Ng, and L. Hanzo, "Reduced-complexity coherent versus non-coherent qam-aided space-time shift keying," *IEEE Transactions on Communications*, vol. 59, pp. 3090–3101, November 2011.

[49] S. Sugiura, S. Chen, H. Haas, P. M. Grant, and L. Hanzo, "Coherent versus non-coherent decode-and-forward relaying aided cooperative space-time shift keying," *IEEE Transactions on Communications*, vol. 59, pp. 1707–1719, June 2011.

[50] R. Rajashekar, C. Xu, N. Ishikawa, S. Sugiura, K. V. S. Hari, and L. Hanzo, "Algebraic differential spatial modulation is capable of approaching the performance of its coherent counterpart," *IEEE Transactions on Communications*, vol. 65, pp. 4260–4273, Oct 2017.

[51] M. Schwartz, W. Bennett, and S. Stein, *Communication Systems and Techniques*. New York: McGraw-Hill, 1966.

[52] A. Glenn and G. Lieberman, "Performance of digital communications systems in an arbitrary fading rate and jamming environments," *IEEE Transactions on Communications Systems*, vol. 11, pp. 57–68, March 1963.

[53] W. Osborne and M. Luntz, "Coherent and noncoherent detection cpfsk," *IEEE Transactions on Communications*, vol. 22, pp. 1023–1036, August 1974.

[54] T. Schonhoff, "Symbol error probabilities for m-ary cpfsk: Coherent and noncoherent detection," *IEEE Transactions on Communications*, vol. 24, pp. 644–652, June 1976.

[55] S. Stein, "Unified analysis of certain coherent and noncoherent binary communications systems," *IEEE Transactions on Information Theory*, vol. 10, pp. 43–51, January 1964.

[56] J. Oetting, "A comparison of modulation techniques for digital radio," *IEEE Transactions on Communications*, vol. 27, pp. 1752–1762, December 1979.

[57] S. Maslamani and M. Ghanbari, "Digital demodulation by a non-coherent differential psk modem," *Electronics Letters*, vol. 26, pp. 2028–2029, Nov 1990.

[58] J. Henry, "Dpsk versus fsk with frequency uncertainty," *IEEE Transactions on Communication Technology*, vol. 18, pp. 814–817, December 1970.

[59] F. Adachi, "Reduced-state viterbi differential detection using a recursively estimated phase reference for m-ary dpsk," *IEE Proceedings - Communications*, vol. 142, pp. 263–270, Aug 1995.

[60] F. Adachi, "Adaptive differential detection for m-ary dpsk," *IEE Proceedings - Communications*, vol. 143, pp. 21–28, Feb 1996.

[61] S. G. Wilson, J. Freebersyser, and C. Marshall, "Multi-symbol detection of m-dpsk," in *1989 IEEE Global Telecommunications Conference and Exhibition 'Communications Technology for the 1990s and Beyond'*, pp. 1692–1697 vol.3, Nov 1989.

[62] H. Huynh and M. Lecours, "Impulsive noise in noncoherent m-ary digital systems," *IEEE Transactions on Communications*, vol. 23, pp. 246–252, February 1975.

[63] S. Doyle and S. Hryckiewicz, "Performance comparison of noncoherent dpsk with coherent bandwidth efficient modulation signals in simultaneous fading and optimized jamming," *IEEE MILCOM Conference*, Oct 1990 1990.

[64] W. H. G. R. Schober and J. B. Huber, "Improving differential detection of mdpsk by nonlinear noise prediction and sequence estimation," *IEEE Transactions on Communications*, vol. 47, pp. 1161–1172, 1999.

[65] N. Hamamoto, "Differential detection with iir filter for improving dpsk detection performance," *IEEE Transactions on Communications*, vol. 44, pp. 959–966, Aug 1996.

[66] W. Lindsey and M. Simon, "Detection of digital fsk and psk using a first-order phase-locked loop," *IEEE Transactions on Communications*, vol. 25, pp. 200–214, February 1977.

[67] R. L. Brewster and W. W. S. Jibrail, "Detection of fsk and dpsk data signals by pulse compression," *IEE Proceedings F - Communications, Radar and Signal Processing*, vol. 129, pp. 273–280, August 1982.

[68] R. Wilson and J. Richter, "Generation and performance of quadraphase welti codes for radar and synchronization of coherent and differentially coherent psk," *IEEE Transactions on Communications*, vol. 27, pp. 1296–1301, Sep. 1979.

[69] E. Geraniotis, "Performance of noncoherent direct-sequence spread-spectrum multiple-access communications," *IEEE Journal on Selected Areas in Communications*, vol. 3, pp. 687–694, Sep. 1985.

[70] M. Kavehrad and G. Bodeep, "Design and experimental results for a direct-sequence spread-spectrum radio using differential phase-shift keying modulation for indoor, wireless communications," *IEEE Journal on Selected Areas in Communications*, vol. 5, pp. 815–823, June 1987.

[71] J. Siuzdak and W. van Etten, "Ber evaluation for phase and polarization diversity optical homodyne receivers using noncoherent ask and dpsk demodulation," *Journal of Lightwave Technology*, vol. 7, pp. 584–599, April 1989.

[72] M. Li, T. Li, X. Zhang, Y. Song, and Y. Liu, "Bit error rate analysis of ook modulation scheme under non-coherent demodulation for space uplink optical communication systems," in *2015 IEEE 16th International Conference on Communication Technology (ICCT)*, pp. 695–698, Oct 2015.

[73] D. A. Fishman, J. A. Nagel, T. W. Cline, R. E. Tench, T. C. Pleiss, T. Miller, D. G. Coult, M. A. Milbrodt, P. D. Yeates, A. Chraplyvy, R. Tkach, A. B. Piccirilli, J. R. Simpson, and C. M. Miller, "A high capacity noncoherent fsk lightwave field experiment using er/sup 3+/-doped fiber optical amplifiers," *IEEE Photonics Technology Letters*, vol. 2, pp. 662–664, Sep. 1990.

[74] P. Liu, S. Gazor, I. Kim, and D. I. Kim, "Noncoherent relaying in energy harvesting communication systems," *IEEE Transactions on Wireless Communications*, vol. 14, pp. 6940–6954, Dec 2015.

[75] P. Liu, S. Gazor, I. Kim, and D. I. Kim, "Energy harvesting noncoherent cooperative communications," *IEEE Transactions on Wireless Communications*, vol. 14, pp. 6722–6737, Dec 2015.

[76] A. B. Sergienko, "Dpsk-qam combination as a signal set for spectrally efficient noncoherent communication," in *2018 IEEE East-West Design Test Symposium (EWDTS)*, pp. 1–6, Sep. 2018.

[77] B. Selim, S. Muhaidat, P. C. Sofotasios, B. S. Sharif, T. Stouraitis, G. K. Karagiannidis, and N. Al-Dhahir, "Performance analysis of single carrier coherent and noncoherent modulation under i/q imbalance," in *2018 IEEE 87th Vehicular Technology Conference (VTC Spring)*, pp. 1–5, June 2018.

[78] R. Haeb, "A comparison of coherent and differentially coherent detection schemes for fading channels," in *38th IEEE Vehicular Technology Conference*, pp. 364–370, June 1988.

[79] R. Lupas and S. Verdu, "Linear multiuser detectors for synchronous code-division multiple-access channels," *IEEE Transactions on Information Theory*, vol. 35, pp. 123–136, Jan 1989.

[80] S. Tomisato, K. Fukawa, and H. Suzuki, "Coherent frequency hopping multiple access (cfhma) with multiuser detection for mobile communication systems," *IEEE Transactions on Vehicular Technology*, vol. 49, pp. 531–539, March 2000.

[81] J. G. Koo, "Performance analysis of an iterative group-wise parallel interference cancellation for multiuser detection of coherent w-cdma system," in *Global Telecommunications Conference, 2002. GLOBECOM '02. IEEE*, vol. 1, pp. 519–523 vol.1, Nov 2002.

[82] M. K. Varanasi and D. Das, "Noncoherent decision-feedback multiuser detection," *IEEE Transactions on Communications*, vol. 48, pp. 259–269, Feb 2000.

[83] A. Russ and M. K. Varanasi, "Noncoherent multiuser detection for nonlinear modulation over the rayleigh-fading channel," *IEEE Transactions on Information Theory*, vol. 47, pp. 295–307, Jan 2001.

[84] D. Das and M. K. Varanasi, "Optimum noncoherent multiuser decision feedback detection," *IEEE Transactions on Information Theory*, vol. 50, pp. 1974–1988, Sep. 2004.

[85] R. J. Kozick and B. M. Sadler, "Maximum likelihood multi-user detection for fast frequency hopping/multiple frequency shift keying systems," in *2000 IEEE Wireless Communications and Networking Conference. Conference Record (Cat. No.00TH8540)*, vol. 1, pp. 67–72 vol.1, Sep. 2000.

[86] Y. T. Su, Y.-S. Shen, and C.-Y. Hsiao, "On the detection of a class of fast frequency-hopped multiple access signals," *IEEE Journal on Selected Areas in Communications*, vol. 19, pp. 2151–2164, Nov 2001.

[87] R. Schober and L. H. . Lampe, "Noncoherent receivers for multichip differentially encoded ds-cdma," *IEEE Transactions on Wireless Communications*, vol. 3, pp. 2129–2140, Nov 2004.

[88] B. M. Hochwald and T. L. Marzetta, "Unitary space-time modulation for multiple-antenna communications in rayleigh flat fading," *IEEE Transactions on Information Theory*, vol. 46, pp. 543–564, March 2000.

[89] B. M. Hochwald and W. Sweldens, "Differential unitary space-time modulation," *IEEE Transactions on Communications*, vol. 48, pp. 2041–2052, Dec 2000.

[90] T. Cui and C. Tellambura, "On multiple symbol detection for diagonal dustm over ricean channels," *IEEE Transactions on Wireless Communications*, vol. 7, pp. 1146–1151, April 2008.

[91] M. Hajiaghayi and C. Tellambura, "Unitary signal constellations for differential space-time modulation," *IEEE Communications Letters*, vol. 11, pp. 25–27, Jan 2007.

[92] M. J. Borran, A. Sabharwal, and B. Aazhang, "On design criteria and construction of noncoherent space-time constellations," *IEEE Transactions on Information Theory*, vol. 49, pp. 2332–2351, Oct 2003.

[93] M. Beko, J. Xavier, and V. A. N. Barroso, "Further results on the capacity and error probability analysis of noncoherent mimo systems in the low snr regime," *IEEE Transactions on Signal Processing*, vol. 56, pp. 2915–2930, July 2008.

[94] R. H. Gohary and T. N. Davidson, "Noncoherent mimo communication: Grassmannian constellations and efficient detection," *IEEE Transactions on Information Theory*, vol. 55, pp. 1176–1205, March 2009.

[95] I. Kammoun, A. M. Cipriano, and J. Belfiore, "Non-coherent codes over the grassmannian," *IEEE Transactions on Wireless Communications*, vol. 6, pp. 3657–3667, October 2007.

[96] A. Schenk and R. F. H. Fischer, "Noncoherent detection in massive mimo systems," in *WSA 2013; 17th International ITG Workshop on Smart Antennas*, pp. 1–8, March 2013.

[97] M. C. A. Manolakos and A. Goldsmith, "Csi is not needed for optimal scaling in multiuser massive simo systems," in *Proceedings of ISIT.*, (Honolulu), Jul 2014.

[98] M. Chowdhury, A. Manolakos, and A. J. Goldsmith, "Coherent versus noncoherent massive simo systems: Which has better performance?," in *2015 IEEE International Conference on Communications (ICC)*, pp. 1691–1696, June 2015.

[99] M. Chowdhury, A. Manolakos, and A. J. Goldsmith, "Design and performance of noncoherent massive simo systems," in *2014 48th Annual Conference on Information Sciences and Systems (CISS)*, pp. 1–6, March 2014.

[100] H. A. J. Alshamary, T. Al-Naffouri, A. Zaib, and W. Xu, "Optimal non-coherent data detection for massive simo wireless systems: A polynomial complexity solution," in *2015 IEEE Signal Processing and Signal Processing Education Workshop (SP/SPE)*, pp. 172–177, Aug 2015.

[101] E. Leung, Z. Dong, and J. Zhang, "Uniquely factorable hexagonal constellation designs for noncoherent simo systems," *IEEE Transactions on Vehicular Technology*, vol. 66, pp. 5495–5501, June 2017.

[102] D. Kong, X. Xia, and T. Jiang, "A differential qam detection in uplink massive mimo systems," *IEEE Transactions on Wireless Communications*, vol. 15, pp. 6371–6383, Sep. 2016.

[103] A. G. Armada and L. Hanzo, "A non-coherent multi-user large scale simo system relaying on m-ary dpsk," in *2015 IEEE International Conference on Communications (ICC)*, pp. 2517–2522, June 2015.

[104] M. Chowdhury, A. Manolakos, and A. Goldsmith, "Scaling laws for noncoherent energy-based communications in the simo mac," *IEEE Transactions on Information Theory*, vol. 62, pp. 1980–1992, April 2016.

[105] A. Manolakos, M. Chowdhury, and A. Goldsmith, "Energy-based modulation for noncoherent massive simo systems," *IEEE Transactions on Wireless Communications*, 2016.

[106] M. A. El-Azizy, R. H. Gohary, and T. N. Davidson, "A bicm-idd scheme for noncoherent mimo communication," *IEEE Transactions on Wireless Communications*, vol. 8, pp. 541–546, Feb 2009.

[107] J. Camp and E. Knightly, "Modulation rate adaptation in urban and vehicular environments: Cross-layer implementation and experimental evaluation," *IEEE/ACM Transactions on Networking*, vol. 18, pp. 1949–1962, Dec 2010.

[108] S. Hur, S. Baek, B. Kim, Y. Chang, A. F. Molisch, T. S. Rappaport, K. Haneda, and J. Park, "Proposal on millimeter-wave channel modeling for 5g cellular system," *IEEE Journal of Selected Topics in Signal Processing*, vol. 10, pp. 454–469, April 2016.

[109] S. Sun, T. S. Rappaport, M. Shafi, P. Tang, J. Zhang, and P. J. Smith, "Propagation models and performance evaluation for 5g millimeter-wave bands," *IEEE Transactions on Vehicular Technology*, vol. 67, pp. 8422–8439, Sep. 2018.

[110] B. Knott, M. Chowdhury, A. Manolakos, and A. J. Goldsmith, "Benefits of coding in a noncoherent massive simo system," in *2015 IEEE International Conference on Communications (ICC)*, pp. 2350–2355, June 2015.

[111] M. Matthaiou, P. J. Smith, H. Ngo, and H. Tataria, "Does massive mimo fail in rician channels?," *IEEE Wireless Communication Letters*, vol. 1, pp. 1–4, July 2018.

[112] A. Sengupta and P. Miltra, "Capacity of multivariate channels with multiplicative noise," *Tech. Repo. AT&TBell Labs*, 2004.

[113] S. Ray, M. Medard, and L. Zheng, "Wideband non-coherent mimo capacity," in *Proceedings. International Symposium on Information Theory, 2005. ISIT 2005.*, pp. 646–650, Sep. 2005.

[114] S. Verdu, "Spectral efficiency in the wideband regime," *IEEE Transactions on Information Theory*, vol. 48, pp. 1319–1343, June 2002.

[115] V. M. Baeza, A. G. Armada, W. Zhang, M. El-Hajjar, and L. Hanzo, "A noncoherent multiuser large-scale simo system relying on m-ary dpsk and bicm-id," *IEEE Transactions on Vehicular Technology*, vol. 67, pp. 1809–1814, Feb 2018.

[116] V. Baeza and A. Armada, "Analysis of the performance of a non-coherent large scale simo system based on m-dpsk under rician fading," in *EUSIPCO*, (Kos, Greece), EUSIPCO, Sep 2016.

[117] V. M. Baeza and A. Garcia-Armada, "Non-coherent massive simo system based on m-dpsk for rician channels," *IEEE Transactions on Vehicular Technology*, pp. 1–1, 2019.

[118] M. E.-H. V.M. Baeza, A.G. Armada and L. Hanzo, "Performance of a non-coherent massive simo m-dpsk system," in *Vehicular Technology Conference*, (Toronto, Canada), pp. 1–5, Sep 2017.

[119] *Radio Technologies for 5G*, ch. Non-Coherent Massive MIMO. Wiley, 2019.

[120] A. Goldsmith, *Wireless communications*. Cambridge University Press, 2005.

[121] T. S. Rappaport, *Wireless Communications: Principles and Practice*. Prentice-Hall, Jan 2002.

[122] J. I. Smith, "A computer generated multipath fading simulation for mobile radio," *IEEE Transactions on Vehicular Technology*, vol. 24, pp. 39–40, Aug 1975.

[123] G. T. 36.211, *LTE; Evolved Universal Terrestrial Radio Access (E- UTRA); Physical channels and modulation*. 3GPP Standard version 10.0.0 Release 10, Jan 2011.

[124] T. L. Marzetta, "How much training is required for multiuser mimo," in *Proc. of IEEE Asilomar Conference on Signals, Systems and Computers*, pp. 359–363, Pacific Grove, USA, Nov 2006.

[125] R. Wei and X. Wang, "Differential 16-qam and 16-apsk for uplink massive mimo systems," *IEEE Wireless Communications Letters*, vol. 7, pp. 170–173, April 2018.

[126] M. C. A. Manolakos and A. J. Goldsmith, "Constellation design in noncoherent massive simo systems," in *Proc. IEEE Global Commun. Conf*, pp. 3690–3695, December 2014.

[127] X. Li and J. A. Ritcey, "Bit-interleaved coded modulation with iterative decoding," *IEEE Commununication Letters*, vol. 1, pp. 169–171, Nov 1997.

[128] E. Zehavi, "8-psk trellis codes for a rayleigh channel," *IEEE Transactions on Communications*, vol. 40, pp. 873–884, May 1992.

[129] G. Ungerböck, "Trellis-coded modulation with redundant signal sets. part 1 and 2," *IEEE Communications Magazine*, vol. 25, pp. 5–21, February 1987.

[130] C. Berrou, A. Glavieux, and P. Thitimajshima, "Near shannon limit error-correcting coding and decoding: Turbo-codes. 1," in *Proceedings of ICC '93 - IEEE International Conference on Communications*, vol. 2, pp. 1064–1070 vol.2, May 1993.

[131] S. Benedetto and G. Montorsi, "Serial concatenation of block and convolutional codes," *Electronics Letters*, vol. 32, pp. 887–888, May 1996.

[132] L. Bahl, J. Cocke, F. Jelinek, and J. Raviv, "Optimal decoding of linear codes for minimizing symbol error rate (corresp.)," *IEEE Transactions on Information Theory*, vol. 20, pp. 284–287, March 1974.

[133] M. El-Hajjar and L. Hanzo, "Exit charts for system design and analysis," *IEEE Communications Surveys Tutorials*, vol. 16, pp. 127–153, First 2014.

[134] M. Ivanov, C. Häger, F. Brännström, A. G. i Amat, A. Alvarado, and E. Agrell, "On the information loss of the max-log approximation in bicm systems," *IEEE Transactions on Information Theory*, vol. 62, pp. 3011–3025, June 2016.

[135] S. ten Brink, "Designing iterative decoding schemes with the extrinsic information chart," *AEU International Journal Electronic Communications*, vol. 54, pp. 389–398, Sep 2000.

[136] C. Shannon, "A mathematical theory of communication," *Bell Systemms Technical Journal*, vol. 27, pp. 623–656, October 1948.

[137] M. Tuchler, S. Brink, and J. Hagenauer, "Measures for tracing convergence of iterative decoding algorithms," in *Proc. 4th International ITG Conference on Source and Channel Coding*, (Berlin Germany,), pp. 53–60, 2002.

[138] S. T. Brink, "Design of serially concatenated codes based on iterative decoding converge," in *2nd International Symposium on Turbo Codes and Related Topics*, pp. 319–322, September 2000.

[139] S. T. Brink, "Code characteristic matching for iterative decoding of serially concatenated codes," *Annals of Telecommunications*, vol. 56, pp. 394–408, 2001.

[140] S. ten Brink, "Convergence behavior of iteratively decoded parallel concatenated codes," *IEEE Transactions on Communications*, vol. 49, pp. 1727–1737, Oct 2001.

[141] M. Tuchler and J. Hagenauer, "Exit charts of irregular codes," in *Proceedings of Conference on Information Science and Systems*, pp. 20–22, Princeton University, 2002.

[142] M. Tuchler, "Design of serially concatenated systems depending on the block length," *IEEE Transactions on Communications*, vol. 52, pp. 209–218, Feb 2004.

[143] L. Hanzo, R. G. Maunder, J. Wang, and L.-L. Yang, *Near-capacity variable-length coding: regular and EXIT-chart-aided irregular designs*. John Wiley & Sons, 2011.

[144] T. Krner and S. Priebe, "Towards thz communications-status in research, standardization and regulation," *Journal of Infrared, Milimetter and Terahertz Waves*, vol. 35, no. 1, pp. 547–558, 2014.

[145] H. N. S. Jin, D. Yue, "Equal-gain transmission in massive mimo systems under ricean fading," *IEEE Trans. on Vehicular Technology*, vol. 1, pp. 1–10, July.

[146] Y. Wang and Z. Tian, "Multiple symbol differential detection for noncoherent communications with large-scale antenna arrays," *EEE Wireless Communications Letters*, vol. 7, pp. 190–193, Apr 2018.

[147] Q. Liu, "Doppler measurement and compensation in mobile satellite communications systems," in *MILCOM 1999. IEEE Military Communications. Conference Proceedings (Cat. No.99CH36341)*, vol. 1, pp. 316–320 vol.1, Oct 1999.

[148] J. S. L. HE, J. WANG and L. HANZO, "Bandwidth efficiency maximization for single-cell massive spatial modulation mimo: An adaptive power allocation perspective," *IEEE Access*, Mar 2017.

[149] J. S. L. HE, J. WANG and L. Hanzo, "On the multi-user multi-cell massive spatial modulation uplink: How many antennas for each user?," *IEEE Transactions on Wireless Communications*, vol. 16, Mar 2017.

[150] G. K. Karagiannidis and A. S. Lioumpas, "An improved approximation for the gaussian q-function," *IEEE Communications Letters*, vol. 11, pp. 644–646, August 2007.

[151] Y. Isukapalli and B. D. Rao, "An analytically tractable approximation for the gaussian q-function," *IEEE Communications Letters*, vol. 12, pp. 669–671, Sep. 2008.

[152] Y. Chen and N. C. Beaulieu, "A simple polynomial approximation to the gaussian q-function and its application," *IEEE Communications Letters*, vol. 13, pp. 124–126, February 2009.

[153] R. Li, P. Y. Kam, and H. Fu, "New representations and bounds for the generalized marcum q-function via a geometric approach, and an application," *IEEE Transactions on Communications*, vol. 58, pp. 157–169, January 2010.

[154] P. C. Sofotasios and S. Freear, "Novel expressions for the one and two dimensional gaussian q-functions," in *2010 IEEE International Conference on Wireless Information Technology and Systems*, pp. 1–4, Aug 2010.

[155] M. Lopez-Benitez and F. Casadevall, "Versatile, accurate, and analytically tractable approximation for the gaussian q-function," *IEEE Transactions on Communications*, vol. 59, pp. 917–922, April 2011.

[156] Q. Shi and Y. Karasawa, "An accurate and efficient approximation to the gaussian q-function and its applications in performance analysis in nakagami-m fading," *IEEE Communications Letters*, vol. 15, pp. 479–481, May 2011.

[157] W. M. Jang, "A simple upper bound of the gaussian q-function with closed-form error bound," *IEEE Communications Letters*, vol. 15, pp. 157–159, February 2011.

[158] M. Wu, X. Lin, and P. Kam, "New exponential lower bounds on the gaussian q-function via jensen's inequality," in *2011 IEEE 73rd Vehicular Technology Conference (VTC Spring)*, pp. 1–5, May 2011.

[159] Q. Shi and Y. Karasawa, "An intuitive methodology for efficient evaluation of the nuttall q-function and performance analysis of energy detection in fading channels," *IEEE Wireless Communications Letters*, vol. 1, pp. 109–112, April 2012.

[160] G. Abreu, "Very simple tight bounds on the q-function," *IEEE Transactions on Communications*, vol. 60, pp. 2415–2420, Sep. 2012.

[161] S. Malluri and V. K. Pamula, "Gaussian q-function and its approximations," in *2013 International Conference on Communication Systems and Network Technologies*, pp. 74–77, April 2013.